
Electronic Thesis and Dissertation Repository

August 2019

Elucidating the mechanism of NUAK1 function in Ovarian Cancer Metastasis

Jamie Fritz

The University of Western Ontario

Supervisor

Dr. Trevor Shepherd

The University of Western Ontario

Graduate Program in Anatomy and Cell Biology

A thesis submitted in partial fulfillment of the requirements for the degree in Master of Science

© Jamie Fritz 2019

Follow this and additional works at: <https://ir.lib.uwo.ca/etd>



Part of the [Cancer Biology Commons](#)

Recommended Citation

Fritz, Jamie, "Elucidating the mechanism of NUAK1 function in Ovarian Cancer Metastasis" (2019). *Electronic Thesis and Dissertation Repository*. 6364.

<https://ir.lib.uwo.ca/etd/6364>

Abstract

Epithelial ovarian cancer (EOC) has a unique mode of metastasis, where upon shedding from the primary tumor, cells form spheroids and spread through the peritoneal cavity. There is a need to elucidate pathways driving spheroid formation to identify novel therapeutic targets. We previously showed that LKB1 is required for EOC metastasis. Using multiplex inhibitor bead-mass spectrometry, we identified NUAK1 as a top LKB1 substrate candidate. We confirmed LKB1 maintains NUAK1 phosphorylation and expression. *NUAK1* KO cells had lower cell adhesion and generated spheroids with reduced integrity. We identified a cell attachment pathway that was enriched in parental compared with *NUAK1* KO spheroids. The *FN1* gene, encoding fibronectin, exhibited the greatest differential expression in *NUAK1* KO spheroids. Parental spheroids have enhanced fibronectin expression, which was undetectable in *NUAK1* KO spheroids. Treatment of *NUAK1* KO cells with fibronectin restored a compact spheroid phenotype. We have identified a novel mechanism where NUAK1 promotes spheroid formation through fibronectin deposition.

Keywords

Liver Kinase B1, AMPK-related kinase, NUAK1, spheroid, fibronectin, adhesion, epithelial ovarian cancer, metastasis

Co-Authorship Statement

OVCAR8 *STK11*KO, *NUAK1*KO, HEYA8 and OVCAR3 *NUAK1* overexpressing cells were established by Dr. Trevor Shepherd and Olga Collins.

iOvCa series, ascites-derived cell lines, were established by Dr. Gabriel DiMatta.

Multiplex inhibitor bead-mass spectrometry preparation and analysis was completed by Dr. Adrian Buensuceso, Dr. Trevor Shepherd, Kyle Francis, Kevin Brown, Karen Colwill, Anne-Claude Gingras, and Robert Rottapel.

Parima Saxena completed the phostagTM western blot analysis.

Tumor samples used for this study were collected from an EOC xenograft study completed by Dr. Adrian Buensuceso.

Experiments to assess single cell adhesion, morphology of *NUAK1*KO spheroids, and live cells in *NUAK1*KO spheroids labelled with GFP were completed by Olga Collins.

Immunofluorescence was completed by Olga Collins.

Experiments that measured the viability of spheroids with *NUAK1* knocked down were completed by Parima Saxena. Western blots confirming *NUAK1* knockdown were completed by Parima. Experiments measuring the doubling time of cells treated with WZ4003 were completed by Parima.

Experiments that measured viability and doubling time of *NUAK1*KO spheroids and spheroids overexpressing *NUAK1* were completed by Olga Collins.

Tritiated thymidine incorporation assay was performed in collaboration with Pirunthan Perampalam and Dr. Fred Dick.

Dr. Trevor Shepherd wrote the method sections describing the generation of *NUAK1*KO and *NUAK1* overexpressing cells. Parima Saxena wrote the method sections for experiments she completed, including the phostagTM western blot, spheroid viability assay, and tritiated thymidine incorporation assay. Dr. Karen Colwill wrote the method sections describing Multiplexed Inhibitor Bead (MIB) Chromatography, Mass Spectrometry Analysis, and Mass Spectrometry Data Analysis.

Acknowledgments

First, I am sincerely thankful to my supervisor, Dr. Trevor Shepherd, for his support, encouragement, and guidance throughout my master's program. I would also like to thank Dr. Gabriel DiMatta for providing valuable insight into my project and for allowing me to use cells from the repository of patient ascites-derived cell lines. I would also like to acknowledge my advisory committee, Dr. Paul Walton, Dr. Silvia Penuela, and Dr. Chris Pin for all of their guidance during my master's degree. Finally, I would like to thank all members of the Translational Ovarian Cancer Research Unit, including Adrian, Olga, Judith, Bart, and Jeremi for helping me learn lab techniques, providing technical assistance, and creating an enjoyable lab environment.

Table of Contents

Abstract	ii
Co-Authorship Statement.....	iii
Acknowledgments	iv
Table of Contents	v
List of Figures	vii
List of Supplementary Figures	viii
List of Supplementary Tables	ix
List of Abbreviations	x
Chapter 1.....	1
1 Introduction	1
1.1 Ovarian cancer epidemiology, clinical presentation, and diagnosis	1
1.2 Treatment for advanced-stage ovarian cancer	2
1.3 High-grade serous ovarian cancer.....	3
1.4 Ovarian cancer metastasis and experimental model system.....	4
1.5 Ovarian cancer spheroid formation.....	8
1.6 The role of LKB1 in ovarian cancer metastasis.....	9
1.7 NUAK1: Structure and Regulation	13
1.8 The role of NUAK1 in tumor progression	16
1.9 Research goal, hypothesis, and objectives	20
1.10 References	21
Chapter 2.....	30
2 A novel role for the LKB1 target NUAK1 in promoting ovarian cancer spheroid formation through regulation of fibronectin deposition.....	30
2.1 Introduction	30
2.2 Materials and Methods.....	33
2.2.1 Antibodies and Reagents	33
2.2.2 Cell culture and treatments	33
2.2.3 Generation of OVCAR8 STK11-KO and OVCAR8 NUAK1-KO Cells..	34
2.2.4 Generation of HEYA8 and OVCAR3 <i>NUAK1</i> overexpressing cells.....	35
2.2.5 Immunoblot analysis	35
2.2.6 Phostag™ Western Blot	36
2.2.7 Immunofluorescence	37
2.2.8 Quantitative RT-PCR	37
2.2.9 Tandem Ubiquitin Binding Entities (TUBEs)	37
2.2.10 Determination of Doubling Time	38
2.2.11 IncuCyte Zoom Live Cell Analysis System to image spheroid morphology in real-time	39
2.2.12 Phase contrast images of spheroids	39
2.2.13 Spheroid viability assay	39
2.2.14 Timed adhesion assay	39
2.2.15 Small-interfering RNA Transfection	40
2.2.16 Tritiated Thymidine Incorporation Assay.....	40
2.2.17 Multiplexed Inhibitor Bead (MIB) Chromatography	41
2.2.18 Mass Spectrometry Analysis.....	42
2.2.19 Mass Spectrometry Data Analysis	42
2.2.20 Transcriptome analysis and GSEA.....	44

2.2.21 Statistical analysis	44
2.3 Results	45
2.3.1 NUAK1 expression is regulated by the master stress kinase LKB1 in ovarian cancer spheroids and xenograft tumors	45
2.3.2 NUAK1 expression is differentially expressed in spheroids and this is mediated by the <i>ubiquitin</i> -proteasome system and lysosomal degradation	48
2.3.3 NUAK1 controls EOC cell adhesion and ovarian cancer spheroid integrity	54
2.3.4 NUAK1 promotes EOC spheroid formation through up-regulating fibronectin deposition	57
2.3.5 Transient and sustained loss of NUAK1 increases spheroid viability without altering proliferation of EOC cells	61
2.3.6 Loss of NUAK1 increases NF- κ B signaling in EOC spheroids	65
2.4 Discussion.....	67
2.5 References	73
2.6 Supplementary Figures.....	82
2.7 Supplementary Tables	84
Chapter 3.....	124
3 Discussion	124
3.1 Summary of Findings.....	124
3.2 LKB1-NUAK1 Signaling	125
3.3 Pro-metastatic function of NUAK1 in ovarian cancer.....	126
3.4 Loss of NUAK1 up-regulates NF- κ B signaling	129
3.5 Limitations of current study and future studies	130
3.6 Therapeutic implications	131
3.7 Overall Conclusion	132
3.8 References	132
Curriculum Vitae	141

List of Figures

Figure 1.1 Ovarian cancer peritoneal metastasis and experimental model system	7
Figure 1.2 Overview of LKB1 signaling	12
Figure 1.3 Structure and function of NUAK1	14
Figure 1.4 Roles for NUAK1 in tumor progression	17
Figure 2.1 NUAK1 expression is regulated by the master stress kinase LKB1 in ovarian cancer spheroids and xenograft tumors	47
Figure 2.2 NUAK1 expression is differentially expressed in spheroids and this is mediated by the ubiquitin-proteasome system and lysosomal degradation.....	51
Figure 2.3 NUAK1 regulates EOC cell adhesion and ovarian cancer spheroid integrity	56
Figure 2.4 NUAK1 promotes EOC spheroid formation through fibronectin deposition	59
Figure 2.5 Transient and sustained loss of NUAK1 increases spheroid viability without altering proliferation of EOC cells	64
Figure 2.6 Loss of NUAK1 increases NF- κ B signaling in EOC spheroids.....	67

List of Supplementary Figures

Figure S 2.1 Tandem ubiquitin binding entities (TUBEs) to detect ubiquitinated-NUAK1 in EOC cells and spheroids.....	82
Figure S 2.2 Validation experiments for KRAS signaling signature. (A) KRAS Signaling enrichment plot is presented.	83

List of Supplementary Tables

Table S 2.1 Primer sequences for qPCR.....	84
Table S 2.2 Differentially expressed genes from MIB/MS analysis completed using OVCAR8 parental and OVCAR8 STK11-KO adherent cells	85
Table S 2.3 Differentially expressed genes from MIB/MS analysis completed using OVCAR8 parental and OVCAR8 STK11-KO spheroids.....	89
Table S 2.4 Differentially expressed genes from the Affymetrix Clariom S array using OVCAR8 parental and OVCAR8 NUAK1-KO spheroids	95
Table S 2.5 Signatures from the GSEA Hallmark database that were enriched in the OVCAR8 parental spheroids compared to NUAK1-KO spheroids.....	103
Table S 2.6 Signatures from the Curated Canonical database that were enriched in the OVCAR8 parental spheroids compared to NUAK1-KO spheroids	104
Table S 2.7 Core enriched gene set from REACTOME_INTEGRIN_CELL_SURFACE_INTERACTION signature	120
Table S 2.8 Core enriched genes from HALLMARK_TNFA_SIGNALING_VIA_NF-κB	121

List of Abbreviations

Abbreviation	Term
AMPK	AMP-activated protein kinase
ARK	AMPK related kinase
BRSK	Brain specific serine-threonine kinase
CDK	Cyclin dependent kinase
CQ	Chloroquine
DMSO	Dimethyl sulfoxide
dNTP	Deoxyribose nucleoside triphosphate
EDTA	Ethylenediaminetetraacetic acid
EOC	Epithelial ovarian cancer
EMT	Epithelial-to-mesenchymal transition
FN	Fibronectin
F11R	F11 Receptor
GFP	Green fluorescent protein
HGSOC	High-grade serous ovarian cancer
ITGB5	Integrin Subunit Beta 5
ITGB8	Integrin Subunit Beta 8
KO	Knockout
LKB1	Liver kinase B1
L1CAM	L1 Cell Adhesion Molecule
MARK	Microtubule affinity regulatory kinase
Adh	Adherent culture
MLC2	Myosin light chain 2
MMP	Matrix metalloproteinase
MYPT1	Myosin phosphatase targeting subunit 1
NT	No treatment
NUAK1	Nua kinase 1
PBS	Phosphate-buffered saline
PLK1	Polo-like kinase 1
PMSF	Phenylmethane sulfonyl fluoride
PP1	Protein phosphatase 1
PVDF	Polyvinylidene fluoride
RIPA	Radioimmunoprecipitation assay
STIC	Serous tubal intraepithelial carcinoma
SIK	Salt inducible kinase
SNRK	Sucrose nonfermenting 1 (SNF-1) related kinase
SDS	Sodium dodecyl sulfate
TBST	Tris-buffered saline tween
THBS1	Thrombospondin 1
Sph	Spheroid culture
ULA	Ultra-low attachment
WT	Wild-type

Chapter 1

1 Introduction

1.1 Ovarian cancer epidemiology, clinical presentation, and diagnosis

Epithelial ovarian cancer (EOC) is the most lethal gynecologic malignancy in the developed world and is characterized by early and rapid metastasis (Lheureux, Gourley, Vergote, & Oza, 2019). Most women are diagnosed with advanced-stage disease with a 5-year survival rate of 29% (Siegel, Miller, & Jemal, 2019). The standard treatment plan for patients with late-stage ovarian cancer is maximal surgical cytoreduction with adjuvant chemotherapy of carboplatin and paclitaxel (Lheureux et al., 2019). However, with the current standard of care, the majority of patients will eventually have disease recurrence and resistance to chemotherapy (Bowtell et al., 2015b).

A diagnosis of EOC at an advanced-stage is common because patients are often asymptomatic until the cancer has metastasized (Lheureux et al., 2019). When symptoms present they are not-specific and include abdominal fullness, abnormal vaginal bleeding, gastrointestinal and urinary symptoms (Roett & Evans, 2009). A physician's initial investigation will involve performing a pelvic and rectovaginal examination to check for an ovarian mass, measuring serum levels of CA125, and completing a transvaginal ultrasonography (American College of Obstetricians and Gynecologists., 2002). CA125 is raised in 90 percent of patients with advanced-stage disease yet only 50 percent of patients in the early stage of the disease have elevated levels of CA125 (American College of Obstetricians and Gynecologists., 2002). Moreover, a transvaginal ultrasound is associated with false-positive results and often detects ovarian masses that have already metastasized (Karst & Drapkin, 2009). Therefore, new strategies are required to diagnose EOC in the early stages.

To stage EOC, the chest, abdomen, and pelvic regions are imaged with a CT and MRI, but surgery is required to adequately stage the disease (Lheureux et al., 2019). In stage I, EOC is localized to the ovaries (Bast, Hennessy, & Mills, 2009). If the cancer has

metastasized within the pelvic region, it is stage II. Once the cancer has spread to the abdominal region it is stage III; and distant metastasis beyond the abdomen into areas, such as the liver parenchyma, lung, and brain, is considered stage IV. In addition to staging EOC, the pathology of the tumor tissues is assessed because EOC is a heterogeneous disease with multiple histological subtypes (Lheureux et al., 2019). The four EOC histotypes include serous, endometriod, mucinous, and clear cell (Bast et al., 2009)

1.2 Treatment for advanced-stage ovarian cancer

The standard first-line treatment plan for patients with advanced-stage ovarian cancer is primary surgical cytoreduction with the goal of no residual tumor burden (Goff, 2012; Lheureux et al., 2019). Debulking surgery is the most important prognostic factor for survival. Surgery is then followed by chemotherapy of paclitaxel and carboplatin. Neoadjuvant chemotherapy is an option for patients with preexisting medical comorbidities or when tumors cannot be completely resected (Coleman, Monk, Sood, & Herzog, 2013). Carboplatin and paclitaxel are administered intravenously every 3 weeks for 6 cycles (Lheureux et al., 2019). Carboplatin forms crosslinks in the deoxyribonucleic acid (DNA), inhibiting replication and transcription in proliferating tumor cells (Martin, Hamilton, & Schilder, 2008). On the other hand, paclitaxel is a microtubule-stabilizing drug that leads to mitotic arrest (Weaver, 2014) . To reduce the risk for disease recurrence, maintenance therapies of anti-angiogenic therapies, including Bevacizumab, and PARP inhibitors (PARPi), such as Olaparib, can be given. PARPi are given to patients with defective homologous recombination (HR) particularly with germ line mutations in BRCA1 or BRCA2 (Lheureux et al., 2019). Mechanistically, inhibition of PARP prevents the repair of single-stranded breaks (Banerjee, Kaye, & Ashworth, 2010). In tumors absent of HR genes which repair double stranded breaks, the addition of PARPi leads to a loss of DNA repair mechanisms due to synthetic lethality and cell death.

If cancer progresses during first-line chemotherapy, patients have refractory disease and prognosis is very poor (Lheureux et al., 2019). Moreover, even after first-line treatment, more than 75% of patients will have disease recurrence. Platinum-sensitive

recurrent ovarian cancer is defined as a disease free interval of at least 6 months (Matulonis, 2018). These patients have the option for a secondary debulking surgery, a platinum doublet with 6-8 cycles of carboplatin and paclitaxel, and maintenance therapy. In the case of platinum-resistant recurrent ovarian cancer, cancer recurs after an interval of less than 6 months. Many different non-platinum-containing chemotherapeutic agents can be selected, including paclitaxel alone, with the addition of bevacizumab can be implemented; however platinum-resistant recurrent patients tend to have a very low responses to these treatments.

HGSOC is a highly genetically unstable disease; thus, during treatment, tumor cells can rapidly evolve, leading to chemoresistance (Lheureux et al., 2019). In addition to this issue of temporal tumor heterogeneity, spatial heterogeneity can occur within a tumor which makes treating this disease with a single therapeutic agent challenging. To address the complexity of HGSOC, combination therapy targeting DNA repair mechanisms, the cell cycle, and novel critical metastatic pathways will be necessary.

1.3 High-grade serous ovarian cancer

High-grade serous ovarian cancer (HGSOC) is the most common diagnosed histological subtype, representing 75 % of all cases of EOC (Lheureux et al., 2019). This subtype progresses rapidly, is typically diagnosed at an advanced-stage, and represents the majority of ovarian cancer-related deaths (Bowtell et al., 2015a; Goff, 2012). It is now widely regarded that the primary site of origin for HGSOC is the secretory epithelial cells of the distal fallopian tube (Bowtell et al., 2015a; Labidi-Galy et al., 2017; Lheureux et al., 2019). Cells undergo malignant transformation with mutations occurring in the *TP53* gene to form serous tubal intraepithelial carcinoma (STIC) lesions which then spread to the ovary. In some cases of HGSOC, ovarian cancer can arise without fallopian tube involvement and instead from precursor cells on the ovary (Bowtell et al., 2015a).

HGSOC appears heterogeneous with papillary, glandular, solid, and necrotic regions (Lheureux et al., 2019). Cancer cells have large and atypical nuclei. This subtype is characterized by mutations in *TP53* and to a lesser extent mutations in *NFI*, *BRCA1*, *BRCA2*, *RBI*, and *CDK12* genes. Oncogenic mutations in HGSOC are infrequent.

HGSOC has genome instability with widespread DNA copy number gains and losses being common. The prevalence of DNA alterations can make this cancer susceptible to acquiring chemoresistance. Furthermore, DNA repair mechanisms involving mutations in HR genes, such *BRCA1* or *BRCA2*, are deficient in 50% of HGSOC (Matulonis, 2018).

1.4 Ovarian cancer metastasis and experimental model system

In EOC metastasis, cancer cells shed from the primary ovarian tumor and spread into the peritoneal cavity (Sodek, Murphy, Brown, & Ringuette, 2012). Ascites fluid commonly accumulates in the peritoneal cavity of patients with advanced-stage disease and disease recurrence (Al Habyan, Kalos, Szymborski, & McCaffrey, 2018; Sodek et al., 2012). This build-up of ascites fluid results from cancer cells impairing lymphatic drainage and secreting vascular endothelial growth factor (VEGF) which enhances vascular permeability. The ascites microenvironment consists of diverse cell types, including ovarian cancer cells, fibroblasts, immune cells, and endothelial cells (Cho, Howell, & Colvin, 2015). It also contains acellular components, such as extracellular matrix (ECM) proteins, matrix metalloproteinases (MMP), growth factors, and cytokines (Ahmed & Stenvvers, 2013). The tumor microenvironment regulates cancer survival and invasion (Cho et al., 2015). For instance, cancer-associated fibroblasts (CAFs) interact with ovarian cancer cells to promote their invasiveness (Schauer et al., 2015). The release of *interleukin 1 β* (IL-1β) from ovarian cancer cells communicates to CAFs to down-regulate levels of the tumor suppressor p53. The diminished levels of p53 enhances the transcriptional activation of the *NF-κB* promoter, leading to the release of interleukins that feedback on ovarian cancer cells to promote their invasiveness.

Upon release from the primary tumor, cancer cells will form into multi-cellular structures known as spheroids to evade anoikis, a form of apoptosis due to loss of cell detachment (Figure 1.1A) (Al Habyan et al., 2018; Sodek et al., 2012). Eventually spheroids will adhere to the mesothelium and submesothelium of the peritoneum or omentum and continue to invade at secondary sites (Figure 1.1A) (Lengyel et al., 2014; Sodek et al.,

2012). The phenotypic heterogeneity of the primary tumor is often retained in spheroids and at sites of peritoneal metastases (Al Habyan et al., 2018).

Spheroids are heterogeneous structures with a necrotic core, a middle layer of quiescent cells, and a peripheral layer of actively proliferating cells (Weiswald, Bellet, & Dangles-Marie, 2015). The ascites microenvironment is hypoxic and devoid of glucose due to insufficient vascularization, and so spheroids adopt unique survival mechanisms (Figure 1.1A) (Emmings et al., 2019). Our group has shown that spheroids exhibit decreased cell proliferation and are arrested in the cell cycle at G0/G1 (Correa et al., 2014). However, they can reverse their dormant phenotype and enhance proliferation upon reattachment by reactivating AKT signaling. Spheroids also up-regulate autophagy, a system that degrades large and damaged proteins (Correa, Valdes, Shepherd, & DiMattia, 2015; Lilienbaum, 2013; Lu et al., 2008; Wang et al., 2018). Autophagy serves as a survival mechanism in response to stress from nutrient deprivation and hypoxia in the ascites microenvironment by recycling cellular components and nutrients.

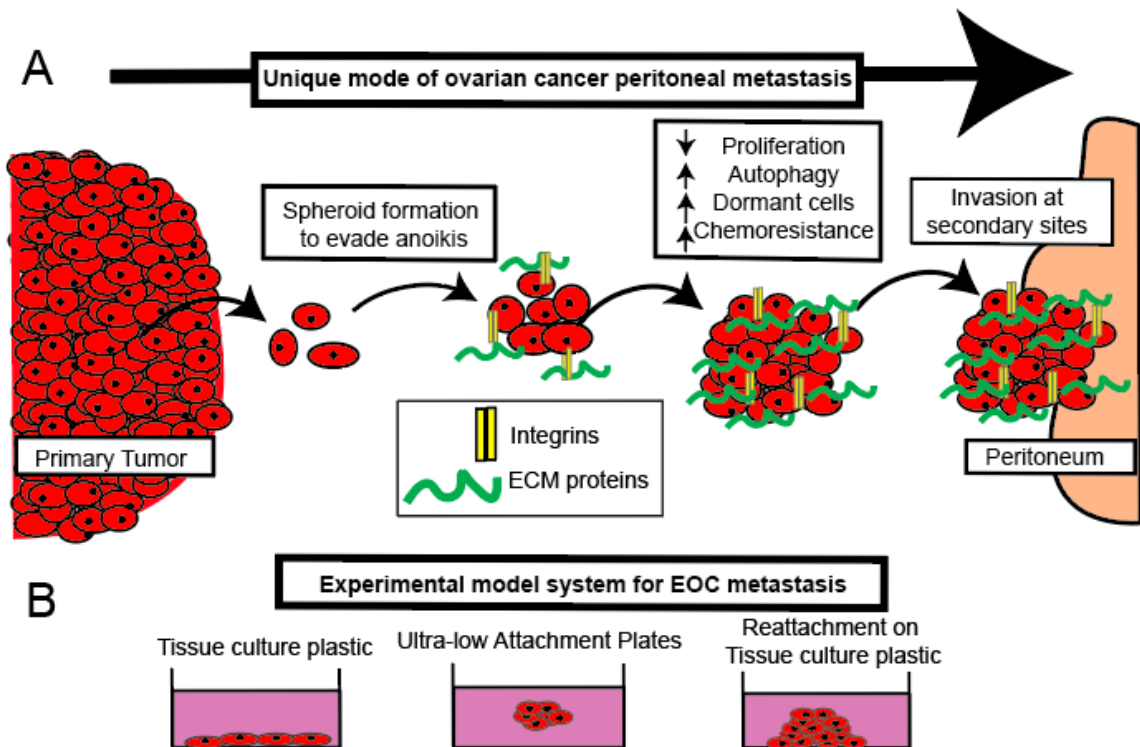


Figure 1.1 Ovarian cancer peritoneal metastasis and experimental model system. (A) Malignant cells shed from the primary ovarian tumor and aggregate into spheroids in the peritoneal cavity to evade anoikis. In this hypoxic and nutrient-poor microenvironment, spheroids adopt unique survival mechanisms. The interaction between integrins and ECM proteins are critical for spheroid formation. These multi-cellular aggregates can seed on secondary sites, such as the peritoneum, to form new tumor nodules. (B) Metastasis can be modelled *in vitro* by seeding cells on ultra-low attachment plates to facilitate spheroid formation and reattaching spheroids on tissue culture plastic.

Prior studies have provided evidence that targeting the ovarian cancer spheroid could be an effective therapeutic strategy because it is the primary mediator of peritoneal metastasis (Lengyel et al., 2014; Sodek et al., 2012). In addition, EOC cells that have a greater disposition to form compact spheroids have enhanced invasive properties (Sodek, Ringuette, & Brown, 2009). EOC spheroids can also develop resistance to paclitaxel and cisplatin in contrast to cells grown as a monolayer (Pease, Brewer, & Tirnauer, 2012). In fact, dissociation of spheroids can reestablish sensitivity to chemotherapeutic agents. This resistance to chemotherapy in spheroids can arise from inhibition of apoptosis or quiescent cells that can regrow after actively dividing peripheral cells die (Desoize & Jardillier, 2000).

To model EOC metastasis *in vitro*, cells can be grown on ultra-low attachment plates (ULA) to facilitate spheroid formation (Figure 1.1B) (Sant & Johnston, 2017). Due to the hydrophilic and neutral coating of the ULA plates, cells grow in suspension and form aggregates. To mimic the process of spheroids seeding on secondary surfaces, spheroids can then be transferred to regular tissue culture plastic (Figure 1.1B) (Shepherd, Thériault, Campbell, & Nachtigal, 2007). In this system, both established cell lines and patient-derived ascites cell lines can be used. To derive primary cells, ascites fluid is taken from patients during paracentesis (Shepherd et al., 2007). Spheroids are found in this ascites fluid and can be transferred to tissue culture plastic to grow as adherent cells. These patient-derived ascites cells can be grown in ULA dishes to directly maintain them in culture.

1.5 Ovarian cancer spheroid formation

Cell-cell attachments mediate the formation of spheroids through cadherins and indirectly through extracellular matrix (ECM) proteins (Sodek et al., 2012). Cadherins are transmembrane proteins that have homophilic interactions with other cadherin receptors (Lin, Chou, Chien, & Chang, 2006). Integrins are the primary adhesion receptor that anchors the ECM to the intracellular cytoskeleton (Johansson, Svineng, Wennerberg, Armulik, & Lohikangas, 1997). These heterodimeric receptors are comprised of alpha and β subunits. The compaction of spheroids occurs when integrins and cadherins signal to the actin cytoskeleton to induce contraction through actomyosin-mediated forces (Schiller & Fässler, 2013; Sodek et al., 2012). In ovarian cancer, the interaction between α5β1 integrins and fibronectin has been shown to be critical for the formation and cohesiveness of spheroids (Figure 1.1A) (Casey et al., 2001).

Fibronectin is an ECM protein that can exist in multiple forms due to alternate splicing (Pankov & Yamada, 2002). It has a soluble globular form in the plasma (pFN) and an insoluble fibrillar form in the ECM. While pFN is secreted by hepatocytes, ECM fibronectin is derived predominately from fibroblasts and a fraction from the plasma (White & Muro, 2011). EOC cells have also been shown to produce their own fibronectin matrix (Iwanicki et al., 2016). This glycoprotein is comprised of three types of different repeating units: type I, II, and III repeats (White & Muro, 2011). Fibronectin is a ligand for multiple integrins, however the canonical receptor is the α5β1 integrin. A tripeptide Arg-Gly-Asp (*RGD*) sequence in fibronectin interacts with the α5β1 integrin. Beyond its role in ovarian cancer spheroid formation, there have been multiple studies that have suggested a key role for fibronectin in ovarian cancer tumor progression. Elevated fibronectin expression has been correlated with increased tumor stage and decreased overall survival in ovarian cancer patients (Franke, Von Georgi, Zygmunt, & Münstedt, 2003). Furthermore, the loss of fibronectin in the omentum reduced ovarian cancer cell adhesion, invasion, and tumor metastasis in mouse models (Kenny et al., 2014). In addition to being found in the ECM of metastatic sites, fibronectin also accumulates in

the ascites fluid of patients with advanced-stage ovarian cancer (Linke, Babic, & Gossner, 1988).

Besides fibronectin and $\alpha 5\beta 1$ integrin supporting the integrity of ovarian cancer spheroids, L1 Cell Adhesion Molecule (L1CAM) can also promote spheroid formation (Doberstein et al., 2018). Intriguingly, L1CAM controls fibronectin and $\alpha 5\beta 1$ integrin expression in ovarian cancer spheroids. L1CAM is a transmembrane glycoprotein that can have homophilic interactions with other L1CAM molecules or heterophilic interactions with different adhesion molecules, such as integrins (Altevogt, Doberstein, & Fogel, 2016). The presence of type III fibronectin repeats in L1CAM suggest that it also interacts with fibronectin. L1CAM can exist as a soluble form after cleavage of its extracellular domain at the cell surface membrane (Beer, Oleszewski, Gutwein, Geiger, & Altevogt, 1999). Tumor-promoting roles for L1CAM have been demonstrated based on its ability to control cell invasion, metastasis, and chemoresistance (Altevogt et al., 2016). In ovarian cancer, high levels of membranous L1CAM was associated with greater lymphogenous metastases and a greater risk for incomplete debulking surgery (Bondong et al., 2012). Elevated levels of soluble L1CAM in the ascites fluid was correlated with lower overall survival and greater chemoresistance.

1.6 The role of LKB1 in ovarian cancer metastasis

The elucidation of key molecular pathways in ovarian cancer spheroids would allow for improved understanding of metastatic processes and would aid in the identification of novel therapeutic targets. Our group previously showed that the master stress kinase liver kinase B1 (LKB1) is critical for ovarian cancer metastasis (Buensuceso, Valdes, Figueredo, DiMatta, & Shepherd, 2018; Peart et al., 2015). LKB1 is commonly expressed in established ovarian cancer cell lines and patient-derived ascites cell lines (Peart et al., 2015). Furthermore, LKB1 expression increases in ovarian cancer spheroids compared to monolayer cells. The sustained loss of LKB1 decreased anchorage-independent growth of EOC cells and decreased the viability of ovarian cancer spheroids (Buensuceso et al., 2018). In a xenograft model of peritoneal metastasis, LKB1 loss extended survival and decreased tumor burden.

LKB1 (encoded by the *STK11* gene) is a serine-threonine kinase which becomes activated in a complex with the accessory proteins STRAD and MO25 (Hardie & Alessi, 2013). There is a large body of literature implicating *STK11* as a tumor suppressor. Inactivating mutations of *STK11* lead to Peutz-Jeghers syndrome, a condition characterized by gastrointestinal polyps and an increased risk for cancer (Beggs et al., 2010; Hemminki et al., 1998). *STK11* is commonly deleted in non-small cell lung cancer and somatic nonsense mutations occur in melanoma (Gill et al., 2011; Guldberg et al., 1999). While the gene for LKB1 is frequently described as a tumor suppressor, there is evidence indicating the role of LKB1 is more complex because it can have tumor-promoting functions under certain contexts. LKB1 overexpression is associated with worse survival outcomes in hepatocellular carcinoma (Lee et al., 2015). It is also important for tumor growth by promoting cell survival under energetic stress in non-small cell lung cancer (Shackelford et al., 2013). Indeed, as described above, our group showed that LKB1 is required for ovarian cancer metastasis (Buensuceso et al., 2018; Peart et al., 2015).

The canonical downstream target of LKB1 is AMP-activated protein kinase (AMPK), a regulator of metabolic stress (Shackelford & Shaw, 2009). LKB1 activates AMPK by a phosphorylation modification at threonine 172 on the activation loop of its catalytic domain (Bright, Thornton, & Carling, 2009). Under conditions of nutrient deprivation, LKB1-AMPK signaling is induced and decreases cell growth by inhibiting mammalian target of rapamycin complex 1 (mTORC1). Surprisingly, our group showed that LKB1's pro-metastatic role in ovarian cancer occurs through AMPK-independent signaling; in spheroids lacking LKB1, phospho-AMPK levels were maintained (Buensuceso et al., 2018). While AMPK is the commonly studied substrate of LKB1, LKB1 is known as a master upstream kinase due to its ability to also regulate 12 other AMPK-related kinases (ARKs): BRSK1, BRSK2, NUAK1, NUAK2, QIK, QSK, SIK, MARK1, MARK2, MARK3, MARK4, and SNRK (Figure 1.2). The ARKs show sequence similarity to AMPK at the N-terminal serine-threonine kinase domain (Lizcano et al., 2004). Similar to AMPK, ARK phosphorylation at an equivalent threonine residue of the T-loop by

LKB1 leads to their activation . It has been reported that the ARKs have roles in cell polarity, motility, and cancer metastasis (Bright et al., 2009). It would be important to elucidate the key downstream substrate that is allowing LKB1 to elicit its pro-metastatic functions in ovarian cancer. In this report, we use a multiplexed kinase inhibitor bead-mass spectrometry (MIB/MS) analysis with spheroids lacking LKB1 to identify NUAK1 as a top substrate candidate in EOC cells.

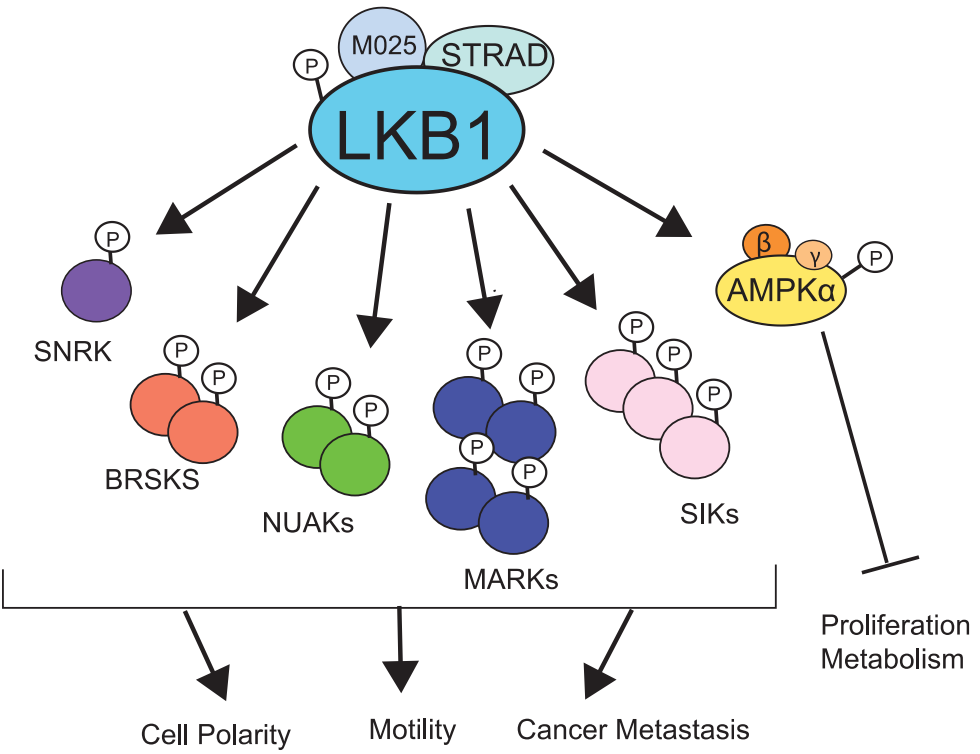


Figure 1.2 Overview of LKB1 signaling

Under conditions of cell stress, LKB1 complexes with the STRAD and MO25 and initiates signalling to AMPK to decrease cell growth and metabolism. LKB1 can also control 12 AMPK related kinases (ARKs). This downstream signaling serves to regulate cell polarity, cell motility, and cancer metastasis.

1.7 NUAK1: Structure and Regulation

The gene for NUAK1 is found on chromosome 12 at position q23.3 (Scherer et al., 2006). This gene encodes a 660 amino acid protein and has an estimated molecular weight of 74 kDa (Nagase et al., 2000; Suzuki et al., 2003). NUAK1 is a member of the ARK family with 47% and 46 % sequence homology to AMPK- α 1 and AMPK- α 2, respectively. Its most closely related ARK family member is NUAK2 with a sequence homology of 55%. NUAK1 has a serine-threonine kinase domain near the N-terminus which is conserved amongst AMPK and the ARKs (Lizcano et al., 2004) (Figure 1.3). NUAK1 is predominately localized to the cytoplasm but can also be found in the nucleus (Hou et al., 2011).

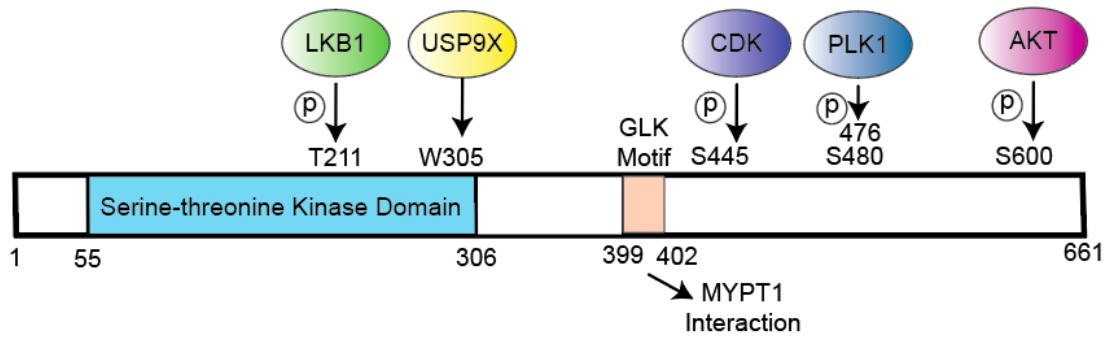


Figure 1.3 Structure and function of NUAK1

NUAK1 has sites for LKB1 phosphorylation and activation. USP9X binds to NUAK1 at W305 and can remove the polyubiquitin chain. NUAK1 is phosphorylated and activated by AKT at S600 near the c-terminus. NUAK1 can also be phosphorylated by cyclin-dependent kinases (CDKs) at serine 445 which creates a docking site for polo kinase (PLK) to then phosphorylate NUAK1 at ser 476 and serine 480

Several upstream kinases have been shown to activate NUAK1. When LKB1 complexes with its accessory proteins STRAD and MO25, it can phosphorylate and activate NUAK1 at the conserved residue threonine 211 on the T-loop of its catalytic domain (Figure 1.3) (Lizcano et al., 2004). Furthermore, NUAK1 ubiquitination was shown to control its activation by LKB1 (Al-Hakim et al., 2008). NUAK1 can be ubiquitinated by unique Lys29 and or Lys33 linkages which do not signal for degradation. Instead these modifications block phosphorylation and activation by LKB1. The deubiquitinase Ubiquitin Specific Peptidase 9 X-Linked (USP9X) can bind to NUAK1 at W305 and cleave the polyubiquitin modification, allowing for LKB1 phosphorylation and activation (Figure 1.3).

Besides regulation by LKB1, NUAK1 can also be controlled by LKB1-independent mechanisms. In response to glucose starvation NUAK1 is phosphorylated and activated by AKT at its C-terminus (Figure 1.3) (Suzuki et al., 2003). Furthermore, in Myc-overexpressing tumors calcium-dependent activation of PKC can activate NUAK1 (Monteverde et al., 2018). NUAK1 can also be phosphorylated by cyclin-dependent kinases (CDKs) at Serine 445 which creates a docking site for polo kinase (PLK) to then phosphorylate NUAK1 at Serines 476 and 480 (Figure 1.3) (Banerjee et al., 2014). These phosphorylation modifications promote binding to the SCF^{BTrcp} E3 ligase which leads to ubiquitination and degradation of NUAK1.

1.8 The role of NUAK1 in tumor progression

Prior studies have shown that NUAK1 can function in tumor progression through regulating apoptosis, the cell cycle, invasion and metastasis, and metabolic stress in tumors. NUAK1 blocked cell death induced by glucose starvation or various death-receptor stimuli in human hepatoma cells (Suzuki et al., 2003). The authors proposed that NUAK1 suppresses apoptosis by inhibiting the activation of caspase 8 (Figure 1.4). Specifically, this inhibition occurs through NUAK1 resisting the degradation of FLICE (FADD-like IL-1 β -converting enzyme)-inhibitory protein (FLIP), which blocks the activation of caspase 8. Moreover, NUAK1 allows colorectal cancer cells to resist cell death stimulated by the Fas ligand (FasL) binding to the cell death receptor Fas (Suzuki et al., 2004). NUAK1 blocked apoptosis in these cells by phosphorylating caspase 6, leading to its inactivation (Figure 1.4). Caspase 6 is known to cleave the anti-apoptotic protein FLIP. Thus, inactivation of caspase 6 by NUAK1 sustained levels of FLIP and also inhibited caspase 8 in the apoptotic pathway.

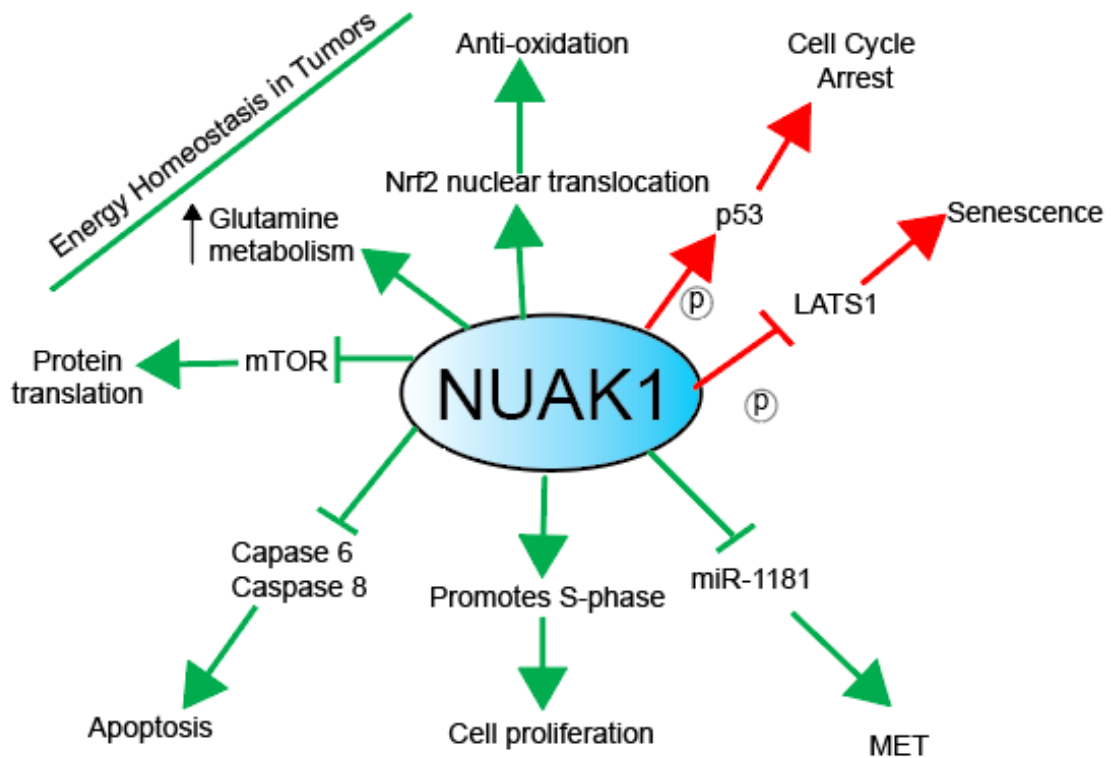


Figure 1.4 Roles for NUAK1 in tumor progression.

Roles for NUAK1 in tumor progression. NUAK1 can function in tumor progression (green arrows) through regulating apoptosis, the cell cycle, EMT, invasion, and metabolic stress in tumors. NUAK1 can also have tumor-suppressive functions (red arrows) because it can induce cell cycle arrest and senescence.

Along with promoting cell survival through inhibiting apoptosis, NUAK1 can regulate the cell cycle. NUAK1 can induce the S-phase and cell proliferation (Banerjee et al., 2014). During the cell cycle, PLK and NUAK1 are reciprocally regulated. In S-phase there are high levels of NUAK1 and low levels of PLK. In G2/M phase, PLK levels are high while NUAK1 levels are low. The mechanism proposed for this reciprocal control is PLK phosphorylates NUAK1 which results in its binding to SCF^{BTrcp}, ubiquitination and subsequent degradation.

NUAK1 has also been shown to promote EMT in multiple cancer cell types (Ye, Chen, & Chen, 2018; Zhang, Li, Li, & Wang, 2015). In ovarian cancer cells, NUAK1 overexpression increased levels of mesenchymal markers, decreased levels of epithelial markers, and increased the invasion and migratory properties of cells (Zhang et al., 2015). Mechanistically, NUAK1 was shown to inhibit miR-1181 which promotes mesenchymal–epithelial transition (MET). miR-1181 also degrades homeobox protein Hox-A10 (HOXA10) which stimulates EMT. Altogether, this study suggested that a NUAK1/miR-1181/HOXA10 signaling axis can induce EMT in ovarian cancer cells (Figure 1.4). Moreover, another study showed that siRNA-mediated knockdown of *NUAK1* decreased the migration of ovarian cancer monolayer cells in a wound healing assay (Phippen et al., 2016). Furthermore, in hepatocellular carcinoma cells NUAK1 has been shown to promote EMT (Ye et al., 2018). In line with a role for NUAK1 in EMT, a prior study has implicated NUAK1 in promoting tumor invasion and metastasis (Kusakai, Suzuki, Ogura, Kaminishi, & Esumi, 2004). SCID mice injected with pancreatic cancer cells overexpressing NUAK1 had metastasis to the liver and in some cases to peritoneal sites whereas metastasis was not detectable in control mice. A previous report investigated the molecular basis by which NUAK1 can facilitate cell detachment (Zagórska et al., 2010). Using HEK293 and MEF cells, the authors showed that NUAK1 can induce cell detachment through regulation of the myosin phosphatase complex. In response to LKB1 activation, NUAK1 interacts with the myosin phosphatase targeting-1 (MYPT1)-protein phosphatase-1B (PP1B) complex (Figure 1.2). NUAK1 phosphorylates MYPT1, which facilitates its binding to 14-3-3, an adaptor protein that inhibits MYPT1

phosphatase activity. This leads to enhanced myosin light chain-2 (MLC2) phosphorylation and subsequent cell detachment.

Several studies have shown that NUAK1 can also promote cancer survival through sustaining metabolic homeostasis (Liu et al., 2012; Port et al., 2018). It was shown that NUAK1 is needed to maintain energy homeostasis in tumors overexpressing *myc* (Liu et al., 2012). Myc is known to enhance activation of anabolic pathways and cell proliferation in tumors. To manage energetic stress, NUAK1 inhibits mTORC1 to suppress protein translation (Figure 1.4). It also sustains glutamine metabolism in these Myc-driven cancers by maintaining efficient mitochondrial respiration (Figure 1.4). Loss of NUAK1 led to a reduction of ATP levels and decreased proliferation in hepatocellular and pancreatic carcinoma cells. Moreover, in colorectal tumors NUAK1 can provide protection from oxidative stress by promoting nuclear translocation of the anti-oxidant regulator, Nrf2 (Port et al., 2018). In response to oxidative stress, NUAK1 inhibits PP1B which has been shown to block AKT-mediated suppression of GSK3B, a negative regulator of Nrf2 (Figure 1.4). Furthermore, loss of NUAK1 reduced colorectal tumor burden in mouse models, and the addition of an exogenous anti-oxidant reversed this phenotype.

A tumor-promoting role for NUAK1 is further strengthened by studies showing that elevated levels of NUAK1 correlates with poor prognosis in multiple cancer types (Phippen et al., 2016; Port et al., 2018). It was shown that high NUAK1 transcript levels in serous ovarian cancer patients was associated with lower progression free survival and lower overall survival (Phippen et al., 2016). There was also an increased risk for diagnosis at an advanced stage and residual disease after cytoreductive surgery. Similarly, high levels of NUAK1 was associated with advanced stage colorectal cancer and reduced overall survival in patients (Port et al., 2018).

While there is a large body of literature suggesting that NUAK1 serves to promote cancer survival, several studies have suggested that NUAK1 can have tumor suppressive roles under certain contexts. Using lung adenocarcinoma and melanoma cells, it was shown

that in response to LKB1 activation NUAK1 phosphorylates p53, leading to cell cycle arrest (Figure 1.4) (Hou et al., 2011). More specifically, LKB1, NUAK1, and p53 form a complex in the nucleus and bind to the *CDKN1A* promoter to induce expression of genes for arrest at the G1/S checkpoint. Beyond regulating the cell cycle, a potential tumor suppressive role for NUAK1 was shown by its ability to induce senescence and gross aneuploidies (Figure 1.4) (Humbert et al., 2010). Using normal human diploid fibroblast cells, NUAK1 was shown to phosphorylate Large Tumor Suppressor Drosophila Homolog 1 (LATS1) leading to its degradation and an induction of senescence. NUAK1 was also shown to elevate aberrant DNA content in breast epithelial cells which led to increased apoptosis.

1.9 Research goal, hypothesis, and objectives

To further elucidate LKB1 signalling in ovarian cancer, I sought to investigate the regulation and function of one of its AMPK-related kinase targets, NUAK1. I hypothesized that the LKB1 target NUAK1 promotes ovarian cancer metastasis by regulating EOC cell adhesion and spheroid integrity. To test this hypothesis, I examined whether LKB1 regulates the expression of NUAK1 in ovarian cancer spheroids and tumor samples. I used a metastatic model to investigate the regulatory mechanisms controlling NUAK1 levels between monolayer cells and quiescent spheroids. I next examined whether NUAK1 functions in EOC cell adhesion and spheroid integrity. To discover the molecular basis for NUAK1-dependent adhesion phenotype, I completed transcriptome analysis using Clariom S microarrays with RNA isolated from OVCAR8 parental and OVCAR8 *NUAK1*-KO cells and spheroids followed by pathway analysis using Gene Set Enrichment Analysis and subsequently validated fibronectin as a key target. This project has allowed me to elucidate the LKB1-NUAK1 pathway as critically functional in ovarian cancer metastasis.

1.10 References

- Ahmed, N., & Stenvers, K. L. (2013). Getting to Know Ovarian Cancer Ascites: Opportunities for Targeted Therapy-Based Translational Research. *Frontiers in Oncology*. <https://doi.org/10.3389/fonc.2013.00256>
- Al-Hakim, A. K., Zagorska, A., Chapman, L., Deak, M., Peggie, M., & Alessi, D. R. (2008). Control of AMPK-related kinases by USP9X and atypical Lys 29 /Lys 33 - linked polyubiquitin chains . *Biochemical Journal*. <https://doi.org/10.1042/bj20080067>
- Al Habyan, S., Kalos, C., Szymborski, J., & McCaffrey, L. (2018). Multicellular detachment generates metastatic spheroids during intra-abdominal dissemination in epithelial ovarian cancer. *Oncogene*. <https://doi.org/10.1038/s41388-018-0317-x>
- Altevogt, P., Doberstein, K., & Fogel, M. (2016). L1CAM in human cancer. *International Journal of Cancer*. <https://doi.org/10.1002/ijc.29658>
- American College of Obstetricians and Gynecologists. (2002). ACOG Committee Opinion Number 280: The Role of the Generalist Obstetrician-Gynecologist in the Early Detection of Ovarian Cancer. *Obstetrics & Gynecology*, 100(6), 1413–1416. [https://doi.org/10.1016/s0029-7844\(02\)02630-3](https://doi.org/10.1016/s0029-7844(02)02630-3)
- Banerjee, Sourav, Zagórska, A., Deak, M., Campbell, D. G., Prescott, A. R., & Alessi, D. R. (2014). Interplay between Polo kinase, LKB1-activated NUAK1 kinase, PP1 β MYPT1 phosphatase complex and the SCF β TrCP E3 ubiquitin ligase . *Biochemical Journal*. <https://doi.org/10.1042/bj20140408>
- Banerjee, Susana, Kaye, S. B., & Ashworth, A. (2010). Making the best of PARP inhibitors in ovarian cancer. *Nature Reviews Clinical Oncology*. <https://doi.org/10.1038/nrclinonc.2010.116>
- Bast, R. C., Hennessy, B., & Mills, G. B. (2009). The biology of ovarian cancer: New opportunities for translation. *Nature Reviews Cancer*. <https://doi.org/10.1038/nrc2644>
- Beer, S., Oleszewski, M., Gutwein, P., Geiger, C., & Altevogt, P. (1999). Metalloproteinase-mediated release of the ectodomain of L1 adhesion molecule. *Journal of Cell Science*.
- Beggs, A. D., Latchford, A. R., Vasen, H. F. A., Moslein, G., Alonso, A., Aretz, S., ... Hodgson, S. V. (2010). Peutz - Jeghers syndrome: A systematic review and recommendations for management. *Gut*. <https://doi.org/10.1136/gut.2009.198499>
- Bell, D., Berchuck, A., Birrer, M., Chien, J., Cramer, D. W., Dao, F., ... Thomson, E. (2011). Integrated genomic analyses of ovarian carcinoma. *Nature*. <https://doi.org/10.1038/nature10166>
- Bondong, S., Kiefel, H., Hielscher, T., Zeimet, A. G., Zeillinger, R., Pils, D., ... Altevogt, P. (2012). Prognostic significance of L1CAM in ovarian cancer and its role in constitutive NF- κ B activation. *Annals of Oncology*.

- <https://doi.org/10.1093/annonc/mdr568>
- Bonnans, C., Chou, J., & Werb, Z. (2014). Remodelling the extracellular matrix in development and disease. *Nature Reviews. Molecular Cell Biology*.
<https://doi.org/10.1038/nrm3904>
- Bowtell, D. D., Böhm, S., Ahmed, A. A., Aspuria, P.-J., Bast, R. C., Beral, V., ...
 Balkwill, F. R. (2015a). Rethinking ovarian cancer II: reducing mortality from high-grade serous ovarian cancer. *Nature Reviews. Cancer*.
<https://doi.org/10.1038/nrc4019>
- Bright, N. J., Thornton, C., & Carling, D. (2009). The regulation and function of mammalian AMPK-related kinases. *Acta Physiologica*.
<https://doi.org/10.1111/j.1748-1716.2009.01971.x>
- Buensuceso, A., Valdes, Y. R., Figueredo, R., DiMattia, G. E., & Shepherd, T. G. (2018). *Abstract A12: The metabolic stress mediator LKB1 is required for ovarian cancer metastasis*. <https://doi.org/10.1158/1557-3265.ovca17-a12>
- Casey, R. C., Burleson, K. M., Skubitz, K. M., Pambuccian, S. E., Oegema, T. R., Ruff, L. E., & Skubitz, A. P. N. (2001). $\beta 1$ -integrins regulate the formation and adhesion of ovarian carcinoma multicellular spheroids. *American Journal of Pathology*.
[https://doi.org/10.1016/S0002-9440\(10\)63058-1](https://doi.org/10.1016/S0002-9440(10)63058-1)
- Cho, A., Howell, V. M., & Colvin, E. K. (2015). The Extracellular Matrix in Epithelial Ovarian Cancer – A Piece of a Puzzle. *Frontiers in Oncology*.
<https://doi.org/10.3389/fonc.2015.00245>
- Coleman, R. L., Monk, B. J., Sood, A. K., & Herzog, T. J. (2013). Latest research and treatment of advanced-stage epithelial ovarian cancer. *Nature Reviews Clinical Oncology*. <https://doi.org/10.1038/nrclinonc.2013.5>
- Correa, R. J. M., Valdes, Y. R., Peart, T. M., Fazio, E. N., Bertrand, M., McGee, J., ... Shepherd, T. G. (2014). Combination of AKT inhibition with autophagy blockade effectively reduces ascites-derived ovarian cancer cell viability. *Carcinogenesis*.
<https://doi.org/10.1093/carcin/bgu049>
- Correa, R. J. M., Valdes, Y. R., Shepherd, T. G., & DiMattia, G. E. (2015). Beclin-1 expression is retained in high-grade serous ovarian cancer yet is not essential for autophagy induction in vitro. *Journal of Ovarian Research*.
<https://doi.org/10.1186/s13048-015-0182-y>
- Desoize, B., & Jardillier, J. C. (2000). Multicellular resistance: A paradigm for clinical resistance? *Critical Reviews in Oncology/Hematology*.
[https://doi.org/10.1016/S1040-8428\(00\)00086-X](https://doi.org/10.1016/S1040-8428(00)00086-X)
- Doberstein, K., Spivak, R., Feng, Y., Stuckelberger, S., Mills, G. B., Devins, K. M., ... Affiliations. (2018). Fallopian tube precursor lesions of serous ovarian carcinoma require L1CAM for dissemination and metastasis. *BioRxiv Preprint First*.
<https://doi.org/10.1101/270785>
- Domcke, S., Sinha, R., Levine, D. A., Sander, C., & Schultz, N. (2013). Evaluating cell

- lines as tumour models by comparison of genomic profiles. *Nature Communications*. <https://doi.org/10.1038/ncomms3126>
- Duncan, J. S., Whittle, M. C., Nakamura, K., Abell, A. N., Midland, A. A., Zawistowski, J. S., ... Johnson, G. L. (2012). Dynamic reprogramming of the kinase in response to targeted MEK inhibition in triple-negative breast cancer. *Cell*. <https://doi.org/10.1016/j.cell.2012.02.053>
- Emmerich, C. H., & Cohen, P. (2015). Optimising methods for the preservation, capture and identification of ubiquitin chains and ubiquitylated proteins by immunoblotting. *Biochemical and Biophysical Research Communications*. <https://doi.org/10.1016/j.bbrc.2015.08.109>
- Emmings, E., Mullany, S., Chang, Z., Landen, C. N., Linder, S., & Bazzaro, M. (2019). Targeting Mitochondria for Treatment of Chemoresistant Ovarian Cancer. *International Journal of Molecular Sciences*, 20(1). <https://doi.org/10.3390/ijms20010229>
- Espín-Palazón, R., & Traver, D. (2016). The NF-κB family: Key players during embryonic development and HSC emergence. *Experimental Hematology*. <https://doi.org/10.1016/j.exphem.2016.03.010>
- F Ann Ran, Patrick D Hsu, Jason Wright, Vineeta Agarwala, D. A. S. & F. Z. (2013). Genome engineering using crispr-cas9 system. *Nature Protocols*, 8(11), 2281–2308. https://doi.org/10.1007/978-1-4939-1862-1_10
- Franke, F. E., Von Georgi, R., Zygmunt, M., & Münstedt, K. (2003). Association between Fibronectin Expression and Prognosis in Ovarian Carcinoma. *Anticancer Research*.
- Gill, R. K., Yang, S. H., Meerzaman, D., Mechanic, L. E., Bowman, E. D., Jeon, H. S., ... Jen, J. (2011). Frequent homozygous deletion of the LKB1/STK11 gene in non-small cell lung cancer. *Oncogene*. <https://doi.org/10.1038/onc.2011.98>
- Goff, B. A. (2012). Advanced ovarian cancer: What should be the standard of care? *Journal of Gynecologic Oncology*. <https://doi.org/10.3802/jgo.2013.24.1.83>
- Gopal, S., Veracini, L., Grall, D., Butori, C., Schaub, S., Audebert, S., ... Van Obberghen-Schilling, E. (2017). Fibronectin-guided migration of carcinoma collectives. *Nature Communications*. <https://doi.org/10.1038/ncomms14105>
- Guldberg, P., Straten, P. T., Ahrenkiel, V., Seremet, T., Kirkin, A. F., & Zeuthen, J. (1999). Somatic mutation of the Peutz-Jeghers syndrome gene, LKB1/STK11, in malignant melanoma. *Oncogene*. <https://doi.org/10.1038/sj.onc.1202486>
- Hardie, D. G., & Alessi, D. R. (2013). LKB1 and AMPK and the cancer-metabolism link - ten years after. *BMC Biology*. <https://doi.org/10.1186/1741-7007-11-36>
- Hemminki, a, Avizienyte, E., Roth, S., Loukola, A., Aaltonen, L. a, Järvinen, H., & de la Chapelle, A. (1998). A serine/threonine kinase gene defective in Peutz-Jeghers syndrome. *Nature*, 391(January), 184–187. Retrieved from <http://www.ncbi.nlm.nih.gov/pubmed/11524750>

- Hernandez, L., Kim, M. K., Lyle, L. T., Bunch, K. P., House, C. D., Ning, F., ... Annunziata, C. M. (2016). Characterization of ovarian cancer cell lines as in vivo models for preclinical studies. *Gynecologic Oncology*. <https://doi.org/10.1016/j.ygyno.2016.05.028>
- Hew, K. E., Miller, P. C., El-Ashry, D., Sun, J., Besser, A. H., Ince, T. A., ... Simpkins, F. (2016). MAPK activation predicts poor outcome and the MEK inhibitor, selumetinib, reverses antiestrogen resistance in ER-positive high-grade serous ovarian cancer. *Clinical Cancer Research*. <https://doi.org/10.1158/1078-0432.CCR-15-0534>
- Hou, X., Liu, J.-E., Liu, W., Liu, C.-Y., Liu, Z.-Y., & Sun, Z.-Y. (2011). A new role of NUAK1: directly phosphorylating p53 and regulating cell proliferation. *Oncogene*. <https://doi.org/10.1038/onc.2011.19>
- House, C. D., Jordan, E., Hernandez, L., Ozaki, M., James, J. M., Kim, M., ... Annunziata, C. M. (2017). NF κ B promotes ovarian tumorigenesis via classical pathways that support proliferative cancer cells and alternative pathways that support ALDH β cancer stem-like cells. *Cancer Research*. <https://doi.org/10.1158/0008-5472.CAN-17-0366>
- Humbert, N., Navaratnam, N., Augert, A., Da Costa, M., Martien, S., Wang, J., ... Bernard, D. (2010). Regulation of ploidy and senescence by the AMPK-related kinase NUAK1. *EMBO Journal*. <https://doi.org/10.1038/emboj.2009.342>
- Iwanicki, M. P., Chen, H.-Y., Iavarone, C., Zervantonakis, I. K., Muranen, T., Novak, M., ... Brugge, J. S. (2016). Mutant p53 regulates ovarian cancer transformed phenotypes through autocrine matrix deposition. *JCI Insight*. <https://doi.org/10.1172/jci.insight.86829>
- Johansson, S., Svineng, G., Wennerberg, K., Armulik, A., & Lohikangas, L. (1997). Fibronectin-integrin interactions. *Frontiers in Bioscience : A Journal and Virtual Library*.
- Karst, A. M., & Drapkin, R. (2009). Ovarian Cancer Pathogenesis: A Model in Evolution. *Journal of Oncology*. <https://doi.org/10.1155/2010/932371>
- Kedves, A. T., Gleim, S., Liang, X., Bonal, D. M., Sigoillot, F., Harbinski, F., ... Forrester, W. C. (2017). Recurrent ubiquitin B silencing in gynecological cancers establishes dependence on ubiquitin C. *Journal of Clinical Investigation*. <https://doi.org/10.1172/JCI92914>
- Keller, A., Nesvizhskii, A. I., Kolker, E., & Aebersold, R. (2002). Empirical statistical model to estimate the accuracy of peptide identifications made by MS/MS and database search. *Analytical Chemistry*, 74(20), 5383–5392. <https://doi.org/10.1021/ac025747h>
- Kenny, H. A., Chiang, C. Y., White, E. A., Schryver, E. M., Habis, M., Romero, I. L., ... Lengyel, E. (2014). Mesothelial cells promote early Ovarian cancer metastasis through fibronectin secretion. *Journal of Clinical Investigation*. <https://doi.org/10.1172/JCI74778>

- Kusakai, G., Suzuki, A., Ogura, T., Kaminishi, M., & Esumi, H. (2004). Strong association of ARK5 with tumor invasion and metastasis. *Journal of Experimental & Clinical Cancer Research : CR.*
- Labidi-Galy, S. I., Papp, E., Hallberg, D., Niknafs, N., Adleff, V., Noe, M., ... Velculescu, V. E. (2017). High grade serous ovarian carcinomas originate in the fallopian tube. *Nature Communications.* <https://doi.org/10.1038/s41467-017-00962-1>
- Lee, J., Rhee, M. H., Kim, E., & Cho, J. Y. (2012). BAY 11-7082 is a broad-spectrum inhibitor with anti-inflammatory activity against multiple targets. *Mediators of Inflammation.* <https://doi.org/10.1155/2012/416036>
- Lee, S. W., Li, C. F., Jin, G., Cai, Z., Han, F., Chan, C. H., ... Lin, H. K. (2015). Skp2-Dependent Ubiquitination and Activation of LKB1 Is Essential for Cancer Cell Survival under Energy Stress. *Molecular Cell.* <https://doi.org/10.1016/j.molcel.2015.01.015>
- Lengyel, E., Burdette, J. E., Kenny, H. A., Matei, D., Pilrose, J., Haluska, P., ... Stack, M. S. (2014). Epithelial ovarian cancer experimental models. *Oncogene.* <https://doi.org/10.1038/onc.2013.321>
- Leung, B. M., Lesher-Perez, S. C., Matsuoka, T., Moraes, C., & Takayama, S. (2015). Media additives to promote spheroid circularity and compactness in hanging drop platform. *Biomaterials Science.* <https://doi.org/10.1039/c4bm00319e>
- Lheureux, S., Gourley, C., Vergote, I., & Oza, A. M. (2019). Epithelial ovarian cancer. *The Lancet.* [https://doi.org/10.1016/S0140-6736\(18\)32552-2](https://doi.org/10.1016/S0140-6736(18)32552-2)
- Lilienbaum, A. (2013). Relationship between the proteasomal system and autophagy. *International Journal of Biochemistry and Molecular Biology.*
- Lin, R. Z., Chou, L. F., Chien, C. C. M., & Chang, H. Y. (2006). Dynamic analysis of hepatoma spheroid formation: Roles of E-cadherin and β 1-integrin. *Cell and Tissue Research.* <https://doi.org/10.1007/s00441-005-0148-2>
- Linke, R., Babic, R., & Gossner, W. (1988). Fibrin-Fibronectin Compounds in Human Ovarian Tumor Ascites and Their Possible Relation to the Tumor Stroma. *Cancer Research.*
- Liu, F., Yang, X., Geng, M., & Huang, M. (2018). Targeting ERK, an Achilles' Heel of the MAPK pathway, in cancer therapy. *Acta Pharmaceutica Sinica B.* <https://doi.org/10.1016/j.apsb.2018.01.008>
- Liu, G., Zhang, J., Larsen, B., Stark, C., Breitkreutz, A., Lin, Z.-Y., ... Gingras, A.-C. (2010). ProHits: integrated software for mass spectrometry-based interaction proteomics. *Nature Biotechnology.* <https://doi.org/10.1038/nbt1010-1015>
- Liu, L., Ulbrich, J., Müller, J., Wüstefeld, T., Aeberhard, L., Kress, T. R., ... Murphy, D. J. (2012). Deregulated MYC expression induces dependence upon AMPK-related kinase 5. *Nature.* <https://doi.org/10.1038/nature10927>
- Livak, K. J., & Schmittgen, T. D. (2001). Analysis of relative gene expression data using

- real-time quantitative PCR and the 2- $\Delta\Delta$ CT method. *Methods*. <https://doi.org/10.1006/meth.2001.1262>
- Lizcano, J. M., Göransson, O., Toth, R., Deak, M., Morrice, N. A., Boudeau, J., ... Alessi, D. R. (2004). LKB1 is a master kinase that activates 13 kinases of the AMPK subfamily, including MARK/PAR-1. *EMBO Journal*. <https://doi.org/10.1038/sj.emboj.7600110>
- Lu, Z., Luo, R. Z., Lu, Y., Zhang, X., Yu, Q., Khare, S., ... Bast, R. C. (2008). The tumor suppressor gene ARHI regulates autophagy and tumor dormancy in human ovarian cancer cells. *Journal of Clinical Investigation*. <https://doi.org/10.1172/JCI35512>
- MacDonald, J., Ramos-Valdes, Y., Perampalam, P., Litovchick, L., DiMatta, G. E., & Dick, F. A. (2016). A Systematic Analysis of Negative Growth Control Implicates the DREAM Complex in Cancer Cell Dormancy. *Molecular Cancer Research*. <https://doi.org/10.1158/1541-7786.mcr-16-0323-t>
- Manning, G., Whyte, D. B., Martinez, R., Hunter, T., & Sudarsanam, S. (2002). The protein kinase complement of the human genome. *Science*. <https://doi.org/10.1126/science.1075762>
- Martin, L. P., Hamilton, T. C., & Schilder, R. J. (2008). Platinum resistance: The role of DNA repair pathways. *Clinical Cancer Research*. <https://doi.org/10.1158/1078-0432.CCR-07-2238>
- Matulonis, U. A. (2018). Management of newly diagnosed or recurrent ovarian cancer. *Clinical Advances in Hematology and Oncology*.
- Monteverde, T., Tait-Mulder, J., Hedley, A., Knight, J. R., Sansom, O. J., & Murphy, D. J. (2018). Calcium signalling links MYC to NUAK1. *Oncogene*. <https://doi.org/10.1038/onc.2017.394>
- Nagase, T., Kikuno, R., Hattori, A., Kondo, Y., Okumura, K., & Ohara, O. (2000). Prediction of the coding sequences of unidentified human genes. XIX. The complete sequences of 100 new cDNA clones from brain which code for large proteins in vitro. *DNA Research : An International Journal for Rapid Publication of Reports on Genes and Genomes*. <https://doi.org/10.1093/dnare/7.6.347>
- Nakamura, K., Nakayama, K., Ishikawa, N., Ishikawa, M., Sultana, R., Kiyono, T., & Kyo, S. (2017). Reconstitution of high-grade serous ovarian carcinoma from primary fallopian tube secretory epithelial cells. *Oncotarget*, 9(16), 12609–12619. <https://doi.org/10.18632/oncotarget.23035>
- Nesvizhskii, A. I., Keller, A., Kolker, E., & Aebersold, R. (2003). A statistical model for identifying proteins by tandem mass spectrometry. *Analytical Chemistry*.
- Pankov, R., & Yamada, K. M. (2002). Fibronectin at a glance. *Journal of Cell Science*, 115(Pt 20), 3861–3863. <https://doi.org/10.1242/jcs.00059>
- Peart, T., Valdes, Y. R., Correa, R. J. M., Fazio, E., Bertrand, M., McGee, J., ... Shepherd, T. G. (2015). Intact LKB1 activity is required for survival of dormant ovarian cancer spheroids. *Oncotarget*. <https://doi.org/10.18632/oncotarget.4211>

- Pease, J. C., Brewer, M., & Tirnauer, J. S. (2012). Spontaneous spheroid budding from monolayers: a potential contribution to ovarian cancer dissemination. *Biology Open*. <https://doi.org/10.1242/bio.2012653>
- Perumal, D., Leshchenko, V. V., Kuo, P. Y., Jiang, Z., Divakar, S. K. A., Jay Cho, H., ... Parekh, S. (2016). Dual targeting of CDK4 and ARK5 using a novel kinase inhibitor ON123300 exerts potent anticancer activity against multiple myeloma. *Cancer Research*. <https://doi.org/10.1158/0008-5472.CAN-15-2934>
- Phippen, N. T., Bateman, N. W., Wang, G., Conrads, K. A., Ao, W., Teng, P., ... Conrads, T. P. (2016). NUAK1 (ARK5) Is Associated with Poor Prognosis in Ovarian Cancer. *Frontiers in Oncology*. <https://doi.org/10.3389/fonc.2016.00213>
- Port, J., Muthalagu, N., Raja, M., Ceteci, F., Monteverde, T., Kruspig, B., ... Murphy, D. J. (2018). Colorectal tumors require NUAK1 for protection from oxidative stress. *Cancer Discovery*. <https://doi.org/10.1158/2159-8290.CD-17-0533>
- Roett, M. A., & Evans, P. (2009). Ovarian cancer: An overview. *American Family Physician*.
- Sabio, G., & Davis, R. J. (2014). TNF and MAP kinase signalling pathways. *Seminars in Immunology*. <https://doi.org/10.1016/j.smim.2014.02.009>
- Sant, S., & Johnston, P. A. (2017). The production of 3D tumor spheroids for cancer drug discovery. *Drug Discovery Today: Technologies*. <https://doi.org/10.1016/j.ddtec.2017.03.002>
- Schauer, I. G., Zhang, J., Xing, Z., Guo, X., Mercado-Uribe, I., Sood, A. K., ... Liu, J. (2015). Interleukin-1 β Promotes Ovarian Tumorigenesis through a p53/NF- κ B-Mediated Inflammatory Response in Stromal Fibroblasts. *Neoplasia*, 15(4), 409-IN18. <https://doi.org/10.1593/neo.121228>
- Scherer, S. E., Muzny, D. M., Buhay, C. J., Chen, R., Cree, A., Ding, Y., ... Gibbs, R. A. (2006). The finished DNA sequence of human chromosome 12. *Nature*. <https://doi.org/10.1038/nature04569>
- Schiller, H. B., & Fässler, R. (2013). Mechanosensitivity and compositional dynamics of cell-matrix adhesions. *EMBO Reports*. <https://doi.org/10.1038/embor.2013.49>
- Shackelford, D. B., Abt, E., Gerken, L., Vasquez, D. S., Seki, A., Leblanc, M., ... Shaw, R. J. (2013). LKB1 Inactivation Dictates Therapeutic Response of Non-Small Cell Lung Cancer to the Metabolism Drug Phenformin. *Cancer Cell*. <https://doi.org/10.1016/j.ccr.2012.12.008>
- Shackelford, D. B., & Shaw, R. J. (2009). The LKB1-AMPK pathway: Metabolism and growth control in tumour suppression. *Nature Reviews Cancer*. <https://doi.org/10.1038/nrc2676>
- Shepherd, T. G., Thériault, B. L., Campbell, E. J., & Nachtigal, M. W. (2007). Primary culture of ovarian surface epithelial cells and ascites-derived ovarian cancer cells from patients. *Nature Protocols*. <https://doi.org/10.1038/nprot.2006.328>
- Shteynberg, D., Deutsch, E. W., Lam, H., Eng, J. K., Sun, Z., Tasman, N., ...

- Nesvizhskii, A. I. (2011). iProphet: Multi-level Integrative Analysis of Shotgun Proteomic Data Improves Peptide and Protein Identification Rates and Error Estimates. *Molecular & Cellular Proteomics*.
<https://doi.org/10.1074/mcp.M111.007690>
- Siegel, R. L., Miller, K. D., & Jemal, A. (2019). Cancer statistics, 2019. *CA: A Cancer Journal for Clinicians*. <https://doi.org/10.3322/caac.21551>
- Sodek, K. L., Murphy, K. J., Brown, T. J., & Ringuette, M. J. (2012). Cell-cell and cell-matrix dynamics in intraperitoneal cancer metastasis. *Cancer and Metastasis Reviews*. <https://doi.org/10.1007/s10555-012-9351-2>
- Sodek, K. L., Ringuette, M. J., & Brown, T. J. (2009). Compact spheroid formation by ovarian cancer cells is associated with contractile behavior and an invasive phenotype. *International Journal of Cancer*. <https://doi.org/10.1002/ijc.24188>
- Stuhlmiller, T. J., Miller, S. M., Zawistowski, J. S., Nakamura, K., Beltran, A. S., Duncan, J. S., ... Johnson, G. L. (2015). Inhibition of lapatinib-induced kinase reprogramming in ERBB2-positive breast cancer by targeting BET family bromodomains. *Cell Reports*. <https://doi.org/10.1016/j.celrep.2015.03.037>
- Subramanian, A., Tamayo, P., Mootha, V. K., Mukherjee, S., Ebert, B. L., Gillette, M. A., ... Mesirov, J. P. (2005). Gene set enrichment analysis: a knowledge-based approach for interpreting genome-wide expression profiles. *Proceedings of the National Academy of Sciences of the United States of America*.
<https://doi.org/10.1073/pnas.0506580102>
- Suzuki, A., Lu, J., Kusakai, G. -i., Kishimoto, A., Ogura, T., & Esumi, H. (2004). ARK5 Is a Tumor Invasion-Associated Factor Downstream of Akt Signaling. *Molecular and Cellular Biology*. <https://doi.org/10.1128/MCB.24.8.3526-3535.2004>
- Suzuki, Atsushi, Kusakai, G. I., Kishimoto, A., Lu, J., Ogura, T., Lavin, M. F., & Esumi, H. (2003). Identification of a novel protein kinase mediating Akt survival signaling to the ATM protein. *Journal of Biological Chemistry*.
<https://doi.org/10.1074/jbc.M206025200>
- Teo, G., Kim, S., Tsou, C. C., Collins, B., Gingras, A. C., Nesvizhskii, A. I., & Choi, H. (2015). MapDIA: Preprocessing and statistical analysis of quantitative proteomics data from data independent acquisition mass spectrometry. *Journal of Proteomics*, 129, 108–120. <https://doi.org/10.1016/j.jprot.2015.09.013>
- Tomida, J., Kitao, H., Kinoshita, E., & Takata, M. (2008). Detection of phosphorylation on large proteins by western blotting using Phos-tag containing gel. *Protocol Exchange*. <https://doi.org/10.1038/nprot.2008.232>
- Tsou, C. C., Avtonomov, D., Larsen, B., Tucholska, M., Choi, H., Gingras, A. C., & Nesvizhskii, A. I. (2015). DIA-Umpire: Comprehensive computational framework for data-independent acquisition proteomics. *Nature Methods*.
<https://doi.org/10.1038/nmeth.3255>
- Venstrom, K., & Reichardt, L. (1995). Beta 8 integrins mediate interactions of chick sensory neurons with laminin-1, collagen IV, and fibronectin. *Molecular Biology of*

- the Cell. <https://doi.org/10.1091/mbc.6.4.419>
- Viatour, P., Merville, M. P., Bours, V., & Chariot, A. (2005). Phosphorylation of NF-kB and IkkB proteins: Implications in cancer and inflammation. *Trends in Biochemical Sciences*. <https://doi.org/10.1016/j.tibs.2004.11.009>
- Wang, Q., Bu, S., Xin, D., Li, B., Wang, L., & Lai, D. (2018). Autophagy Is Indispensable for the Self-Renewal and Quiescence of Ovarian Cancer Spheroid Cells with Stem Cell-Like Properties. *Oxidative Medicine and Cellular Longevity*. <https://doi.org/10.1155/2018/7010472>
- Ware, M. J., Colbert, K., Keshishian, V., Ho, J., Corr, S. J., Curley, S. A., & Godin, B. (2016). Generation of Homogenous Three-Dimensional Pancreatic Cancer Cell Spheroids Using an Improved Hanging Drop Technique. *Tissue Engineering Part C: Methods*. <https://doi.org/10.1089/ten.tec.2015.0280>
- Weaver, B. A. (2014). How Taxol/paclitaxel kills cancer cells. *Molecular Biology of the Cell*, 25(18), 2677–2681. <https://doi.org/10.1091/mbc.e14-04-0916>
- Weiswald, L. B., Bellet, D., & Dangles-Marie, V. (2015). Spherical Cancer Models in Tumor Biology. *Neoplasia (United States)*. <https://doi.org/10.1016/j.neo.2014.12.004>
- White, E. S., & Muro, A. F. (2011). Fibronectin splice variants: Understanding their multiple roles in health and disease using engineered mouse models. *IUBMB Life*. <https://doi.org/10.1002/iub.493>
- Ye, Z., Chen, X., & Chen, X. (2018). ARK5 promotes invasion and migration in hepatocellular carcinoma cells by regulating epithelial-mesenchymal transition. *Oncology Letters*, 15(2), 1511–1516. <https://doi.org/10.3892/ol.2017.7453>
- Zagórska, A., Deak, M., Campbell, D. G., Banerjee, S., Hirano, M., Aizawa, S., ... Alessi, D. R. (2010). New roles for the LKB1-NUAK pathway in controlling myosin phosphatase complexes and cell adhesion. *Science Signaling*. <https://doi.org/10.1126/scisignal.2000616>
- Zhang, H. Y., Li, J. H., Li, G., & Wang, S. R. (2015). Activation of ARK5/miR-1181/HOXA10 axis promotes epithelial-mesenchymal transition in ovarian cancer. *Oncology Reports*. <https://doi.org/10.3892/or.2015.4113>

Chapter 2

2 A novel role for the LKB1 target NUAK1 in promoting ovarian cancer spheroid formation through regulation of fibronectin deposition

2.1 Introduction

Ovarian cancer is the most lethal gynecologic malignancy and is characterized by early and rapid metastasis (Lheureux et al., 2019). Most women are diagnosed with advanced-stage disease with a 5- year survival rate of only 29% (Siegel et al., 2019). The standard treatment plan for patients with late-stage ovarian cancer is maximal surgical cytoreduction with adjuvant chemotherapy of carboplatin and paclitaxel (Lheureux et al., 2019). However, the majority of patients will eventually develop disease recurrence and resistance to chemotherapy (Bowtell et al., 2015b). Therefore, there is a need to develop novel therapeutic strategies to impede ovarian cancer metastasis.

In ovarian cancer metastasis, malignant cells shed from the primary ovarian tumor and spread into the peritoneal cavity (Sodek et al., 2012). Ascites commonly accumulates in the peritoneal cavity of patients with advanced-stage disease (Al Habyan et al., 2018; Sodek et al., 2012). In the ascites fluid, cancer cells will form multi-cellular structures known as spheroids to evade anoikis, a form of apoptosis due to loss of cell attachment. Eventually spheroids will adhere to the peritoneum to continue to invade at secondary sites (Al Habyan et al., 2018; Lengyel et al., 2014). In addition to playing a key role in efficient peritoneal metastasis, spheroids acquire resistance to chemotherapy due to the acquisition of cellular quiescence (Desoize & Jardillier, 2000; Pease et al., 2012). The formation of spheroids is controlled by several cell attachments through cadherins and indirectly through extracellular matrix (ECM) proteins and integrins (Sodek et al., 2012). In ovarian cancer, the interaction between the ECM protein fibronectin and the $\alpha 5\beta 1$ integrin is known to be critical for the formation of spheroids (Casey et al., 2001). Integrins are the primary adhesion receptor that anchors the ECM to the intracellular cytoskeleton (Pankov & Yamada, 2002). These heterodimeric receptors are comprised of alpha and β subunits. Fibronectin exists as a soluble form in the plasma and as an

insoluble fibrillar form in the ECM (Pankov & Yamada, 2002). Fibronectin is a ligand for multiple integrins, however its canonical receptor is the $\alpha 5\beta 1$ integrin. Multiple studies have indicated a key role for fibronectin in ovarian cancer tumor progression. Elevated fibronectin expression has been correlated with worsened tumor stage and decreased overall survival in ovarian cancer patients (Franke et al., 2003). In mouse models, the loss of fibronectin reduced ovarian cancer cell adhesion, invasion, and tumor metastasis (Kenny et al., 2014).

The elucidation of key intracellular signaling pathways in ovarian cancer spheroids would allow for improved understanding of metastatic processes and would aid in the identification of novel therapeutic targets. Our group previously showed that liver kinase B1 (LKB1) is critical for ovarian cancer metastasis (Buensuceso et al., 2018; Peart et al., 2015). LKB1 (encoded by the *STK11* gene) is a serine-threonine kinase that is frequently described as having tumor suppressive-like activity in other cancers (Gill et al., 2011; Guldberg et al., 1999). *STK11* inactivating mutations lead to Peutz-Jeghers syndrome, a condition characterized by gastrointestinal polyps and an increased risk for cancer (Beggs et al., 2010; Hemminki et al., 1998). However, we have shown that it has context-specific functions because in late-stage ovarian cancer LKB1 facilitates tumor progression (Buensuceso et al., 2018; Peart et al., 2015). LKB1 is commonly expressed in established ovarian cancer cell lines, patient-derived ascites cells, and tumor extracts (Buensuceso et al., 2018). The sustained loss of LKB1 decreased anchorage-independent growth of EOC cells and decreased the viability of ovarian cancer spheroids. In a xenograft model of peritoneal metastasis, LKB1 loss extended survival and decreased tumor burden.

The canonical downstream target of LKB1 is AMP-activated protein kinase (AMPK), a regulator of metabolic stress (Shackelford & Shaw, 2009). Interestingly, our group showed that LKB1's pro-metastatic role in ovarian cancer occurs through AMPK-independent signaling (Buensuceso et al., 2018; Peart et al., 2015). LKB1 is known as a master upstream kinase due to its ability to also regulate 12 other AMPK-related kinases (ARKs): BRSK1, BRSK2, NUAK1, NUAK2, QIK, QSK, SIK, MARK1, MARK2, MARK3, MARK4, and SNRK (Lizcano et al., 2004; Manning, Whyte, Martinez, Hunter, & Sudarsanam, 2002). It would be important to identify the key downstream substrate

that is allowing LKB1 to elicit its pro-metastatic function in ovarian cancer. In the study, we use a multiplex inhibitor bead-mass spectrometry analysis with cells and spheroids lacking LKB1 to show that NUAK1 is likely a key substrate enabling LKB1 to drive ovarian cancer metastasis.

NUAK1 is a serine-threonine kinase that can be phosphorylated by LKB1 at a *conserved threonine 211 residue on the T-loop of its catalytic domain* (Lizcano *et al.*, 2004). Prior studies have shown that NUAK1 has pro-tumorigenic functions. NUAK1 can promote cancer survival by inhibiting apoptosis and inducing the S-phase in the cell cycle. It can also protect tumors from oxidative stress by increasing nuclear translocation of the anti-oxidant regulator, Nrf2 (Port *et al.*, 2018). Previous work has also suggested that NUAK1 can play a role in cell adhesion (Zagórska *et al.*, 2010; Zhang *et al.*, 2015). In ovarian cancer cells, NUAK1 has been shown to increase epithelial–mesenchymal transition EMT. It can also stimulate cell detachment by regulating the myosin phosphatase complexes. A tumor-promoting role for NUAK1 is strengthened by studies showing that elevated levels of NUAK1 correlate with poor prognosis in several cancers, including ovarian cancer (Phippen *et al.*, 2016; Port *et al.*, 2018).

In this study, we aimed to elucidate how NUAK1 facilitates LKB1 pro-tumorigenic functions in ovarian cancer. We show that LKB1 regulates the phosphorylation and expression of NUAK1 in ovarian cancer. We present evidence that NUAK1 controls key steps of the metastatic cascade by regulating ovarian cancer cell adhesion and spheroid integrity. Mechanistically, NUAK1 regulates fibronectin along with a network of adhesion molecules to control spheroid formation. We have identified novel function for the LKB1 target NUAK1 in promoting efficient ovarian cancer metastasis. Therefore, strategies targeting the downstream target of this master upstream kinase may have therapeutic potential in advanced-stage ovarian cancer.

2.2 Materials and Methods

2.2.1 Antibodies and Reagents

Antibodies obtained against NUAK1(#4458S), LKB1 (#3050S), p-LKB1-Ser428 (#3482S), LC3B (#2775), p65 (#D14E12), p-p65- Ser536 (#3033S), MEK1/2 (#9122), p-MEK1/2-Ser217/221 (#9121), ERK1/2 (#9102), p-ERK1/2-Thr202/204 (#9101), JNK (#9252), p-JNK-Thr182/Tyr185 (#9251), and c-myc (#5605) were obtained from Cell Signaling Technology (Danvers, MA). Anti-Tubulin antibody (#T5168), Anti-Actin antibody (#A2066), anti-rabbit FITC secondary antibody (# F9887), HRP-conjugated antibodies against mouse IgG (NA931V) and rabbit IgG (NA934V), and 4', 6-diamidino-2-phenylindole were purchased from Sigma (St. Lewis, MO). Chloroquine (#C-6628), MG132 (#M8699), and methylcellulose (#M0512) were also obtained from Sigma. Anti-fibronectin (#ab2413) was purchased from Abcam (Cambridge, Ma). Antibody against L1CAM (#SIG-3911) was obtained from Biolegend (San Diego, CA). Anti-USP9X (A301-350A) was purchased from Bethyl Laboratories (Montgomery, TX). PR-619, control agarose beads, agarose-TUBE2, and anti-ubiquitin antibody (#VU101) were purchased from Lifesensors (Malvern, PA). Alexa Fluor phalloidin and plasma human fibronectin (#PHE0023) was obtained from Thermo Fisher Scientific (Waltham, MA). WZ400 (#5177) was purchased from Tocris Bioscience.

2.2.2 Cell culture and treatments

OVCAR8 (ATCC, Manassas, VA) and HEYA8 (ATCC) cells were cultured in RPMI-1640 (Wisent, St. Bruno, QC). OVCAR5 cells (ATCC) were cultured in DMEM-F12 (Life Technologies, Carlsbad, CA). Early passage ascites-derived cell lines (iOvCa147, iOvCa198, iOvCa247) were generated based on a protocol described by us previously and cultured in DMEM-F12 (Shepherd et al., 2007). The growth media was supplemented with 10% fetal bovine serum (Wisent) for all cell lines. Cells were grown in a humidified incubator at 37°C with 5% CO₂.

Adherent cells were maintained on tissue cultured-treated polystyrene (Sarstedt, Newton, NC). Spheroids were formed by maintaining cells on ultra-low attachment dishes

(Corning, NY) which have a hydrophilic and neutral coating to prevent cell attachment as described previously (Correa et al., 2014).

For specific experiments, day 3 adherent cells and spheroids were treated with DMSO or MG132 (10 µM) for 8 hours. Cells were also treated or untreated with chloroquine (25 µM) for 8 hours.

2.2.3 Generation of OVCAR8 STK11-KO and OVCAR8 NUAK1-KO Cells

The 20-nucleotide guide sequence targeting the *STK11* gene 5'-AGCTT GGCCC GCTTG CGGCG-3' was selected using CRISPR Design Tool (<http://tools.genome-engineering.org>). Complementary oligonucleotides 5'-CACCG AGCTT GGCCC GCTTG CGGCG-3' and 5'- AAACC GCCGC AAGCG GGCCA AGCTC-3' (Sigma-Genosys) were annealed and ligated into the BbsI-digested restriction endonuclease site of pSpCas9(BB)-2A-Puro plasmid (gift from Dr. F. Dick, Western University) to generate the pSpCas9-sgSTK11 plasmid (Ran et al., 2013). Cells were seeded at 200,000 cells/well into 6-well plates and transfected with 1 µg of pSpCas9-sgSTK11 plasmid using LipofectAMINE 2000 (Invitrogen) according to manufacturer's instructions. Media containing 1 µg/mL puromycin was replaced the following day, and cells were treated for one day. After growth recovery, cells were trypsinized, counted, and seeded into 96-well plates to perform limiting dilution subcloning of potential *STK11*-knockout cells. Single colonies were expanded for protein isolation and confirmation of *STK11* knockout by western blotting for LKB1. A minimum of five clones lacking LKB1 protein expression were positively identified and subsequently mixed in equal ratios to generate the *STK11*KO cell line populations.

A similar protocol was followed to create *NUAK1*-KO cells. The 20-nucleotide guide sequence targeting the *NUAK1* gene 5'-GTGGC GGGGG ACCGC CCCGA-3' was selected using CRISPR Design Tool (<http://tools.genome-engineering.org>). Complementary oligonucleotides 5'- CACCG TCG GGG CGG TCC CCC GCC AC -3' and 5'- CACCG GGG TCT CCT GCA GCT CGT AG -3' (Sigma-Genosys) were annealed and ligated into the BbsI-digested restriction endonuclease site of

pSpCas9(BB)-2A-Puro plasmid. The same protocol described above was used for transfection and selection of clones lacking NUAK1

2.2.4 Generation of HEYA8 and OVCAR3 *NUAK1* overexpressing cells

HeyA8 and OVCAR3 cells were transfected with pPHAGE C-TAP-NUAK1 ([HsCD00462473](#); Harvard PlasmID Database) using Lipofectamine 2000 (Invitrogen) according to manufacturer's instructions. Forty-eight hours post-transfection, 1ug/mL puromycin (Sigma) treatment was started until single colonies remained. Cells were re-plated into 10-cm dishes and selection was continued at 1ug/mL puromycin. Colonies were picked and expanded prior to screening for NUAK1 expression by western blot using lysates from parental cell lines for comparison. Empty vector control (EVC) cells were generated using the pPHAGE C-TAP plasmid for both cell lines and represent four pooled clones of each line subjected to the same puromycin selection process.

2.2.5 Immunoblot analysis

To obtain whole cell lysates from adherent culture, cells were collected after washing the plate with PBS and scraping cells in lysis buffer [50mM HEPES pH7.4, 150 mM NaCl, 10% glycerol, 1.5 mM MgCl₂, 1 mM EGTA, 1 mM sodium orthovanadate, 10 mM sodium pyrophosphate, 10 mM NaF, 1% Triton X-100, 1% sodium deoxycholate, 0.1% SDS, 1 mM PMSF, 1X protease inhibitor cocktail (Roche, Laval, QC), and 225mM β-glycerophosphate]. For spheroids, after centrifugation (2400 rpm for 5 minutes) the media was aspirated and the pellet was resuspended in PBS and then centrifuged. After removal of PBS, lysis buffer was added to the pellet. Protein was isolated and the protein concentration in the supernatant was measured with a Bradford assay (Bio-Rad Laboratories, Hercules, CA)

To isolate cytoplasmic and nuclear fractions, adherent cells and spheroids were washed in PBS, resuspended in a hypotonic lysis buffer (20 mM HEPES (pH 7.4), 1 mM EGTA, 1 mM EDTA and 1 mM DTT), and incubated on ice for 15 minutes. Spheroid lysates were passed through a 26G needle three times. After lysates were centrifuged, supernatant was collected for the cytoplasmic fraction. The nuclear pellet was washed three times with

wash buffer [10 nM HEPES (pH 7.4), 10 mM KCl, 0.1 mM EGTA and 0.1 mM EDTA]. The nuclear pellet was then resuspended in lysis buffer and clarified by centrifugation. Protein was isolated from tumor samples by homogenizing flash-frozen tissue in lysis buffer (50 mM HEPES pH7.4, 150 mM NaCl, 10% glycerol, 1.5 mM MgCl₂, 1 mM EGTA, 1 mM sodium orthovanadate, 10 mM sodium pyrophosphate, 10 mM NaF, 1% Triton X-100, 1% sodium deoxycholate, 0.1% SDS, 1 mM PMSF, 1X protease inhibitor cocktail). Solid tumor specimens had been collected from a xenotransplantation experiment described previously (Buensuceso et al., 2018).

For immunoblot analysis, 30-50ug of protein was resolved by SDS-PAGE using 6%, 8% or 12 % gels. Proteins were transferred at 100V for 1 hour to a PVDF membrane (Roche), blocked with 5% milk or 5% BSA diluted in TBST (10mM Tris-HCl, pH 8.0, 150mM NaCl and 0.1% Tween-20). Membranes were incubated with primary antibodies overnight at 4°C. To visualize immunoreactive bands, membranes were incubated for 1h with peroxidase-conjugated anti-rabbit or anti-mouse antibodies (1:10 000 in 5% BSA/TBST) and exposed to chemiluminescence reagent (Luminata Forte, Millipore, Temecula, CA). Images were captured using the ChemiDoc™ Imaging System (Bio-Rad) and bands were quantified using Image Lab 4.1 software.

2.2.6 Phostag™ Western Blot

PhostagTM lysis buffer was prepared similar to above, however EGTA, sodium pyrophosphate and β-glycerophosphate were excluded from preparation. PhostagTM gels were prepared using PhostagTM solution (Wako Chem, Richmond, VA) and 10mM MnCl₂, as 8% acrylamide gels, according to manufacturer's protocol. Electrophoresis was run for ~3 hours, after which gels were washed for 10 minutes with 1x transfer buffer with 1mM EDTA, followed by 10 minutes with 1x transfer buffer without EDTA. Wet transfer was run for 1 hour on PVDF membranes (Immobilon-P). Membranes were incubated in primary antibody for 2 days, and imaging was performed as described above.

2.2.7 Immunofluorescence

Spheroids were embedded in cryo-matrix (Thermo Fisher) and sectioned with Shandon cryostat microtome at 5 μ M. Cryosections were fixed (10% formalin solution), permeabilized (0.1% Triton X-100 in PBS), and blocked (5% BSA in 0.1% Triton X-100). After overnight incubation with Anti-fibronectin antibody (1:100; #ab2413), sections were washed with PBS and then incubated for 1 hour with anti-rabbit FITC secondary antibody (1:300; # F9887). For counterstaining, sections were incubated for 1h with Alexa Fluor phalloidin (1:1000) followed by incubation for 1 hour with 4', 6-diamidino-2-phenylindole (1:1000). Sections were mounted on coverslips with Vectashield (Vector Laboratories, Burlingame CA). Fluorescence images were captured using Olympus AX70 upright microscope and ImagePro image capture software.

2.2.8 Quantitative RT-PCR

Total RNA was isolated from adherent cells and spheroids using the RNeasy Mini Kit (Qiagen, Hilden, Germany). The concentration and purity of the RNA was determined with the ND-1000 spectrophotometer (NanoDrop Technologies, Wilmington, DE). Reverse transcription was performed using High Capacity cDNA Reverse Transcription Kit (*Applied Biosystems*, Foster City, CA). The resulting cDNA was used for qRT-PCR using Brilliant SYBR Green QPC1R Master Mix (Agilent Technologies/Stratagene, Mississauga, ON) and was run on the Quantstudios 3 (*Applied Biosystems*). Human-specific primer sequences (*Sigma*) are described in table 2.1. GAPDH was used as an internal control. Relative gene expression was quantified by calculating $2^{-\Delta\Delta Ct}$ (Livak & Schmittgen, 2001).

2.2.9 Tandem Ubiquitin Binding Entities (TUBEs)

OVCAR8 cells cultured as adherent cells or as spheroids were treated with MG132 (10 μ M, 8 hours) and a deubiquitinating enzyme inhibitor PR-619 (20 μ M, 2 hours). Cells were collected, washed and lysed in buffer containing 50mM Tris-HCl, pH 7.5, 0.15M NaCl, 1mM EDTA, 1% NP-40, 10% glycerol, 10x protease inhibitor, and 100 μ M PR-619. Protein was isolated and the concentration was determined using a Bradford assay. Lysates were passed through a 25G needle three times on ice. Lysates containing 1 mg of

protein was incubated with 40 uL of pre-washed control agarose beads for 60 minutes at 4°C. Unbound supernatant was removed and then incubated with 100 uL Agarose-TUBE2 overnight at 4°C. Beads were washed in 20mM Tris-HCl, pH 8.0, 0.15M NaCl, 0.1% Tween-20 (TBS-T) and the unbound supernatant was removed. Beads were re-suspended in 2x SDS loading buffer and boiled for 5 minutes to elute ubiquitinated proteins. Eluted samples were analyzed by western blot, immunoblotting for NUAK1, c-myc, and total ubiquitin. An input of 50ug of protein lysate along with an aliquot from the fraction not bound to control agarose or agarose-TUBEs were also analyzed by western blot. The western blot procedure was completed as described above except transfer occurred at 30V for 2.5 hours and the stacking gel was included for the transfer.

2.2.10 Determination of Doubling Time

Cells were seeded into a 96-well adherent culture at a density of 2000 cells per well. The following day, cells were treated with DMSO or 0.5 μ M of WZ4003. Using the Incucyte ZOOM (Essen Bioscience, Ann Arbor, MI), confluence was measured for 3 days by capturing phase contrast images every 3 hours. To calculate doubling time, an exponential growth curve was fitted to the confluence-over-time results in Graphpad PRISM.

To calculate doubling time for OVCAR8 *NUAK1*-KO and HEYA8 *NUAK1* overexpressing cells along with their respective controls, cells were transfected with NucLight Green Lentivirus Reagent (Essen BioScience) and selection was completed using bleomycin (10 μ g/ml) (#203408) (Sigma). OVCAR8 cells and OVCAR8 *NUAK1*-KO cells labelled with GFP were seeded at 1500 cells per well in ultra-low attachment dishes (ULA, Corning). HEYA8 cells and HEYA8 *NUAK1* overexpressing cells labelled with GFP were seeded at 1000 cells per well in ULA plates. IncuCyte Zoom imaging system measured number of GFP-labeled nuclei per field of view every 2 hours. Doubling time was calculated by fitting an exponential growth curve to GFP-labeled nuclei-over-time data in GraphPad Prism.

2.2.11 IncuCyte Zoom Live Cell Analysis System to image spheroid morphology in real-time

OVCAR8 cells and OVCAR8 *NUAK1*-KO cells labelled with GFP were seeded at 5000 cells/ well in round bottom ultra-low attachment dishes (ULA, Corning). The ULA plates were placed in IncuCyte Zoom (Essen BioScience) for 17 days and spheroids were imaged every 3 hours.

2.2.12 Phase contrast images of spheroids

To facilitate spheroid formation, cells were seeded in a 24 well ULA dish (1000 cells per well) and cultured in complete media and methylcellulose (Leung, Lesher-Perez, Matsuoka, Moraes, & Takayama, 2015; Ware et al., 2016). For the fibronectin rescue experiment, 5 ug/ml of plasma fibronectin was also included in the media. After 11 days, spheroids were washed with PBS and transferred to a new ULA dish with only complete media. Images were immediately taken with the Leica DMI 4000B inverted microscope using the Leica Application Suite version 4.4 software.

2.2.13 Spheroid viability assay

Spheroids from 24-well ULA plates were transferred to 1.5mL Eppendorf tubes and centrifuged at 4000rpm for 5 minutes. Media was completely aspirated from tubes, without disturbing spheroid pellet. Pellets were washed twice with 1mL of PBS, and centrifuged at 4000rpm for 5 minutes between each wash. A volume of 250 μ L of trypsin-EDTA (0.25%) was added to each sample and pellet was resuspended in trypsin-EDTA. Samples were left in 37°C water bath for 30 minutes, and were vortexed every 10 minutes during this time. After incubation, 250 μ L of FBS was added to each sample to inactivate trypsin. Pellet was resuspended in mixture and completely dissociated using trituration. Each sample was aliquoted at 50 μ L into new Eppendorf tubes. An additional 50 μ L of Trypan Blue dye (ThermoFischer Scientific) was added to each tube and vortexed. The mixture was pipetted at a 15 μ L volume on to cell counter slide and viability readings were taken using TC10 cell counter (Bio-Rad). Total cell number and live cell number were recorded, indicating Trypan Blue excluded cells (Strober, 2001).

2.2.14 Timed adhesion assay

Cells were seeded in a 24 well adherent dish at 200 000 cells per well. After a specified amount of time (15 minutes for HEYA8 cells, 2 hours for OVCAR3 cells, and 4 hours for

OVCAR8 cells), non-adherent cells were aspirated, the plate was washed with PBS, and adherent cells were counted with Trypan blue cell counting to quantify single cell adhesion.

2.2.15 Small-interfering RNA Transfection

Cells were seeded at a density of 2.5×10^5 cells/well in a 6-well dish. The following day cells were transfected according to the manufacturer's protocol (Dharmacon, Thermo Fisher Scientific). Briefly, 4 μ L of DharmaFECT-1 (T-2001-02) was combined with 10 nM of siRNA in 2 ml of media and allowed to incubate for 20 minutes. *NUAK1* (M-004931-00), *USP9X* (M-006099-02), and non-targeting control pool (D-001206-14-05) siGenome SMARTpool siRNAs were obtained from Dharmacon. The siRNA/DharmaFect1 complexes were then added to the wells. 24 hours after transfection the media was replaced. After transfection (72 hours) cells were trypsinized and seeded for experimental conditions (6-well, 24-well, 96-well). Three days after seeding cell viability was measured with the TC10 cell counter as described above (Bio-Rad). Lysates were also collected 3 days post-seeding for western blot analysis.

2.2.16 Tritiated Thymidine Incorporation Assay

Cells were seeded in adherent and spheroid culture in 24-well format, at a density of 50 000 cells/well. Spheroids were immediately treated with 0.5 μ M WZ4003 at time of seeding. Adherent cells were treated with 0.5 μ M WZ4003 the following day. Cells were exposed to tritiated thymidine 24 hours after treatment. Tritiated thymidine was added (1 μ Ci/ μ L) to each well and incubated for either 24 hours for spheroids or 2 hours for adherent cells. For spheroids, media was collected and cells were pelleted. Cell pellets were washed twice in cold 1x PBS followed by cold 10% TCA (trichloroacetic acid, Sigma). Cells were lysed by adding 500 μ L of lysis buffer (1N NaOH/0.1% SDS) to the pellet and resuspending. For adherent cells, wells were washed twice in cold 1x PBS followed by a wash with cold 10% TCA. Cells were lysed in the wells by adding 500 μ L of lysis buffer. For spheroids and adherent cells, 400 μ L of cell lysate was then added to 400 μ L of 1N HCl and mixed with 5 mL of scintillation fluid (ScintiVerse BD Cocktail, Fisher Chemical) in scintillation vials. Counts per minute (cpm) was measured using a

liquid scintillation counter (MacDonald et al., 2016).

2.2.17 Multiplexed Inhibitor Bead (MIB) Chromatography

Lysates were collected from OVCAR8 parental and OVCAR8 *STK11*-KO cells cultured as adherent cells and spheroids. Multiplexed Inhibitor Bead (MIB) Chromatography was performed as described below.

Broad spectrum Type I kinase inhibitors (CTx0294885, VI-16832, PP58, Purvalanol B, UNC-2147A, UNC-8088A) were custom-synthesized with hydrocarbon linkers and terminal amine groups and covalently attached to ECH-activated Sepharose beads as previously described (Stuhlmiller et al., 2015) to form the multiplexed inhibitor beads. Enrichment of kinases from OVCAR8 cells by MIB chromatography was adapted from (Duncan et al., 2012). Cell pellets were lysed in MIB lysis buffer (50 mM Hepes pH 7.5, 150 mM NaCl, 0.5% Triton X-100, 1 mM EDTA, 1 mM EGTA freshly supplemented with 10 mM NaF, 2.5 mM NaVO₄, protease inhibitor cocktail (Sigma-Aldrich, Catalog #P8340), phosphatase inhibitor cocktail 2 (Sigma-Aldrich, Catalog #P5726) and phosphatase inhibitor cocktail 3 (Sigma-Aldrich, Catalog #P0044)) while on ice for 20 minutes. The lysate was homogenized with an 18-gauge syringe needle and centrifuged at 20,800 x g for 15 minutes at 4°C. The total protein amount in the supernatant was quantified using the Bio-Rad protein assay (Catalog #5000006) according to the manufacturer's instructions. The supernatant was brought to 1M NaCl and 4 mg of total protein was loaded on a column (Bio-Rad, Catalog #731-1550) of 100 µl packed ECH sepharose 4B (GE Healthcare, Catalog # 17057101), pre-equilibrated with 2 ml of high salt Buffer B (50 mM Hepes pH 7.5, 1 M NaCl, 0.5% Triton X-100, 1 mM EDTA, 1 mM EGTA). The flowthrough was transferred to a column consisting of layered MIBs (50 µl each of a 50% slurry of CTx0294885, VI-16832, PP58, Purvalanol B, UNC-2147A, and UNC-8088A) pre-equilibrated with 2 ml of Buffer B. The flowthrough was reapplied to the column and the column was then washed with 5 ml of Buffer B and 5 ml of 50 mM ammonium bicarbonate (ABC). After washing, the beads were transferred to 1.5 ml centrifuge tubes in 1 ml of 50 mM ABC and washed twice more in 1 ml of 50 mM ABC. The samples were digested overnight at 37°C with 1 µg trypsin and LysC (Promega, Catalog # V5073). The supernatant was collected and the samples were reduced in 5mM

DTT at 53oC for 30 min, cooled to room temperature and then alkylated in 10 mM iodoacetamide in the dark at RT for 45 min. Trypsin (Sigma-Aldrich, Catalog # T6567) was added and the samples were incubated at 37°C for 4 hours. Formic Acid was added to a final concentration of 2%, and the samples were dried by speed vac.

2.2.18 Mass Spectrometry Analysis

Digested peptides were dissolved in 5% Formic Acid and transferred to autosampler vials for analysis by nano-LC-MS/MS using a SCIEX 5600 TripleTOF mass spectrometer and an Eksigent Ultra nanoHPLC. Samples were loaded onto a home-packed emitter tip column (15 cm x 75 um; 3 µm C18, Reprosil, Dr. Maisch). After sample loading, a linear gradient from 2% acetonitrile to 35% acetonitrile over 90 min at 200 nl/min was used to elute all peptides. A further increase to 80% acetonitrile from 90 min – 95 min, hold from 95 min – 105 min at 80% acetonitrile and return to 2% acetonitrile from 105 min to 120 min was used to ensure full peptide elution. During peptide elution, data was acquired on the mass spectrometer in data-independent acquisition (DIA) mode. Cycle time was 3.5 seconds, consisting of a 250 ms MS1 scan (400-1250 Da) and 34 x 25 Da SWATH windows covering the range of 400-1250 m/z.

2.2.19 Mass Spectrometry Data Analysis

All raw MS files were saved in our local interaction proteomics LIMS, ProHits (G. Liu et al., 2010). The WIFF raw files were converted into mzXML format using the SCIEX converter through the Proteowizard module implemented within ProHits. The mzXML files were processed by the signal extraction (SE) module of DIA-Umpire (version 2.0, [Tsou et al., 2015]). to generate pseudo MS/MS spectra for data base searches. The following parameters were used: isolation window (fixed, 25 Da), fragment grouping (RPmax 25, RFmax 300, correlation threshold 0.2, delta apex 0.6, RT overlap 0.3), signal extraction parameters (mass tolerance (30 ppm MS1, 40 ppm MS2), signal to noise (2 for MS1 and MS2), minimum intensity threshold (1 for MS1, 0.1 for MS2), charge state range (2+ to 4+ for MS1 and MS2), maximum curve in RT range (1.5), and resolution (17,000). Files were searched using X! tandem (version Jackhammer, 2013.06.15.1) and Comet (version 2014.02 revision 2) using the following parameters: allow tryptic peptides only, carbamidomethylation on cysteine as a fixed modification, and deamidation on asparagine and glutamine, oxidation on methionine, and phosphorylation

on serine, threonine and tyrosine as variable modifications. Additional Comet parameters were 2 missed cleavages, monoisotopic parent and fragment mass, 35 ppm peptide mass tolerance, 2+ to 4+ precursor charge state, fragment ion binding (1.005 amu with 0.4 offset). Additional X! tandem parameters were: 1 missed cleavage, 50 ppm parent mass error, 40 ppm fragment mass error, monoisotopic fragment, 4+ maximum parent charge. The searched database contained the human and adenovirus complements of the RefSeq protein database (version 57) supplemented with “common contaminants” from the Max Planck Institute (<http://141.61.102.106:8080/share.cgi?ssid=0f2gfub>) and the Global Proteome Machine (GPM; <http://www.thegpm.org/crap/index.html>) as well as sequences from common fusion proteins and epitope tags. The sequence database consisted of forward and reversed sequences; in total 72,226 sequences were searched. The resulting Comet and X! tandem search results were individually processed by PeptideProphet (Keller, Nesvizhskii, Kolker, & Aebersold, 2002), and peptides were assembled into proteins using parsimony rules first described in ProteinProphet (Nesvizhskii, Keller, Kolker, & Aebersold, 2003) into a final iProphet (Shteynberg et al., 2011) protein output using the Trans-Proteomic Pipeline (TPP; Linux version, v4.7, Polar Vortex rev 1, Build 201410231114). TPP options were as follows: general options were -p0.05 -x20 -PPM -d”DECOY,” iProphet options were pPRIME and PeptideProphet options were pPAEd. Parameters for DIA-Umpire Quant (version 2.0) were peptide FDR (0.05), protein FDR (0.05), probability threshold (0.9), filter weight (group), minimum weight (0.9), top number of fragments (20), top number peptides (20), and frequency (0). mapDIA analysis (version 2.3.3, [Teo et al., 2015]) was then performed on the DIA-Umpire results for intensity normalization, selection of fragments and peptides and determination of significantly changed proteins. For this, only peptides that were unique at the gene level were considered. mapDIA used the following parameters: impute (group 0.9, missing values are assigned 0.9 of the smallest value of the group in the row; if none above zero, then 0.9 the smallest value of the column), experimental design (replicate), normalization (retention time normalized with standard deviation of 10, rounded to 2 decimal places (RT 10 2)), standard deviation factor (SDF) filter (2), minimum correlation (2), minimum observation (2), minimum fragments per peptide (3), maximum fragments per peptide (5), minimum peptides per protein (2), maximum peptides per protein (infinity),

minimum proportion of differentially expressed proteins (0.01), and maximum proportion of differentially expressed proteins (0.99).

2.2.20 Transcriptome analysis and GSEA

RNA was isolated from OVCAR8 parental spheroids and OVCAR8 *NUAK1*-KO spheroids as described above. The RNA was reverse transcribed into cDNA and then labelled with biotin using the Affymetrix Genechip WT pico kit (Thermo Fisher Scientific). The labelled cDNA was hybridized to the Human Clariom S microarray (Thermo Fisher Scientific). After washing, the microarray was scanned using the Affymetrix Gene Chip Scanner 3000. Data analysis was completed with the Transcriptome Analysis Console software at the Centre for Applied Genomics at SickKids (University of Toronto).

Pathway analysis was completed using Gene set enrichment analysis (GSEA) version 3.0 developed by the Broad institute at MIT (Subramanian et al., 2005). The gene list was imported into GSEA without limiting the genes by applying cut-offs. GSEA identifies groups of genes that are enriched in a gene list. The Hallmark collection of 50 gene sets and the Curated Canonical collection of 1329 gene sets from the Molecular Signatures Database (MSigDB, Broad Institute) were used for the analysis. These gene sets were limited to those with 15 to 500 genes. Permutations were completed 1000 times. Signal-to-noise was calculated and used to rank genes based on their differential expression. Significant gene sets were those with a $p < 0.05$ and an $FDR < 0.25$.

2.2.21 Statistical analysis

Statistical analysis was completed using Graphpad PRISM 7 (GraphPad Software, San Diego, CA). Analyses were performed using two-tailed Student's *t*-test, one-way ANOVA, and two-way ANOVA followed by Sidak's or Tukey's *post-hoc* test. A *p*-value less than 0.05 was considered statistically significant.

2.3 Results

2.3.1 NUAK1 expression is regulated by the master stress kinase LKB1 in ovarian cancer spheroids and xenograft tumors

We previously showed that the master upstream kinase LKB1 is needed for efficient ovarian cancer metastasis (Buensuceso et al., 2018; Peart et al., 2015). While AMPK is the canonical target of LKB1, our group showed that LKB1's pro-metastatic role in ovarian cancer likely occurs through AMPK-independent signaling (Shackelford & Shaw, 2009). To elucidate at least one key substrates of LKB1 mediating its tumor-promoting functions in ovarian cancer, multiplex inhibitor bead-mass spectrometry (*MIB/MS*) was completed. Briefly this involves the use of multiplex inhibitor beads (MIBs) which are immobilized kinase inhibitors that will capture kinases present in lysates. MIBs can be coupled to mass spectrometry to identify and quantify the kinases. Our *MIB/MS* analysis was completed using OVCAR8 parental and OVCAR8 *STK11*-KO cells generated by CRISPR/CAS9 that lack LKB1 expression (Figure 2.1A-B). Out of 12 ARKs, NUAK1 was the only ARK that was significantly decreased in *STK11*-KO adherent cells and spheroids. It was also the 6th most down-regulated kinase overall (-2.8 fold change in adherent cells; -8.75 fold change in spheroids) (Table S 2.2 and Table S 2.3). Therefore, this discovery based the *MIB/MS* analysis provided a rationale to pursue LKB1-NUAK1 signaling in ovarian cancer.

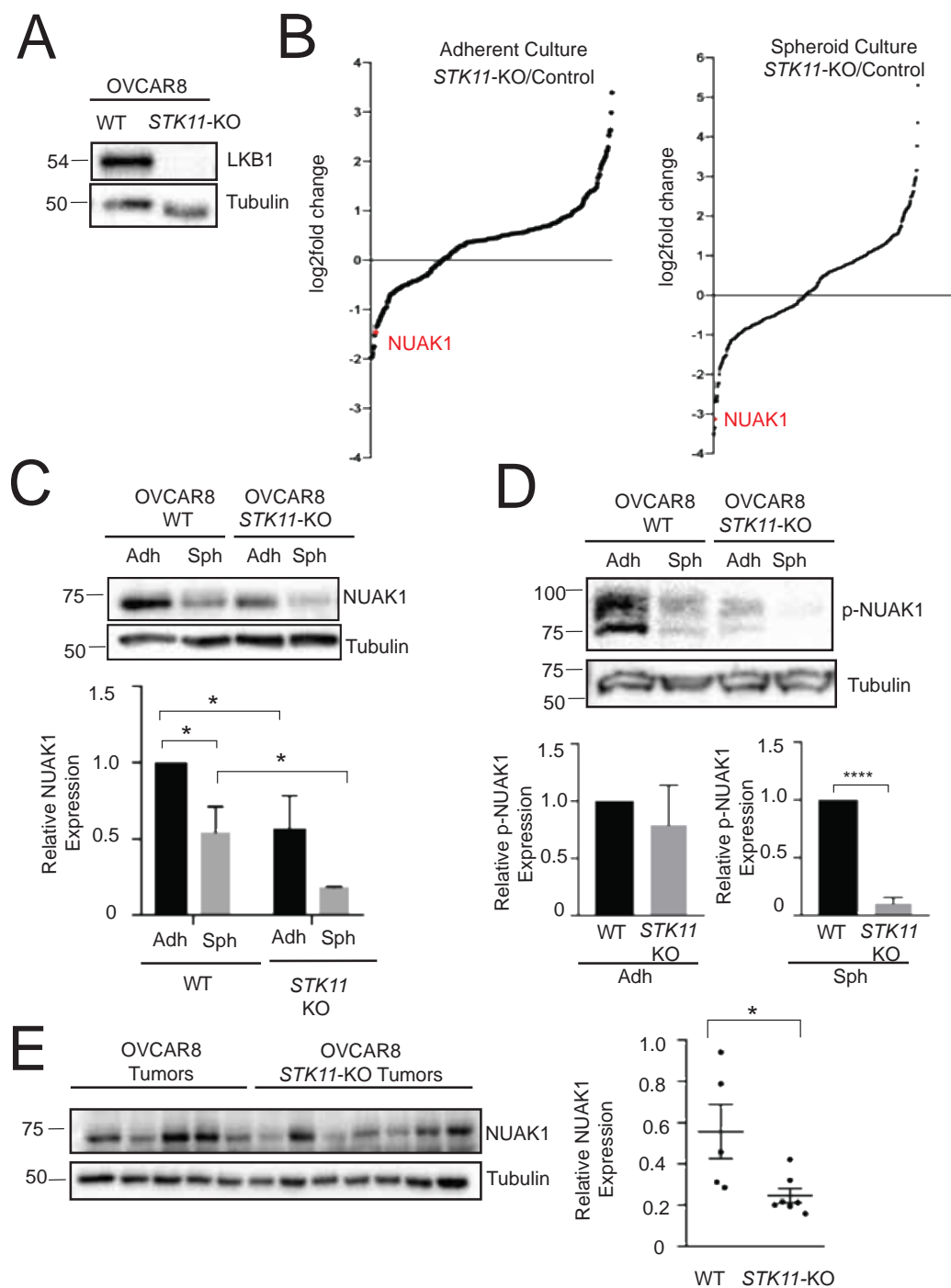


Figure 2.1 NUAK1 expression is regulated by the master stress kinase LKB1 in ovarian cancer spheroids and xenograft tumors.

(A) Western blot analysis of OVCAR8 parental and OVCAR8 *STK11*-KO cells to confirm the loss of LKB1 expression in CRISPR/CAS9 genome edited cell lines. (B) Multiplexed kinase inhibitor bead-mass spectrometry analysis was completed using OVCAR8 *STK11*-KO cells and OVCAR8 parental cells. Log₂fold change is presented for *STK11* -KO/parental for both adherent culture and spheroid culture. Points on graph represent differentially expressed kinases as determined by multiplex inhibitor beads-mass spectrometry (*NUAK1* colored in red). (C) Immunoblot analysis to determine NUAK1 levels in OVCAR8 parental and OVCAR8 *STK11*-KO cells cultured as monolayer cells (Adh) or as spheroids (Sph). Tubulin was used as a loading control. Densitometric analysis shows NUAK1 expression relative to tubulin and normalized to parental control. Two-way ANOVA was performed followed by Tukey's *post-hoc* test (*, p<0.05; ****, p<0.0001). (n=3) (D) Immunoblot analysis was completed using Phostag™ acrylamide gels to determine phosphorylated NUAK1 expression in OVCAR8 parental and OVCAR8 *STK11*-KO cells cultured as adherent cells (adh) and spheroids (sph). Tubulin was used as a loading control. Densitometric analysis shows p-NUAK1 expression relative to tubulin and normalized to parental control. Two-tailed Student's *t*-test was performed (****, p<0.0001). (n=3) (E) Immunoblot analysis of NUAK1 expression in OVCAR8 parental and OVCAR8 *STK11*-KO tumors. 6-week old NOD-SCID females were administered OVCAR8 parental or OVCAR8 *STK11*-KO cells by intraperitoneal injection. Necropsy was performed on day 51 to remove tumors. Densitometric analysis showing NUAK1 expression relative to tubulin for parental tumors (n=5) and *STK11*-KO tumors (n=7). Analysis was performed using two-tailed Student's *t*-test (*, p<0.05). *MIB/MS preparation and analysis was completed by Dr. Adrian Buensuceso and Dr. Trevor Shepherd. Parima Saxena completed the Phostag western blot analysis.*

To confirm the *MIB/MS* results, we assessed NUAK1 expression by immunoblot analysis. There was a significant decrease in NUAK1 expression levels in OVCAR8 *STK11*-KO spheroids (Figure 2.1C). To further study the regulation of NUAK1 by this master upstream kinase, the ability of LKB1 to control NUAK1 phosphorylation was examined. Because there are no commercially available antibodies to detect NUAK1 phosphorylation by LKB1 at threonine 211, the established target site for NUAK1, PhostagTM acrylamide gels were used (Lizcano et al., 2004; Tomida, Kitao, Kinoshita, & Takata, 2008). There was a significant decrease in phosphorylated-NUAK1 in OVCAR8 *STK11*-KO spheroids (Figure 2.1D). Thus, NUAK1 expression and phosphorylation both appear to be regulated by LKB1 in EOC cells and spheroids.

Next, we wanted to test if LKB1 also regulates NUAK1 expression levels in tumors. Tumor samples were collected from a prior EOC xenograft study (Buensuceso et al., 2018). NOD-SCID female mice were administered OVCAR8 parental cells or OVCAR8 *STK11*-KO cells. Tumors were removed on day 51 and protein was isolated for western blot analysis. Despite variability in NUAK1 expression amongst the tumor sample conditions, there was a significant decrease in NUAK1 expression in *STK11*-KO tumors (Figure 2.1E). Altogether, our findings suggest that LKB1 regulates NUAK1 expression in ovarian cancer spheroids and tumor samples.

2.3.2 NUAK1 expression is differentially expressed in spheroids and this is mediated by the *ubiquitin-proteasome system* and lysosomal degradation

In ovarian cancer, spheroids are the primary mediator of metastasis. Spheroids are commonly found in patient ascites and are critical for efficient dissemination as they resist anoikis and adhere to the peritoneum to invade at secondary sites (Lengyel et al., 2014; Sodek et al., 2012, 2009). Using an *in vitro* model for metastasis, we sought to understand if NUAK1 expression levels change. NUAK1 expression was compared between proliferative adherent cells and quiescent spheroids (Al Habyan et al., 2018). By examining spheroids generated from high-grade serous ovarian cancer (HGSOC) established cells lines (OVCAR8 and OVCAR5), we found that NUAK1 protein levels are down-regulated in spheroids compared to monolayer (Figure 2.2A) (Domcke, Sinha, Levine, Sander, & Schultz, 2013). This trend was also apparent in multiple ascites-

derived cell lines cultured as spheroids , including cells from a stage IIIB HGSOC patient when she received 6 cycles of carboplatin and paclitaxel (iOvCa198) and later when she developed carboplatin resistance (iOvCa247) (Figure 2.2A). As a control, a non-HGSOC cell line (HEYA8) was examined. HEYA8 cells are a moderately differentiated papillary cystadenocarcinoma (Hernandez et al., 2016). In contrast to HGSOC spheroids, HEYA8 spheroids showed increased NUAK1 compared to monolayer cells, suggesting this down-regulation of NUAK1 may be subtype specific (Figure 2.2A).

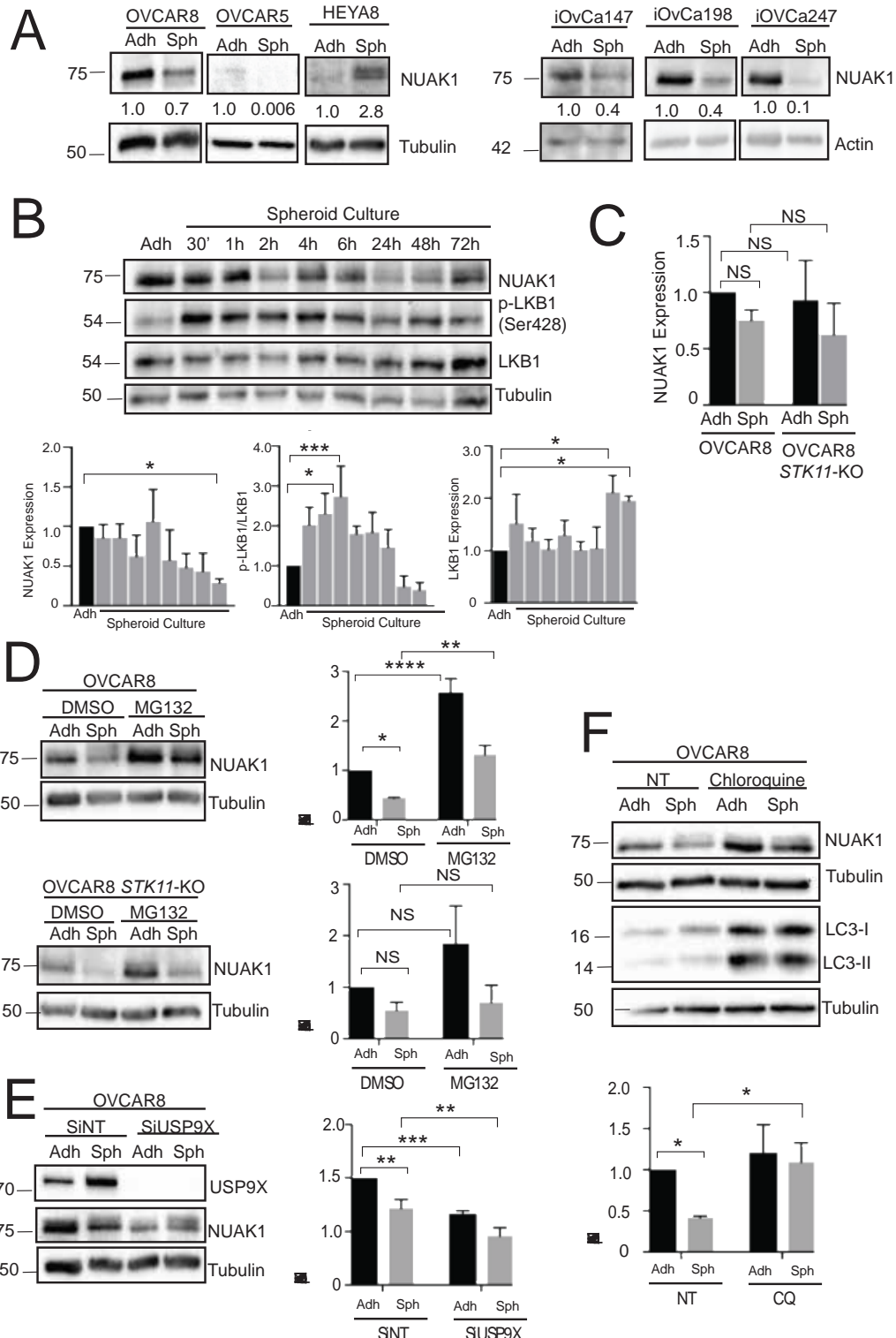


Figure 2.2 NUAK1 expression is differentially expressed in spheroids and this is mediated by the ubiquitin-proteasome system and lysosomal degradation.

(A) Immunoblot analysis to assess NUAK1 expression in HGSOC cell lines (OVCAR8, OVCAR5), a non-HGSOC cell line (HEYA8), and patient-derived ascites cell lines (iOvCa147, iOvCa198, iOvCa247) cultured under adherent (adh) or suspension (sph) conditions. Tubulin and actin were used as loading controls. NUAK1 expression fold change is indicated on the immunoblots. (B) Time course analysis of NUAK, p-LKB1 (S428), and total LKB1 in OVCAR8 spheroid formation. Densitometric analysis shows pixel intensity volume for NUAK1 relative to tubulin, p-LKB1 relative to LKB1, and LKB1 relative to tubulin. One-way ANOVA and Sidak's multiple comparison test was performed (*, p<0.05; ***, p<0.001). (n=3) (C) RT-qPCR analysis of *NUAK1* gene expression in OVCAR8 parental and *STK11*-KO cells cultured under adherent (adh) conditions or as spheroids (sph). Gene expression is relative to GADPH and normalized to parental adherent. Two-way ANOVA and Tukey's multiple comparisons test was performed (NS= non-significant). (n=3) (D) Immunoblot analysis of NUAK1 expression in OVCAR8 cells and OVCAR8 *STK11*-KO cells treated with DMSO or MG132 (10 µM for 8h). Cells were cultured in adherent (adh) conditions or as spheroids (sph). Data is quantified as NUAK1 expression relative to tubulin and normalized to DMSO adherent. Two-way ANOVA and Tukey's multiple comparisons test was performed (NS= not significant; *, p< 0.05, **, p<0.01, ****, p<0.0001) (n=3) (E) Immunoblot analysis of NUAK1 and USP9X expression in OVCAR8 cells transfected with control siRNA (siNT) or siRNA targeting *USP9X*. Cells were cultured in adherent (adh) conditions or as spheroids (sph). Data is quantified as NUAK1 expression relative to tubulin and normalized to siNT control. Two-way ANOVA and Tukey's multiple comparisons test was performed (**, p<0.01, ***, p<0.001). (n=3) (F) Immunoblot analysis of NUAK1 and LC3 I and II expression in OVCAR8 cells treated with chloroquine (8h; 25 µM) or untreated. Cells were cultured in adherent (adh) conditions or as spheroids (sph). Data is quantified as NUAK1 relative to tubulin and normalized no treatment control. Two-way ANOVA and Tukey's multiple comparisons test was performed (*, p<0.05). (n=3)

To study these changes in NUAK1 expression in greater detail, time course analysis was completed in OVCAR8 spheroids (Figure 2.2B). During early spheroid formation, NUAK1 expression is relatively high and this parallels the increased levels of phospho-LKB1 levels in spheroids (Figure 2.2B). NUAK1 levels decrease significantly compared to monolayer later during spheroid formation and this correlates with the drop in phospho-LKB1. NUAK1 continues to be expressed at a lower yet detectable level at these later points (Figure 2.2B). Interestingly, total LKB1 expression starts to increase in late spheroid formation (Figure 2.2B). This trend supports our previous data which implicates LKB1 as being critical for ovarian cancer metastasis (Buensuceso et al., 2018; Peart et al., 2015)

To understand the mechanism that mediates this decrease in NUAK1 levels in spheroids, we first performed RT-qPCR to determine whether *NUAK1* is regulated at the transcript level. There was no significant difference in *NUAK1* gene expression between adherent cells and 24h spheroids (Figure 2.2C). Furthermore, there was no significant difference in *NUAK1* mRNA between parental and *STK11*-KO conditions. These results suggest that the regulation is not occurring at the transcriptional level but rather NUAK1 expression is being controlled at the protein level whether it be translational or post-translational. Interestingly, previous studies have shown that NUAK1 protein levels can be regulated by the ubiquitin-proteasome system (UPS) (Banerjee et al., 2014). Hence, we sought to test whether the UPS was playing a role in NUAK1 down-regulation by treating cells with the proteasome inhibitor, MG132. The addition of MG132 to OVCAR8 cells prevented the decrease in NUAK1 levels in spheroids and significantly increased levels of this kinase (Figure 2.2D). These findings suggest that the UPS regulates NUAK1 expression in spheroids and contributes to the down-regulation of this kinase. Intriguingly, in spheroids absent of LKB1, MG132 did not significantly increase NUAK1 levels in OVCAR8 cells (Figure 2.2D). These results support the importance of LKB1 in regulating NUAK1 expression levels in spheroids.

A previous report indicated that NUAK1 is ubiquitinated and the Ubiquitin Specific Peptidase 9 X-Linked (USP9X) can remove the polyubiquitin modification on NUAK1

(Al-Hakim et al., 2008). To continue to examine the involvement of the UPS in controlling NUAK1 expression, we tested whether USP9X regulates NUAK1 levels in spheroids. Using an siRNA-mediated approach to knockdown *USP9X*, we predicted that reduced levels of USP9X would lead to decreased NUAK1 expression possibly by promoting its degradation at the proteasome. Indeed, *USP9X* knockdown significantly decreased levels of NUAK1 in OVCAR8 adherent cells and spheroids (Figure 2.2E). Therefore, USP9X regulates NUAK1 expression in EOC spheroids.

Based on our results implicating the UPS in regulating NUAK1 levels in spheroids, we next examined levels of ubiquitinated-NUAK1 in EOC. We predicted that if the UPS was contributing to the down-regulation of NUAK1 in spheroids there may be increased levels of ubiquitinated-NUAK1 in spheroids compared to adherent cells. To test this, cells were treated with a proteasome inhibitor and deubiquitinase inhibitor to preserve the ubiquitin modification (Emmerich & Cohen, 2015). To pulldown ubiquitinated proteins, lysates were incubated with Tandem Ubiquitin Binding Entities (TUBEs) which capture all types of ubiquitin linkages (Emmerich & Cohen, 2015). Subsequently, immunoblotting for NUAK1 should be able to detect endogenous ubiquitinated-NUAK1. c-myc was used as a positive control based on a prior report showing that it is ubiquitinated in OVCAR8 cells (Kedves et al., 2017). While ubiquitinated-c-myc was present in spheroids, *ubiquitinated*-NUAK1 was not detected in adherent cells or spheroids (Figure S2.1). These results suggest that NUAK1 may not be highly *ubiquitinated* in ovarian cancer cells.

While the UPS is the primary degradation pathway for short-lived and small proteins, the autophagy-lysosome pathway is another degradation system in eukaryotic cells responsible for the clearance of large and damaged proteins. In response to stress from nutrient deprivation and hypoxia, autophagy can be activated as a survival mechanism due to its ability to recycle cellular components and nutrients. Indeed, our group and others have shown that autophagy is activated in ovarian cancer and spheroids have higher levels of autophagy compared to monolayer cells (Correa et al., 2014; Lu et al., 2008; Wang et al., 2018). To determine if lysosomal degradation contributes to NUAK1

down-regulation spheroids were treated with the lysosome inhibitor, chloroquine. Chloroquine treatment led to a significant increase in NUAK1 expression levels in spheroids; NUAK1 levels in adherent cells approached significance after chloroquine treatment (Figure 2.2F). Altogether these findings suggest while the UPS controls NUAK1 expression, the lysosome is also implicated in regulating NUAK1 in spheroids compared to adherent cells.

2.3.3 NUAK1 controls EOC cell adhesion and ovarian cancer spheroid integrity

Prior studies have indicated that NUAK1 can play a role in cell adhesion (Ye et al., 2018; Zagórska et al., 201[^] Zhang et al., 2015). NUAK1 promotes EMT in cancer cells and induces cell detachment by regulating the MYPT-PP1 β complex. Cell adhesion is critical in the context of ovarian cancer metastasis because cell-ECM interactions have been shown to mediate the formation of ovarian cancer spheroids (Casey et al., 2001; Doberstein et al., 2018). Therefore, we aimed to determine whether NUAK1 regulates cell adhesion in ovarian cancer in several EOC cell lines. To investigate the role of NUAK1 in ovarian cancer metastasis, we used OVCAR8 cells (HGSOC), OVCAR3 (HGSOC), and HEYA8 (moderately-differentiated high-grade ovarian cancer) because they readily form dense spheroids *in vitro* and can establish tumors when injected i.p into immune-compromised mice. OVCAR8 cells express high levels of NUAK1, while OVCAR3 and HEYA8 cells express very low levels of NUAK1. We generated a stable line lacking NUAK1 expression (OVCAR8 *NUAK1*-KO) using CRISPR-Cas9 genome editing (Figure 2.3A). We engineered the OVCAR3 and HEYA8 cell lines to stably overexpress *NUAK1* (Figure 2.3A). To examine NUAK1's ability to regulate adhesion timed adhesion assays were completed. By measuring the number of cells that adhered to a tissue culture plate after 15 minutes, we found that HEYA8 *NUAK1* overexpressing cells had significantly greater single cell adhesion compared to HEYA8 cells (Figure 2.3B). Similarly, after 2 hours OVCAR3 *NUAK1* overexpressing cells had significantly greater cell adhesion (Figure 2.3B). In examining the reciprocal system, after 4 hours OVCAR8 *NUAK1*-KO cells had significantly lower cell adhesion compared to OVCAR8 parental cells (Figure 2.3B). These results suggest that NUAK1 acts to enhance EOC cell adhesion.

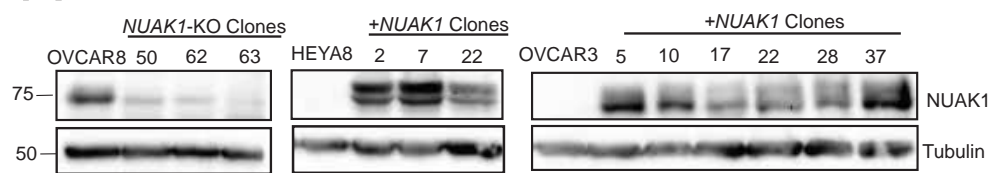
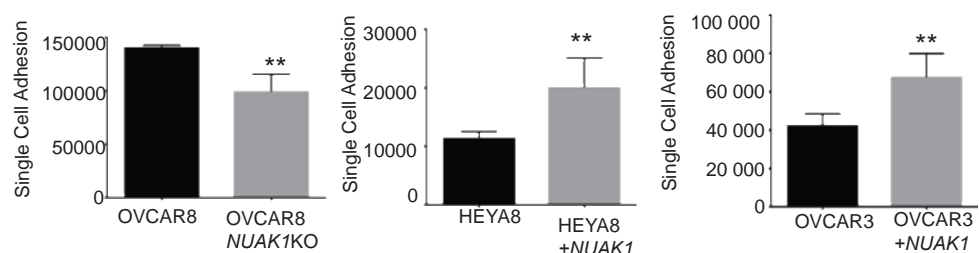
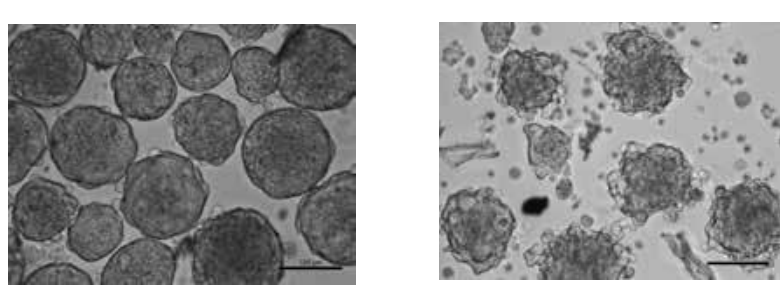
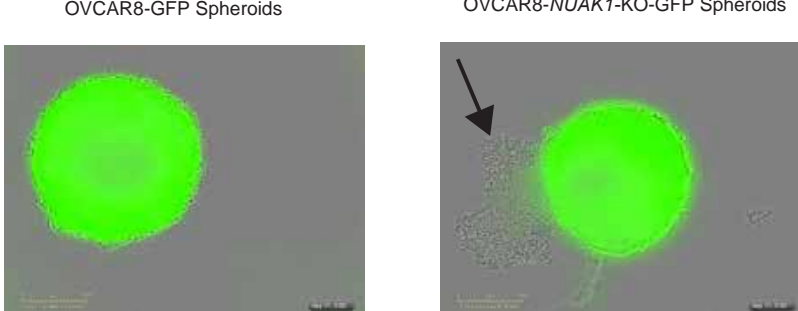
A**B****C****D**

Figure 2.3 NUAK1 regulates EOC cell adhesion and ovarian cancer spheroid integrity
(A) Immunoblot analysis of OVCAR8 *NUAK1*-KO, HEYA8 *NUAK1*-overexpressor, and OVCAR3 *NUAK1* cells and matched controls to validate loss or overexpression of NUAK1. Tubulin is used as a loading control. (B) Single cell adhesion was quantified with Trypan blue cell counting for OVCAR8 *NUAK1*-KO, HEYA8 *NUAK1* and OVCAR3 *NUAK1* cells and matched controls. Data is presented as absolute cell counts from pooled data among multiple clones. Analysis was performed using two-tailed Student's *t*-test (**, $p < 0.01$). ($n=3$) (C) Images of OVCAR8 parental and OVCAR8 *NUAK1*-KO spheroids cultured for 11 days in ultra-low attachment dishes with methylcellulose. Scale bars represent 125 μ M. ($n=3$) (D) Images of 11 day OVCAR8 parental and OVCAR8 *NUAK1*-KO spheroids transduced with NucLight Green Lentivirus Reagent. Live cells were imaged in real-time with IncuCyte Zoom imaging system. ($n=3$) *Experiments were completed by Olga Collins.*

Given our data suggesting a role for NUAK1 in EOC cell adhesion we next investigated whether NUAK1 may also regulate the formation of ovarian cancer spheroids. To facilitate spheroid formation, cells were cultured in ultra-low attachment (ULA) culture plates and methylcellose was added to the media (Leung et al., 2015). After 11 days in culture, OVCAR8 spheroids formed dense spheroids (Figure 2.3C). However, OVCAR8 *NUAK1*-KO spheroids were less compact and there was an abundance of budding cells at the periphery (Figure 2.3C). To further examine this altered phenotype, OVCAR8 and OVCAR8 *NUAK1*-KO cells were transfected NucLight Green Lentivirus Reagent and live cells were imaged during single spheroid culture in real-time with IncuCyte Zoom imaging system. At 11 days, there were an abundance of live cells in highly compact OVCAR8-GFP spheroids (Figure 2.3D). In contrast, OVCAR8 *NUAK1*-KO-GFP spheroids showed decreased integrity with many protruding non-viable cells as visualized by loss of GFP expression. Altogether, NUAK1 loss reduces EOC spheroid integrity (Figure 2.3D).

2.3.4 NUAK1 promotes EOC spheroid formation through up-regulating fibronectin deposition

To understand the molecular basis for the impaired spheroid integrity in *NUAK1*-KO spheroids, global transcriptome analysis was performed to compare OVCAR8 *NUAK1*-KO spheroids and parental spheroids. A total of 606 genes were differentially expressed with Affymetrix's Clariom S array (fold change ≥ 2 or ≤ -2) (Table 2.4). Hierarchical clustering demonstrated that there were distinct gene expression profiles between OVCAR8 parental spheroids and OVCAR8 *NUAK1*-KO spheroids (Figure 2.4A); thus, to determine the pathways through which NUAK1 may act, Gene Set Enrichment analysis (GSEA) was completed. Using the Hallmark database in GSEA it was revealed that interferon, metabolism, and epithelial mesenchymal transition signatures were enriched in the OVCAR8 parental spheroids compared to *NUAK1*-KO spheroids (Figure 2.4B; Table 2.5). A previous study had shown that NUAK1 can promote epithelial mesenchymal transition in ovarian cancer (Zhang et al., 2015). In examining the curated canonical database, several metabolism pathways were up-regulated, including electron transport chain and oxidative phosphorylation pathways (Figure 2.4B, Table 2.6). Interestingly, in line with our *in vitro* cell adhesion data we found multiple pathways involved in integrin cell attachment that were enriched in parental compared to *NUAK1*-KO spheroids.

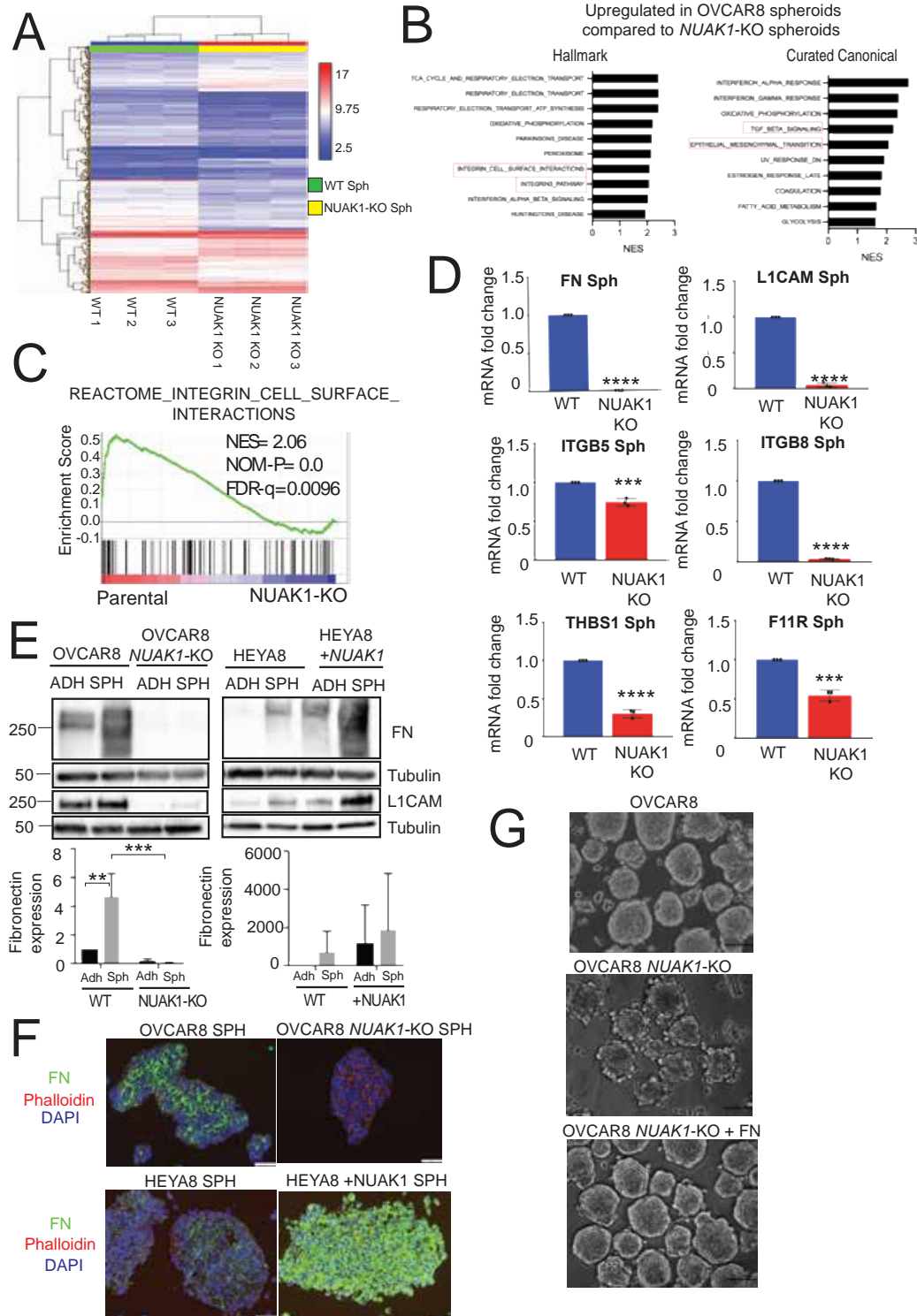


Figure 2.4 NUAK1 promotes EOC spheroid formation through fibronectin deposition

(A) Hierarchical clustering heat map showing gene expression profiles for OVCAR8 parental and OVCAR8 *NUAK1*-KO 24h spheroids. Up-regulated genes and down-regulated genes are shown in red and blue, respectively. Differentially expressed genes with a fold change ≥ 2 or ≤ -2 with a $p < 0.05$ are displayed. Three replicates were used for each respective group. (B) Top 10 gene sets up-regulated in OVCAR8 parental spheroids compared to OVCAR8 *NUAK1*-KO spheroids. Gene sets were derived from GSEA Hallmark database and Curated Canonical database. Normalized enrichment score (NES) is presented. (C) Integrin cell surface interaction enrichment plot is presented. Vertical black lines represent the position of genes in the ordered data set. Green line represents the enrichment score curve. Normalized enrichment score (NES), nominal p-value, and FDR are shown. (D) RT-qPCR analysis to validate core enriched genes from the integrin cell surface interaction signature. Fold change in mRNA levels is presented for OVCAR8 parental and OVCAR8 *NUAK1*-KO 24h spheroids. Analysis was performed using two-tailed Student's *t*-test (***, $p < 0.001$; ****, $p < 0.0001$). ($n=3$) (E) Immunoblot analysis showing fibronectin and L1CAM expression for OVCAR8 *NUAK1*-KO and HEYA8 *NUAK1*-overexpressor cells along with their respective controls cells cultured in adherent conditions (adh) or in suspension (sph). Tubulin was used as a loading control. Data is quantified as fibronectin expression relative to tubulin and normalized to adherent control. Two-way ANOVA and Tukey's multiple comparisons test was performed (**, $p < 0.01$, ***, $p < 0.001$) ($n=3$) (F) Immunofluorescence images showing fibronectin, phalloidin (cytoskeleton stain), and DAPI (nuclear stain) for OVCAR8 *NUAK1*-KO and HEYA8 *NUAK1* cells along with their respective control cells cultured in adherent conditions (adh) or in suspension (sph). Images were captured using Olympus AX70 upright microscope and ImagePro image capture software. Scale bar represents 100 μM . ($n=3$) (G) Images of OVCAR8 parental and OVCAR8 *NUAK1*-KO spheroids cultured for 11 days in ultra-low attachment dishes with methylcellulose and supplemented with 5 $\mu\text{g}/\text{ml}$ of plasma fibronectin (pFN). Scale bars represent 100 μM . Images were captured using a Leica light microscope. ($n=3$) *Immunofluorescence was completed by Olga Collins.*

To confirm this adhesion signature, key target genes were chosen to validate by RT-qPCR. This list of target genes was based on the core enriched gene set from the REACTOME_INTEGRIN_CELL_SURFACE_INTERACTION signature and genes with a fold change greater than 2 were chosen to be validated (Figure 2.4C-D; Table 2.7). While *LICAM* was not a core enriched gene, it was included in the gene list to validate because this transmembrane adhesion molecule promotes EOC spheroid formation (Doberstein et al., 2018). Furthermore, out of 605 differentially expressed genes it was the 10th most down-regulated gene in *NUAK1*-KO spheroids (fold change = -10) (Table 2.4). We validated a significant decrease in *FNI* mRNA levels in OVCAR8 *NUAK1*-KO spheroids (Figure 2.4D), and mRNA levels of *LICAM* were also significantly decreased (Figure 2.4D). Interestingly, while there was no change in levels of the canonical fibronectin receptor, $\alpha 5 \beta 1$ integrins, there was a significant decrease in components of non-canonical receptors, such as integrin $\beta 5$ and integrin $\beta 8$ (Johansson et al., 1997; Venstrom & Reichardt, 1995) (Figure 2.4D). There was a significant decrease in several other adhesion molecules, including Thrombospondin 1 (*THBS1*) and F11 Receptor (*F11R*) (Figure 2.4D). Therefore, key core enriched genes from the integrin cell surface interaction signature were validated by RT-qPCR analysis.

To further investigate this adhesion signature at the protein level, we focused on assessing the expression of fibronectin in *NUAK1*-KO spheroids. Fibronectin showed the greatest differential expression, with a 745-fold decrease in *NUAK1*-KO spheroids, which drove the enrichment score for the integrin cell attachment pathway (Figure 2.4C) (Table 2.4). Moreover, several reports have implicated fibronectin as being critical for spheroid formation (Casey et al., 2001; Doberstein et al., 2018). In comparison to OVCAR8 monolayer cells, spheroids had increased levels of fibronectin with a multiple isoforms appearing by western blot analysis (Figure 2.4E). Previous reports have similarly shown many fibronectin bands and this has been attributed to an up-regulation of cleaved fibronectin fragments due to proteinases (Bonnans, Chou, & Werb, 2014; Gopal et al., 2017). In ovarian cancer metastasis, *matrix metalloproteinase-2* (*MMP-2*) is up-regulated and cleaves fibronectin (Kenny et al., 2014). Smaller fibronectin fragments increase

ovarian cancer adhesion because they can more easily bind to integrin receptors compared to uncleaved fragments. Strikingly, there was no detectable fibronectin in OVCAR8 *NUAK1*-KO spheroids (Figure 2.4E). In a reciprocal fashion, HEYA8 *NUAK1* overexpressing cells and spheroids had a dramatic increase in fibronectin expression compared to HEYA8 parental cells and spheroids (Figure 2.4E). Similar to fibronectin, L1CAM decreased in OVCAR8 *NUAK1*-KO spheroids compared to parental and increased in HEYA8 *NUAK1*-overexpressor spheroids relative to HEYA8 spheroids (Figure 2.4E). Moreover, the fibronectin immunoblot results were further supported by immunofluorescence data showing a loss of fibronectin in OVCAR8 *NUAK1*-KO spheroids and increased fibronectin in HEYA8 *NUAK1*-overexpressor spheroids (Figure 2.4F). Therefore, our results strongly suggest that NUAK1 regulates fibronectin expression in ovarian cancer spheroids.

To understand the mechanism by which NUAK1 controls spheroid integrity, we tested whether NUAK1 regulates fibronectin deposition in spheroids to establish spheroid formation. To test this, exogenous plasma fibronectin was added to the culture to observe whether a compact spheroid morphology could be rescued in OVCAR8 *NUAK1*-KO spheroids. Plasma fibronectin (5 ug/ml) was supplemented to OVCAR8 *NUAK1*-KO cells in suspension and after 11 days spheroids appeared densely packed without protruding peripheral cells (Figure 2.4G). Thus, NUAK1 is required to promote cell cohesion in spheroids through its regulation of fibronectin deposition.

2.3.5 Transient and sustained loss of NUAK1 increases spheroid viability without altering proliferation of EOC cells

The results from our adhesion experiments suggest that NUAK1 increases cell adhesion and promotes spheroid formation. Using our OVCAR8 GFP-labeled spheroids, we found that with NUAK1 loss there was diminished spheroid integrity and an increase in dead cells that accumulated around the periphery of the spheroid. This up-regulation of dead cells could be a consequence of impaired spheroid integrity due to a loss of adhesion molecules and cell death by anoikis. However, these results could also be due to NUAK1's ability to regulate cell growth (Banerjee et al., 2014). Therefore, we investigated whether NUAK1 has a role in EOC cell proliferation in addition to its ability

to regulate cell adhesion. We first transiently knocked down *NUAK1* using an siRNA-mediated approach and confirmed NUAK1 loss in OVCAR8 and HEYA8 cells (Figure 2.5A). *NUAK1* knockdown significantly increased viability in HEYA8 spheroids and there was a trend toward increased viability in OVCAR8 spheroids (Figure 2.5B). To assess the effect on viability with sustained loss of NUAK1, we used our OVCAR8 *NUAK1*-KO spheroids. There was a significant increase in spheroid viability in OVCAR8 *NUAK1*-KO spheroids (Figure 2.5C). In the reciprocal system, HEYA8 *NUAK1*-overexpressor spheroids showed a significant decrease in viability. Therefore, loss of NUAK1 appeared to increase the viability of spheroids and cells.

Next, we wanted to discern whether these changes in viability were because of altered EOC cell proliferation. To test this cells were treated with the dual NUAK1/2 inhibitor WZ4003 and doubling time was measured (Banerjee et al., 2014). While WZ4003 treatment led to a significant decrease in doubling time in HEYA8 cells, there was no difference in doubling time for OVCAR8 cells (Figure 2.5D). Furthermore, there was no change in doubling time for both OVCAR8 *NUAK1*-KO spheroids and HEYA8 *NUAK1*-overexpressor cells (Figure 2.5E). A thymidine incorporation assay is another method to measure proliferating cells. However, we found no significant difference in thymidine incorporation between OVCAR8 and HEYA8 cells treated with the WZ4003 compound and their respective controls (Figure 2.5F). Altogether, these findings suggest that NUAK1 loss can increase spheroid viability however these effects are not due to increased proliferation.

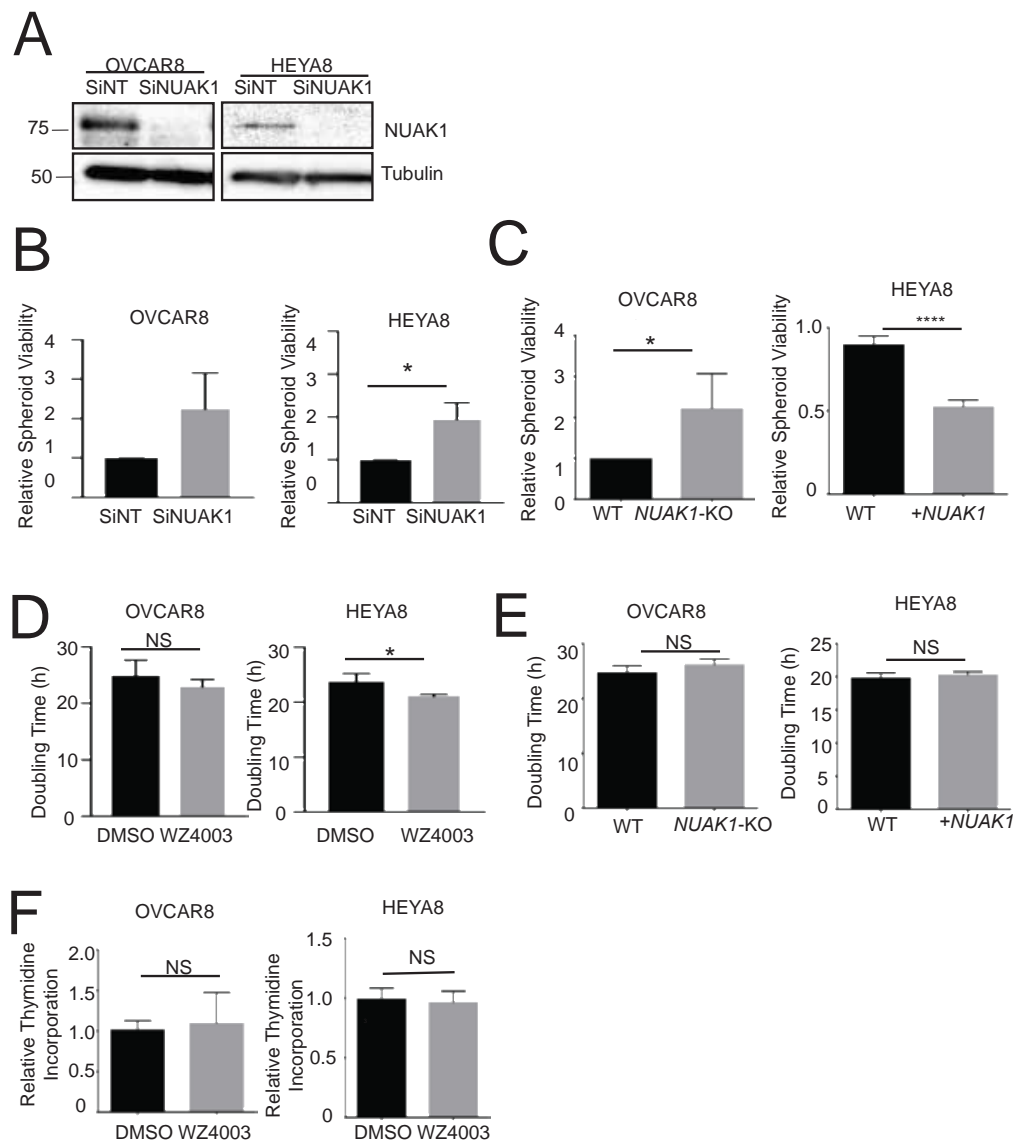


Figure 2.5 Transient and sustained loss of NUAK1 increases spheroid viability without altering proliferation of EOC cells

(A) Immunoblot analysis of OVCAR8 and HEYA8 cells transfected with control siRNA (siNT) or siRNA targeting *NUAK1* (si*NUAK1*) to confirm transient loss of NUAK1. Tubulin was used as a loading control. (B) Spheroid viability for OVCAR8 si*NUAK1* and HEYA8 si*NUAK1* and their respective siNT controls. Viable cell number was determined by trypan blue exclusion cell counting 3 days after transfection. Data is presented as viable cell number normalized to siNT control. Analysis was performed using a two-tailed Student's *t*-test (*, p<0.05). (n=3) (C) Spheroid viability for OVCAR8 *NUAK1*-KO and HEYA8 *NUAK1* cells and their respective controls. Viable cell number was determined by trypan blue exclusion cell counting after 7 days (OVCAR8) or 14 days (HEYA8) in culture. Data is presented as viable cell number normalized to OVCAR8 and HEYA8 controls. Analysis was performed using a two-tailed Student's *t*-test (*, p<0.05, ****, p<0.0001). (n=3) (D) Doubling time for OVCAR8 and HEYA8 cells treated with DMSO or WZ4003 (0.5 µM). IncuCyte Zoom Imaging system measured percent confluence over 3 days. Graphpad PRISM was used to generate growth curves. Using non-linear regression analysis, doubling times were calculated with Graphpad PRISM. (*, p<0.05) (n=3) (E) Doubling time for OVCAR8 *NUAK1*-KO and HEYA8 *NUAK1* cells and their respective controls. Cells were transduced with NucLight Green Lentivirus Reagent and GFP-labeled cells were counted in real-time using the IncuCyte Zoom imaging system. Analysis was performed using a two-tailed Student's *t*-test (NS= not significant). (n=3) (F) Thymidine incorporation assay was completed on OVCAR8 and HEYA8 spheroids treated with DMSO or WZ4003 (0.5 µM). Spheroids were pulsed with tritiated thymidine for 24 hours. Counts per minute (cpm) was measured using a liquid scintillation counter. Analysis was performed using a two-tailed Student's *t*-test (NS= not significant). (n=3) *Experiments shown in figure 5A and B were completed by Parima Saxena. Experiment shown in figure 5F was completed by Parima in collaboration Pirunthan Perampelam and Dr. Fred Dick. Experiments were also performed by Olga Collins as shown in figure 5C and 5E.*

2.3.6 Loss of NUAK1 increases NF-κB signaling in EOC spheroids

To understand the molecular basis for the increased spheroid viability, we reinvestigated our transcriptome analysis data. Using the hallmark database, we found that Kras, *TNF-a*/NF-κB, and inflammatory signaling were up-regulated in OVCAR8 *NUAK1*-KO spheroids compared to parental spheroids (Figure 2.6A). The curated canonical database also showed enrichment of several NF-κB signaling pathways (Figure 2.6A).

Interestingly, KRAS and NF-κB signaling both contribute to cell survival and tumor progression (Figure 2.6B; Figure S2.2A) (Bell et al., 2011; Hew et al., 2016; House et al., 2017; Nakamura et al., 2017). Because KRAS activates the MAPK signaling we assessed the expression of several MAP kinases in *NUAK1*-KO spheroids as a readout of its activity (F. Liu, Yang, Geng, & Huang, 2018; Sabio & Davis, 2014). We found that there was no change in phosphorylated protein levels of ERK, MEK, and JNK (Figure S2.2B-D). To determine if NF-κB signaling was up-regulated in *NUAK1*-KO spheroids, we assessed the activation of the canonical p65 transcription factor by its phosphorylation status in whole cell lysates (Espín-Palazón & Traver, 2016; Viatour, Merville, Bours, & Chariot, 2005). Phospho-p65 was significantly higher in *NUAK1*-KO spheroids, indicating increased activation of this transcription factor (Figure 2.6C). Next, to investigate if loss of NUAK1 promotes nuclear translocation of the p65 transcription factor, we examined p65 expression in nuclear and cytoplasmic fractions. Nuclear p65 was increased in *NUAK1*-KO spheroids (Figure 2.6D). Because our data suggests enhanced activation of the p65 transcription in *NUAK1*-KO spheroids, we subsequently examined which target genes were being expressed by p65. To generate a list of NF-κB target genes, we used the core enriched genes from the HALLMARK_ *TNFA_SIGNALING_VIA_NF-κB* (Figure 2.6B) and focused on 6 up-regulated genes and 1 down-regulated gene for validation since they represent established NF-κB target genes using the “NF-κB Target Genes” list maintained by Thomas Gilmore’s lab (Boston University) (<http://www.bu.edu/nf-kb/gene-resources/target-genes/>) (Table 2.8). Inflammatory target genes were found to be significantly upregulated in *NUAK1*-KO spheroids, including *IL-1α* and *IL-1β* (Figure 2.6E). Interestingly, NF-κB2 (*p100*), a transcription factor in the non-canonical NF-κB pathway, was the only NF-κB family member that showed differential expression by RT-qPCR (Figure 2.6E).

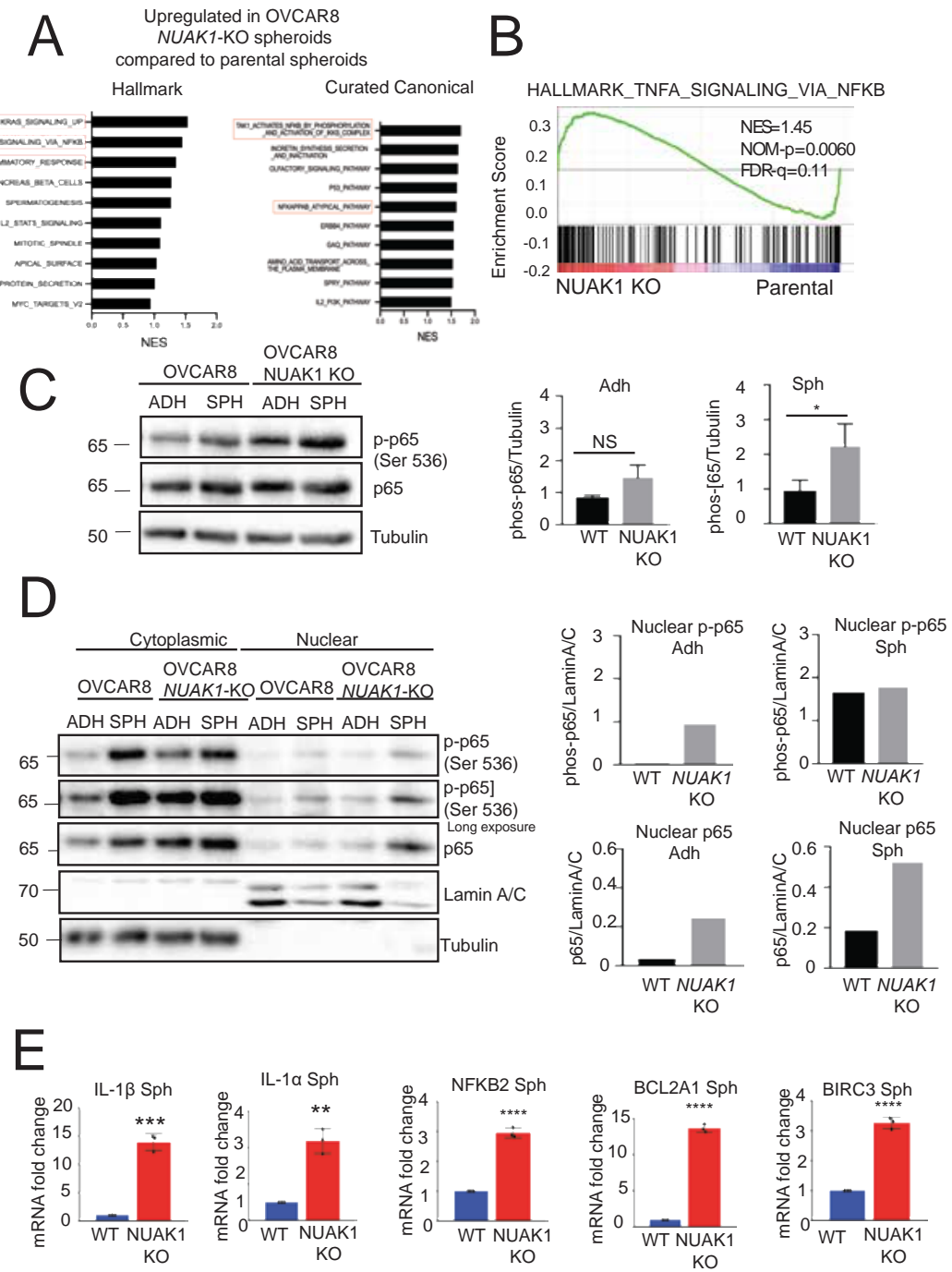


Figure 2.6 Loss of NUAK1 increases NF-κB signaling in EOC spheroids.

(A) Top 10 gene sets up-regulated in OVCAR8 *NUAK1*-KO spheroids compared to OVCAR8 parental spheroids. Gene sets were derived from GSEA Hallmark database and Curated Canonical database. Normalized enrichment score (NES) is presented. (B) TNF α signaling through NF-κB enrichment plot is shown. Vertical black lines represent the position of genes in the ordered data set. Green line represents the enrichment score curve. Normalized enrichment score (NES), nominal p-value, and FDR are presented. (C) Immunoblot analysis showing p-p65 (S536) and p65 in OVCAR8 *NUAK1*-KO and OVCAR8 parental cells cultured on monolayer conditions (adh) or in suspension (sph). Tubulin was used as a loading control. Densitometric analysis showing the pixel intensity volume for p-p65 relative to tubulin. Analysis was performed using a Two-tailed Student's *t*-test (NS= not significant; *, p<0.05). (n=3) (D) Immunoblot analysis showing p-p65 (S536) and p65 in the nuclear and cytoplasmic fractions from OVCAR8 *NUAK1*-KO and OVCAR8 parental cells cultured on monolayer conditions (adh) or in suspension (sph). Tubulin was used as a loading control for the cytoplasmic fraction. Lamin A/C was used as a loading control for the nuclear fraction. Densitometric analysis showing the pixel intensity volume for nuclear p-p65 and nuclear p65 relative to lamin A/C. (n=2) (E) RT-qPCR analysis to validate core enriched genes from the TNF α signaling through NF-κB signature. Fold change in mRNA is presented for OVCAR8 parental and OVAR8 *NUAK1*-KO 24h spheroids. Statistical analysis was performed using two-tailed Student's *t*-test (**, p<0.01; ***, p < 0.001; ****, p<0.0001). (n=3)

Furthermore, several anti-apoptotic genes were significantly increased in *NUAK1*-KO spheroids, including *BCL2A1* and *BIRC3* (Figure 2.6E). Therefore, NF-κB signaling is up-regulated in *NUAK1*-KO spheroids and may represent a means for increased cell viability in EOC spheroids lacking NUAK1.

2.4 Discussion

Advanced-stage EOC is characterized by the accumulation of ascites fluid in the peritoneal cavity (Al Habyan et al., 2018; Sodek et al., 2009). Ascites contains spheroids

which are a key mediator of peritoneal metastasis and can facilitate chemoresistance (Al Habyan et al., 2018; Desoize & Jardillier, 2000; Lengyel et al., 2014; Pease et al., 2012). Our group previously reported that the master kinase LKB1 is required for efficient ovarian cancer metastasis (Buensuceso et al., 2018; Peart et al., 2015). To elucidate the downstream target eliciting the pro-metastatic function of LKB1, we completed a multiplex inhibitor beads-mass spectrometry analysis and identified NUAK1 as a top candidate substrate. NUAK1 is differentially expressed in quiescent spheroids compared to proliferative monolayer cells and this is regulated by lysosome degradation and the UPS. Furthermore, NUAK1 increases EOC cell adhesion and promotes spheroid integrity. Using transcriptome analysis with GSEA and subsequent validation experiments we demonstrated that NUAK1 regulates spheroid formation by controlling fibronectin deposition in spheroids. Thus, we propose that the LKB1 target NUAK1 has tumor-promoting functions by facilitating spheroid integrity through matrix deposition.

LKB1 is known as a master kinase in the literature due to its ability to regulate AMPK as well as 12 AMPK-related kinases (Shackelford & Shaw, 2009). Through these substrates, LKB1 can have multiple functions related to cell polarity, metabolism and growth. While LKB1 is commonly known as a tumor suppressor, there is a growing body of literature implicating it as having pro-metastatic roles under certain contexts (Lee et al., 2015; Shackelford et al., 2013; Shackelford & Shaw, 2009). In fact, we previously demonstrated that LKB1 is required for EOC spheroid viability and metastasis in *in vivo* xenograft models (Buensuceso et al., 2018; Peart et al., 2015). Because LKB1 can have a broad range of functions it is critical to elucidate its downstream targets to identify specific substrates that could serve as more suitable therapeutic targets. Most of the literature examining targets of LKB1 have focused on AMPK, which is a regulator of metabolic stress (Shackelford & Shaw, 2009). However, our prior work indicated that in EOC, LKB1 elicits its tumorigenic functions through AMPK-independent signalling (Buensuceso et al., 2018; Peart et al., 2015). Thus to determine the critical target for LKB1 in EOC, we completed multiplexed kinase inhibitor bead-mass spectrometry and identified the ARK NUAK1 as a top candidate substrate. To confirm these findings, we showed that LKB1 regulates the phosphorylation and expression of NUAK1 in EOC

adherent cells and spheroids. We found that early in spheroid formation NUAK1 is highly expressed and this correlates with the levels of phosphorylated-LKB1. However, later during spheroid formation NUAK1 levels decrease but are still expressed at detectable levels. This down-regulation of NUAK1 was observed in several HGSOC established cell lines and patient-derived ascites cells cultured as spheroids. We showed that lysosome degradation and the UPS both contribute to the down-regulation of NUAK1 in spheroids. Previous studies have shown that the UPS plays a role in regulating NUAK1. NUAK1 can be phosphorylated by cyclin-dependent kinases and polo kinase which lead to NUAK1 binding to the SCF^{BTrp} E3 ligase, its ubiquitination and subsequent degradation (Banerjee et al., 2014). NUAK1 was also shown to be ubiquitinated by unique Lys29 and or Lys33 linkages which block phosphorylation and activation by LKB1 (Al-Hakim et al., 2008). USP9X can bind to NUAK1 and cleave the polyubiquitin modification, allowing for LKB1 phosphorylation and activation. In this report, we show that USP9X also regulates NUAK1 expression in EOC. Therefore, we found that NUAK1 is a target of LKB1 in EOC and shows differential expression between proliferative adherent cells and quiescent spheroids.

Multiple studies have provided evidence that NUAK1 can have tumor-promoting functions. In human hepatoma cells, NUAK1 blocked cell death by inhibiting caspase 8 (Suzuki et al., 2003). Along with increasing cell survival through inhibiting apoptosis, NUAK1 can induce the S-phase in the cell cycle and increase cell proliferation (Banerjee et al., 2014). Several reports have shown that NUAK1 can also enhance cancer survival through supporting metabolic homeostasis (Liu et al., 2012). In tumors overexpressing *myc*, NUAK1 reduces metabolic stress by inhibiting mTORC1 and sustaining glutamine metabolism. A tumor-promoting role for NUAK1 is strengthened by studies showing that elevated levels of NUAK1 correlate with poor prognosis (Phippen et al., 2016; Port et al., 2018). High NUAK1 transcript levels in serous ovarian cancer patients was associated with lower progression free survival and lower overall survival (Phippen et al., 2016). There was also an increased risk for diagnosis at an advanced stage and residual disease after cytoreductive surgery. The molecular basis underlying the poor prognosis in EOC had not previously been elucidated. Herin, we found that NUAK1 regulates EOC cell

adhesion and the formation of spheroids, which are the key mediators of metastasis in ovarian cancer.

In the context of EOC metastasis, cell adhesion is critical as cancer cells aggregate through cell-ECM interactions to form spheroids which then spread through the peritoneal cavity (Casey et al., 2001). Previous research has suggested NUAK1 plays a role in cell adhesion due to its roles in promoting EMT and invasion. In ovarian cancer cells, NUAK1 increases EMT and migration of cells by inhibiting miR-1181 (Zhang et al., 2015). Furthermore, NUAK1 overexpression in a pancreatic cancer mouse model increased *in vivo* metastasis (Kusakai et al., 2004). Mechanistically, NUAK1 has been shown to promote cell detachment by controlling the myosin phosphatase complex in HEK293 and MEF cells (Zagórska et al., 2010). Moreover, in colorectal cancer, loss of NUAK1 reduced tumor-initiating capacity because spheroids appeared smaller in size and were less abundant. To identify the molecular basis for this phenotype, the authors proposed that NUAK1 protects tumors from oxidative stress through nuclear translocation of Nrf2 (Port et al., 2018). In our study, we show that loss of NUAK1 impairs single cell adhesion and spheroid formation as spheroids appeared less compact. By examining spheroid formation in real-time *NUAK1*-KO-GFP spheroids showed decreased integrity with an accumulation of dead cells around the periphery. We propose that in EOC the ability of NUAK1 to control adhesion molecules is likely the primary mechanism mediating EOC spheroid formation. Two of the top signatures up-regulated in OVCAR8 parental spheroids compared to OVCAR8 *NUAK1*-KO spheroids were related to cell attachment. Interestingly, in the Nrf2 study described above they also observed several cell adhesion pathways using the Metacore GeneGO analysis (Port et al., 2018). These cell adhesion pathway had a higher ranking than the Nrf2 oxidative stress response pathway yet were not pursued in that study. We observed FN1 as the most differentially expressed gene in OVCAR8 *NUAK1*-KO spheroids with a 745-fold decrease. Importantly, the addition of soluble fibronectin also completely restored the native phenotype in *NUAK1*-KO spheroids. Altogether, we have elucidated a novel mechanism of NUAK1 in promoting EOC cell adhesion and spheroid compaction through fibronectin matrix production.

Our GSEA indicated a cell attachment signature that was enriched in OVCAR8 spheroids compared to OVCAR8 *NUAK1*-KO spheroids. Multiple adhesion molecules were identified, including *FN*, *L1CAM*, *ITG β 8*, *ITG β 5*, *THBS1*, and *F11R* (Table 2.7). This suggests that NUAK1 regulates a network of adhesion molecules. We focused our validation experiments on fibronectin because it demonstrated the greatest differential expression and prior studies have shown it plays a key role in spheroid formation. Previous work in OVCAR5 cells showed that fibronectin mediates the formation of spheroids (Casey et al., 2001). The authors showed that the fibronectin receptor $\alpha 5\beta 1$ integrin also contributes to spheroid integrity. Interestingly, the canonical fibronectin receptor subunits were not present in our transcriptome analysis with only the *ITG β 5* and *ITG β 8* subunits being differentially expressed (Table 2.4). A prior study showed that *ITG β 8* may interact with fibronectin, however this interaction has only been shown in chick sensory neurons and the alpha subunit has not yet been elucidated (Venstrom & Reichardt, 1995). In addition, *ITG β 8* had a relatively small fold change of 10, while *FNI* has a fold change of 745, suggesting that regulation of matrix expression is the principal mechanism by which NUAK1 is controlling cell adhesion in spheroids. Another study similarly demonstrated the importance of fibronectin in spheroids generated from fallopian tube epithelial cells (FTE) which represent the putative cell of origin in HGSOC (Iwanicki et al., 2016; Labidi-Galy et al., 2017). FTE cells with *p53* mutations have an increased propensity to aggregate into spheroids due to autocrine fibronectin deposition. In addition to *FNI*, *L1CAM* was differentially expressed in our analysis with a fold change of 10. Indeed, L1CAM was previously shown to promote OVCAR8 and FTE spheroid formation (Doberstein et al., 2018). In FTE spheroids, L1CAM up-regulated expression of integrins and fibronectin to facilitate spheroid formation. In our study, we similarly showed an interesting relationship between L1CAM and fibronectin expression. In OVCAR8 *NUAK1*-KO spheroids there was no detectable levels of either L1CAM or fibronectin expression. Therefore, we may have identified a novel signaling pathway controlling fibronectin and its molecules that mediates the formation of EOC spheroids.

In conclusion, we have identified NUAK1 as a key target of LKB1 in EOC. We show

that NUAK1 has pro-metastatic functions because it increases EOC cell adhesion and promotes spheroid integrity. Mechanistically, NUAK1 controls the deposition of fibronectin in spheroids to facilitate spheroid formation. Altogether, we provide evidence that the LKB1 substrate NUAK1 could serve as a potential therapeutic target in ovarian cancer metastasis.

2.5 References

- Ahmed, N., & Stenvers, K. L. (2013). Getting to Know Ovarian Cancer Ascites: Opportunities for Targeted Therapy-Based Translational Research. *Frontiers in Oncology*. <https://doi.org/10.3389/fonc.2013.00256>
- Al-Hakim, A. K., Zagorska, A., Chapman, L., Deak, M., Peggie, M., & Alessi, D. R. (2008). Control of AMPK-related kinases by USP9X and atypical Lys 29 /Lys 33 - linked polyubiquitin chains . *Biochemical Journal*. <https://doi.org/10.1042/bj20080067>
- Al Habyan, S., Kalos, C., Szymborski, J., & McCaffrey, L. (2018). Multicellular detachment generates metastatic spheroids during intra-abdominal dissemination in epithelial ovarian cancer. *Oncogene*. <https://doi.org/10.1038/s41388-018-0317-x>
- Altevogt, P., Doberstein, K., & Fogel, M. (2016). L1CAM in human cancer. *International Journal of Cancer*. <https://doi.org/10.1002/ijc.29658>
- American College of Obstetricians and Gynecologists. (2002). ACOG Committee Opinion Number 280: The Role of the Generalist Obstetrician-Gynecologist in the Early Detection of Ovarian Cancer. *Obstetrics & Gynecology*, 100(6), 1413–1416. [https://doi.org/10.1016/s0029-7844\(02\)02630-3](https://doi.org/10.1016/s0029-7844(02)02630-3)
- Banerjee, Sourav, Zagórska, A., Deak, M., Campbell, D. G., Prescott, A. R., & Alessi, D. R. (2014). Interplay between Polo kinase, LKB1-activated NUAK1 kinase, PP1 β MYPT1 phosphatase complex and the SCF β TrCP E3 ubiquitin ligase . *Biochemical Journal*. <https://doi.org/10.1042/bj20140408>
- Banerjee, Susana, Kaye, S. B., & Ashworth, A. (2010). Making the best of PARP inhibitors in ovarian cancer. *Nature Reviews Clinical Oncology*. <https://doi.org/10.1038/nrclinonc.2010.116>
- Bast, R. C., Hennessy, B., & Mills, G. B. (2009). The biology of ovarian cancer: New opportunities for translation. *Nature Reviews Cancer*. <https://doi.org/10.1038/nrc2644>
- Beer, S., Oleszewski, M., Gutwein, P., Geiger, C., & Altevogt, P. (1999). Metalloproteinase-mediated release of the ectodomain of L1 adhesion molecule. *Journal of Cell Science*.
- Beggs, A. D., Latchford, A. R., Vasen, H. F. A., Moslein, G., Alonso, A., Aretz, S., ... Hodgson, S. V. (2010). Peutz - Jeghers syndrome: A systematic review and recommendations for management. *Gut*. <https://doi.org/10.1136/gut.2009.198499>
- Bell, D., Berchuck, A., Birrer, M., Chien, J., Cramer, D. W., Dao, F., ... Thomson, E. (2011). Integrated genomic analyses of ovarian carcinoma. *Nature*. <https://doi.org/10.1038/nature10166>
- Bondong, S., Kiefel, H., Hielscher, T., Zeimet, A. G., Zeillinger, R., Pils, D., ... Altevogt, P. (2012). Prognostic significance of L1CAM in ovarian cancer and its role in constitutive NF- κ B activation. *Annals of Oncology*. <https://doi.org/10.1093/annonc/mdr568>

- Bonnans, C., Chou, J., & Werb, Z. (2014). Remodelling the extracellular matrix in development and disease. *Nature Reviews. Molecular Cell Biology*.
<https://doi.org/10.1038/nrm3904>
- Bowtell, D. D., Böhm, S., Ahmed, A. A., Aspuria, P.-J., Bast, R. C., Beral, V., ...
 Balkwill, F. R. (2015a). Rethinking ovarian cancer II: reducing mortality from high-grade serous ovarian cancer. *Nature Reviews. Cancer*.
<https://doi.org/10.1038/nrc4019>
- Bowtell, D. D., Böhm, S., Ahmed, A. A., Aspuria, P.-J., Bast, R. C., Beral, V., ...
 Balkwill, F. R. (2015b). Rethinking ovarian cancer II: reducing mortality from high-grade serous ovarian cancer. *Nature Reviews Cancer*, 15(11), 668–679.
<https://doi.org/10.1038/nrc4019>
- Bright, N. J., Thornton, C., & Carling, D. (2009). The regulation and function of mammalian AMPK-related kinases. *Acta Physiologica*.
<https://doi.org/10.1111/j.1748-1716.2009.01971.x>
- Buensuceso, A., Valdes, Y. R., Figueredo, R., DiMatta, G. E., & Shepherd, T. G. (2018). *Abstract A12: The metabolic stress mediator LKB1 is required for ovarian cancer metastasis*. <https://doi.org/10.1158/1557-3265.ovca17-a12>
- Casey, R. C., Burleson, K. M., Skubitz, K. M., Pambuccian, S. E., Oegema, T. R., Ruff, L. E., & Skubitz, A. P. N. (2001). $\beta 1$ -integrins regulate the formation and adhesion of ovarian carcinoma multicellular spheroids. *American Journal of Pathology*.
[https://doi.org/10.1016/S0002-9440\(10\)63058-1](https://doi.org/10.1016/S0002-9440(10)63058-1)
- Cho, A., Howell, V. M., & Colvin, E. K. (2015). The Extracellular Matrix in Epithelial Ovarian Cancer – A Piece of a Puzzle. *Frontiers in Oncology*.
<https://doi.org/10.3389/fonc.2015.00245>
- Coleman, R. L., Monk, B. J., Sood, A. K., & Herzog, T. J. (2013). Latest research and treatment of advanced-stage epithelial ovarian cancer. *Nature Reviews Clinical Oncology*. <https://doi.org/10.1038/nrclinonc.2013.5>
- Correa, R. J. M., Valdes, Y. R., Peart, T. M., Fazio, E. N., Bertrand, M., McGee, J., ...
 Shepherd, T. G. (2014). Combination of AKT inhibition with autophagy blockade effectively reduces ascites-derived ovarian cancer cell viability. *Carcinogenesis*.
<https://doi.org/10.1093/carcin/bgu049>
- Correa, R. J. M., Valdes, Y. R., Shepherd, T. G., & DiMatta, G. E. (2015). Beclin-1 expression is retained in high-grade serous ovarian cancer yet is not essential for autophagy induction in vitro. *Journal of Ovarian Research*.
<https://doi.org/10.1186/s13048-015-0182-y>
- Desoize, B., & Jardillier, J. C. (2000). Multicellular resistance: A paradigm for clinical resistance? *Critical Reviews in Oncology/Hematology*.
[https://doi.org/10.1016/S1040-8428\(00\)00086-X](https://doi.org/10.1016/S1040-8428(00)00086-X)
- Doberstein, K., Spivak, R., Feng, Y., Stuckelberger, S., Mills, G. B., Devins, K. M., ...
 Affiliations. (2018). Fallopian tube precursor lesions of serous ovarian carcinoma require L1CAM for dissemination and metastasis. *BioRxiv Preprint First*.

- <https://doi.org/10.1101/270785>
- Domcke, S., Sinha, R., Levine, D. A., Sander, C., & Schultz, N. (2013). Evaluating cell lines as tumour models by comparison of genomic profiles. *Nature Communications*. <https://doi.org/10.1038/ncomms3126>
- Duncan, J. S., Whittle, M. C., Nakamura, K., Abell, A. N., Midland, A. A., Zawistowski, J. S., ... Johnson, G. L. (2012). Dynamic reprogramming of the kinaseome in response to targeted MEK inhibition in triple-negative breast cancer. *Cell*. <https://doi.org/10.1016/j.cell.2012.02.053>
- Emmerich, C. H., & Cohen, P. (2015). Optimising methods for the preservation, capture and identification of ubiquitin chains and ubiquitylated proteins by immunoblotting. *Biochemical and Biophysical Research Communications*. <https://doi.org/10.1016/j.bbrc.2015.08.109>
- Emmings, E., Mullany, S., Chang, Z., Landen, C. N., Linder, S., & Bazzaro, M. (2019). Targeting Mitochondria for Treatment of Chemoresistant Ovarian Cancer. *International Journal of Molecular Sciences*, 20(1). <https://doi.org/10.3390/ijms20010229>
- Espín-Palazón, R., & Traver, D. (2016). The NF-κB family: Key players during embryonic development and HSC emergence. *Experimental Hematology*. <https://doi.org/10.1016/j.exphem.2016.03.010>
- F Ann Ran, Patrick D Hsu, Jason Wright, Vineeta Agarwala, D. A. S. & F. Z. (2013). Genome engineering using crispr-cas9 system. *Nature Protocols*, 8(11), 2281–2308. https://doi.org/10.1007/978-1-4939-1862-1_10
- Franke, F. E., Von Georgi, R., Zygmunt, M., & Münstedt, K. (2003). Association between Fibronectin Expression and Prognosis in Ovarian Carcinoma. *Anticancer Research*.
- Gill, R. K., Yang, S. H., Meerzaman, D., Mechanic, L. E., Bowman, E. D., Jeon, H. S., ... Jen, J. (2011). Frequent homozygous deletion of the LKB1/STK11 gene in non-small cell lung cancer. *Oncogene*. <https://doi.org/10.1038/onc.2011.98>
- Goff, B. A. (2012). Advanced ovarian cancer: What should be the standard of care? *Journal of Gynecologic Oncology*. <https://doi.org/10.3802/jgo.2013.24.1.83>
- Gopal, S., Veracini, L., Grall, D., Butori, C., Schaub, S., Audebert, S., ... Van Obberghen-Schilling, E. (2017). Fibronectin-guided migration of carcinoma collectives. *Nature Communications*. <https://doi.org/10.1038/ncomms14105>
- Guldberg, P., Straten, P. T., Ahrenkiel, V., Seremet, T., Kirkin, A. F., & Zeuthen, J. (1999). Somatic mutation of the Peutz-Jeghers syndrome gene, LKB1/STK11, in malignant melanoma. *Oncogene*. <https://doi.org/10.1038/sj.onc.1202486>
- Hardie, D. G., & Alessi, D. R. (2013). LKB1 and AMPK and the cancer-metabolism link - ten years after. *BMC Biology*. <https://doi.org/10.1186/1741-7007-11-36>
- Hemminki, a, Avizienyte, E., Roth, S., Loukola, A., Aaltonen, L. a, Järvinen, H., & de la Chapelle, A. (1998). A serine/threonine kinase gene defective in Peutz-Jeghers

- syndrome. *Nature*, 391(January), 184–187. Retrieved from <http://www.ncbi.nlm.nih.gov/pubmed/11524750>
- Hernandez, L., Kim, M. K., Lyle, L. T., Bunch, K. P., House, C. D., Ning, F., ... Annunziata, C. M. (2016). Characterization of ovarian cancer cell lines as *in vivo* models for preclinical studies. *Gynecologic Oncology*. <https://doi.org/10.1016/j.ygyno.2016.05.028>
- Hew, K. E., Miller, P. C., El-Ashry, D., Sun, J., Besser, A. H., Ince, T. A., ... Simpkins, F. (2016). MAPK activation predicts poor outcome and the MEK inhibitor, selumetinib, reverses antiestrogen resistance in ER-positive high-grade serous ovarian cancer. *Clinical Cancer Research*. <https://doi.org/10.1158/1078-0432.CCR-15-0534>
- Hou, X., Liu, J.-E., Liu, W., Liu, C.-Y., Liu, Z.-Y., & Sun, Z.-Y. (2011). A new role of NUAK1: directly phosphorylating p53 and regulating cell proliferation. *Oncogene*. <https://doi.org/10.1038/onc.2011.19>
- House, C. D., Jordan, E., Hernandez, L., Ozaki, M., James, J. M., Kim, M., ... Annunziata, C. M. (2017). NFkB promotes ovarian tumorigenesis via classical pathways that support proliferative cancer cells and alternative pathways that support ALDH β cancer stem-like cells. *Cancer Research*. <https://doi.org/10.1158/0008-5472.CAN-17-0366>
- Humbert, N., Navaratnam, N., Augert, A., Da Costa, M., Martien, S., Wang, J., ... Bernard, D. (2010). Regulation of ploidy and senescence by the AMPK-related kinase NUAK1. *EMBO Journal*. <https://doi.org/10.1038/emboj.2009.342>
- Iwanicki, M. P., Chen, H.-Y., Iavarone, C., Zervantonakis, I. K., Muranen, T., Novak, M., ... Brugge, J. S. (2016). Mutant p53 regulates ovarian cancer transformed phenotypes through autocrine matrix deposition. *JCI Insight*. <https://doi.org/10.1172/jci.insight.86829>
- Johansson, S., Svineng, G., Wennerberg, K., Armulik, A., & Lohikangas, L. (1997). Fibronectin-integrin interactions. *Frontiers in Bioscience : A Journal and Virtual Library*.
- Karst, A. M., & Drapkin, R. (2009). Ovarian Cancer Pathogenesis: A Model in Evolution. *Journal of Oncology*. <https://doi.org/10.1155/2010/932371>
- Kedves, A. T., Gleim, S., Liang, X., Bonal, D. M., Sigoillot, F., Harbinski, F., ... Forrester, W. C. (2017). Recurrent ubiquitin B silencing in gynecological cancers establishes dependence on ubiquitin C. *Journal of Clinical Investigation*. <https://doi.org/10.1172/JCI92914>
- Keller, A., Nesvizhskii, A. I., Kolker, E., & Aebersold, R. (2002). Empirical statistical model to estimate the accuracy of peptide identifications made by MS/MS and database search. *Analytical Chemistry*, 74(20), 5383–5392. <https://doi.org/10.1021/ac025747h>
- Kenny, H. A., Chiang, C. Y., White, E. A., Schryver, E. M., Habis, M., Romero, I. L., ... Lengyel, E. (2014). Mesothelial cells promote early Ovarian cancer metastasis

- through fibronectin secretion. *Journal of Clinical Investigation*. <https://doi.org/10.1172/JCI74778>
- Kusakai, G., Suzuki, A., Ogura, T., Kaminishi, M., & Esumi, H. (2004). Strong association of ARK5 with tumor invasion and metastasis. *Journal of Experimental & Clinical Cancer Research : CR*.
- Labidi-Galy, S. I., Papp, E., Hallberg, D., Niknafs, N., Adleff, V., Noe, M., ... Velculescu, V. E. (2017). High grade serous ovarian carcinomas originate in the fallopian tube. *Nature Communications*. <https://doi.org/10.1038/s41467-017-00962-1>
- Lee, J., Rhee, M. H., Kim, E., & Cho, J. Y. (2012). BAY 11-7082 is a broad-spectrum inhibitor with anti-inflammatory activity against multiple targets. *Mediators of Inflammation*. <https://doi.org/10.1155/2012/416036>
- Lee, S. W., Li, C. F., Jin, G., Cai, Z., Han, F., Chan, C. H., ... Lin, H. K. (2015). Skp2-Dependent Ubiquitination and Activation of LKB1 Is Essential for Cancer Cell Survival under Energy Stress. *Molecular Cell*. <https://doi.org/10.1016/j.molcel.2015.01.015>
- Lengyel, E., Burdette, J. E., Kenny, H. A., Matei, D., Pilrose, J., Haluska, P., ... Stack, M. S. (2014). Epithelial ovarian cancer experimental models. *Oncogene*. <https://doi.org/10.1038/onc.2013.321>
- Leung, B. M., Lesher-Perez, S. C., Matsuoka, T., Moraes, C., & Takayama, S. (2015). Media additives to promote spheroid circularity and compactness in hanging drop platform. *Biomaterials Science*. <https://doi.org/10.1039/c4bm00319e>
- Lheureux, S., Gourley, C., Vergote, I., & Oza, A. M. (2019). Epithelial ovarian cancer. *The Lancet*. [https://doi.org/10.1016/S0140-6736\(18\)32552-2](https://doi.org/10.1016/S0140-6736(18)32552-2)
- Lilienbaum, A. (2013). Relationship between the proteasomal system and autophagy. *International Journal of Biochemistry and Molecular Biology*.
- Lin, R. Z., Chou, L. F., Chien, C. C. M., & Chang, H. Y. (2006). Dynamic analysis of hepatoma spheroid formation: Roles of E-cadherin and β 1-integrin. *Cell and Tissue Research*. <https://doi.org/10.1007/s00441-005-0148-2>
- Linke, R., Babic, R., & Gossner, W. (1988). Fibrin-Fibronectin Compounds in Human Ovarian Tumor Ascites and Their Possible Relation to the Tumor Stroma. *Cancer Research*.
- Liu, F., Yang, X., Geng, M., & Huang, M. (2018). Targeting ERK, an Achilles' Heel of the MAPK pathway, in cancer therapy. *Acta Pharmaceutica Sinica B*. <https://doi.org/10.1016/j.apsb.2018.01.008>
- Liu, G., Zhang, J., Larsen, B., Stark, C., Breitkreutz, A., Lin, Z.-Y., ... Gingras, A.-C. (2010). ProHits: integrated software for mass spectrometry-based interaction proteomics. *Nature Biotechnology*. <https://doi.org/10.1038/nbt1010-1015>
- Liu, L., Ulbrich, J., Müller, J., Wüstefeld, T., Aeberhard, L., Kress, T. R., ... Murphy, D. J. (2012). Deregulated MYC expression induces dependence upon AMPK-related

- kinase 5. *Nature*. <https://doi.org/10.1038/nature10927>
- Livak, K. J., & Schmittgen, T. D. (2001). Analysis of relative gene expression data using real-time quantitative PCR and the 2- $\Delta\Delta CT$ method. *Methods*. <https://doi.org/10.1006/meth.2001.1262>
- Lizcano, J. M., Göransson, O., Toth, R., Deak, M., Morrice, N. A., Boudeau, J., ... Alessi, D. R. (2004). LKB1 is a master kinase that activates 13 kinases of the AMPK subfamily, including MARK/PAR-1. *EMBO Journal*. <https://doi.org/10.1038/sj.emboj.7600110>
- Lu, Z., Luo, R. Z., Lu, Y., Zhang, X., Yu, Q., Khare, S., ... Bast, R. C. (2008). The tumor suppressor gene ARHI regulates autophagy and tumor dormancy in human ovarian cancer cells. *Journal of Clinical Investigation*. <https://doi.org/10.1172/JCI35512>
- MacDonald, J., Ramos-Valdes, Y., Perampalam, P., Litovchick, L., DiMattia, G. E., & Dick, F. A. (2016). A Systematic Analysis of Negative Growth Control Implicates the DREAM Complex in Cancer Cell Dormancy. *Molecular Cancer Research*. <https://doi.org/10.1158/1541-7786.mcr-16-0323-t>
- Manning, G., Whyte, D. B., Martinez, R., Hunter, T., & Sudarsanam, S. (2002). The protein kinase complement of the human genome. *Science*. <https://doi.org/10.1126/science.1075762>
- Martin, L. P., Hamilton, T. C., & Schilder, R. J. (2008). Platinum resistance: The role of DNA repair pathways. *Clinical Cancer Research*. <https://doi.org/10.1158/1078-0432.CCR-07-2238>
- Matulonis, U. A. (2018). Management of newly diagnosed or recurrent ovarian cancer. *Clinical Advances in Hematology and Oncology*.
- Monteverde, T., Tait-Mulder, J., Hedley, A., Knight, J. R., Sansom, O. J., & Murphy, D. J. (2018). Calcium signalling links MYC to NUAK1. *Oncogene*. <https://doi.org/10.1038/onc.2017.394>
- Nagase, T., Kikuno, R., Hattori, A., Kondo, Y., Okumura, K., & Ohara, O. (2000). Prediction of the coding sequences of unidentified human genes. XIX. The complete sequences of 100 new cDNA clones from brain which code for large proteins in vitro. *DNA Research : An International Journal for Rapid Publication of Reports on Genes and Genomes*. <https://doi.org/10.1093/dnares/7.6.347>
- Nakamura, K., Nakayama, K., Ishikawa, N., Ishikawa, M., Sultana, R., Kiyono, T., & Kyo, S. (2017). Reconstitution of high-grade serous ovarian carcinoma from primary fallopian tube secretory epithelial cells. *Oncotarget*, 9(16), 12609–12619. <https://doi.org/10.18632/oncotarget.23035>
- Nesvizhskii, A. I., Keller, A., Kolker, E., & Aebersold, R. (2003). A statistical model for identifying proteins by tandem mass spectrometry. *Analytical Chemistry*.
- Pankov, R., & Yamada, K. M. (2002). Fibronectin at a glance. *Journal of Cell Science*, 115(Pt 20), 3861–3863. <https://doi.org/10.1242/jcs.00059>
- Peart, T., Valdes, Y. R., Correa, R. J. M., Fazio, E., Bertrand, M., McGee, J., ...

- Shepherd, T. G. (2015). Intact LKB1 activity is required for survival of dormant ovarian cancer spheroids. *Oncotarget*. <https://doi.org/10.18632/oncotarget.4211>
- Pease, J. C., Brewer, M., & Tirnauer, J. S. (2012). Spontaneous spheroid budding from monolayers: a potential contribution to ovarian cancer dissemination. *Biology Open*. <https://doi.org/10.1242/bio.2012653>
- Perumal, D., Leshchenko, V. V., Kuo, P. Y., Jiang, Z., Divakar, S. K. A., Jay Cho, H., ... Parekh, S. (2016). Dual targeting of CDK4 and ARK5 using a novel kinase inhibitor ON123300 exerts potent anticancer activity against multiple myeloma. *Cancer Research*. <https://doi.org/10.1158/0008-5472.CAN-15-2934>
- Phippen, N. T., Bateman, N. W., Wang, G., Conrads, K. A., Ao, W., Teng, P., ... Conrads, T. P. (2016). NUAK1 (ARK5) Is Associated with Poor Prognosis in Ovarian Cancer. *Frontiers in Oncology*. <https://doi.org/10.3389/fonc.2016.00213>
- Port, J., Muthalagu, N., Raja, M., Ceteci, F., Monteverde, T., Kruspiig, B., ... Murphy, D. J. (2018). Colorectal tumors require NUAK1 for protection from oxidative stress. *Cancer Discovery*. <https://doi.org/10.1158/2159-8290.CD-17-0533>
- Roett, M. A., & Evans, P. (2009). Ovarian cancer: An overview. *American Family Physician*.
- Sabio, G., & Davis, R. J. (2014). TNF and MAP kinase signalling pathways. *Seminars in Immunology*. <https://doi.org/10.1016/j.smim.2014.02.009>
- Sant, S., & Johnston, P. A. (2017). The production of 3D tumor spheroids for cancer drug discovery. *Drug Discovery Today: Technologies*. <https://doi.org/10.1016/j.ddtec.2017.03.002>
- Schauer, I. G., Zhang, J., Xing, Z., Guo, X., Mercado-Uribe, I., Sood, A. K., ... Liu, J. (2015). Interleukin-1 β Promotes Ovarian Tumorigenesis through a p53/NF- κ B-Mediated Inflammatory Response in Stromal Fibroblasts. *Neoplasia*, 15(4), 409-IN18. <https://doi.org/10.1593/neo.121228>
- Scherer, S. E., Muzny, D. M., Buhay, C. J., Chen, R., Cree, A., Ding, Y., ... Gibbs, R. A. (2006). The finished DNA sequence of human chromosome 12. *Nature*. <https://doi.org/10.1038/nature04569>
- Schiller, H. B., & Fässler, R. (2013). Mechanosensitivity and compositional dynamics of cell-matrix adhesions. *EMBO Reports*. <https://doi.org/10.1038/embor.2013.49>
- Shackelford, D. B., Abt, E., Gerken, L., Vasquez, D. S., Seki, A., Leblanc, M., ... Shaw, R. J. (2013). LKB1 Inactivation Dictates Therapeutic Response of Non-Small Cell Lung Cancer to the Metabolism Drug Phenformin. *Cancer Cell*. <https://doi.org/10.1016/j.ccr.2012.12.008>
- Shackelford, D. B., & Shaw, R. J. (2009). The LKB1-AMPK pathway: Metabolism and growth control in tumour suppression. *Nature Reviews Cancer*. <https://doi.org/10.1038/nrc2676>
- Shepherd, T. G., Thériault, B. L., Campbell, E. J., & Nachtigal, M. W. (2007). Primary culture of ovarian surface epithelial cells and ascites-derived ovarian cancer cells

- from patients. *Nature Protocols*. <https://doi.org/10.1038/nprot.2006.328>
- Shteynberg, D., Deutsch, E. W., Lam, H., Eng, J. K., Sun, Z., Tasman, N., ... Nesvizhskii, A. I. (2011). iProphet: Multi-level Integrative Analysis of Shotgun Proteomic Data Improves Peptide and Protein Identification Rates and Error Estimates. *Molecular & Cellular Proteomics*. <https://doi.org/10.1074/mcp.M111.007690>
- Siegel, R. L., Miller, K. D., & Jemal, A. (2019). Cancer statistics, 2019. *CA: A Cancer Journal for Clinicians*. <https://doi.org/10.3322/caac.21551>
- Sodek, K. L., Murphy, K. J., Brown, T. J., & Ringuette, M. J. (2012). Cell-cell and cell-matrix dynamics in intraperitoneal cancer metastasis. *Cancer and Metastasis Reviews*. <https://doi.org/10.1007/s10555-012-9351-2>
- Sodek, K. L., Ringuette, M. J., & Brown, T. J. (2009). Compact spheroid formation by ovarian cancer cells is associated with contractile behavior and an invasive phenotype. *International Journal of Cancer*. <https://doi.org/10.1002/ijc.24188>
- Stuhlmiller, T. J., Miller, S. M., Zawistowski, J. S., Nakamura, K., Beltran, A. S., Duncan, J. S., ... Johnson, G. L. (2015). Inhibition of lapatinib-induced kinase reprogramming in ERBB2-positive breast cancer by targeting BET family bromodomains. *Cell Reports*. <https://doi.org/10.1016/j.celrep.2015.03.037>
- Subramanian, A., Tamayo, P., Mootha, V. K., Mukherjee, S., Ebert, B. L., Gillette, M. A., ... Mesirov, J. P. (2005). Gene set enrichment analysis: a knowledge-based approach for interpreting genome-wide expression profiles. *Proceedings of the National Academy of Sciences of the United States of America*. <https://doi.org/10.1073/pnas.0506580102>
- Suzuki, A., Lu, J., Kusakai, G. -i., Kishimoto, A., Ogura, T., & Esumi, H. (2004). ARK5 Is a Tumor Invasion-Associated Factor Downstream of Akt Signaling. *Molecular and Cellular Biology*. <https://doi.org/10.1128/MCB.24.8.3526-3535.2004>
- Suzuki, Atsushi, Kusakai, G. I., Kishimoto, A., Lu, J., Ogura, T., Lavin, M. F., & Esumi, H. (2003). Identification of a novel protein kinase mediating Akt survival signaling to the ATM protein. *Journal of Biological Chemistry*. <https://doi.org/10.1074/jbc.M206025200>
- Teo, G., Kim, S., Tsou, C. C., Collins, B., Gingras, A. C., Nesvizhskii, A. I., & Choi, H. (2015). MapDIA: Preprocessing and statistical analysis of quantitative proteomics data from data independent acquisition mass spectrometry. *Journal of Proteomics*, 129, 108–120. <https://doi.org/10.1016/j.jprot.2015.09.013>
- Tomida, J., Kitao, H., Kinoshita, E., & Takata, M. (2008). Detection of phosphorylation on large proteins by western blotting using Phos-tag containing gel. *Protocol Exchange*. <https://doi.org/10.1038/nprot.2008.232>
- Tsou, C. C., Avtonomov, D., Larsen, B., Tucholska, M., Choi, H., Gingras, A. C., & Nesvizhskii, A. I. (2015). DIA-Umpire: Comprehensive computational framework for data-independent acquisition proteomics. *Nature Methods*. <https://doi.org/10.1038/nmeth.3255>

- Venstrom, K., & Reichardt, L. (1995). Beta 8 integrins mediate interactions of chick sensory neurons with laminin-1, collagen IV, and fibronectin. *Molecular Biology of the Cell*. <https://doi.org/10.1091/mbc.6.4.419>
- Viatour, P., Merville, M. P., Bours, V., & Chariot, A. (2005). Phosphorylation of NF- κ B and IkkB proteins: Implications in cancer and inflammation. *Trends in Biochemical Sciences*. <https://doi.org/10.1016/j.tibs.2004.11.009>
- Wang, Q., Bu, S., Xin, D., Li, B., Wang, L., & Lai, D. (2018). Autophagy Is Indispensable for the Self-Renewal and Quiescence of Ovarian Cancer Spheroid Cells with Stem Cell-Like Properties. *Oxidative Medicine and Cellular Longevity*. <https://doi.org/10.1155/2018/7010472>
- Ware, M. J., Colbert, K., Keshishian, V., Ho, J., Corr, S. J., Curley, S. A., & Godin, B. (2016). Generation of Homogenous Three-Dimensional Pancreatic Cancer Cell Spheroids Using an Improved Hanging Drop Technique. *Tissue Engineering Part C: Methods*. <https://doi.org/10.1089/ten.tec.2015.0280>
- Weaver, B. A. (2014). How Taxol/paclitaxel kills cancer cells. *Molecular Biology of the Cell*, 25(18), 2677–2681. <https://doi.org/10.1091/mbc.e14-04-0916>
- Weiswald, L. B., Bellet, D., & Dangles-Marie, V. (2015). Spherical Cancer Models in Tumor Biology. *Neoplasia (United States)*. <https://doi.org/10.1016/j.neo.2014.12.004>
- White, E. S., & Muro, A. F. (2011). Fibronectin splice variants: Understanding their multiple roles in health and disease using engineered mouse models. *IUBMB Life*. <https://doi.org/10.1002/iub.493>
- Ye, Z., Chen, X., & Chen, X. (2018). ARK5 promotes invasion and migration in hepatocellular carcinoma cells by regulating epithelial-mesenchymal transition. *Oncology Letters*, 15(2), 1511–1516. <https://doi.org/10.3892/ol.2017.7453>
- Zagórska, A., Deak, M., Campbell, D. G., Banerjee, S., Hirano, M., Aizawa, S., ... Alessi, D. R. (2010). New roles for the LKB1-NUAK pathway in controlling myosin phosphatase complexes and cell adhesion. *Science Signaling*. <https://doi.org/10.1126/scisignal.2000616>
- Zhang, H. Y., Li, J. H., Li, G., & Wang, S. R. (2015). Activation of ARK5/miR-1181/HOXA10 axis promotes epithelial-mesenchymal transition in ovarian cancer. *Oncology Reports*. <https://doi.org/10.3892/or.2015.4113>

2.6 Supplementary Figures

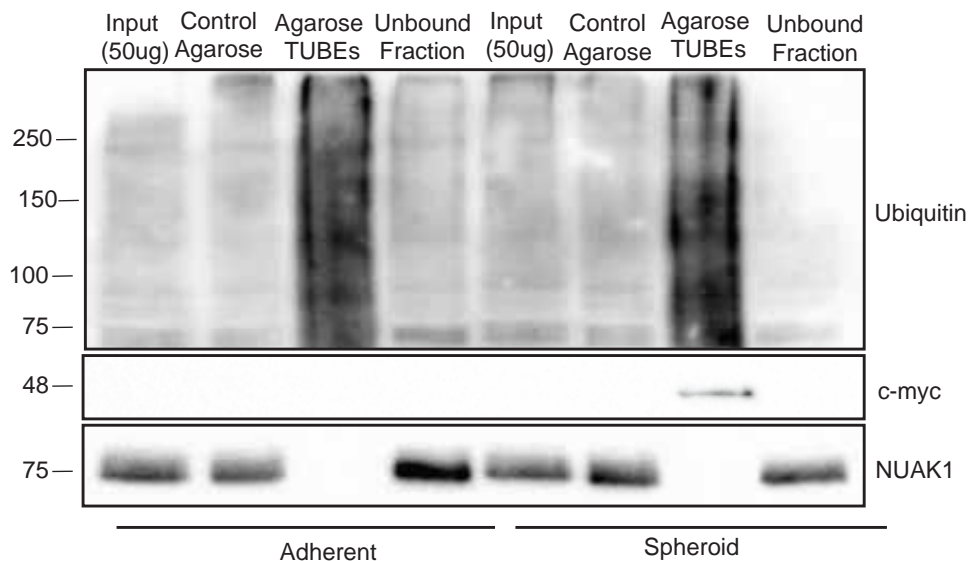


Figure S 2.1 Tandem ubiquitin binding entities (TUBEs) to detect ubiquitinated-NUAK1 in EOC cells and spheroids.

Immunoblot analysis was completed to assess ubiquitinated-c-myc (positive control) and ubiquitnated-NUAK1. Input, lysates unbound to control agarose and Agarose-TUBEs were loaded as controls. (n=3)

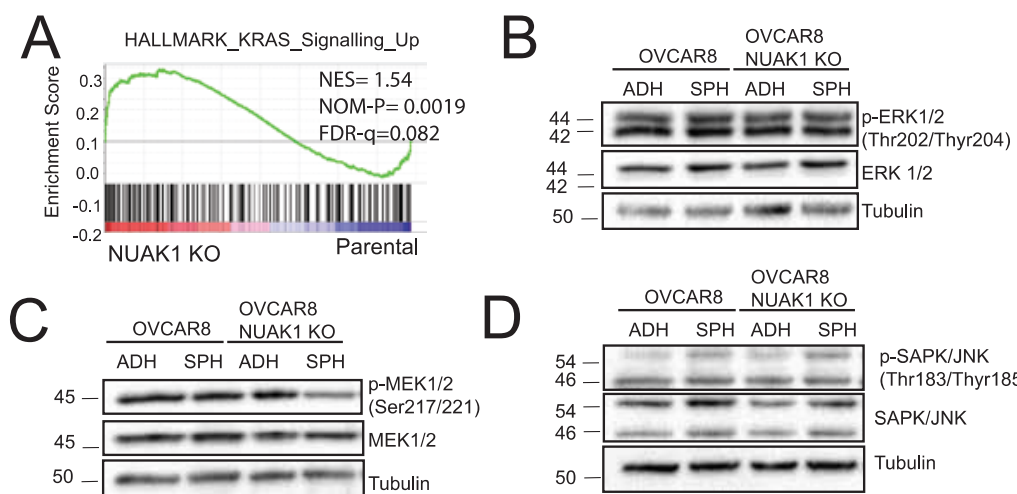


Figure S 2.2 Validation experiments for KRAS signaling signature. (A) KRAS Signaling enrichment plot is presented.

Vertical black lines represent the position of genes in the ordered data set. Green line represents the enrichment score curve. Normalized enrichment score (NES), nominal p-value, and FDR are presented. (B-D) Immunoblot analysis showing (B) p-ERK1/2 (Thr202/Thyr204) and ERK, (C) p-MEK1/2 (Ser217/221) and MEK, and (D) p-SAPK/JNK (Thr183/Thyr185) and SAPK/JNK in OVCAR8 *NUAK1*-KO and OVCAR8 parental cells cultured on monolayer conditions (Adh) or in suspension (sph). Tubulin was used as a loading control. (n=1)

2.7 Supplementary Tables

Table S 2.1 Primer sequences for qPCR

Gene	Forward Primer	Reverse Primer
IL1B	5'CCACAGACCTTCAGGAGAATG3'	5'GTGCAGTTCACTGATCGTACAGG3'
NFKB2	5'GGCAGACCCAGTGTCATTGAGCA3'	5'CAGCAGAAAGCTACCCACACTC3'
BCL2A1	5'GGATAAGGCCAACCGGAGGCTG3'	5'CAGTATTGCTTCAGGAGAGATAGC3'
IL1A	5'TGTATGTGACTGCCAACGATGAAG3'	5'AGAGGAGGTTGGCTCACTACCC3'
BIRC3	5'GCTTTTGCTGTGATGGTGGACTC3'	5'CTTGACGGATGAACTCCGTCC3'
G0S2	5'GCCTGATGGAGACTGTGTGAG3'	5'TCC TGCTGCTTGCCCTTCTCT3'
iI6	5'AGACAGCCACTCACCTTTCAG3'	5'TTC TGCCAGTGCCCTTTGCTTG3'
FN1	5'ACAACACCAGGGTGAAGAC3'	5'GGACACAACGATCTTCTGAG3'
THBS1	5'GCTGAAATGTGGTGCTTGCC3'	5'CTCCATTGTGGTTGAAGCAGGC3'
F11R	5'GTGAAGTTGCTCTGCGCTACTC3'	5'ACCAGTTGCAAGAAGGTCACC3'
ITGB5	5'GCC TCTGTGAGTGGACAAAC3'	5'CCGATGTAACCTGCATGGCACT3'
INTGB8	5'CTGTTGCAGTGGCTTACCTGGAGAC3'	5'TGCC TGCTTCACACTCTCATG3'
COL4A1	5'TGTTGACGGCTTACCTGGAGAC3'	5'GGTAGACCAACTCCAGGCCTCT3'
L1CAM	5'TCGCCCTATGTCCACTACACCT3'	5'ATCCACAGGGTTCTCTGG3'
NUAK1	5'CTCATTGGCAAATCAGCAGCG3'	5'CACCAGTGGTTGGCAATGTCT3'

Table S 2.2 Differentially expressed kinases from MIB/MS analysis completed using OVCAR8 parental and OVCAR8 STK11-KO adherent cells

Comparison	log2Foldchange	FDR	Kinases
Adh STK11KO/Adh WT	-1.97366	0	CSNK1G3
Adh STK11KO/Adh WT	-1.95801	1.73E-12	CYB5B
Adh STK11KO/Adh WT	-1.89108	0	FYN
Adh STK11KO/Adh WT	-1.78728	0	VAV2
Adh STK11KO/Adh WT	-1.74778	3.64E-15	UNC50
Adh STK11KO/Adh WT	-1.51883	0	NUAK1
Adh STK11KO/Adh WT	-1.46016	4.06E-05	NDUFB4
Adh STK11KO/Adh WT	-1.34657	1.57E-09	SFXN3
Adh STK11KO/Adh WT	-1.32789	8.01E-10	INTS5
Adh STK11KO/Adh WT	-1.28441	1.49E-07	PFKL
Adh STK11KO/Adh WT	-1.23542	4.04E-13	EPHB1
Adh STK11KO/Adh WT	-1.20998	1.66E-05	TAOK1
Adh STK11KO/Adh WT	-1.16754	8.87E-08	NBEAL2
Adh STK11KO/Adh WT	-1.12512	3.12E-13	SLC25A13
Adh STK11KO/Adh WT	-1.0996	2.33E-09	VDAC3
Adh STK11KO/Adh WT	-1.06842	0.00207	SPTLC1
Adh STK11KO/Adh WT	-1.01661	0	TEX10
Adh STK11KO/Adh WT	-0.994782	2.16E-07	UOCRC2
Adh STK11KO/Adh WT	-0.969536	0.000820923	PPP6R3
Adh STK11KO/Adh WT	-0.964587	0	ARFGEF1
Adh STK11KO/Adh WT	-0.946974	9.08E-14	PRDX1
Adh STK11KO/Adh WT	-0.846994	0.00555427	CAMK2D
Adh STK11KO/Adh WT	-0.841552	0.00165305	TUBA4A
Adh STK11KO/Adh WT	-0.781043	1.05E-07	INCENP
Adh STK11KO/Adh WT	-0.737074	1.28E-07	MRPS21
Adh STK11KO/Adh WT	-0.69114	0.000243573	ELOVL2
Adh STK11KO/Adh WT	-0.68825	7.25E-09	TBCD
Adh STK11KO/Adh WT	-0.678653	2.04E-13	RPL15
Adh STK11KO/Adh WT	-0.670448	0.0053879	MRPS5
Adh STK11KO/Adh WT	-0.662074	1.28E-14	KRT1
Adh STK11KO/Adh WT	-0.636737	0.00204682	SLC25A32
Adh STK11KO/Adh WT	-0.624303	0.0141178	RPL19
Adh STK11KO/Adh WT	-0.618517	4.05E-08	AURKB
Adh STK11KO/Adh WT	-0.590932	5.68E-17	TIMM44
Adh STK11KO/Adh WT	-0.587071	0	BRAF
Adh STK11KO/Adh WT	-0.584215	0.00292699	CCNE2
Adh STK11KO/Adh WT	-0.583903	0	HSD17B4
Adh STK11KO/Adh WT	-0.55642	0.037613	RPS6KB1
Adh STK11KO/Adh WT	-0.556194	0.00789811	HSP90B1
Adh STK11KO/Adh WT	-0.554032	1.93E-06	GNB2L1
Adh STK11KO/Adh WT	-0.523702	0.0159977	UBE2J1
Adh STK11KO/Adh WT	-0.523676	4.92E-10	RPL8
Adh STK11KO/Adh WT	-0.513712	0.000342438	HSPD1
Adh STK11KO/Adh WT	-0.507747	2.48E-06	STK3
Adh STK11KO/Adh WT	-0.50498	0.0280614	ATAD3B
Adh STK11KO/Adh WT	-0.503351	1.66E-09	ACAD10
Adh STK11KO/Adh WT	-0.497607	0.000139223	NNT
Adh STK11KO/Adh WT	-0.497478	9.49E-06	COX5B
Adh STK11KO/Adh WT	-0.4915	0.0226465	GRK6
Adh STK11KO/Adh WT	-0.459123	0.00362162	COX2
Adh STK11KO/Adh WT	-0.454173	0.0200689	SCD5
Adh STK11KO/Adh WT	-0.450508	7.32E-16	EPHB2
Adh STK11KO/Adh WT	-0.44844	0.0498535	RPS23
Adh STK11KO/Adh WT	-0.442644	0.000129016	MAP4K3
Adh STK11KO/Adh WT	-0.423766	0.0236518	MELK
Adh STK11KO/Adh WT	-0.423274	0.0139878	COX6C
Adh STK11KO/Adh WT	-0.422743	6.89E-13	VAC14
Adh STK11KO/Adh WT	-0.416894	0.00718978	FAM213A
Adh STK11KO/Adh WT	-0.41585	0	TUBGCP3
Adh STK11KO/Adh WT	-0.410997	0	AGK
Adh STK11KO/Adh WT	-0.399654	0.0284335	CERS5
Adh STK11KO/Adh WT	-0.397477	0.0419112	OXA1L
Adh STK11KO/Adh WT	-0.384582	0.00346759	HIST1H2BD
Adh STK11KO/Adh WT	-0.378792	0.0179724	ACVR1
Adh STK11KO/Adh WT	-0.366113	0.00269768	DPH5
Adh STK11KO/Adh WT	-0.357246	0.00471562	PRSS21
Adh STK11KO/Adh WT	-0.352448	0.00145417	TM9SF1
Adh STK11KO/Adh WT	-0.337459	1.76E-15	RPL17
Adh STK11KO/Adh WT	-0.327478	0.00260508	SLC43A3
Adh STK11KO/Adh WT	-0.318707	0.00354371	YIF1B
Adh STK11KO/Adh WT	-0.317724	0.000296681	PDE1C
Adh STK11KO/Adh WT	-0.316452	0.00903223	FAR1
Adh STK11KO/Adh WT	-0.313114	0.000383626	COA3
Adh STK11KO/Adh WT	-0.28207	4.25E-11	VDAC1
Adh STK11KO/Adh WT	-0.261335	0.00424384	OPA1
Adh STK11KO/Adh WT	-0.258441	0.0489084	CEPT1
Adh STK11KO/Adh WT	-0.239501	8.45E-13	ISOC2
Adh STK11KO/Adh WT	-0.231117	0	EDC4
Adh STK11KO/Adh WT	-0.178488	5.57E-10	TM9SF3
Adh STK11KO/Adh WT	-0.171577	0.0416818	GIGYF2
Adh STK11KO/Adh WT	-0.159034	0.000190905	COG6
Adh STK11KO/Adh WT	-0.149491	0	RPL18A

Adh STK11KO/Adh WT	-0.129702	5.92E-05	ABCC1
Adh STK11KO/Adh WT	-0.128553	0.00178038	ATM
Adh STK11KO/Adh WT	-0.0972751	0.0493807	STK17B
Adh STK11KO/Adh WT	-0.0845323	0	SLC25A11
Adh STK11KO/Adh WT	-0.0845323	0	SLC25A11
Adh STK11KO/Adh WT	-0.0736675	2.07E-10	MTOR
Adh STK11KO/Adh WT	-0.0731486	1.26E-07	MYH9
Adh STK11KO/Adh WT	-0.051941	0.000482044	TAOK2
Adh STK11KO/Adh WT	-0.0339553	0.000147797	ATP6V1H
Adh STK11KO/Adh WT	-0.00184483	3.41E-18	PAICS
Adh STK11KO/Adh WT	0.000899655	0	GAPDH
Adh STK11KO/Adh WT	0.0040975	0.00725857	CALU
Adh STK11KO/Adh WT	0.0352471	0.0264291	SCFD1
Adh STK11KO/Adh WT	0.0379827	5.63E-06	RPS10
Adh STK11KO/Adh WT	0.0553931	1.22E-09	HSPB1
Adh STK11KO/Adh WT	0.0618257	3.04E-08	DCK
Adh STK11KO/Adh WT	0.0657621	0.0015314	CCNT2
Adh STK11KO/Adh WT	0.0704602	1.04E-08	RPL10A
Adh STK11KO/Adh WT	0.0707662	0	HSPA9
Adh STK11KO/Adh WT	0.0941577	0	RPL21
Adh STK11KO/Adh WT	0.105502	2.64E-09	PHB2
Adh STK11KO/Adh WT	0.14163	2.75E-05	TIA1
Adh STK11KO/Adh WT	0.157962	0.000729769	RNF213
Adh STK11KO/Adh WT	0.166101	0.00457025	MINK1
Adh STK11KO/Adh WT	0.169961	0.03418	FAM162A
Adh STK11KO/Adh WT	0.181769	0	PI4K2A
Adh STK11KO/Adh WT	0.185245	3.40E-17	PRKCSH
Adh STK11KO/Adh WT	0.215049	0.0153185	ARF4
Adh STK11KO/Adh WT	0.222232	0.0295811	BSG
Adh STK11KO/Adh WT	0.225771	0.0005843	TBC1D9B
Adh STK11KO/Adh WT	0.255818	8.07E-08	SLC25A6
Adh STK11KO/Adh WT	0.260043	3.71E-09	SLC16A1
Adh STK11KO/Adh WT	0.26512	0	RPN1
Adh STK11KO/Adh WT	0.2865	0.0276945	CCNA2
Adh STK11KO/Adh WT	0.288231	0	COG8
Adh STK11KO/Adh WT	0.289714	2.93E-05	RPS8
Adh STK11KO/Adh WT	0.291447	0.000857973	RPS26
Adh STK11KO/Adh WT	0.303143	0.000332934	TARBP1
Adh STK11KO/Adh WT	0.304468	0.00011446	SACM1L
Adh STK11KO/Adh WT	0.30747	0.000121591	PIK3C3
Adh STK11KO/Adh WT	0.347208	0.030947	XPO4
Adh STK11KO/Adh WT	0.347277	3.90E-06	HIST1H4J
Adh STK11KO/Adh WT	0.363014	0.00251438	LIMS1
Adh STK11KO/Adh WT	0.363014	0.00254449	LIMS1
Adh STK11KO/Adh WT	0.366503	0.036514	VPS51
Adh STK11KO/Adh WT	0.367443	1.44E-05	HNRNPK
Adh STK11KO/Adh WT	0.373718	0.000542926	RPL27
Adh STK11KO/Adh WT	0.373779	1.02E-17	THADA
Adh STK11KO/Adh WT	0.373941	0.0396227	TUBB
Adh STK11KO/Adh WT	0.377802	4.60E-05	NCAPD2
Adh STK11KO/Adh WT	0.38051	0.00138048	COPG1
Adh STK11KO/Adh WT	0.381063	0.0387216	VPS53
Adh STK11KO/Adh WT	0.382492	0.0133487	LRRC59
Adh STK11KO/Adh WT	0.383964	0.0122381	DECR2
Adh STK11KO/Adh WT	0.385521	0.000288474	RPL7A
Adh STK11KO/Adh WT	0.389964	0.014379	CHP1
Adh STK11KO/Adh WT	0.391984	1.54E-07	PRKAB1
Adh STK11KO/Adh WT	0.394835	0.00639954	HNRNPH1
Adh STK11KO/Adh WT	0.396247	9.00E-05	HLA-C
Adh STK11KO/Adh WT	0.396505	8.50E-05	FER
Adh STK11KO/Adh WT	0.397083	4.63E-17	NPEPPS
Adh STK11KO/Adh WT	0.40146	4.48E-07	RPS15A
Adh STK11KO/Adh WT	0.401673	0.000173157	COPB1
Adh STK11KO/Adh WT	0.402277	0.00257458	PSMC4
Adh STK11KO/Adh WT	0.405217	2.95E-15	MAP4K5
Adh STK11KO/Adh WT	0.412628	0.002318	SLC38A2
Adh STK11KO/Adh WT	0.413082	0.0231467	MTX2
Adh STK11KO/Adh WT	0.413623	0.00108195	RAB3B
Adh STK11KO/Adh WT	0.426703	4.39E-05	ZAK
Adh STK11KO/Adh WT	0.430613	1.01E-05	UNC45A
Adh STK11KO/Adh WT	0.434	0.0299697	BMPR2
Adh STK11KO/Adh WT	0.436717	8.18E-11	AAK1
Adh STK11KO/Adh WT	0.437721	0.00124144	GCDH
Adh STK11KO/Adh WT	0.439058	4.67E-05	KHSRP
Adh STK11KO/Adh WT	0.439397	4.74E-05	SYMPK
Adh STK11KO/Adh WT	0.43977	4.25E-05	PGRMC1
Adh STK11KO/Adh WT	0.446492	0.0439828	MEST
Adh STK11KO/Adh WT	0.448815	0.000870669	RAB5A
Adh STK11KO/Adh WT	0.449834	0.0398511	CSNK1E
Adh STK11KO/Adh WT	0.450538	0.00147347	CSK
Adh STK11KO/Adh WT	0.451037	0.0453831	RRAS2
Adh STK11KO/Adh WT	0.451862	4.07E-07	HSD17B11
Adh STK11KO/Adh WT	0.453166	0.0472618	ARLB8
Adh STK11KO/Adh WT	0.471068	0.0271477	MAPK3
Adh STK11KO/Adh WT	0.476938	3.26E-05	LRPPRC
Adh STK11KO/Adh WT	0.480287	8.61E-06	PIK3R4
Adh STK11KO/Adh WT	0.49383	0.00342963	RPN2

Adh STK11KO/Adh WT	0.497743	0.00835616	VAPB
Adh STK11KO/Adh WT	0.497771	0.00481327	NIPA1
Adh STK11KO/Adh WT	0.498001	1.46E-05	C2CD5
Adh STK11KO/Adh WT	0.505949	2.53E-10	SGPL1
Adh STK11KO/Adh WT	0.50667	0.000264912	ESYT1
Adh STK11KO/Adh WT	0.507799	8.38E-05	MAP2K4
Adh STK11KO/Adh WT	0.51111	9.21E-11	PSMC5
Adh STK11KO/Adh WT	0.513231	0.000158839	CCDC132
Adh STK11KO/Adh WT	0.514691	0.0303599	VAPA
Adh STK11KO/Adh WT	0.521043	0	HSP90AB1
Adh STK11KO/Adh WT	0.52197	0.000178115	EXOC4
Adh STK11KO/Adh WT	0.527881	0.00117524	DHRS1
Adh STK11KO/Adh WT	0.530027	0.0145119	TMED2
Adh STK11KO/Adh WT	0.531871	1.39E-07	CDC42
Adh STK11KO/Adh WT	0.532354	0.00171648	TMEM115
Adh STK11KO/Adh WT	0.536388	1.58E-05	STX7
Adh STK11KO/Adh WT	0.541503	0.0105622	SCD
Adh STK11KO/Adh WT	0.543172	3.07E-18	ATP5C1
Adh STK11KO/Adh WT	0.545072	6.50E-07	RPL27A
Adh STK11KO/Adh WT	0.545172	0	CAD
Adh STK11KO/Adh WT	0.551233	0.00491254	RPS11
Adh STK11KO/Adh WT	0.552937	1.10E-05	RAB32
Adh STK11KO/Adh WT	0.553884	0	JAK1
Adh STK11KO/Adh WT	0.555762	4.13E-06	PRKAR2A
Adh STK11KO/Adh WT	0.557391	1.36E-09	SUN2
Adh STK11KO/Adh WT	0.558509	1.62E-07	MST4
Adh STK11KO/Adh WT	0.559623	5.54E-12	RPL18
Adh STK11KO/Adh WT	0.561136	1.07E-06	RAB11B
Adh STK11KO/Adh WT	0.56144	4.45E-06	MFSD10
Adh STK11KO/Adh WT	0.565941	0.00739726	EXOC5
Adh STK11KO/Adh WT	0.56733	0.00234493	DPM1
Adh STK11KO/Adh WT	0.57271	0	ATP5H
Adh STK11KO/Adh WT	0.583931	1.32E-17	PRKAG1
Adh STK11KO/Adh WT	0.587826	0.00143511	HAX1
Adh STK11KO/Adh WT	0.605673	0.0456171	MYLK
Adh STK11KO/Adh WT	0.607101	0.000165845	TMPO
Adh STK11KO/Adh WT	0.610695	4.72E-07	MAP3K2
Adh STK11KO/Adh WT	0.614964	5.37E-12	PRKACA
Adh STK11KO/Adh WT	0.620686	0.0369529	FLOT1
Adh STK11KO/Adh WT	0.621648	8.46E-07	NEK1
Adh STK11KO/Adh WT	0.621813	5.42E-08	ATP2C1
Adh STK11KO/Adh WT	0.623269	0.00313501	PDCD6
Adh STK11KO/Adh WT	0.634237	0.0096666	BCAP31
Adh STK11KO/Adh WT	0.634687	2.47E-11	GANAB
Adh STK11KO/Adh WT	0.64084	5.66E-07	INF2
Adh STK11KO/Adh WT	0.641106	9.33E-07	RPL13
Adh STK11KO/Adh WT	0.642757	2.51E-12	MAP2K3
Adh STK11KO/Adh WT	0.644499	6.85E-06	LGALS1
Adh STK11KO/Adh WT	0.649045	1.10E-12	RPSA
Adh STK11KO/Adh WT	0.655986	0	CKAP4
Adh STK11KO/Adh WT	0.660884	1.95E-11	SLC16A3
Adh STK11KO/Adh WT	0.667495	9.70E-05	TGFBR1
Adh STK11KO/Adh WT	0.674772	0.0021187	GPX8
Adh STK11KO/Adh WT	0.678617	0.0260763	TMEM43
Adh STK11KO/Adh WT	0.682487	3.75E-07	TM9SF4
Adh STK11KO/Adh WT	0.683913	2.38E-07	PNPLA6
Adh STK11KO/Adh WT	0.685659	2.01E-08	RDH11
Adh STK11KO/Adh WT	0.686854	0	EC12
Adh STK11KO/Adh WT	0.690096	0	ADK
Adh STK11KO/Adh WT	0.69751	0.000602095	UBQLN1
Adh STK11KO/Adh WT	0.698872	9.72E-15	GALNT2
Adh STK11KO/Adh WT	0.701559	0	SLK
Adh STK11KO/Adh WT	0.703021	0	PHGDH
Adh STK11KO/Adh WT	0.714852	1.53E-08	TYK2
Adh STK11KO/Adh WT	0.737739	9.18E-09	UBE3C
Adh STK11KO/Adh WT	0.741539	0	HSPA5
Adh STK11KO/Adh WT	0.744566	0.0149142	ACADVL
Adh STK11KO/Adh WT	0.745209	0	ATP5O
Adh STK11KO/Adh WT	0.748681	5.30E-10	SLC3A2
Adh STK11KO/Adh WT	0.757592	0.000257416	PDS5A
Adh STK11KO/Adh WT	0.765241	2.28E-05	G6PC3
Adh STK11KO/Adh WT	0.770124	0.00753697	RALB
Adh STK11KO/Adh WT	0.776687	4.70E-13	TUBGCP2
Adh STK11KO/Adh WT	0.79873	8.70E-08	ADCK5
Adh STK11KO/Adh WT	0.80656	3.81E-05	INSR
Adh STK11KO/Adh WT	0.807434	5.63E-11	EEF1D
Adh STK11KO/Adh WT	0.838763	0.00197884	RPS3A
Adh STK11KO/Adh WT	0.839279	0	RPS13
Adh STK11KO/Adh WT	0.848706	3.10E-14	EXOC7
Adh STK11KO/Adh WT	0.85824	0.00324261	ASPH
Adh STK11KO/Adh WT	0.861662	0	SLC25A24
Adh STK11KO/Adh WT	0.870775	7.32E-17	COMT
Adh STK11KO/Adh WT	0.879903	0.0165513	USMG5
Adh STK11KO/Adh WT	0.880792	2.74E-06	BTAF1
Adh STK11KO/Adh WT	0.882589	0.00578086	COG2
Adh STK11KO/Adh WT	0.898664	0	ATP5J
Adh STK11KO/Adh WT	0.901232	6.22E-09	PRAF2

Adh STK11KO/Adh WT	0.901359	0	PRKACB
Adh STK11KO/Adh WT	0.905981	4.35E-15	ECH1
Adh STK11KO/Adh WT	0.912835	2.10E-14	ATP5J2
Adh STK11KO/Adh WT	0.942541	1.75E-06	DOLK
Adh STK11KO/Adh WT	0.973739	1.78E-13	ACSL3
Adh STK11KO/Adh WT	0.991613	1.79E-09	SLC7A5
Adh STK11KO/Adh WT	0.994583	0.00027255	STK24
Adh STK11KO/Adh WT	1.00966	4.32E-10	DDOST
Adh STK11KO/Adh WT	1.01372	0	MYOF
Adh STK11KO/Adh WT	1.02419	9.36E-10	RPS18
Adh STK11KO/Adh WT	1.02915	1.89E-05	NDUFS8
Adh STK11KO/Adh WT	1.03988	1.33E-16	RHOT2
Adh STK11KO/Adh WT	1.05973	0.00419912	OSTC
Adh STK11KO/Adh WT	1.06171	0	ALDH2
Adh STK11KO/Adh WT	1.06869	0.0005592	SAR1A
Adh STK11KO/Adh WT	1.08542	0	TMED9
Adh STK11KO/Adh WT	1.09571	3.04E-12	EC11
Adh STK11KO/Adh WT	1.13834	3.58E-13	VAMP7
Adh STK11KO/Adh WT	1.17824	1.93E-16	RPL35A
Adh STK11KO/Adh WT	1.237	1.26E-05	TAPBP
Adh STK11KO/Adh WT	1.26017	1.92E-10	ITM2C
Adh STK11KO/Adh WT	1.26472	1.69E-06	QPCTL
Adh STK11KO/Adh WT	1.28596	1.09E-15	RPL38
Adh STK11KO/Adh WT	1.32405	0	TAP1
Adh STK11KO/Adh WT	1.34945	3.94E-11	TXLNA
Adh STK11KO/Adh WT	1.35898	0	SCAMP1
Adh STK11KO/Adh WT	1.37277	6.97E-07	ATP5L
Adh STK11KO/Adh WT	1.39034	2.06E-18	PIK3C2A
Adh STK11KO/Adh WT	1.40418	0	ATP5F1
Adh STK11KO/Adh WT	1.40572	0	PDS5B
Adh STK11KO/Adh WT	1.40666	0.0491441	TM9SF2
Adh STK11KO/Adh WT	1.41433	2.29E-12	RRBP1
Adh STK11KO/Adh WT	1.41741	5.52E-16	ICAM1
Adh STK11KO/Adh WT	1.44288	0	ATP5A1
Adh STK11KO/Adh WT	1.45806	0	MAGED2
Adh STK11KO/Adh WT	1.4772	0	TOR1AIP1
Adh STK11KO/Adh WT	1.55833	1.10E-13	SLC25A1
Adh STK11KO/Adh WT	1.66223	0	MAP3K11
Adh STK11KO/Adh WT	1.69199	0	SERPINH1
Adh STK11KO/Adh WT	1.74111	0	MGST1
Adh STK11KO/Adh WT	1.84896	3.54E-10	PIK3R1
Adh STK11KO/Adh WT	1.90803	0	ATP5B
Adh STK11KO/Adh WT	1.95366	0	TAP2
Adh STK11KO/Adh WT	1.98368	0	GNG12
Adh STK11KO/Adh WT	2.00741	0	CDK18
Adh STK11KO/Adh WT	2.04915	6.00E-10	ST13
Adh STK11KO/Adh WT	2.07961	0	ANXA2
Adh STK11KO/Adh WT	2.11967	1.51E-09	CANX
Adh STK11KO/Adh WT	2.19426	0	FECH
Adh STK11KO/Adh WT	2.22504	0	FLT4
Adh STK11KO/Adh WT	2.28825	0	IFIT1
Adh STK11KO/Adh WT	2.52651	0	CSNK1G1
Adh STK11KO/Adh WT	2.61056	0	CYB5A
Adh STK11KO/Adh WT	2.6386	7.09E-12	UQCRCQ
Adh STK11KO/Adh WT	2.98745	0	LMAN1
Adh STK11KO/Adh WT	3.39069	0	AGTRAP

Table S 2.3 Differentially expressed kinases from MIB/MS analysis completed using OVCAR8 parental and OVCAR8 STK11-KO spheroids

Comparison	log2Foldchange	FDR	Kinases
Sph STK11KO/Sph WT	-3.48543	5.19E-17	SCD
Sph STK11KO/Sph WT	-3.37233	0	FLNC
Sph STK11KO/Sph WT	-3.34529	0	STK17B
Sph STK11KO/Sph WT	-3.13482	0	NRAS
Sph STK11KO/Sph WT	-3.13154	0	NUAK1
Sph STK11KO/Sph WT	-2.66969	4.55E-12	RPS6
Sph STK11KO/Sph WT	-2.65475	0	ACSL3
Sph STK11KO/Sph WT	-2.57629	2.44E-14	KRT18
Sph STK11KO/Sph WT	-2.54447	1.17E-09	NCAPG2
Sph STK11KO/Sph WT	-2.30289	0	PYGB
Sph STK11KO/Sph WT	-2.22807	2.63E-12	AGRTRAP
Sph STK11KO/Sph WT	-2.22772	0	PRKCA
Sph STK11KO/Sph WT	-2.21951	5.96E-15	PGRMC1
Sph STK11KO/Sph WT	-1.99452	0	TIMM44
Sph STK11KO/Sph WT	-1.87695	4.78E-12	SYMPK
Sph STK11KO/Sph WT	-1.83333	7.48E-08	SMEK1
Sph STK11KO/Sph WT	-1.8075	0	RHOG
Sph STK11KO/Sph WT	-1.77886	3.25E-07	TUBB2B
Sph STK11KO/Sph WT	-1.73956	1.33E-11	NSDHL
Sph STK11KO/Sph WT	-1.7236	0	RPS16
Sph STK11KO/Sph WT	-1.69924	1.77E-14	RAB32
Sph STK11KO/Sph WT	-1.64759	0	MAPK9
Sph STK11KO/Sph WT	-1.62553	0	FLAD1
Sph STK11KO/Sph WT	-1.60555	0	VPS51
Sph STK11KO/Sph WT	-1.57303	5.50E-15	PLIN3
Sph STK11KO/Sph WT	-1.5591	0	MYBBP1A
Sph STK11KO/Sph WT	-1.55809	2.60E-09	SF3B3
Sph STK11KO/Sph WT	-1.55766	0	LRPPRC
Sph STK11KO/Sph WT	-1.52809	1.63E-09	PPP6R3
Sph STK11KO/Sph WT	-1.52255	7.75E-09	EMD
Sph STK11KO/Sph WT	-1.5114	0	NCAPD2
Sph STK11KO/Sph WT	-1.39845	1.81E-06	PDCD6
Sph STK11KO/Sph WT	-1.35815	1.18E-15	COMT
Sph STK11KO/Sph WT	-1.35057	0	SUN2
Sph STK11KO/Sph WT	-1.32342	0	FUBP1
Sph STK11KO/Sph WT	-1.31536	4.89E-05	FADS2
Sph STK11KO/Sph WT	-1.26534	0	COPA
Sph STK11KO/Sph WT	-1.24441	4.24E-18	RPS18
Sph STK11KO/Sph WT	-1.23605	0.000352212	RRAS2
Sph STK11KO/Sph WT	-1.23138	1.39E-13	SCFD1
Sph STK11KO/Sph WT	-1.20503	8.13E-07	EPHB1
Sph STK11KO/Sph WT	-1.1891	2.30E-16	RPS15
Sph STK11KO/Sph WT	-1.14106	0	GBF1
Sph STK11KO/Sph WT	-1.13765	0	FLT4
Sph STK11KO/Sph WT	-1.12471	2.52E-06	PIK3R1
Sph STK11KO/Sph WT	-1.11742	1.72E-06	CYB5B
Sph STK11KO/Sph WT	-1.11272	0	RPS11
Sph STK11KO/Sph WT	-1.11085	1.46E-16	LIMS1
Sph STK11KO/Sph WT	-1.11085	1.50E-16	LIMS1
Sph STK11KO/Sph WT	-1.11068	3.32E-14	RPS14
Sph STK11KO/Sph WT	-1.10309	0	STK10
Sph STK11KO/Sph WT	-1.08591	0	ECI2
Sph STK11KO/Sph WT	-1.08205	7.90E-13	RPL32
Sph STK11KO/Sph WT	-1.08095	1.72E-15	LIMS1
Sph STK11KO/Sph WT	-1.05264	6.97E-06	CDK12
Sph STK11KO/Sph WT	-1.05	0	EXOC6B
Sph STK11KO/Sph WT	-1.04736	7.51E-17	THADA
Sph STK11KO/Sph WT	-1.03093	6.46E-15	MINK1
Sph STK11KO/Sph WT	-1.02728	0.00339175	UBAP2L
Sph STK11KO/Sph WT	-1.01132	0	TTK
Sph STK11KO/Sph WT	-0.984035	0.00216746	DHCR7
Sph STK11KO/Sph WT	-0.97816	3.30E-09	UBE3C
Sph STK11KO/Sph WT	-0.974436	6.90E-11	RPL38
Sph STK11KO/Sph WT	-0.970422	5.72E-13	EXOC8
Sph STK11KO/Sph WT	-0.966921	6.31E-11	EXOC1
Sph STK11KO/Sph WT	-0.958858	0.000156553	PIP4K2A
Sph STK11KO/Sph WT	-0.955781	0	ATM
Sph STK11KO/Sph WT	-0.942437	2.84E-05	STK35
Sph STK11KO/Sph WT	-0.941719	7.50E-09	RSU1
Sph STK11KO/Sph WT	-0.924964	7.67E-05	TPR
Sph STK11KO/Sph WT	-0.907183	2.92E-11	TUBA4A
Sph STK11KO/Sph WT	-0.900196	0.0496171	CCNB2
Sph STK11KO/Sph WT	-0.894975	1.50E-08	MAP3K2
Sph STK11KO/Sph WT	-0.886649	0	VAC14
Sph STK11KO/Sph WT	-0.882996	2.36E-08	TBCD
Sph STK11KO/Sph WT	-0.869391	7.05E-11	NDUFA5
Sph STK11KO/Sph WT	-0.855434	2.56E-14	RPL27A
Sph STK11KO/Sph WT	-0.848177	0	ECH1
Sph STK11KO/Sph WT	-0.843394	0	RPL23
Sph STK11KO/Sph WT	-0.839247	1.56E-12	FAM213A

Sph STK11KO/Sph WT	-0.838761	0.0229795	HMOX2
Sph STK11KO/Sph WT	-0.838396	2.89E-06	LRRC59
Sph STK11KO/Sph WT	-0.837998	0	RPS13
Sph STK11KO/Sph WT	-0.832002	0.00712098	PDS5A
Sph STK11KO/Sph WT	-0.827391	0.00608555	PARVA
Sph STK11KO/Sph WT	-0.827368	0.00665596	PAM16
Sph STK11KO/Sph WT	-0.827025	0.000175625	PREB
Sph STK11KO/Sph WT	-0.822008	0	CLTC
Sph STK11KO/Sph WT	-0.813709	0.0335604	TMEM109
Sph STK11KO/Sph WT	-0.809857	2.13E-15	ILK
Sph STK11KO/Sph WT	-0.80725	7.45E-06	RAB21
Sph STK11KO/Sph WT	-0.782623	8.15E-09	ACAD10
Sph STK11KO/Sph WT	-0.777727	1.07E-12	MAP2K2
Sph STK11KO/Sph WT	-0.763121	0.00136247	UTP20
Sph STK11KO/Sph WT	-0.757222	0.000446193	CCDC51
Sph STK11KO/Sph WT	-0.757061	1.95E-05	RAN
Sph STK11KO/Sph WT	-0.756724	0.00894558	MLST8
Sph STK11KO/Sph WT	-0.753915	3.86E-10	RPL35A
Sph STK11KO/Sph WT	-0.752124	0	ADK
Sph STK11KO/Sph WT	-0.738901	0.00200141	RPL24
Sph STK11KO/Sph WT	-0.736196	3.43E-07	STX7
Sph STK11KO/Sph WT	-0.731367	8.75E-06	ATP6V1H
Sph STK11KO/Sph WT	-0.729044	0	MAP3K11
Sph STK11KO/Sph WT	-0.726824	1.97E-08	FAM96B
Sph STK11KO/Sph WT	-0.724824	1.59E-07	MAPK3
Sph STK11KO/Sph WT	-0.719494	0.0221523	UQCRH
Sph STK11KO/Sph WT	-0.718692	5.58E-05	ACAD9
Sph STK11KO/Sph WT	-0.718458	5.14E-06	CYB5R3
Sph STK11KO/Sph WT	-0.708042	0	HSPA9
Sph STK11KO/Sph WT	-0.707496	1.76E-17	RPS2
Sph STK11KO/Sph WT	-0.701246	3.86E-14	RPSA
Sph STK11KO/Sph WT	-0.690842	5.01E-09	MAP4K4
Sph STK11KO/Sph WT	-0.687111	3.02E-07	CSK
Sph STK11KO/Sph WT	-0.684726	7.78E-05	ABL1
Sph STK11KO/Sph WT	-0.665492	0.00195647	TBC1D9B
Sph STK11KO/Sph WT	-0.663198	3.37E-07	FASN
Sph STK11KO/Sph WT	-0.662588	3.76E-05	RPS17L
Sph STK11KO/Sph WT	-0.661202	0.0384989	GOSR2
Sph STK11KO/Sph WT	-0.651518	0.00820132	RAP1B
Sph STK11KO/Sph WT	-0.625081	1.56E-14	CDK7
Sph STK11KO/Sph WT	-0.622898	0.0168326	KPNB1
Sph STK11KO/Sph WT	-0.615883	3.50E-07	FIG4
Sph STK11KO/Sph WT	-0.610085	3.97E-10	RPS9
Sph STK11KO/Sph WT	-0.604385	0.000413051	ARL8B
Sph STK11KO/Sph WT	-0.594726	1.30E-05	RAB6A
Sph STK11KO/Sph WT	-0.594431	0.00760757	ATAD3B
Sph STK11KO/Sph WT	-0.592084	4.55E-08	COG5
Sph STK11KO/Sph WT	-0.588008	2.80E-05	RPL28
Sph STK11KO/Sph WT	-0.584233	0.0011594	ROCK2
Sph STK11KO/Sph WT	-0.578767	0.000145634	EBP
Sph STK11KO/Sph WT	-0.573096	0.0067214	CLTB
Sph STK11KO/Sph WT	-0.570763	0	RPL13A
Sph STK11KO/Sph WT	-0.567429	0.0121203	VAV2
Sph STK11KO/Sph WT	-0.562133	0	PRKAG2
Sph STK11KO/Sph WT	-0.561848	5.85E-07	SAV1
Sph STK11KO/Sph WT	-0.561772	0.00134446	COG2
Sph STK11KO/Sph WT	-0.561682	6.78E-09	MAP4K5
Sph STK11KO/Sph WT	-0.560547	7.04E-05	RPS6KA3
Sph STK11KO/Sph WT	-0.556208	0.00282658	SLK
Sph STK11KO/Sph WT	-0.551321	0.015724	PDPK1
Sph STK11KO/Sph WT	-0.540664	0	DYNC1H1
Sph STK11KO/Sph WT	-0.537804	4.79E-10	XPOT
Sph STK11KO/Sph WT	-0.537411	0.0243349	MAGED2
Sph STK11KO/Sph WT	-0.536687	0.012479	ST13
Sph STK11KO/Sph WT	-0.535633	0	RPL4
Sph STK11KO/Sph WT	-0.534414	0.0382769	MTAP
Sph STK11KO/Sph WT	-0.533489	0.000143486	RAB6A
Sph STK11KO/Sph WT	-0.51912	0.000504507	MROH1
Sph STK11KO/Sph WT	-0.514274	1.60E-06	KHSRP
Sph STK11KO/Sph WT	-0.505031	2.34E-12	DOLK
Sph STK11KO/Sph WT	-0.503148	0.000799691	GCDH
Sph STK11KO/Sph WT	-0.501827	0	RAB7A
Sph STK11KO/Sph WT	-0.494759	0	CAD
Sph STK11KO/Sph WT	-0.481615	0	IPO4
Sph STK11KO/Sph WT	-0.46631	6.00E-09	SART3
Sph STK11KO/Sph WT	-0.459903	0.00193414	RPS8
Sph STK11KO/Sph WT	-0.458644	3.21E-05	RARS2
Sph STK11KO/Sph WT	-0.458448	0	PTK2
Sph STK11KO/Sph WT	-0.458448	0	PTK2
Sph STK11KO/Sph WT	-0.45423	1.62E-11	XPO5
Sph STK11KO/Sph WT	-0.432373	0	PRKD6
Sph STK11KO/Sph WT	-0.425538	0	AXL
Sph STK11KO/Sph WT	-0.419782	0	TYK2
Sph STK11KO/Sph WT	-0.419402	5.22E-15	MAP2K1
Sph STK11KO/Sph WT	-0.415588	0.00501328	DPH5
Sph STK11KO/Sph WT	-0.412965	3.39E-13	RAB5C
Sph STK11KO/Sph WT	-0.408632	0	PRKDC

Sph STK11KO/Sph WT	-0.407457	0.0371724	ZAK
Sph STK11KO/Sph WT	-0.404475	5.85E-17	RAB14
Sph STK11KO/Sph WT	-0.397436	0	RPL18A
Sph STK11KO/Sph WT	-0.394666	1.97E-06	KRT1
Sph STK11KO/Sph WT	-0.392986	0	HSPA1B
Sph STK11KO/Sph WT	-0.391635	0.0127224	RTN4
Sph STK11KO/Sph WT	-0.379502	1.95E-12	XPO7
Sph STK11KO/Sph WT	-0.374165	0	EPHB2
Sph STK11KO/Sph WT	-0.367441	0	MAP4K4
Sph STK11KO/Sph WT	-0.360693	3.53E-09	MARK3
Sph STK11KO/Sph WT	-0.357642	0.040308	NEK6
Sph STK11KO/Sph WT	-0.353954	1.46E-10	COPB1
Sph STK11KO/Sph WT	-0.339952	9.77E-17	PKMYT1
Sph STK11KO/Sph WT	-0.336012	0	KIAA0368
Sph STK11KO/Sph WT	-0.333549	3.74E-15	PKMYT1
Sph STK11KO/Sph WT	-0.331876	2.51E-05	ACLY
Sph STK11KO/Sph WT	-0.328222	0.000512077	ACLY
Sph STK11KO/Sph WT	-0.32409	0.000389264	SEC61A1
Sph STK11KO/Sph WT	-0.314597	0.0255496	PNPLA6
Sph STK11KO/Sph WT	-0.313107	0.0233145	UBXN4
Sph STK11KO/Sph WT	-0.310368	0	HNRPNM
Sph STK11KO/Sph WT	-0.306897	2.78E-13	USP34
Sph STK11KO/Sph WT	-0.30457	0.00544312	PI4KA
Sph STK11KO/Sph WT	-0.2942	0.0253741	RALA
Sph STK11KO/Sph WT	-0.292206	0.000527279	RASSF2
Sph STK11KO/Sph WT	-0.288472	0.000253914	SAR1A
Sph STK11KO/Sph WT	-0.285302	4.96E-08	RAB2A
Sph STK11KO/Sph WT	-0.281487	0.0465567	TRIM59
Sph STK11KO/Sph WT	-0.27655	0	IPO7
Sph STK11KO/Sph WT	-0.275875	0.00452219	RPL9
Sph STK11KO/Sph WT	-0.260112	0	RPS15A
Sph STK11KO/Sph WT	-0.245535	0	RPL7
Sph STK11KO/Sph WT	-0.240227	0.0470268	TUBB
Sph STK11KO/Sph WT	-0.237629	1.11E-08	IPO9
Sph STK11KO/Sph WT	-0.234483	1.45E-08	SRC
Sph STK11KO/Sph WT	-0.233395	0	SEC22B
Sph STK11KO/Sph WT	-0.224332	0.00046737	SF3B1
Sph STK11KO/Sph WT	-0.221411	0.00163216	PIK3R4
Sph STK11KO/Sph WT	-0.20482	1.82E-11	RIOK2
Sph STK11KO/Sph WT	-0.17614	1.37E-17	PAICS
Sph STK11KO/Sph WT	-0.154366	0.0435202	RPL6
Sph STK11KO/Sph WT	-0.137936	1.97E-16	PIP5K1A
Sph STK11KO/Sph WT	-0.132278	3.74E-11	HEATR2
Sph STK11KO/Sph WT	-0.132108	7.09E-06	MAGT1
Sph STK11KO/Sph WT	-0.124091	0.00428854	RPL3
Sph STK11KO/Sph WT	-0.109493	0	CSE1L
Sph STK11KO/Sph WT	-0.108647	0.00242741	TAOK2
Sph STK11KO/Sph WT	-0.10796	7.91E-17	USP9X
Sph STK11KO/Sph WT	-0.100679	1.20E-18	PDS5A
Sph STK11KO/Sph WT	-0.10025	0.0026357	AURKB
Sph STK11KO/Sph WT	-0.0967982	0.000202289	CDK9
Sph STK11KO/Sph WT	-0.0945296	0.00302984	STK3
Sph STK11KO/Sph WT	-0.0696641	3.86E-17	PIP5K1A
Sph STK11KO/Sph WT	-0.0434375	0.000657187	RHOT2
Sph STK11KO/Sph WT	-0.0335419	0	EPHA2
Sph STK11KO/Sph WT	-0.0308265	0.000740506	COPE
Sph STK11KO/Sph WT	-0.0188178	0	PAK4
Sph STK11KO/Sph WT	-0.0126456	0	KIAA1524
Sph STK11KO/Sph WT	0.00994845	1.69E-12	HSPA8
Sph STK11KO/Sph WT	0.0305907	3.64E-11	AHNAK
Sph STK11KO/Sph WT	0.0389252	3.65E-09	PKN2
Sph STK11KO/Sph WT	0.0426871	0	PRKACA
Sph STK11KO/Sph WT	0.0557955	9.39E-14	TNPO3
Sph STK11KO/Sph WT	0.056888	0	MNAT1
Sph STK11KO/Sph WT	0.0594787	0.000211225	TNPO1
Sph STK11KO/Sph WT	0.0837652	0	HINT1
Sph STK11KO/Sph WT	0.0911725	0	PHGDH
Sph STK11KO/Sph WT	0.0924039	0	TEX10
Sph STK11KO/Sph WT	0.0938864	1.01E-11	PFKP
Sph STK11KO/Sph WT	0.0968534	5.07E-14	PRKCD
Sph STK11KO/Sph WT	0.100792	0.0460864	INTS8
Sph STK11KO/Sph WT	0.101184	0	UBR4
Sph STK11KO/Sph WT	0.105433	0.0239912	STK24
Sph STK11KO/Sph WT	0.106974	2.77E-07	MRPS21
Sph STK11KO/Sph WT	0.120785	0.000496981	NBEAL2
Sph STK11KO/Sph WT	0.130432	0.0130971	TIMM50
Sph STK11KO/Sph WT	0.131135	0	RPL21
Sph STK11KO/Sph WT	0.131431	4.61E-06	TRIM32
Sph STK11KO/Sph WT	0.163193	0.0267874	SGPL1
Sph STK11KO/Sph WT	0.167619	0.0367335	TUBB3
Sph STK11KO/Sph WT	0.168077	0	TUBGCP2
Sph STK11KO/Sph WT	0.177168	0	HNRNPF
Sph STK11KO/Sph WT	0.178642	0	EXOC7
Sph STK11KO/Sph WT	0.19059	0.0118864	RPL14
Sph STK11KO/Sph WT	0.207646	0	RPS21
Sph STK11KO/Sph WT	0.22576	2.12E-09	FGFR1
Sph STK11KO/Sph WT	0.233995	0.0321386	CDK1

Sph STK11KO/Sph WT	0.238455	0	TUBGCP3
Sph STK11KO/Sph WT	0.301526	0.0245072	SSR1
Sph STK11KO/Sph WT	0.319336	2.34E-07	FRYL
Sph STK11KO/Sph WT	0.323551	6.56E-18	CDKN2A
Sph STK11KO/Sph WT	0.327106	0	HSD17B4
Sph STK11KO/Sph WT	0.334737	4.95E-06	RPL10
Sph STK11KO/Sph WT	0.406535	0	ACAD11
Sph STK11KO/Sph WT	0.412437	0.000337626	EEF1E1
Sph STK11KO/Sph WT	0.419752	0.0339727	IKBKG
Sph STK11KO/Sph WT	0.420021	0.0138581	RAB18
Sph STK11KO/Sph WT	0.436476	0.0184064	TM9SF1
Sph STK11KO/Sph WT	0.44087	0.00415574	YIPF5
Sph STK11KO/Sph WT	0.467627	0	MAP2K3
Sph STK11KO/Sph WT	0.467945	0.0120027	RPS6KA1
Sph STK11KO/Sph WT	0.487755	3.19E-17	EPHB4
Sph STK11KO/Sph WT	0.491705	6.09E-12	LTN1
Sph STK11KO/Sph WT	0.493764	3.93E-05	DYNC1LI1
Sph STK11KO/Sph WT	0.495303	9.42E-16	CCNT2
Sph STK11KO/Sph WT	0.497198	0.00804752	MFSD10
Sph STK11KO/Sph WT	0.498326	0	RRP12
Sph STK11KO/Sph WT	0.512546	0.000188231	SYNGR2
Sph STK11KO/Sph WT	0.521347	0	MTOR
Sph STK11KO/Sph WT	0.523994	3.95E-13	ILVBL
Sph STK11KO/Sph WT	0.525103	0.00386097	SSR4
Sph STK11KO/Sph WT	0.554577	4.18E-08	VIM
Sph STK11KO/Sph WT	0.560299	4.56E-07	RPL18
Sph STK11KO/Sph WT	0.562575	1.58E-11	GALNT2
Sph STK11KO/Sph WT	0.566858	4.90E-18	SMS
Sph STK11KO/Sph WT	0.57452	0	TAP2
Sph STK11KO/Sph WT	0.581634	0.00041941	RPL17
Sph STK11KO/Sph WT	0.589561	0.000924406	ALDH2
Sph STK11KO/Sph WT	0.594809	0.000629128	CANX
Sph STK11KO/Sph WT	0.60419	1.21E-14	GAK
Sph STK11KO/Sph WT	0.605527	3.09E-16	RALB
Sph STK11KO/Sph WT	0.610454	1.95E-07	VDAC1
Sph STK11KO/Sph WT	0.611646	0.000323635	ICAM1
Sph STK11KO/Sph WT	0.614173	0.0146458	SDR39U1
Sph STK11KO/Sph WT	0.614519	0.0479665	SCARB1
Sph STK11KO/Sph WT	0.616813	1.14E-06	AIMP1
Sph STK11KO/Sph WT	0.62146	0	DDX20
Sph STK11KO/Sph WT	0.622915	5.34E-05	ZW10
Sph STK11KO/Sph WT	0.635481	0.00506618	SACM1L
Sph STK11KO/Sph WT	0.639644	0	EPRS
Sph STK11KO/Sph WT	0.640733	0.00141675	ATP5L
Sph STK11KO/Sph WT	0.643645	0	ATP2A2
Sph STK11KO/Sph WT	0.648459	2.20E-11	MET
Sph STK11KO/Sph WT	0.649707	1.01E-10	SLC25A24
Sph STK11KO/Sph WT	0.656151	0.000309939	CAMK2G
Sph STK11KO/Sph WT	0.657703	0	MDN1
Sph STK11KO/Sph WT	0.664574	3.53E-05	STK4
Sph STK11KO/Sph WT	0.667561	0	IMMT
Sph STK11KO/Sph WT	0.673845	8.25E-05	TIA1
Sph STK11KO/Sph WT	0.681871	5.96E-08	SLC25A10
Sph STK11KO/Sph WT	0.683606	4.57E-11	PRKCSH
Sph STK11KO/Sph WT	0.685454	1.09E-08	CSNK1G1
Sph STK11KO/Sph WT	0.691497	3.68E-07	VCP
Sph STK11KO/Sph WT	0.692219	3.01E-10	PRDX1
Sph STK11KO/Sph WT	0.699264	0	IMMT
Sph STK11KO/Sph WT	0.700919	2.04E-09	GNG12
Sph STK11KO/Sph WT	0.701648	0.00032825	NDUFB4
Sph STK11KO/Sph WT	0.709266	1.10E-06	FECH
Sph STK11KO/Sph WT	0.719011	2.83E-12	TM9SF3
Sph STK11KO/Sph WT	0.722003	0.0104575	COX2
Sph STK11KO/Sph WT	0.722561	8.07E-06	SLC25A40
Sph STK11KO/Sph WT	0.729783	0	NNT
Sph STK11KO/Sph WT	0.730483	3.79E-08	LYN
Sph STK11KO/Sph WT	0.734356	0.001038	CAMK2G
Sph STK11KO/Sph WT	0.744702	1.77E-05	LGALS1
Sph STK11KO/Sph WT	0.747761	0.0354334	MCCC2
Sph STK11KO/Sph WT	0.764555	3.01E-16	RPLP0
Sph STK11KO/Sph WT	0.768713	9.35E-09	MARS
Sph STK11KO/Sph WT	0.773101	3.98E-17	RPS10
Sph STK11KO/Sph WT	0.775334	3.07E-05	TMEM43
Sph STK11KO/Sph WT	0.778184	0.032949	TAPBP
Sph STK11KO/Sph WT	0.784423	0.00175903	TMEM115
Sph STK11KO/Sph WT	0.7873	1.61E-08	TMEM209
Sph STK11KO/Sph WT	0.794399	0	PHB2
Sph STK11KO/Sph WT	0.794407	1.23E-11	MST4
Sph STK11KO/Sph WT	0.794935	6.15E-10	AGPAT6
Sph STK11KO/Sph WT	0.80084	4.37E-06	CCT6A
Sph STK11KO/Sph WT	0.801168	6.94E-08	CDS2
Sph STK11KO/Sph WT	0.802242	2.36E-16	GIGYF2
Sph STK11KO/Sph WT	0.808216	0.000845363	SAMM50
Sph STK11KO/Sph WT	0.81053	4.16E-14	DHRS7
Sph STK11KO/Sph WT	0.813699	0.000130982	SLC16A3
Sph STK11KO/Sph WT	0.821761	1.15E-17	ISOC2
Sph STK11KO/Sph WT	0.828303	3.62E-12	ATP2C1

Sph STK11KO/Sph WT	0.828375	1.21E-06	KIAA0196
Sph STK11KO/Sph WT	0.837102	1.74E-05	ALG1
Sph STK11KO/Sph WT	0.837604	0.020383	ABCA3
Sph STK11KO/Sph WT	0.864074	0	RPS29
Sph STK11KO/Sph WT	0.872143	0.000453092	SLC25A5
Sph STK11KO/Sph WT	0.875218	1.48E-12	MLEC
Sph STK11KO/Sph WT	0.880406	0.000832934	ERLIN2
Sph STK11KO/Sph WT	0.885284	3.08E-09	GNB2L1
Sph STK11KO/Sph WT	0.888295	0	SURF4
Sph STK11KO/Sph WT	0.894558	5.85E-13	ABL2
Sph STK11KO/Sph WT	0.899008	1.24E-07	HIGD2A
Sph STK11KO/Sph WT	0.910625	0	TBK1
Sph STK11KO/Sph WT	0.914653	0	HIST1H4J
Sph STK11KO/Sph WT	0.916817	0	NEK9
Sph STK11KO/Sph WT	0.919027	0.00885921	SLC3A2
Sph STK11KO/Sph WT	0.921194	0.00590018	CAMK2G
Sph STK11KO/Sph WT	0.925895	3.44E-10	FER
Sph STK11KO/Sph WT	0.936974	1.77E-10	QARS
Sph STK11KO/Sph WT	0.944069	1.91E-08	OSBPL3
Sph STK11KO/Sph WT	0.949747	2.76E-14	IKBKB
Sph STK11KO/Sph WT	0.949965	1.52E-17	MBOAT7
Sph STK11KO/Sph WT	0.950227	0	JAK1
Sph STK11KO/Sph WT	0.954273	1.51E-05	RER1
Sph STK11KO/Sph WT	0.960666	1.34E-15	THEM6
Sph STK11KO/Sph WT	0.963373	1.32E-07	SLC35F6
Sph STK11KO/Sph WT	0.978513	2.87E-07	ATP6
Sph STK11KO/Sph WT	0.978904	0	DCK
Sph STK11KO/Sph WT	0.992695	4.46E-11	ATP5J2
Sph STK11KO/Sph WT	0.993561	1.33E-09	RPL15
Sph STK11KO/Sph WT	0.993607	9.57E-10	BDH1
Sph STK11KO/Sph WT	0.99791	0	LYN
Sph STK11KO/Sph WT	0.999429	0	PI4K2A
Sph STK11KO/Sph WT	1.00927	0	ATAD3A
Sph STK11KO/Sph WT	1.01155	0.0142484	G6PC3
Sph STK11KO/Sph WT	1.01437	0	ATP5A1
Sph STK11KO/Sph WT	1.03493	0	EIF2AK2
Sph STK11KO/Sph WT	1.04449	4.58E-15	VPS53
Sph STK11KO/Sph WT	1.06255	1.26E-10	KDELR1
Sph STK11KO/Sph WT	1.07429	1.39E-16	FYN
Sph STK11KO/Sph WT	1.08442	9.19E-18	TMX2
Sph STK11KO/Sph WT	1.08648	2.67E-17	PRKAB1
Sph STK11KO/Sph WT	1.08895	1.87E-08	STT3A
Sph STK11KO/Sph WT	1.08895	1.09E-05	SLC25A32
Sph STK11KO/Sph WT	1.09101	3.75E-10	SLC43A3
Sph STK11KO/Sph WT	1.09578	0	ATP5J
Sph STK11KO/Sph WT	1.10222	6.73E-06	YIPF4
Sph STK11KO/Sph WT	1.10245	1.27E-12	UBAC2
Sph STK11KO/Sph WT	1.11123	0	RAB3B
Sph STK11KO/Sph WT	1.11664	9.65E-06	CD44
Sph STK11KO/Sph WT	1.12337	6.58E-17	RPL10A
Sph STK11KO/Sph WT	1.13242	3.03E-14	PDE12
Sph STK11KO/Sph WT	1.13749	2.25E-16	SFXN1
Sph STK11KO/Sph WT	1.14882	9.24E-13	TXLNA
Sph STK11KO/Sph WT	1.15577	1.47E-13	HIST1H2BD
Sph STK11KO/Sph WT	1.15889	2.19E-12	COG6
Sph STK11KO/Sph WT	1.16145	8.73E-09	SFXN3
Sph STK11KO/Sph WT	1.16812	1.09E-16	SMPD4
Sph STK11KO/Sph WT	1.16812	1.12E-16	SMPD4
Sph STK11KO/Sph WT	1.16858	4.64E-07	DARS
Sph STK11KO/Sph WT	1.17451	3.55E-08	PIK3C2A
Sph STK11KO/Sph WT	1.17675	6.10E-05	CLK3
Sph STK11KO/Sph WT	1.18208	2.40E-06	EXOC6
Sph STK11KO/Sph WT	1.19217	3.56E-07	TMEM165
Sph STK11KO/Sph WT	1.197	1.72E-05	MAP2K5
Sph STK11KO/Sph WT	1.20759	7.88E-18	CSNK1E
Sph STK11KO/Sph WT	1.20886	0	DHRS1
Sph STK11KO/Sph WT	1.21131	0	SLC25A3
Sph STK11KO/Sph WT	1.21761	0.000123407	PTDSS1
Sph STK11KO/Sph WT	1.23069	0	VDAC3
Sph STK11KO/Sph WT	1.23647	1.22E-08	IARS
Sph STK11KO/Sph WT	1.23799	2.26E-14	CAMK2G
Sph STK11KO/Sph WT	1.24467	6.46E-11	COX6C
Sph STK11KO/Sph WT	1.25214	1.82E-10	CDK17
Sph STK11KO/Sph WT	1.25507	5.49E-09	FAM3C
Sph STK11KO/Sph WT	1.25942	4.11E-17	SLC1A5
Sph STK11KO/Sph WT	1.26179	0	ATP5B
Sph STK11KO/Sph WT	1.2836	9.45E-13	COX4I1
Sph STK11KO/Sph WT	1.28481	7.19E-15	BSG
Sph STK11KO/Sph WT	1.28798	0	ULK3
Sph STK11KO/Sph WT	1.29375	2.19E-08	INTS5
Sph STK11KO/Sph WT	1.29677	0	ATP5H
Sph STK11KO/Sph WT	1.30073	4.69E-16	DYNC2H1
Sph STK11KO/Sph WT	1.3136	0	MCU
Sph STK11KO/Sph WT	1.33362	2.14E-11	RPS6KA4
Sph STK11KO/Sph WT	1.35614	5.39E-09	PLP2
Sph STK11KO/Sph WT	1.36174	2.36E-06	STX5
Sph STK11KO/Sph WT	1.36681	0	PRKACB

Sph STK11KO/Sph WT	1.37186	0	UNC45A
Sph STK11KO/Sph WT	1.38364	6.19E-08	COX5B
Sph STK11KO/Sph WT	1.38913	0	ABCD3
Sph STK11KO/Sph WT	1.39326	0.00102365	TIMM23B
Sph STK11KO/Sph WT	1.41228	0	ATR
Sph STK11KO/Sph WT	1.41276	3.10E-08	NCLN
Sph STK11KO/Sph WT	1.42546	0	LMAN1
Sph STK11KO/Sph WT	1.45926	1.36E-11	EPT1
Sph STK11KO/Sph WT	1.46067	8.38E-10	PIP4K2B
Sph STK11KO/Sph WT	1.48257	0	ATP5C1
Sph STK11KO/Sph WT	1.49042	0	ARL1
Sph STK11KO/Sph WT	1.50071	6.80E-10	OXA1L
Sph STK11KO/Sph WT	1.50409	0	CHUK
Sph STK11KO/Sph WT	1.50667	2.21E-17	RARS
Sph STK11KO/Sph WT	1.51822	0	MAPK8
Sph STK11KO/Sph WT	1.52171	0	NUP205
Sph STK11KO/Sph WT	1.52609	4.00E-07	YIF1B
Sph STK11KO/Sph WT	1.52701	5.80E-15	FKBP11
Sph STK11KO/Sph WT	1.52828	1.03E-06	SLC35F2
Sph STK11KO/Sph WT	1.52944	0	MON2
Sph STK11KO/Sph WT	1.53392	3.87E-05	PIK3C3
Sph STK11KO/Sph WT	1.53668	0	ANXA2
Sph STK11KO/Sph WT	1.54135	0	TRRAP
Sph STK11KO/Sph WT	1.55556	0	STOM
Sph STK11KO/Sph WT	1.56808	0	SCAMP1
Sph STK11KO/Sph WT	1.58165	4.68E-11	SLC25A17
Sph STK11KO/Sph WT	1.59683	0	ACVR1
Sph STK11KO/Sph WT	1.65054	0	SLC35A3
Sph STK11KO/Sph WT	1.66084	0	YES1
Sph STK11KO/Sph WT	1.70278	0	USMG5
Sph STK11KO/Sph WT	1.72408	3.58E-14	DHCR24
Sph STK11KO/Sph WT	1.72477	2.78E-11	MRPS5
Sph STK11KO/Sph WT	1.75029	1.49E-15	HM13
Sph STK11KO/Sph WT	1.86365	1.40E-11	CLPTM1L
Sph STK11KO/Sph WT	1.88443	2.59E-16	CHEK1
Sph STK11KO/Sph WT	1.88886	3.02E-15	SLC25A13
Sph STK11KO/Sph WT	1.9451	2.57E-07	FLOT1
Sph STK11KO/Sph WT	1.97657	1.11E-17	BMPR2
Sph STK11KO/Sph WT	2.00539	0	HSPA5
Sph STK11KO/Sph WT	2.05881	2.38E-14	IFIT1
Sph STK11KO/Sph WT	2.07378	2.48E-15	SCD5
Sph STK11KO/Sph WT	2.10827	0	TMEM205
Sph STK11KO/Sph WT	2.11547	0	CSNK1G3
Sph STK11KO/Sph WT	2.14808	0	FAR1
Sph STK11KO/Sph WT	2.149	2.96E-14	GOLT1B
Sph STK11KO/Sph WT	2.1772	1.95E-14	PRSS21
Sph STK11KO/Sph WT	2.18722	0	COX20
Sph STK11KO/Sph WT	2.1926	0	AZI2
Sph STK11KO/Sph WT	2.19488	0	SOAT1
Sph STK11KO/Sph WT	2.22416	2.71E-11	EEF1G
Sph STK11KO/Sph WT	2.23739	0	ATP5F1
Sph STK11KO/Sph WT	2.24375	0	BMP2K
Sph STK11KO/Sph WT	2.26545	6.82E-15	RPS23
Sph STK11KO/Sph WT	2.30779	0	LBR
Sph STK11KO/Sph WT	2.37631	0	ATP5O
Sph STK11KO/Sph WT	2.48406	0	TAP1
Sph STK11KO/Sph WT	2.48581	0	PRKAA2
Sph STK11KO/Sph WT	2.50144	2.08E-12	MEST
Sph STK11KO/Sph WT	2.50181	1.18E-14	SLC38A2
Sph STK11KO/Sph WT	2.52814	0	CMTM6
Sph STK11KO/Sph WT	2.55842	0	OPA1
Sph STK11KO/Sph WT	2.59186	0	ANAPC1
Sph STK11KO/Sph WT	2.62651	0	NDUFA11
Sph STK11KO/Sph WT	2.77471	2.87E-13	INTS7
Sph STK11KO/Sph WT	2.77545	0	GAPDH
Sph STK11KO/Sph WT	2.84706	0	PCID2
Sph STK11KO/Sph WT	2.913	0	HSP90B1
Sph STK11KO/Sph WT	2.93831	0	TARBP1
Sph STK11KO/Sph WT	2.98146	2.39E-18	ITM2C
Sph STK11KO/Sph WT	3.14963	0	CYB5A
Sph STK11KO/Sph WT	3.15967	1.03E-18	SLC25A1
Sph STK11KO/Sph WT	3.77099	0	HLA-C
Sph STK11KO/Sph WT	4.35891	7.99E-15	CERS5
Sph STK11KO/Sph WT	5.30894	0	TMEM177

Table S 2.4 Differentially expressed genes from the Affymetrix Clariom S array using OVCAR8 parental and OVCAR8 NUAK1-KO spheroids

Gene	Log2 fold change (NUAK1 Knockout/Parental)	P-value	FDR P-value
FN1	-745.23	3.67E-19	7.87E-15
NFIB	-49.17	2.23E-16	1.19E-12
CD24	-38.36	3.53E-12	3.79E-09
PAX8	-33.57	6.53E-11	4.52E-08
TFAP2A	-23.16	4.28E-14	1.15E-10
NNMT	-22.27	4.44E-15	1.91E-11
IL6	-16.61	4.16E-05	0.0026
NID2	-10.96	6.42E-12	6.26E-09
FAM198B	-10.44	2.75E-09	1.11E-06
L1CAM	-10.43	1.43E-07	2.58E-05
ADGRG1	-10.36	1.64E-09	8.00E-07
ITGB8	-10.21	6.27E-07	8.85E-05
S100A2	-9.84	1.30E-07	2.37E-05
P3H2	-9.46	8.11E-07	0.0001
GNG11	-9.4	9.19E-13	1.23E-09
RUNX2	-9.16	7.88E-08	1.60E-05
GALNT7	-8.46	5.01E-11	3.71E-08
THBS1	-8.33	3.00E-13	5.35E-10
SPOCK1	-8.21	9.93E-08	1.87E-05
SEMA3C	-7.97	4.88E-13	7.47E-10
PLEKHA7	-7.72	9.90E-08	1.87E-05
KRT7	-7.58	4.20E-12	4.29E-09
GDA	-7.21	3.33E-08	8.50E-06
ID3	-6.47	1.24E-07	2.28E-05
PMEPA1	-6.42	7.56E-10	3.86E-07
PDE1C	-6.35	7.13E-10	3.83E-07
SEMA3E	-6.2	6.80E-06	0.0006
IL7R	-6.17	3.33E-07	5.24E-05
TRPC4	-5.9	8.07E-09	2.83E-06
SERTAD4	-5.75	2.21E-10	1.40E-07
TGFBI	-5.67	4.97E-09	1.84E-06
EFEMP1	-5.65	1.92E-08	6.05E-06
RBPM5	-5.46	0.0001	0.0065
FAM129A	-5.46	2.34E-07	3.84E-05
TENM2	-5.44	1.03E-07	1.91E-05
SLC16A2	-5.37	3.12E-08	8.24E-06
SMAD3	-5.33	4.32E-07	6.62E-05
PTPN20	-5.32	4.44E-09	1.70E-06
GFRA1	-5.13	9.59E-07	0.0001
SMAD6	-5.13	1.44E-05	0.0011
PSMB9	-4.93	6.88E-06	0.0007
CLDN1	-4.91	0.0027	0.0494
NREP	-4.8	5.42E-05	0.0032
EDNRA	-4.76	2.23E-05	0.0015
PHLDB2; PLXCD2	-4.68	3.62E-09	1.41E-06
GBP1	-4.67	0.0035	0.0599
LRNN4	-4.66	8.50E-06	0.0007
PLPP3	-4.51	1.36E-06	0.0002
LHX1	-4.5	1.93E-09	9.00E-07
FERMT1	-4.41	5.02E-08	1.12E-05
UBE2L6	-4.38	1.85E-08	6.00E-06
GPR143	-4.35	3.52E-08	8.78E-06
PDPN	-4.24	1.45E-07	2.59E-05
SERTAD4	-4.24	1.73E-08	5.69E-06
THSD4	-4.23	7.50E-05	0.004
METTL7B	-4.23	6.24E-05	0.0035
DDX60	-4.17	4.29E-07	6.62E-05
RBMS3	-4.12	0.0006	0.0189
DNAJA4	-4.05	1.15E-06	0.0001
PARP14	-4.01	0.0001	0.0057
COL1A1	-4	3.26E-10	1.89E-07
KRT80	-3.96	8.98E-05	0.0045
PLXND1	-3.93	1.47E-06	0.0002
HCFC1R1	-3.88	0.0013	0.0306
ARHGEF5	-3.87	2.49E-08	7.20E-06
DPYSL2	-3.86	4.85E-08	1.10E-05
PSMB8	-3.86	1.47E-05	0.0011
MCAM; MIR6756	-3.86	2.31E-06	0.0003
HES1	-3.82	1.32E-05	0.001
SYT17	-3.82	1.19E-07	2.20E-05
OR2A7; ARHGEF34P	-3.75	3.83E-08	9.22E-06
LGR4	-3.75	3.02E-08	8.09E-06
CAMK1D	-3.74	6.53E-10	3.59E-07
ERBB3	-3.73	5.84E-05	0.0033
S100A16	-3.64	8.36E-06	0.0007
ESRP1	-3.64	0.0001	0.0056
VANGL2	-3.63	4.81E-05	0.0029
EGR1	-3.61	0.0011	0.0272
PLXDC2	-3.61	3.71E-08	9.11E-06
OLFML2B	-3.6	2.41E-07	3.89E-05
IGFBP6	-3.6	7.60E-08	1.57E-05

ENAH	-3.59	1.00E-09	5.00E-07
SERTAD4	-3.58	8.66E-08	1.69E-05
PCDHB5	-3.56	8.31E-08	1.65E-05
TLR3	-3.55	6.18E-05	0.0034
F11R	-3.52	2.67E-06	0.0003
ACTBL2	-3.51	5.51E-05	0.0032
PLOD2	-3.48	6.19E-07	8.79E-05
APOL1	-3.4	9.88E-05	0.0048
MAGED1	-3.39	4.42E-05	0.0027
TMEM184A	-3.38	0.0003	0.0109
LOX	-3.35	0.0018	0.0383
MFSD6	-3.33	0.0006	0.0184
MAGED4; MAGED4B; SNORA11D; SNORA11E	-3.33	0.0003	0.012
FAM84B	-3.31	1.24E-05	0.001
SIM1	-3.31	4.96E-07	7.33E-05
TINAGL1	-3.31	0.0009	0.0242
LITAF	-3.29	6.44E-09	2.34E-06
ACTC1	-3.27	0.0315	0.2279
STXBP6	-3.26	1.49E-05	0.0011
IFIT3	-3.26	3.74E-08	9.11E-06
TSPAN2	-3.25	3.12E-07	4.96E-05
CTAGE8	-3.23	9.70E-05	0.0048
GRAMD3	-3.21	8.79E-06	0.0008
AGPAT3	-3.2	6.07E-07	8.68E-05
SCIN	-3.18	0.0048	0.0728
ANXA3	-3.15	3.21E-06	0.0003
LTBP3	-3.14	2.93E-08	8.06E-06
UGT3A2	-3.14	7.96E-08	1.60E-05
FGF2	-3.1	7.38E-10	3.86E-07
TXNIP	-3.09	0.0082	0.1034
PSG9	-3.08	0.0116	0.1271
SAMD9L	-3.06	4.67E-05	0.0028
CELSR2	-3.05	2.45E-06	0.0003
GPER1	-3.03	7.00E-05	0.0038
LIMCH1	-3.02	0.0004	0.0132
IFIT2	-2.99	9.71E-05	0.0048
CNTNAP3B	-2.98	0.0016	0.0344
KLF9	-2.98	0.0043	0.0677
S100A13	-2.97	2.46E-05	0.0017
ITGB4	-2.95	0.0001	0.0051
ERCC6; ERCC6-PGBD3; PGBD3	-2.94	5.57E-05	0.0032
PLEKHG1	-2.94	7.65E-05	0.004
ME3	-2.94	0.0399	0.2601
INPP4B	-2.9	9.08E-06	0.0008
PROSER2	-2.88	6.27E-08	1.32E-05
INADL	-2.87	0.0026	0.049
KRT7	-2.87	1.20E-06	0.0002
FBXO32	-2.86	0.0003	0.0105
PSMB8-AS1	-2.86	1.02E-05	0.0009
FAM167A	-2.85	0.018	0.1653
ZSCAN31	-2.83	7.07E-06	0.0007
MKX	-2.8	2.74E-09	1.11E-06
GSN	-2.8	8.77E-05	0.0044
GPRC5A; MIR614	-2.77	1.19E-05	0.001
DYRK1B	-2.76	0.0001	0.0057
ACSF2	-2.76	0.0006	0.0179
MBNL2	-2.75	9.27E-07	0.0001
PERP	-2.75	2.13E-06	0.0002
SLC26A2	-2.74	1.30E-05	0.001
MAGED4; MAGED4; SNORA11D	-2.73	1.66E-05	0.0012
C1R	-2.71	0.0018	0.0378
FLT1	-2.7	0.002	0.0408
RBM24	-2.69	0.0003	0.0117
CARD16	-2.69	0.0006	0.0186
PROS1	-2.67	1.94E-07	3.32E-05
IFI16	-2.66	1.76E-05	0.0013
APOBEC3G	-2.63	1.15E-05	0.0009
DTX3L	-2.63	0.0002	0.0069
EMP1	-2.62	0.0008	0.0219
LRRC16A	-2.61	1.89E-08	6.05E-06
ACKR3	-2.59	0.0034	0.0582
DENND2D	-2.58	0.0057	0.0819
SHISA2	-2.57	4.00E-06	0.0004
NPAS2	-2.57	0.0005	0.0173
APOL2	-2.56	8.02E-07	0.0001
SGK223	-2.56	2.21E-05	0.0015
APOE	-2.56	0.0001	0.0062
FBXO44	-2.54	0.0007	0.0212
MYO1E	-2.54	3.47E-05	0.0022
MN1	-2.54	0.0362	0.2463
COL4A1	-2.54	0.0005	0.016
S100A6	-2.54	1.57E-06	0.0002
PDE4DIP	-2.53	2.42E-05	0.0016
DSC3	-2.53	1.16E-06	0.0001
SHROOM3	-2.53	3.23E-05	0.0021
TSPAN15	-2.52	2.25E-05	0.0015

DHTKD1	-2.52	9.81E-05	0.0048
CDA	-2.51	0.0019	0.0387
TPD52L1	-2.5	2.06E-05	0.0015
LAMC2	-2.49	0.0017	0.0364
ITGB5	-2.49	6.37E-05	0.0035
BEX1	-2.48	1.16E-06	0.0001
MGST2	-2.48	4.15E-08	9.90E-06
DNAJC15	-2.48	0.0001	0.0058
COL4A2	-2.48	0.0008	0.0221
SPTLC3	-2.47	0.0002	0.0095
SNX9	-2.47	4.21E-08	9.93E-06
TRMT12	-2.46	1.83E-06	0.0002
GSTM2	-2.45	9.57E-06	0.0008
PRSS23	-2.44	0.0002	0.0068
NMU	-2.44	3.09E-06	0.0003
PARP9	-2.44	1.63E-05	0.0012
DENND2A	-2.43	2.54E-06	0.0003
CFAP206	-2.42	3.52E-07	5.52E-05
CLIC3	-2.41	0.0061	0.0855
SEMA3A	-2.41	0.0003	0.0125
TMEM255A	-2.41	9.34E-05	0.0046
MTRR	-2.4	0.0002	0.0068
GLT8D2	-2.4	0.0007	0.0199
PRKCA	-2.38	1.44E-05	0.0011
ST3GAL6	-2.38	0.0037	0.0614
DPYD	-2.38	5.58E-06	0.0005
PTPRJ	-2.38	4.89E-07	7.29E-05
RARG	-2.37	2.14E-07	3.56E-05
PCDHGC3; PCDHGA12; PCDHGB4; PCDHGA8; PCDHGA1; PCDHGA10; PCDHGA11; PCDHGA2; PCDHGA3; PCDHGA4; PCDHGA5; PCDHGA6; PCDHGA7; PCDHGA9; PCDHGB1; PCDHGB2; PCDHGB3; PCDHGB5; PCDHGB6; PCDHGB7; PCDHGC4; PCDHGC5	-2.37	0.0034	0.0588
ITM2A	-2.37	2.44E-06	0.0003
PRKCQ	-2.36	8.41E-05	0.0043
TRPV4	-2.36	2.30E-08	6.94E-06
NHS	-2.36	0.005	0.0753
PTO1; MIR4749	-2.36	8.65E-05	0.0044
EGFLAM	-2.36	0.0023	0.044
AGPAT4	-2.35	0.0033	0.0572
FAM83B	-2.35	4.23E-05	0.0026
ASIC1	-2.34	0.0286	0.2168
VCAN	-2.34	0.0009	0.0234
SLC18B1	-2.34	2.05E-06	0.0002
FOXP1	-2.34	0.0003	0.0108
PLEKHG4B	-2.34	0.002	0.0402
NDRG4	-2.33	0.001	0.0262
TIAM1	-2.33	0.0037	0.0623
SVIL	-2.33	0.0463	0.2818
PTPN6	-2.33	0.0021	0.0416
ATP8B1	-2.32	7.53E-06	0.0007
PIM1	-2.32	0.0173	0.1614
BST1	-2.32	1.83E-06	0.0002
ACAA2	-2.32	1.45E-06	0.0002
CTAGE8; CTAGE4	-2.31	0.0006	0.0178
RAB30	-2.31	2.90E-05	0.0019
SRPX2	-2.3	0.0013	0.0295
NDUFA13	-2.3	0.0048	0.0728
CTSF	-2.3	0.003	0.0532
DGKD	-2.29	1.64E-06	0.0002
SERPINB9	-2.29	0.0023	0.0441
SMAD7	-2.29	0.0165	0.1575
CRISPLD1	-2.28	0.0003	0.0104
KCNMA1	-2.28	0.0014	0.0312
BAIAP2L1	-2.28	0.0003	0.0102
NEDD9	-2.28	0.0008	0.0226
DHRS13	-2.28	0.0001	0.0054
CAPN3	-2.27	0.0017	0.0364
PLBD1	-2.27	6.90E-06	0.0007
EEF1A2	-2.27	6.02E-07	8.66E-05
43160	-2.27	0.0008	0.0217
SERPINB1	-2.26	0.0003	0.0117
IGF1R	-2.26	7.33E-06	0.0007
IFIH1	-2.26	0.002	0.0401
GPR161	-2.25	2.24E-05	0.0015
ABRACL	-2.25	4.44E-05	0.0027
C5	-2.25	0.0362	0.2462
SLC2A12	-2.24	0.0016	0.035
TAPBPL	-2.24	0.0007	0.0197
MBOAT1	-2.24	0.0008	0.0217
OLFML3	-2.24	0.0004	0.0143
TRIM69	-2.24	1.79E-05	0.0013
CASP1	-2.23	0.0038	0.0634
MEIS3	-2.23	0.0072	0.0945

BDH2	-2.23	2.99E-05	0.002
DSC2	-2.23	6.89E-05	0.0037
SMAD7	-2.22	0.0002	0.008
PKP2	-2.22	1.72E-06	0.0002
TP53I3	-2.22	2.12E-06	0.0002
BMP1	-2.22	0.0015	0.0338
VAMP8	-2.21	2.16E-05	0.0015
SYT16	-2.2	2.20E-05	0.0015
SUSD4	-2.2	0.0312	0.2268
DAW1	-2.2	0.0046	0.0712
TPRA1	-2.2	0.0005	0.0173
NIPSNAP1	-2.2	0.0272	0.2105
CES4A	-2.19	3.26E-05	0.0021
DYRK1B	-2.19	7.23E-06	0.0007
MYO1D	-2.18	0.0003	0.0103
SERPINH1	-2.18	0.0004	0.0137
ERAP2	-2.18	6.63E-05	0.0036
MSLN	-2.18	0.0036	0.0602
LUM	-2.18	0.0227	0.1901
SERPINB4	-2.18	0.0074	0.0959
VGLL3	-2.17	0.0036	0.0604
GNL1	-2.17	0.0007	0.021
SMO	-2.17	2.74E-05	0.0018
ROR2	-2.17	0.0006	0.0195
KIAA1644	-2.17	0.0073	0.0951
AP4M1	-2.17	7.19E-05	0.0038
ARL4C	-2.17	0.001	0.0259
RNF144B	-2.16	1.35E-05	0.0011
EXT1	-2.16	1.54E-06	0.0002
CCL28	-2.16	0.001	0.0262
TCEAL2	-2.15	2.43E-06	0.0003
IER3	-2.15	0.0002	0.0084
ECI1	-2.15	0.0018	0.0381
CYP1B1	-2.15	0.0021	0.042
CALHM2	-2.14	0.0002	0.007
PPIC	-2.14	1.17E-05	0.001
PRKD2	-2.13	6.51E-05	0.0036
TFPI2	-2.13	2.58E-08	7.38E-06
DUSP1	-2.13	8.66E-05	0.0044
SPOCD1	-2.13	0.0162	0.1552
CNTNAP3P2; CNTNAP3	-2.13	0.0002	0.0074
TBL1X	-2.13	0.0424	0.2689
P2RX7	-2.13	0.0056	0.0813
OR2A4	-2.13	0.0018	0.0375
MBD5	-2.13	0.0036	0.0605
MID2	-2.12	0.0004	0.0136
PTGFRN	-2.12	0.0284	0.2158
S100A3	-2.11	0.001	0.0252
FOXO1	-2.11	0.0031	0.0554
EPB41L3	-2.11	2.97E-06	0.0003
MYO3A	-2.11	0.0002	0.0087
43347	-2.11	0.0009	0.0234
SCD5	-2.1	0.0026	0.0483
CA13	-2.1	0.0146	0.146
COL18A1	-2.1	0.0003	0.0114
PSG4	-2.1	0.01	0.1159
ETFB	-2.1	0.001	0.0262
CCBE1	-2.1	0.0008	0.0222
GLB1L2	-2.1	5.64E-05	0.0032
ARFRP1	-2.1	4.86E-06	0.0005
NUAK1	-2.1	0.0064	0.0881
CD163L1	-2.09	0.0015	0.0339
CRIP1	-2.08	0.0041	0.0665
SAMD15	-2.08	1.93E-05	0.0014
PTPRK	-2.08	1.63E-06	0.0002
SERPING1	-2.08	0.0011	0.0264
APOL6	-2.08	3.58E-05	0.0023
MGAT4B	-2.08	1.29E-05	0.001
DCLK1	-2.08	0.0007	0.0197
PTRF	-2.07	0.0006	0.0177
MOSPD3	-2.07	0.0155	0.1508
EPCAM	-2.06	4.34E-08	1.01E-05
SEPW1	-2.06	0.0083	0.1034
BTN3A2	-2.06	0.0115	0.1271
SLC6A9	-2.06	0.0353	0.2428
BEX4	-2.06	8.22E-06	0.0007
MARVELD2	-2.06	9.78E-05	0.0048
PCMTD2	-2.05	8.99E-05	0.0045
C19orf66	-2.05	0.0025	0.0477
CXXC5	-2.05	0.0075	0.0965
LRRC6	-2.05	0.0037	0.0615
TCEAL8	-2.05	0.0015	0.0337
GTF2RD2B	-2.05	0.0012	0.0293
TGFBR1	-2.05	0.0007	0.0211
ALDH7A1	-2.05	0.0002	0.0081
GLIPR2	-2.05	0.0003	0.0116
SEL1L3	-2.04	0.0125	0.1327

ZFYVE28	-2.04	0.0042	0.0674
RAB31	-2.04	3.32E-05	0.0021
RRBP1	-2.04	0.0003	0.0102
MYD88	-2.04	0.0012	0.0287
SAT1	-2.03	0.0068	0.0914
MPP7	-2.03	1.60E-06	0.0002
GPC3	-2.03	0.0251	0.2018
SMAD1	-2.03	5.45E-05	0.0032
LRAT	-2.03	0.0001	0.0058
UCP2	-2.03	0.0002	0.0094
STAT6	-2.03	2.88E-06	0.0003
CYB561	-2.02	0.0014	0.0324
CDKL2	-2.02	0.0002	0.0089
SLTRK5	-2.02	4.86E-05	0.0029
OAS3	-2.02	0.0019	0.0396
C11orf70	-2.02	0.0019	0.0399
FRRS1	-2.01	0.0118	0.1284
LRP4	-2.01	0.0063	0.0876
RHOBTB3	-2.01	5.76E-07	8.35E-05
BDH1	-2.01	0.0046	0.0716
PDE4D	-2.01	0.0087	0.107
SP110	-2.01	8.12E-05	0.0042
FIS1	-2.01	0.002	0.0407
CARHSP1	-2	0.001	0.0252
GPC6	-2	0.0113	0.1254
CD74	-2	0.0039	0.0639
CACNA2D4	2	0.0008	0.0221
NRIP3	2	0.0004	0.014
PRAMEF19	2	0.0076	0.0976
PHF20L1	2	0.0153	0.1498
ITGB1BP2	2.01	0.0005	0.0152
RAD54L2	2.01	1.37E-05	0.0011
CCDC84	2.01	0.0135	0.1393
LRIG1	2.02	1.92E-05	0.0014
ACTR3B	2.02	0.001	0.0252
FZD7	2.02	4.01E-05	0.0025
GATA3	2.03	0.011	0.1234
SERPINA1	2.03	0.0114	0.1268
CSF2RA	2.03	0.0008	0.0222
FABP6	2.03	0.0268	0.2093
C8orf88	2.03	5.73E-07	8.35E-05
DNAJB9	2.03	0.012	0.1297
KLF14	2.03	0.0002	0.0089
SERTAD2	2.03	0.0008	0.0217
CCL19	2.03	0.0373	0.2497
DIAPH2	2.03	5.06E-05	0.003
GOLGA8J	2.04	0.0002	0.0086
CSPP1	2.04	0.0003	0.0124
CD274	2.04	0.0012	0.0285
CALB2	2.05	0.0369	0.2491
SAA2; SAA2-SAA4; SAA4	2.05	2.19E-05	0.0015
WDFY2	2.05	2.82E-08	7.95E-06
ANKRD20A3; ANKRD20A2	2.06	0.0057	0.0823
ITPRIP	2.06	0.0011	0.0278
CA2	2.06	6.79E-06	0.0006
BMPER	2.06	0.0024	0.046
GOLGA8N	2.07	2.20E-05	0.0015
YES1	2.07	2.41E-09	1.08E-06
PAG1	2.07	0.0002	0.007
MMP16	2.07	0.0028	0.0506
PPP4R4	2.08	0.0002	0.0074
ADAMTS16	2.08	0.0055	0.0803
NOL4L	2.08	0.0004	0.0136
EEA1	2.08	0.0002	0.0076
STK39	2.08	0.0001	0.0062
ZNF438	2.09	8.50E-06	0.0007
CHUK	2.09	0.0152	0.149
ZDHHC11	2.09	0.0004	0.0144
MERTK	2.09	2.68E-05	0.0018
CIART	2.09	0.0108	0.1211
CSF2RA	2.09	1.12E-05	0.0009
RNF24	2.1	9.29E-05	0.0046
GOLGA8T	2.1	7.29E-05	0.0039
MAN1C1	2.11	0.0005	0.0152
SERTAD1	2.11	0.0336	0.2362
GLDC	2.11	1.60E-05	0.0012
PHYHIPL	2.11	0.0007	0.0204
SLC25A22	2.13	0.001	0.0262
ANO4	2.13	0.0007	0.0197
DENND3	2.13	0.0002	0.007
GRB10	2.13	0.0005	0.0152
GEM	2.13	0.0178	0.1642
ECSCR	2.13	0.0006	0.0181
SLT2	2.14	0.0218	0.1858
CLK1	2.14	0.0005	0.0172
IGIP	2.14	0.0335	0.2357
SLCO1B7; SLCO1B1	2.14	0.0032	0.0556

UACA	2.14	0.0004	0.0136
LHX9	2.14	0.0304	0.224
43163	2.17	6.73E-05	0.0037
NGEF	2.18	0.001	0.0253
FBXO48	2.18	0.0001	0.0065
TTC21B	2.18	1.51E-07	2.66E-05
SESN3	2.2	0.0318	0.2291
ITGA6	2.2	0.0014	0.0324
CPED1	2.2	1.58E-07	2.76E-05
POP1	2.21	5.60E-05	0.0032
RNF217	2.22	9.35E-05	0.0046
MGEA5	2.22	0.042	0.2675
SPRED3	2.22	0.0102	0.1171
NFE4	2.22	6.96E-05	0.0038
USP3	2.23	0.0477	0.2858
NCF2	2.24	5.28E-05	0.0031
DET1	2.25	0.0049	0.0746
ZEB1	2.25	6.30E-06	0.0006
XAGE1E; XAGE1B	2.25	1.62E-07	2.81E-05
JMJD6	2.25	0.0004	0.0145
LIMD1	2.26	2.35E-08	7.00E-06
ARID3B	2.26	5.05E-05	0.003
CHD7	2.27	7.97E-06	0.0007
ZEB2	2.27	0.0001	0.0056
LRRC20	2.27	0.0008	0.0222
ZFP30	2.28	0.0025	0.0477
ANKRD20A1	2.28	0.0061	0.0859
OTUD6B	2.28	7.03E-08	1.46E-05
R3HDM1	2.29	0.0266	0.209
ZNF114	2.31	7.64E-05	0.004
XAGE1B; XAGE1E	2.32	1.09E-08	3.67E-06
E2F5	2.32	1.45E-05	0.0011
CBLN2	2.33	0.0008	0.0221
CLIP4	2.34	0.0009	0.0248
GOLGA8N; GOLGA8H	2.34	0.0002	0.0074
MAP3K14	2.35	0.0008	0.0217
TBC1D4	2.35	1.74E-06	0.0002
CLDN4	2.36	0.0004	0.0136
EXPH5	2.36	0.0003	0.0109
SATB2	2.37	5.59E-08	1.19E-05
GOS2	2.38	0.0023	0.0447
SNX16	2.38	3.73E-06	0.0004
ELL2	2.38	1.29E-05	0.001
ZC3H6	2.4	0.0027	0.0497
ADAMTS1	2.4	0.0369	0.2491
SYCP1	2.41	5.48E-05	0.0032
FAM196B	2.42	0.0069	0.0918
LAMB3; MIR4260	2.44	4.60E-07	6.93E-05
TRIML2	2.45	3.45E-05	0.0022
CPNE3	2.45	2.76E-09	1.11E-06
FAM173B	2.45	0.0054	0.0789
MYH15	2.47	1.43E-05	0.0011
DOC2B	2.47	2.07E-05	0.0015
MYBL1	2.48	5.09E-06	0.0005
43162	2.49	1.45E-05	0.0011
TMEM55A	2.5	0.0002	0.0092
PDCD1LG2	2.51	0.0033	0.0567
ENC1	2.51	0.0002	0.0076
SYTL3	2.51	3.15E-08	8.24E-06
DEFB124	2.51	0.006	0.0853
ITPR1	2.52	7.51E-06	0.0007
KIAA1549L	2.53	2.12E-07	3.56E-05
CD82	2.54	8.47E-06	0.0007
TRIM6-TRIM34	2.54	0.0415	0.2656
COL6A1	2.56	1.24E-05	0.001
ABHD3	2.56	0.0086	0.1061
TIE1	2.56	0.0013	0.0305
PCDH9	2.58	0.0004	0.0145
PDE4DIP	2.58	0.0004	0.0145
ADAMTS6	2.58	3.34E-06	0.0003
RORB	2.59	3.24E-06	0.0003
GPR135	2.59	0.044	0.2747
AJAP1	2.6	0.0094	0.1118
EIF2S2	2.6	0.0349	0.2416
TBX2	2.62	9.13E-07	0.0001
NCEH1	2.63	1.89E-06	0.0002
MSR1	2.64	1.21E-05	0.001
SERINC5	2.64	5.22E-08	1.14E-05
FILIP1	2.66	6.95E-06	0.0007
SAMD3	2.66	1.16E-06	0.0001
ARHGEF10	2.66	0.0439	0.2743
STAMBPL1	2.73	3.49E-05	0.0022
HDAC9	2.75	5.26E-08	1.14E-05
PDE2A	2.76	0.0006	0.0176
MYEOV	2.76	7.14E-05	0.0038
APCDD1L	2.77	1.59E-05	0.0012
TMEM200A	2.79	7.90E-07	0.0001

C4orf22	2.8	7.53E-06	0.0007
AP1S1	2.8	0.0093	0.1108
ZNF697	2.8	1.39E-05	0.0011
EIF5A2	2.8	3.03E-05	0.002
DUSP6	2.82	0.0008	0.0222
TAOK3	2.86	3.46E-08	8.72E-06
PAX6	2.88	0.0229	0.1913
DNAH5	2.88	0.0134	0.1383
ADTRP	2.9	1.25E-05	0.001
TRHDE	2.91	4.82E-09	1.81E-06
MFAP3L	2.93	7.06E-06	0.0007
TACSTD2	2.93	2.34E-06	0.0003
ZNF582-AS1	2.94	5.52E-08	1.18E-05
THRAP3	2.98	9.31E-07	0.0001
SOX30	3.01	1.84E-06	0.0002
SDCCAG8	3.01	3.62E-11	2.99E-08
PITPNC1	3.01	2.30E-06	0.0003
GRPR	3.02	0.0085	0.1052
LRIG1	3.02	1.57E-06	0.0002
NFE2L3	3.02	3.32E-08	8.50E-06
GCNT2	3.04	4.62E-07	6.93E-05
GAL	3.04	0.0039	0.0644
NTN4	3.07	9.26E-06	0.0008
FUBP3	3.08	0.0042	0.0674
NFKB2	3.08	2.50E-09	1.09E-06
RPS6KA5	3.11	0.0002	0.0072
PLAUR	3.11	2.87E-10	1.71E-07
KCNK1	3.15	1.23E-05	0.001
PTPRB	3.16	3.28E-06	0.0003
FMN1	3.16	5.27E-08	1.14E-05
PDE10A	3.17	2.98E-08	8.08E-06
BHLHE41	3.17	3.76E-05	0.0023
EVI2A; EVI2B	3.22	2.88E-06	0.0003
CRNDE	3.22	4.39E-08	1.01E-05
RRAD	3.24	1.50E-05	0.0011
ATP1A3	3.26	2.07E-05	0.0015
ACTR3C	3.28	2.80E-09	1.11E-06
CAMK2N1	3.38	2.37E-07	3.84E-05
FST	3.4	9.86E-07	0.0001
SERPINA9	3.45	0.0018	0.0381
SPRY4	3.48	3.82E-05	0.0024
FBXL13	3.63	2.87E-08	7.99E-06
RCN3	3.72	4.88E-08	1.10E-05
STC1	3.72	0.0091	0.1101
SEMA7A	3.75	7.89E-09	2.82E-06
PRDM1	3.8	1.70E-05	0.0012
FAT4	3.93	9.09E-06	0.0008
ADGRL2	4	2.95E-12	3.34E-09
AKR1E2	4.02	1.08E-10	7.27E-08
OTUD6B	4.06	0.0001	0.0052
SPANXA1	4.15	3.34E-06	0.0003
IL1A	4.19	0.0022	0.0426
SERPINB7	4.26	1.92E-06	0.0002
BIRC3	4.29	1.65E-05	0.0012
GOLGA8M	4.43	2.38E-09	1.08E-06
FMN1	4.52	1.46E-07	2.59E-05
SPANXA2	4.6	8.42E-08	1.66E-05
KCNK1	4.64	1.98E-07	3.37E-05
AFF3	4.7	2.13E-08	6.53E-06
SPANXC; SPANXD	4.72	9.57E-08	1.83E-05
GGT1	4.86	2.02E-12	2.54E-09
PAQR5	4.94	4.83E-10	2.73E-07
ARHGAP18	5.01	2.78E-11	2.49E-08
SPANXD	5.08	2.35E-07	3.84E-05
DUSP10	5.36	6.55E-06	0.0006
SCG5	5.74	7.98E-08	1.60E-05
FGF5	6.04	2.68E-10	1.64E-07
GFP72	6.2	1.96E-08	6.10E-06
TRIM6	6.29	4.33E-06	0.0004
TRIM55	6.29	1.12E-10	7.30E-08
ANTXR2	6.5	2.67E-12	3.18E-09
GOLGA8J; GOLGA8IP	6.66	3.83E-11	3.04E-08
BCL2A1	6.89	6.84E-05	0.0037
PTPN7	7.14	2.46E-08	7.20E-06
NAV3	7.5	8.84E-08	1.71E-05
RFX8	7.56	4.21E-11	3.22E-08
ESM1	7.64	6.97E-07	9.77E-05
HCLS1	8.78	6.28E-11	4.49E-08
SCN4A	8.79	6.61E-13	9.45E-10
MCTP1	11.56	3.01E-11	2.58E-08
ARHGDI	12.7	2.59E-09	1.11E-06
DNAH11	16.7	8.19E-09	2.83E-06
FRMD4A	18.68	2.87E-14	8.78E-11
KCTD4	19.09	4.68E-13	7.47E-10
COL6A3	21.49	2.47E-11	2.30E-08
HMGA2	24.19	1.89E-13	3.68E-10
IL1B	25.75	1.91E-09	9.00E-07

SPANXB1	32.57	1.29E-13	2.76E-10
LSAMP	42.05	8.74E-17	6.25E-13
SLCO1B3	46.88	6.27E-14	1.49E-10
IGF2BP3	79.01	6.20E-18	6.65E-14
IL1RAPL1	83.4	2.11E-14	7.56E-11
CALB1	113.34	9.09E-09	3.10E-06

Table S 2.5 Signatures from the GSEA Hallmark database that were enriched in the OVCAR8 parental spheroids compared to NUAK1-KO spheroids

Signature	SIZE	NES	NOM p-val	FDR q-val
HALLMARK_INTERFERON_ALPHA_RESPONSE	91	-2.7054312	0	0
HALLMARK_INTERFERON_GAMMA_RESPONSE	191	-2.4021258	0	0
HALLMARK_OXIDATIVE_PHOSPHORYLATION	190	-2.3491118	0	0
HALLMARK_TGF_BETA_SIGNALING	53	-2.2527528	0	0
HALLMARK_EPITHELIAL_MESENCHYMAL_TRANSITION	192	-2.0939176	0	0
HALLMARK_UV_RESPONSE_DN	138	-1.9165574	0	0.001234232
HALLMARK_ESTROGEN_RESPONSE_LATE	194	-1.8456159	0	0.001557613
HALLMARK_COAGULATION	134	-1.7818395	0	0.001941036
HALLMARK_FATTY_ACID_METABOLISM	154	-1.6792668	0	0.005176689
HALLMARK_GLYCOLYSIS	192	-1.6327271	0	0.007976532
HALLMARK_ESTROGEN_RESPONSE_EARLY	192	-1.5897167	0	0.015067029
HALLMARK_APOPTOSIS	155	-1.5840265	0.001996008	0.015184187
HALLMARK_XENOBIOTIC_METABOLISM	193	-1.4987085	0.00631579	0.030580582
HALLMARK_PEROXISOME	98	-1.470946	0.018828452	0.036381334
HALLMARK_IL6_JAK_STAT3_SIGNALING	85	-1.4557805	0.02970297	0.038870838
HALLMARK_COMPLEMENT	189	-1.4311881	0.012578616	0.04369105
HALLMARKADIPOGENESIS	189	-1.4024873	0.008350731	0.054584257
HALLMARK_DNA_REPAIR	138	-1.4016854	0.013861386	0.051881213
HALLMARK_APICAL_JUNCTION	193	-1.3409612	0.021097047	0.08460455
HALLMARK_P53_PATHWAY	192	-1.3290477	0.036053132	0.088990174
HALLMARK_ANDROGEN_RESPONSE	95	-1.3151934	0.06464647	0.095708445
HALLMARK_BILE_ACID_METABOLISM	110	-1.2827135	0.067510545	0.11766519
HALLMARK_MYOGENESIS	193	-1.250651	0.077380955	0.14307003
HALLMARK_HYPOXIA	195	-1.2473122	0.05394191	0.14089133
HALLMARK_HEDGEHOG_SIGNALING	33	-1.2160786	0.19161677	0.17120273
HALLMARK_NOTCH_SIGNALING	31	-1.1836603	0.23353294	0.20465736
HALLMARK_CHOLESTEROL_HOMEOSTASIS	69	-1.1732962	0.20762712	0.21209985
HALLMARK_UV_RESPONSE_UP	153	-1.0836782	0.26112187	0.37113476
HALLMARKHEME_METABOLISM	188	-1.057075	0.29892474	0.4191625
HALLMARK_UNFOLDED_PROTEIN_RESPONSE	101	-0.99530345	0.4732334	0.5657768
HALLMARK_ALLOGRAFT_REJECTION	194	-0.96332645	0.54545456	0.6399002
HALLMARK_MTORC1_SIGNALING	194	-0.92412955	0.6653144	0.7322477
HALLMARK_KRAS_SIGNALING_DN	189	-0.9128246	0.68801653	0.7430476
HALLMARK_MYC_TARGETS_V1	182	-0.88959765	0.7632094	0.7847153
HALLMARK_ANGIOGENESIS	34	-0.81437385	0.77124184	0.92550606
HALLMARK_PI3K_AKT_MTOR_SIGNALING	102	-0.77584875	0.9198397	0.951884
HALLMARK_REACTIVE_OXIGEN_SPECIES_PATHWAY	46	-0.7286609	0.90153176	0.96541804

Table S 2.6 Signatures from the Curated Canonical database that were enriched in the OVCAR8 parental spheroids compared to NUAK1-KO spheroids

Signature	SIZE	NES	NOM p-val	FDR q-val
REACTOME_TCA_CYCLE_AND_RESPIRATORY_ELECTRON_TRANSPORT	117	2.4250476	0	0
REACTOME_RESPIRATORY_ELECTRON_TRANSPORT	68	2.3931193	0	0
REACTOME_RESPIRATORY_ELECTRON_TRANSPORT_ATP_SYNTHESIS_BY_CHEMOSMOTIC_COUPLING_AND_HEAT_PRODUCTION_BY_UNCOUPLING_PROTEINS	83	2.3558912	0	0
KEGG_OXIDATIVE_PHOSPHORYLATION	118	2.172282	0	0.002648652
KEGG_PARKINSONS_DISEASE	114	2.1558495	0	0.002933157
KEGG_PEROXISOME	78	2.0882215	0	0.005975086
REACTOME_INTEGRIN_CELL_SURFACE_INTERACTINS	76	2.0570054	0	0.009632743
PID_INTEGRIN3_PATHWAY	43	2.0240114	0	0.014649713
REACTOME_INTERFERON_ALPHA_BETA_SIGNALING	62	2.0232646	0	0.013021966
KEGG_HUNTINGTONS_DISEASE	166	1.9060166	0	0.054231856
REACTOME_CHOLESTEROL BIOSYNTHESIS	21	1.859071	0	0.08791673
KEGG_METABOLISM_OF_XENOBIOTICS_BY_CYP450	58	1.8561774	0	0.082995996
REACTOME_PEROXISOMAL_LIPID_METABOLISM	20	1.8259057	0.006369427	0.1092535
KEGG_ALZHEIMERS_DISEASE	154	1.8171077	0	0.11037827
PID_ALK1_PATHWAY	24	1.7910784	0.004192872	0.13650955
BIOCARTA_IL10_PATHWAY	17	1.7874752	0.005882353	0.13265434
KEGG_TGF_BETA_SIGNALING_PATHWAY	82	1.786499	0	0.12653384
KEGG_VALINE_LEUCINE_AND_ISOLEUCINE_DEGRADATION	43	1.7849728	0	0.12104583
PID_INTEGRINS_PATHWAY	17	1.7796471	0.002155172	0.120900206
PID_INTEGRIN_A4B1_PATHWAY	31	1.778438	0	0.116658404
REACTOME_PYRUVATE_METABOLISM_AND_CITRIC_ACID_TCA_CYCLE	38	1.745068	0.001949318	0.152775
PID_SYNDECAN_4_PATHWAY	31	1.736503	0.006122449	0.15713038
REACTOME_DOWNREGULATION_OF_TGF_BETA_RECEPTOR_SIGNALING	21	1.7352419	0.004338395	0.15202415
NABA_ECM_GLYCOPROTEINS	190	1.7350745	0	0.1457966
REACTOME_GENERATION_OF_SECOND_MESSENGER MOLECULES	25	1.7221626	0.008510638	0.15870148
REACTOME_REGULATION_OF_WATER_BALANCE_BY_RENAL_AQUAPORINS	42	1.7166786	0.00203666	0.15961316
KEGG_BUTANOATE_METABOLISM	34	1.7116945	0.00617284	0.16023678
REACTOME_TGF_BETA_RECECTOR_SIGNALING_ACTIVATES_SMADS	23	1.707847	0.005882353	0.15925156
KEGG_CITRATE_CYCLE_TCA_CYCLE	30	1.7071004	0.015350877	0.15484129
KEGG_LYSOSOME	112	1.69712	0.002070393	0.1625121
REACTOME_INTEGRIN_ALPHA1BETA3_SIGNALING	26	1.6940324	0.012219959	0.16171302
REACTOME_AMINO_ACID_SYNTHESIS_AND_INTERCONVERSION_TRANSAMINATION	16	1.6850712	0.012320329	0.1695966
REACTOME_CITRIC_ACID_CYCLE_TCA_CYCLE	19	1.683228	0.018947368	0.16729201
REACTOME_METABOLISM_OF_AMINO_ACIDS_AND_DERIVATIVES	187	1.6830503	0	0.16256264
BIOCARTA_TGFB_PATHWAY	17	1.6720524	0.010438413	0.17372315
PID_CASPASE_PATHWAY	51	1.6644408	0	0.17951979
REACTOME_REGULATION_OF_INSULIN_SECRETION_BY_GLUCAGON_LIKE_PEPTIDE1	41	1.6560845	0.006122449	0.18740012

KEGG_O_GLYCAN BIOSYN THESIS	26	1.6547316	0.004166667	0.1838521
REACTOME_GLUCAGON_SIGNALING_IN_METABOLIC_ REGULATION	32	1.6478745	0.018404908	0.19089222
REACTOME_ADP_SIGNALLING_THROUGH_P2RY12	21	1.6463863	0.016771488	0.18813518
PID_HNF3A_PATHWAY	40	1.6354098	0.013182675	0.20152982
KEGGARGININE_AND_PR OLINE_METABOLISM	49	1.6323824	0.012244898	0.20134878
REACTOME_INHIBITION_OF_INSULIN_SECRETION_BY _ADRENALINE_NORADREN ALINE	24	1.6316165	0.027559055	0.19779563
NABA_CORE_MATRISOME	266	1.6309464	0	0.19421901
REACTOME_DNA_STRAND_ELONGATION	30	1.6283588	0.028397566	0.19361688
KEGG_ALLOGRAFT_REJECTION	35	1.6252248	0.010504202	0.19454151
REACTOME_G_ALPHA_Z_SIGNALLING_EVENTS	43	1.6224967	0.008264462	0.19412698
REACTOME_AUTODEGRADATION_OF_CDH1_BY_CDH1 _APC_C	55	1.6214255	0.007920792	0.19180961
KEGG_ECM_RECECTOR_IN TERACTION	79	1.6204288	0	0.18929477
REACTOME_GROWTH_HORMONE_RECECTOR_SIGNAL ALING	24	1.6184843	0.015873017	0.1887426
REACTOME_APOPTOSIS	137	1.6184403	0.002123142	0.18514235
BIOCARTA_AMI_PATHWAY	20	1.6128327	0.027083334	0.19010895
BIOCARTA_INTRINSIC_PATH HWAY	23	1.6119828	0.016359918	0.18761066
KEGG_Nicotinate_and_n icotinamide_metabolism	21	1.6096189	0.01724138	0.18777327
BIOCARTA_NKCELLS_PATH WAY	19	1.6088877	0.033333335	0.1852934
REACTOME_APOPTOTIC_C LEAVAGE_OF_CELLULAR_ PROTEINS	35	1.6031371	0.018595042	0.19020115
PID_TAP63_PATHWAY	51	1.6026647	0.008333334	0.18769751
PID_P75_NTR_PATHWAY	68	1.5984294	0.00625	0.1909825
REACTOME_INTERFERON_ SIGNALING	145	1.5983958	0	0.18776758
REACTOME_SIGNALING_B Y_BMP	21	1.5963877	0.01996008	0.1874588
REACTOME_ER_PHAGOSOME_PATHWAY	57	1.5889894	0.012422361	0.19604644
KEGG_DNA_REPLICATION	36	1.5863802	0.016985139	0.1970921
REACTOME_INTRINSIC_PA THWAY_FOR_APOPTOSIS	28	1.5859164	0.024742268	0.19466896
REACTOME_SYNTHESIS_O F_DNA	89	1.5851712	0.006122449	0.19273548
REACTOME_G_PROTEIN_ACTIVATION	27	1.5849619	0.02584493	0.19019404
KEGG_PORPHYRIN_AND_C HLOROPHYLL_METABOLISM	31	1.5838822	0.016064256	0.18908563
REACTOME_INTERFERON_ GAMMA_SIGNALING	59	1.5833796	0.006097561	0.18712942
REACTOME_OPIOID_SIGNALLING	76	1.576013	0.008403362	0.19460455
REACTOME_BRANCHED_C HAIN_AMINO_ACID_CATABOLISM	17	1.5754918	0.028455285	0.19233225
KEGG_GLYCEROLIPID_METABOLISM	42	1.5669012	0.006185567	0.20247081
REACTOME_APCCDH1_MEDIATED_DEGRADATION_OF_CDC20_AND_OTHER_APCCDH1_TARGETED_PROTEINS_IN_LATE_MITOSIS_EARLY_G1	63	1.5635766	0.008547009	0.20472707
REACTOME_RECYLCLING PATHWAY_OF_L1	26	1.5624045	0.023166023	0.20380454
REACTOME_PLATELET_AGGREGATION_PLUG_FORMATION	34	1.5601443	0.022869023	0.20457901
REACTOME_RESOLUTION_OF_AP_SITES_VIA_THE_MULTIPLE_NUCLEOTIDE_PATHWAY_REPLACEMENT_PATHWAY	17	1.5497735	0.042769857	0.21738997
KEGG_AXON_GUIDANCE	125	1.5405525	0.002028398	0.22934508
REACTOME_PROSTACYCLIN_SIGNALLING_THROUGH_PROSTACYCLIN_RECEPTOR	19	1.5380563	0.042283297	0.23040678
PID_AP1_PATHWAY	67	1.5363431	0.00845666	0.23027234

PID_EPHA2_FWD_PATHWAY	19	1.5362239	0.054166667	0.22750781
REACTOME_AQUAPORIN_MEDIATED_TRANSPORT	49	1.5340035	0.021611001	0.22799714
PID_INTEGRIN1_PATHWAY	61	1.5332756	0.006423983	0.22650884
PID_ECADHERIN_NASCENT_AJ_PATHWAY	37	1.5300757	0.027484143	0.2294265
REACTOME_ASSEMBLY_OF_THE_PRE_REPLICATIVE_COMPLEX	62	1.529226	0.022633744	0.2281819
PID_HESHEY_PATHWAY	44	1.5289323	0.023861172	0.2259424
NABA_BASEMENT_MEMBRANES	38	1.5224735	0.031936128	0.2337058
BIOCARTA_HER2_PATHWAY	21	1.5207173	0.04185022	0.23369944
REACTOME_G_BETA_GAMA_SIGNALLING_THROUGH_PLC_BETA	20	1.5197867	0.056962024	0.23223741
PID_SMAD2_3PATHWAY	17	1.517826	0.035490606	0.23293257
KEGG_GLYCOSYLPHOSPHATIDYLINOSITOL_GPLANC_HOR BIOSYNTHESIS	23	1.5174003	0.048523206	0.23106578
PID_AVB3_INTEGRIN_PATHWAY	70	1.515213	0.008032128	0.23194045
BIOCARTA_COMP_PATHWAY	19	1.5141706	0.05394191	0.23093401
PID_AUDISSL2PATHWAY	46	1.508477	0.018556701	0.23700342
REACTOME_PHASE_II_CONJUGATION	57	1.5076764	0.026052104	0.23556963
KEGG_ARRHYTHMOGENIC_RIGHT_VENTRICULAR_CA_RDIOMYOPATHY_ARVC	71	1.5042404	0.016877636	0.23883425
PID_ATF2_PATHWAY	54	1.5029099	0.016736401	0.23807319
REACTOME_SIGNALLING_BY_TGF_BETA_RECECTOR_COMPLEX	59	1.5025319	0.010245902	0.236288
KEGG_GLYOXALATE_AND_DICARBOXYLATE_METABOLISM	16	1.5023569	0.056603774	0.23414253
REACTOME_VIF_MEDIATE_D_DEGRADATION_OF_APO_BEC3G	48	1.501078	0.025423728	0.23369037
BIOCARTA_CASPASE_PATHWAY	23	1.4991196	0.039832287	0.23434655
REACTOME_MRNA_SPLICING_MINOR_PATHWAY	38	1.4943633	0.030947777	0.23950861
REACTOME_REGULATION_OF_ORNITHINE_DECARBOXYLASE_ODC	46	1.4941695	0.034907598	0.237467
REACTOME_G_PROTEIN_BETA_GAMMA_SIGNALLING	28	1.4922813	0.042944785	0.2384413
KEGG_ASCORBATE_AND_ALDARATE_METABOLISM	15	1.4905654	0.048728812	0.23891298
REACTOME_CYTOKINE_SIGNALING_IN_IMMUNE_SYSTEM	251	1.4859794	0.0041841	0.24373905
REACTOME_MITOCHONDRIAL_PROTEIN_IMPORT	48	1.4854137	0.028747434	0.24241784
KEGG_ALANINE ASPARTATE_AND GLUTAMATE_METABOLISM	31	1.4851748	0.043841336	0.24050972
KEGG_INTESTINAL_IMMUNE_NETWORK_FOR_IGA_PRODUCTION	45	1.4738513	0.035789475	0.25693157
REACTOME_METABOLISM_OF_NUCLEOTIDES	65	1.4695488	0.026915114	0.26149666
BIOCARTA_ALK_PATHWAY	35	1.466976	0.039748956	0.26325598
KEGG_HYPERTROPHIC_CARDIOMYOPATHY_HCM	80	1.4649509	0.021653544	0.2639134
KEGG_TRYPTOPHAN_METABOLISM	38	1.4645885	0.046184737	0.2621237
REACTOME_REGULATION_OF_APOTOPSIS	54	1.4624798	0.050916497	0.26320863
REACTOME_ORC1_REMOVE_AL_FROM_CHROMATIN	64	1.462169	0.018480493	0.26137525
REACTOME_PKA_MEDIATE_D_PHOSPHORYLATION_OF_CREB	16	1.4615057	0.057082452	0.26017174
REACTOME_CELL_CYCLE_CHECKPOINTS	109	1.4586178	0.018480493	0.26268274
REACTOME_MHC_CLASS_II_ANTIGEN_PRESENTATION	87	1.458269	0.018255578	0.26099625
REACTOME_SCFSKP2_ME DIATED_DEGRADATION_OF_P27_P21	52	1.4552923	0.04828974	0.26384956
REACTOME_DESTABILIZATION_OF_MRNA_BY_AUF1_HNRNP_D0	46	1.4532164	0.032719836	0.26526627
REACTOME_RESPONSE_TO_ELEVATED_PLATELET_C	76	1.4456699	0.033333335	0.27596062

YTOSOLIC_CA2				
KEGG GLUTATHIONE_MET_ABOLISM	47	1.4452895	0.058189657	0.27441123
REACTOME_AP_C_CDC20_MEDIATED_DEGRADATION_OF_MITOTIC_PROTEINS	64	1.4413111	0.032719836	0.27927876
REACTOME_MITOCHONDRIAL_TRNA_AMINOACYLATION	19	1.4376354	0.06823028	0.28373176
REACTOME_AXON_GUIDANCE	232	1.4360907	0.002016129	0.28412792
REACTOME_O_LINKED_GLYCOSYLATION_OF_MUCINS	52	1.4360363	0.050209206	0.28187135
REACTOME_G_BETA_GAMA_SIGNALLING_THROUGH_PI3KGAMMA	25	1.4359705	0.06521739	0.2797048
KEGG_FATTY_ACID_METABOLISM	41	1.4352506	0.045454547	0.27877176
BIOCARTA_STATHMIN_PATHWAY	19	1.4341376	0.065979384	0.27850756
BIOCARTA_BIOPEPTIDES_PATHWAY	41	1.4334395	0.06637168	0.27751234
BIOCARTA_PPPARA_PATHWAY	54	1.4308294	0.05050505	0.28013918
REACTOME_AUTODEGRADATION_OF_THE_E3_UBIQUITIN_LIGASE_COP1	46	1.4302399	0.03862661	0.27889702
REACTOME_GLUCONEOGENESIS	31	1.4284494	0.06944445	0.2798538
BIOCARTA_NTHI_PATHWAY	22	1.4241819	0.07459678	0.28511232
REACTOME_PLC_BETA_ME DIATED_EVENTS	41	1.4226469	0.04158004	0.28536105
REACTOME_ANTIGEN_PRESENTATION_FOLDING_ASSEMBLY_AND_PEPTIDE_LOADING_OF_CLASS_I_MHC	20	1.4222279	0.09445585	0.28399003
KEGG_BETA_ALANINE_METABOLISM	22	1.4204473	0.073068894	0.2850732
REACTOME_SYNTHESIS_OF_BILE_ACIDS_AND_BILE_SALTS_VIA_7ALPHA_HYDROXYCHOLESTEROL	15	1.4190136	0.10759494	0.28531414
ST_GRANULE_CELL_SURVIVAL_PATHWAY	26	1.4145983	0.080912866	0.29086304
BIOCARTA_IGF1R_PATHWAY	23	1.4081068	0.08130081	0.30137894
REACTOME_M_G1_TRANSITION	77	1.404145	0.022357723	0.30706486
KEGG_PROTEASOME	43	1.4038216	0.05263158	0.3056058
REACTOME_SEMAPHORIN_INTERACTIONS	62	1.4031359	0.043650795	0.30476323
REACTOME_CDK_MEDIATE_D_PHOSPHORYLATION_AN D_REMOVAL_OF_CDC6	45	1.4027147	0.05870021	0.30335867
REACTOME_SIGNAL_AMPLIFICATION	31	1.4025677	0.06736842	0.3014733
REACTOME_SIGNAL_TRANSDUCTION_BY_L1	33	1.4009938	0.07489879	0.3023463
REACTOME_SCF_BETA_TRCP_MEDiated_DEGRADATION_OF_EM1	48	1.3943431	0.052287582	0.31198832
REACTOME_S_PHASE	105	1.3923216	0.03937008	0.31380975
REACTOME_CHONDROITIN_SULFATE_DERMATAN_SULFATE_METABOLISM	46	1.3918942	0.055555556	0.312446
PID_TOLL_ENDOGENOUS_PATHWAY	24	1.3889744	0.09221312	0.31561768
PID_P53_REGULATION_PATHWAY	53	1.3886273	0.07355865	0.31401545
KEGG_ANTIGEN_PROCESSING_AND_PRESENTATION	68	1.3864337	0.0513347	0.3164378
KEGG_DRUG_METABOLISM_OTHER_ENZYMES	37	1.3834212	0.055776894	0.32025695
REACTOME_ANTIGEN_PROCESSING_CROSS_PRESENTATION	71	1.3825823	0.053892214	0.31977093
BIOCARTA_PROTEASOME_PATHWAY	28	1.3795207	0.0927835	0.32381332
REACTOME_SIGNALING_BY_WNT	61	1.3795192	0.050607286	0.32169688
BIOCARTA_PML_PATHWAY	16	1.3790128	0.12981744	0.32048893
REACTOME_CELL_DEATH_SIGNALLING_VIA_NRAGE_NRIF_AND_NADE	56	1.3743217	0.067940556	0.32792503
KEGG_LYSINE_DEGRADATION	40	1.3719423	0.07272727	0.33042938
REACTOME_AP_C_CDC20_MEDIATED_DEGRADATION	21	1.371304	0.109126985	0.32949287

_OF_NEK2A				
KEGG_SPliceosome	116	1.3685038	0.031712472	0.33274302
REACTOME_P53_INDEPENDENT_G1_S_DNA_DAMAGE_CHECKPOINT	47	1.3685005	0.07858546	0.3306503
PID_UPA_UPAR_PATHWAY	42	1.3655357	0.07643312	0.33455923
REACTOME_REGULATION_OF_MITOTIC_CELL_CYCLE	76	1.363621	0.058139537	0.33615276
REACTOME_APOPTOTIC_EXECUTION_PHASE	49	1.3584377	0.06048387	0.3441212
REACTOME_GLYCOSPHINGOLIPID_METABOLISM	36	1.356716	0.10580913	0.34512013
REACTOME_CELL_SURFACE_INTERACTIONS_AT_THE_VASCULAR_WALL	81	1.3563334	0.07465619	0.34377578
REACTOME_CDT1_ASSOCIATION_WITH_THE_CDC6_ORC_ORIGIN_COMPLEX	53	1.3545519	0.06779661	0.3452327
PID_SYNDECAN_2_PATHWAY	31	1.3529468	0.100603625	0.34632286
KEGG_DRUG_METABOLISM_CYTOCHROME_P450	60	1.35216	0.070866145	0.34573102
REACTOME_BASE_EXCISION_REPAIR	19	1.3510861	0.118644066	0.34577295
KEGG_CSTEINE_AND_METHIONINE_METABOLISM	33	1.3494531	0.08118812	0.34694788
BIOCARTA_RHO_PATHWAY	31	1.3479638	0.10433071	0.3478268
KEGG BIOSYNTHESIS_OF_UNSATURATED_FATTY_ACIDS	18	1.3464526	0.12228797	0.34845555
REACTOME_HS_GAG_DEGRADATION	19	1.346061	0.12068965	0.34707668
REACTOME_PURINE_METABOLISM	32	1.3449745	0.11196911	0.3472988
REACTOME_DEVELOPMENTAL_BIOLOGY	368	1.3437004	0.003846154	0.34777343
REACTOME_OXYGEN_DEPENDENT_PROLINE_HYDROXYLATION_OF_HYPOXIA_INDUCIBLE_FACTOR_ALPHA	16	1.3423727	0.14717741	0.3483318
REACTOME_CROSS_PRESENTATION_OF_SOLUBLE_EXOGENOUS_ANTIGENS_ENDOSOMES	46	1.3418329	0.09650924	0.3474075
KEGG_TERPENOID_BACKBONE BIOSYNTHESIS	15	1.3417426	0.11825726	0.3456439
PID_SMAD2_3NUCLEAR_PATHWAY	79	1.340966	0.04592902	0.34527993
PID_LYMPHANGIOGENESIS_PATHWAY	23	1.3390052	0.12698413	0.34728825
REACTOME_CHONDROITIN_SULFATE BIOSYNTHESIS	18	1.3381987	0.13948497	0.34675038
PID_ENDOTHELIN_PATHWAY	61	1.3360196	0.08366534	0.34911
KEGG_GLYCOSAMINOGLYCAN_BIOSYNTHESIS_CHO_NDROITIN_SULFATE	21	1.3334126	0.10897436	0.35247245
REACTOME_PYRIMIDINE_METABOLISM	22	1.3328283	0.13247864	0.35198689
PID_CXCR3_PATHWAY	42	1.3292997	0.089324616	0.35729763
REACTOME_P53_DEPENDENT_G1_DNA_DAMAGE_RESPONSE	52	1.3274026	0.092402466	0.35894677
REACTOME_GOLGI_ASSOCIATED_VESICLE_BIOGENESIS	48	1.3266934	0.10123967	0.3584592
PID_INTEGRIN_CS_PATHWAY	25	1.3259953	0.12179487	0.35778698
PID_BMP_PATHWAY	42	1.3249217	0.08835341	0.35786015
REACTOME_SULFUR_AMINO_ACID_METABOLISM	24	1.3242701	0.108481266	0.3572813
REACTOME_MYOGENESIS	26	1.3224808	0.13721414	0.35902554
REACTOME_CLASS_I_MHC_MEDIATED_ANTIGEN_PRESENTATION	231	1.3202465	0.012552301	0.36134368
BIOCARTA_chemical_PATHWAY	21	1.3166109	0.14967462	0.3670731
REACTOME_COMPLEMENT CASCADE	29	1.3158318	0.10300429	0.36681148
PID_CDC42_PATHWAY	68	1.3147354	0.08085106	0.36733884
REACTOME_GLYCOSAMINOGLYCAN_METABOLISM	104	1.3146957	0.06138614	0.36553633
BIOCARTA_MITOCHONDRIAL_PATHWAY	21	1.3143437	0.13219616	0.364259
BIOCARTA_CYTOKINE_PATHWAY	20	1.3117241	0.13943355	0.3677875
BIOCARTA_MTA3_PATHWAY	18	1.3114395	0.136	0.36656293
PID_ECADHERIN_STABILIZATION_PATHWAY	41	1.3088132	0.10040161	0.3700528

REACTOME_BASIGIN_INTEGRATIONS	23	1.3070875	0.14020619	0.3716592
REACTOME_TRANS_GOLGI_NETWORK_VESICLE_BUDGING	55	1.3066349	0.081196584	0.3707941
PID_ERBB1_DOWNSTREAM_PATHWAY	103	1.3038006	0.057654075	0.3747982
REACTOME_ACTIVATION_OF_BH3_ONLY_PROTEINS	15	1.3001963	0.16561845	0.3804921
PID_GLYCAN_1PATHWAY	26	1.2992476	0.13636364	0.38056624
REACTOME_THROMBOXANE_SIGNALLING_THROUGH_TP_RECECTOR	23	1.2983276	0.16255145	0.38070503
REACTOME_PLATELET_ACTIVATION_SIGNALING_AND_AGGREGATION	191	1.2960998	0.03292181	0.38332626
PID_BETA_CATENIN_NUC_PATHWAY	78	1.29261	0.08074534	0.388585
REACTOME_SMOOTH_MUSCLE_CONTRACTION	21	1.2918873	0.13747646	0.38830063
SA_CASPASE CASCADE	19	1.2895951	0.16465864	0.39093965
REACTOME_ANTIGEN_PROCESSING_UBIQUITINATION_PROTEASOME_DEGRADATION	194	1.2891651	0.043841336	0.390076
KEGG_HISTIDINE_METABOLISM	28	1.2890482	0.14649682	0.3884272
PID_P53_DOWNSTREAM_PATHWAY	131	1.2867934	0.073839664	0.39093602
REACTOME_AP_C_CDC20_MEDIATED_DEGRADATION_OF_CYCLIN_B	19	1.2840316	0.16494845	0.3949651
BIOCARTA_TNFR1_PATHWAY	28	1.2839679	0.14838709	0.39326632
REACTOME_GLUCAGON_TYPE_LIGAND_RECEPTORS	33	1.28217	0.13100436	0.39534697
REACTOME_ADIPONECTIN_SIGNALLING_THROUGH_P2RY1	25	1.278918	0.14880952	0.40044922
REACTOME_DARPP_32_EVENTS	24	1.2774442	0.15923567	0.40159053
REACTOME_INHIBITION_OF_THE_PROTEOLYTIC_ACTIVITY_OF_AP_C_REQUIREMENT_FOR_THE_ONSET_OF_ANAPHASE_BY_MITOTIC_SPINDLE_CHECKPOINT_COMPONENTS	18	1.2771515	0.15821502	0.40047273
REACTOME_LAGGING_STRAND_SYNTHESIS	19	1.2763091	0.1724846	0.40036678
BIOCARTA_FAS_PATHWAY	29	1.2748996	0.15169661	0.40142906
BIOCARTA_TOLL_PATHWAY	35	1.2725172	0.11904762	0.4048366
BIOCARTA_GPCR_PATHWAY	33	1.271753	0.13742071	0.40458906
BIOCARTA_LAIR_PATHWAY	16	1.2710832	0.19361702	0.40416557
REACTOME_METABOLISM_OF_MRNA	179	1.2708623	0.056485355	0.40290046
REACTOME_NOTCH1_INTRACELLULAR_DOMAIN_REGULATES_TRANSCRIPTION	43	1.2698809	0.13763441	0.4033905
REACTOME_SIGNALLING_BY_NFNG	206	1.2681046	0.036437247	0.4054737
REACTOME_HEPARAN_SULFATE_HEPARIN_HS_GAG_METABOLISM	50	1.2679164	0.1211499	0.40399522
KEGG_REGULATION_OF_ACTIN_CYTOSKELETON	205	1.2657347	0.047904193	0.40670586
KEGG_PYRUVATE_METABOLISM	39	1.2650473	0.14315353	0.40641722
PID_NFAT_TFPATHWAY	46	1.262468	0.15904573	0.41022274
PID_ERBB1_RECEPATOR_PRINCIPAL_PATHWAY	32	1.2569407	0.14004377	0.42012954
REACTOME_ACTIVATION_OF_KAINATE_RECEPTORS_UPON GLUTAMATE_BINDING	31	1.2569343	0.17038539	0.41833034
REACTOME_YAP1_AND_WWTR1_TAZ_STIMULATED_GENE_EXPRESSION	23	1.2529324	0.16898608	0.4247278
REACTOME_L1CAM_INTERACTIONS	80	1.2526073	0.09430256	0.42368495
KEGG_PROPANOATE_METABOLISM	32	1.2520785	0.18552037	0.42307425
PID_FRA_PATHWAY	34	1.2517784	0.14020619	0.42196354
BIOCARTA_NFAT_PATHWAY	52	1.2513741	0.14314115	0.4210289
KEGG_SYSTEMIC_LUPUS_ERYTHEMATOSUS	120	1.2509726	0.08423326	0.42015368
PID_S1P_S1P2_PATHWAY	24	1.2463957	0.17054264	0.42823133
REACTOME_METABOLISM	384	1.245598	0.045454547	0.4281194

OF_PROTEINS				
REACTOME_SIGNALING_BY_NODAL	17	1.245027	0.18085106	0.42757112
PID_ANGIOPOETIN_RECEP_TOR_PATHWAY	50	1.2436651	0.13721414	0.42886978
KEGG_OTHER_GLYCAN_DEGRADATION	15	1.241906	0.22678186	0.43075255
KEGG_PHENYLALANINE_METABOLISM	17	1.2405703	0.1987315	0.43200192
BIOCARTA_IL22BP_PATHWAY	16	1.2395805	0.2153518	0.43217775
REACTOME_REGULATION_OF_MRNA_STABILITY_BY_PROTEINS_THAT_BIND_AU_RICH_ELEMENTS	75	1.2388806	0.13541667	0.43194094
BIOCARTA_MPR_PATHWAY	34	1.2374402	0.17735043	0.43327296
PID_A6B1_A6B4_INTEGRIN_PATHWAY	43	1.2357967	0.17729084	0.4352656
KEGG_ADHERENS_JUNCTION	70	1.2352532	0.14256619	0.4347976
REACTOME_REGULATION_OF_HYPOXIA_INDUCIBLE_FACTOR_HIF_BY_OXYGEN	22	1.2350552	0.18393235	0.4335034
REACTOME_NRAGE_SIGNALS_DEATH_THROUGH_JNK	41	1.2349473	0.15918367	0.43201908
PID_RAC1_PATHWAY	53	1.2309629	0.16966067	0.4388325
REACTOME_DOWNREGULATION_OF_SMAD2_3_SMA_D4_TRANSCRIPTIONAL_ACTIVITY	19	1.2298297	0.21267894	0.43943214
REACTOME_SYNTHESIS_OF_BILE_ACIDS_AND_BILE_SALTS	19	1.2295988	0.18834081	0.43822008
REACTOME_POST_CHAPERONIN_TUBULIN_FOLDING_PATHWAY	17	1.2295223	0.21442886	0.43668836
BIOCARTA_IL7_PATHWAY	16	1.2285291	0.22516556	0.43711108
PIDNECTIN_PATHWAY	29	1.2244577	0.19027483	0.44409105
REACTOME_CELL_CELL_COMMUNICATION	112	1.224034	0.105058365	0.44319782
PID_IL6_7_PATHWAY	46	1.2240045	0.17088607	0.44154856
REACTOME_ACTIVATION_OF_ATR_IN_RESPONSE_TO_REPLICATION_STRESS	34	1.2227597	0.17489712	0.44251665
REACTOME_METABOLISM_OF_RNA	221	1.2208753	0.07676349	0.44482574
BIOCARTA_IL6_PATHWAY	22	1.2176566	0.19315895	0.44985697
REACTOME_EXTENSION_OF_TELOMERES	26	1.216419	0.21205822	0.4509872
REACTOME_HOST_INTERACTIONS_OF_HIV_FACTORS	115	1.2158347	0.13457558	0.45058656
PID_LYSOPHOSPHOLIPID_PATHWAY	62	1.2122517	0.1573499	0.45680046
REACTOME_GABA_B_RECPTOR_ACTIVATION	37	1.2122144	0.18604651	0.45516706
REACTOME GLUTATHIONE_CONJUGATION	23	1.209929	0.19409283	0.45859396
KEGG_GRAFT_VERSUS_HOST_DISEASE	33	1.2096334	0.187251	0.45751047
REACTOME_DEADENYLATION_OF_MRNA	15	1.2083007	0.22520661	0.4588063
KEGG_FOCAL_ADHESION	191	1.2074447	0.0734127	0.4588754
PID_RHOA_REG_PATHWAY	44	1.2073356	0.1755102	0.45739502
NABA_ECM_AFFILIATED	162	1.2072409	0.12058212	0.45594892
REACTOME_P75_NTR_RECPTOR_MEDiated_SIGNALLING	76	1.2065825	0.17731959	0.45562923
REACTOME_TRIGLYCERIDE BIOSYNTHESIS	32	1.205922	0.176	0.45540994
REACTOME_NETRIN1_SIGNALING	36	1.2051767	0.20594479	0.4554365
KEGG_ASTHMA	28	1.2042783	0.20124482	0.45587027
REACTOME_G_ALPHA1213_SIGNALLING_EVENTS	70	1.2033397	0.15463917	0.4564222
REACTOME_G2_M_CHECK_POINTS	40	1.2033105	0.19620253	0.45485592
REACTOME_METABOLISM_OF_LIPIDS_AND_LIPOPROTEINS	448	1.2018013	0.0349345	0.45635274
PID_MYC_PATHWAY	24	1.2007858	0.2208589	0.45694143
KEGG_INOSITOL_PHOSPHATE_METABOLISM	53	1.1988648	0.1755424	0.45968112
REACTOME_CA_DEPENDENT_EVENTS	28	1.197744	0.18329939	0.4604455
REACTOME_CYCLINE_ASOCIATED_EVENTS_DURING_G1_S_TRANSITION	61	1.1968601	0.18110237	0.46081057
REACTOME_MEMORY_TRAFFICKING	119	1.1955295	0.13195877	0.46202788
REACTOME_METABOLISM	223	1.1927696	0.10759494	0.46664566

OF_CARBOHYDRATES				
REACTOME_THROMBIN_SIGNALLING_THROUGH_PROTEINASE_ACTIVATED_RECEPTEORS_PARS	32	1.192358	0.20675105	0.46592125
NABA_PROTEOGLYCANS	35	1.1859107	0.23382045	0.47842845
REACTOME_PLATELET_HOMOSTASIS	75	1.1851165	0.17735043	0.47861108
REACTOME_RNA_POL_III_TRANSCRIPTION_TERMINATION	18	1.1847438	0.22175732	0.47782165
REACTOME_SIGNALING_BY_NOTCH1	66	1.1845057	0.17515275	0.4767474
BIOCARTA_PYK2_PATHWAY	26	1.1823118	0.2281746	0.48000294
REACTOME_INTEGRATION_OF_ENERGY_METABOLISM	113	1.1823074	0.15576923	0.47837254
REACTOME_SIGNALING_BY_ROBO_RECECTOR	28	1.1806213	0.23173277	0.48052916
KEGG_CARDIAC_MUSCLE_CONTRACTION	74	1.1800472	0.18548387	0.48020235
KEGG_DILATED_CARDIOMYOPATHY	86	1.1786551	0.17453799	0.48166502
REACTOME_G1_S_TRANSITION	105	1.1780953	0.16962525	0.48130462
PID_REG_GR_PATHWAY	78	1.1773695	0.18558952	0.48128504
REACTOME_A_TETRASACCHARIDE_LINKER_SEQUENCE_REQUIRED_FOR_GAG_SYNTHESIS	25	1.177149	0.22360249	0.48028237
KEGG_SMALL_CELL_LUNG_CANCER	81	1.1760714	0.16016427	0.4811401
PID_INTEGRIN2_PATHWAY	29	1.1751229	0.22175732	0.4816548
REACTOME_KERATAN_SULFATE_KERATIN_METABOLISM	27	1.1748356	0.2402464	0.4806985
REACTOME_TCR_SIGNALING	49	1.1748091	0.20758483	0.47915816
PID_NFAT_3PATHWAY	51	1.1739318	0.21822034	0.4796431
REACTOME_PHOSPHORYLATION_OF_THE_AP_C	17	1.1714292	0.27405858	0.48346868
BIOCARTA_TOB1_PATHWAY	18	1.1702245	0.2542735	0.4845516
KEGG_PROGESTERONE_MEDiated_OOCYTE_MATURATION	82	1.1690614	0.16839917	0.48565003
KEGG_PURINE_METABOLISM	147	1.1689179	0.13436124	0.48435017
BIOCARTA_INFLAM_PATHWAY	27	1.1680384	0.2707889	0.48467195
REACTOME_LYSOSOME_VESICLE_BIOGENESIS	21	1.1663203	0.23991935	0.4870856
REACTOME_HS_GAG BIOSYNTHESIS	30	1.1662683	0.24236253	0.4856321
BIOCARTA_ACTINY_PATHWAY	20	1.1658527	0.2795031	0.48501176
REACTOME_INFAMMASOMES	16	1.1602263	0.26844263	0.49611852
PID_RETINOIC_ACID_PATHWAY	29	1.1581625	0.23732251	0.49907774
BIOCARTA_GSK3_PATHWAY	25	1.1555285	0.2631579	0.5034341
KEGG_GLYCINE_SERINE_AND_THREONINE_METABOLISM	29	1.1549215	0.24536082	0.5032427
PID_SHP2_PATHWAY	58	1.1546503	0.23061225	0.50224596
BIOCARTA_ERK_PATHWAY	28	1.1527913	0.25792813	0.5047303
PID_AR_NONGENOMIC_PATHWAY	30	1.1517929	0.252505	0.5054457
KEGG_ABC_TRANSPORTERS	44	1.1509537	0.2392638	0.5056224
REACTOME_NGF_SIGNALLING_VIA_TRKA_FROM_THE_PLASMA_MEMBRANE	131	1.1487507	0.20164609	0.50901383
PID_P38_ALPHA_BETA_DOWNSTREAM_PATHWAY	36	1.1485236	0.24946696	0.50799906
REACTOME_ACTIVATION_OF_NFKAPPAB_IN_B CELLS	60	1.1478461	0.21084337	0.50802785
REACTOME_MRNA_SPLICING	96	1.1465719	0.19750519	0.5095155
KEGG_BASE_EXCISION_REPAIR	33	1.1460731	0.25531915	0.5091339
KEGG_JAK_STAT_SIGNALING_PATHWAY	147	1.1458316	0.20295984	0.5080585
BIOCARTA_GATA3_PATHWAY	16	1.145746	0.31543624	0.50669235
PID_IL23_PATHWAY	37	1.1403216	0.27348644	0.51786673
ST_WNT_BETA_CATEPIN_P	29	1.1402211	0.26914662	0.51648617

ATHWAY				
REACTOME_ASSOCIATION_OF_TRIC_CCT_WITH_TAR_GET_PROTEINS_DURING_BIOSYNTHESIS	24	1.1396415	0.27865613	0.51631373
REACTOME_ADAPTIVE_IMMUNE_SYSTEM	495	1.139043	0.09255533	0.51617795
REACTOME_KERATAN_SULFATE BIOSYNTHESIS	24	1.1380419	0.26839826	0.5169712
PID_AR_TF_PATHWAY	50	1.135453	0.23043478	0.5213752
REACTOME_POST_TRANSLATIONAL_PROTEIN_MODIFICATION	176	1.1344062	0.19246861	0.5221052
REACTOME_PKB_MEDIATE_D_EVENTS	28	1.1329242	0.2813187	0.5239958
REACTOME_REGULATION_OF_INSULIN_SECRETION	87	1.1328231	0.20625	0.5226631
REACTOME_SMAD2_SMAD3_SMAD4_HETEROTRIMER_REGULATES_TRANSCRIPTION	25	1.1320785	0.27216494	0.5228225
KEGG_MELANOGENESIS	97	1.1303623	0.22403258	0.525154
PID_RHODOPSIN_PATHWAY	24	1.1281251	0.31558186	0.5288796
KEGG_CELL_ADHESION_MOLECULES_CAMS	130	1.1258861	0.19488189	0.53253585
REACTOME_DAG_AND_IP3_SIGNALING	29	1.1253929	0.29124236	0.5322447
REACTOME_TRANSCRIPTITIONAL_ACTIVITY_OF_SMAD2_SMAD3_SMAD4_HETERO TRIMER	36	1.1239011	0.25955734	0.53418523
REACTOME_CIRCADIAN_RHYTHM_EXPRESSION_OF_EXPRESSION_BY_REV_ERBA	21	1.1232257	0.29613733	0.53434956
REACTOME_G_ALPHA_I_SIGNALLING_EVENTS	185	1.1216449	0.17755102	0.53643286
REACTOME_CELL_JUNCTION_ORGANIZATION	72	1.1187555	0.24418604	0.54171276
PID_IFNG_PATHWAY	39	1.1172634	0.2815735	0.5434162
REACTOME_GABA_RECEP TOR_ACTIVATION	50	1.117246	0.29508197	0.54186463
REACTOME_PROTEIN_FOLDING	47	1.1153871	0.2860215	0.5446053
REACTOME_INTRINSIC_PATHWAY	16	1.115182	0.31235954	0.5435185
REACTOME_FORMATION_OF_FIBRIN_CLOT_CLOTTING CASCADE	31	1.1113133	0.29411766	0.5508337
KEGG_PATHWAYS_IN_CANCER	312	1.1112031	0.182	0.5495383
PID_TGFBR_PATHWAY	53	1.1100712	0.26640928	0.5507136
SA_PTEN_PATHWAY	17	1.1090823	0.32317072	0.55148745
REACTOME_SIGNALING_BY_ILS	102	1.1086859	0.24894515	0.5509285
REACTOME_IRON_UPTAKE_AND_TRANSPORT	36	1.1086203	0.29132232	0.54952097
REACTOME_PROCESSIVE_SYNTHESIS_ON_THE_LAGGING STRAND	15	1.1071781	0.31827113	0.55150265
BIOCARTA_WNT_PATHWAY	25	1.1070898	0.31650487	0.55015707
PID_RET_PATHWAY	39	1.103382	0.31327802	0.55746377
KEGG_VASCULAR_SMOOTH_MUSCLE_CONTRACTION	112	1.0999734	0.25650558	0.5639956
REACTOME_CLASS_B_2_SECRETIN_FAMILY_RECEP TORS	82	1.0994343	0.26923078	0.56376946
BIOCARTA_CK1_PATHWAY	17	1.0973475	0.34672305	0.56720513
KEGG_GLYCEROPOPHOSPHOLIPID_METABOLISM	68	1.0971801	0.27083334	0.5660149
KEGG_ARACHIDONIC_ACID_METABOLISM	56	1.0967717	0.28719008	0.56546414
KEGG_PATHOGENIC_ESCHERICHIA_COLI_INFECTION	54	1.0935924	0.30515465	0.5717673
PID_HIF2PATHWAY	33	1.0930377	0.32238194	0.57158476
BIOCARTA_CSK_PATHWAY	22	1.0913918	0.3254818	0.5739648
REACTOME_GLYCEROPOSPHOLIPID BIOSYNTHESIS	78	1.091105	0.28163266	0.5730684
BIOCARTA_BARRESTIN_SR_C_PATHWAY	15	1.0907445	0.34790874	0.57236886
REACTOME_MITOTIC_G1_G1_S_PHASES	129	1.0879343	0.2664016	0.577634
REACTOME_SYNTHESIS_OF_PA	24	1.0867049	0.34055117	0.5790784
REACTOME_PYRUVATE_METABOLISM	17	1.0861466	0.33909288	0.5788507
PID_HDAC_CLASSII_PATHWAY	34	1.0859255	0.3304721	0.5778516
KEGG_SPHINGOLIPID_METABOLISM	36	1.0823631	0.32461873	0.584836

BIOCARTA_CDC42RAC_PA THWAY	16	1.0802321	0.3713693	0.5885627
PID_DELTA_NP63_PATHWA Y	46	1.0795356	0.3264887	0.58867943
BIOCARTA_MCM_PATHWA Y	18	1.0784736	0.375969	0.589592
PID_P73PATHWAY	74	1.0777467	0.34221312	0.589781
KEGG_P53_SIGNALING_PA THWAY	65	1.0772532	0.30041152	0.5894158
REACTOME_SEMA4D_INDU CED_CELL_MIGRATION_AN D_GROWTH_CONE_COLLA PSE	24	1.0772135	0.33808553	0.5879675
REACTOME_CIRCADIAN_C LOCK	48	1.0765046	0.3432836	0.58801734
REACTOME_NEUROTRANS MITTER_RECECTOR_BINDI NG_AND_DOWNSTREAM_T RANSMISSION_IN_THE_PO STSYNAPTIC_CELL	132	1.0710846	0.305835	0.59988415
REACTOME_NCAM1_INTER ACTIONS	38	1.0690138	0.37787056	0.6034601
REACTOME_INNATE_IMMU NE_SYSTEM	250	1.0669271	0.2747934	0.6069042
BIOCARTA_SHH_PATHWAY	16	1.0663655	0.34989202	0.606678
KEGG_PPAR_SIGNALING_P ATHWAY	68	1.0660598	0.34419551	0.6057865
REACTOME_DEADENYLATI ON_DEPENDENT_MRNA_D ECAY	39	1.0649866	0.3548387	0.60681164
SA_B_CELL_RECEPTOR_C OMPLEXES	24	1.0622936	0.37551022	0.6119343
PID_CDC42_REG_PATHWA Y	26	1.0612622	0.35812134	0.6127678
REACTOME_SIGNALING_B Y_NOTCH	91	1.0611032	0.3346856	0.6115392
REACTOME_PHOSPHOLIPI D_METABOLISM	185	1.0585644	0.3140187	0.6161881
KEGG_VIBRIO_CHOLERAE_ INFECTION	50	1.0563129	0.34435797	0.6201513
SIG_IL4RECEPTOR_IN_B_L YPHOCYTES	27	1.0540915	0.36419752	0.6241885
REACTOME_SYNTHESIS_O F_GLYCOSYLPHOSPHATID YLINOSITOL_GPI	16	1.0519863	0.38562092	0.6278963
REACTOME_SYNTHESIS_O F_PC	18	1.049786	0.37555555	0.6316769
KEGG_PRION_DISEASES	34	1.0487392	0.38641188	0.63275087
REACTOME_HDL_MEDIADE D_LIPID_TRANSPORT	15	1.0473258	0.398773	0.63487786
BIOCARTA_NO1_PATHWAY	30	1.0465542	0.36575875	0.63526344
KEGG_MISMATCH_REPAIR	23	1.0431523	0.40208334	0.64230806
KEGG_GLYCOSAMINOGLY CAN BIOSYNTHESIS_HEPA RAN SULFATE	26	1.041781	0.3970894	0.64412093
PID_RB_1PATHWAY	61	1.0411791	0.37006238	0.64400136
REACTOME_GLUCOSE_ME TABOLISM	62	1.0391171	0.3946281	0.6474477
PID_S1P_S1P3_PATHWAY	28	1.0383162	0.39807692	0.64786816
KEGG_TOLL_LIKE_RECEPT OR_SIGNALING_PATHWAY	96	1.034983	0.37021276	0.654331
PID_INTEGRIN_A9B1_PATH WAY	25	1.0330826	0.39278132	0.6575539
PID_RXR_VDR_PATHWAY	26	1.0326474	0.3863179	0.6569353
PID_VEGFR1_2_PATHWAY	67	1.0284303	0.39034206	0.66601706
REACTOME_SPHINGOLIPID METABOLISM	64	1.0250795	0.41304347	0.6732003
REACTOME_SIGNALING_B Y_PDFG	114	1.0249064	0.4097363	0.6719303
BIOCARTA_IL12_PATHWAY	21	1.0221239	0.43644068	0.6772579
REACTOME_HEMOSTASIS	433	1.0197251	0.3849287	0.68174374
REACTOME_SEMA4D_IN_S EMAPHORIN_SIGNALING	29	1.0192342	0.39430895	0.68140656
BIOCARTA_BAD_PATHWAY	26	1.0187533	0.4238683	0.6809814
SIG_PIP3_SIGNALING_IN_C ARDIAC_MYOCTES	66	1.0178779	0.41431263	0.68162686
BIOCARTA_TID_PATHWAY	17	1.0098147	0.45059288	0.700892
BIOCARTA_CREB_PATHWA Y	27	1.0076572	0.45929018	0.70487696
KEGG_MTOR_SIGNALING_ PATHWAY	50	1.0073588	0.446	0.70393723
KEGG_CALCIUM_SIGNALIN G_PATHWAY	174	1.0047442	0.43089432	0.708842
REACTOME_FATTY_ACID_ TRIACYLGLYCEROL_AND_ KETONE_BODY_METABOLI SM	155	1.0044982	0.4312115	0.7077482
PID_BETA_CATENIN_DEG_ PATHWAY	17	1.0043929	0.46072188	0.7063199
REACTOME_ANTIVIRAL_ME	57	1.0042169	0.43237704	0.70511925

CHANISM_BY_IFN_STIMULATED_GENES				
REACTOME_BIOLOGICAL_OXIDATIONS	124	1.0028334	0.44163424	0.7068459
REACTOME_SIGNALING_BY_ERBB2	94	1.001995	0.45859873	0.7073658
KEGG_PRIMARY_BILE_ACID_BIOSYNTHESIS	16	1.0006084	0.44813278	0.7092343
PID_ARF_3PATHWAY	17	0.9992103	0.48131868	0.7112345
PID_HEDGEHOG_GLI_PATHWAY	47	0.99681926	0.47420636	0.7158853
KEGG_CHEMOKINE_SIGNALING_PATHWAY	179	0.99669623	0.46626985	0.71449286
REACTOME_ACTIVATED_NOTCH1_TRANSmits_SIGNAL_TO_THE_NUCLEUS	25	0.99635035	0.45041323	0.7136762
ST_P38_MAPK_PATHWAY	35	0.99549687	0.45417514	0.7139666
BIOCARTA_P53HYPoxIA PATHWAY	20	0.99547625	0.45887446	0.71236014
BIOCARTA_GH_PATHWAY	26	0.994967	0.46092185	0.7119962
PID_IL4_2PATHWAY	62	0.9945383	0.44467214	0.71140075
REACTOME_NEGATIVE_REGULATORS_OF_RIG_IMDA5_SIGNALING	28	0.9936149	0.4409938	0.7121954
BIOCARTA_RARRXR_PATHWAY	15	0.9907814	0.47686118	0.71788996
KEGG_NOTCH_SIGNALING_PATHWAY	44	0.98869276	0.47764227	0.72171104
REACTOME_ACTIVATION_OF_THE_PRE_REPLICATIVE_COMPLEX	30	0.9883037	0.4680851	0.72100914
REACTOME_DOWNSTREAM_SIGNALING_EVENTS_OF_B_CELL_RECEPtor_BCR	91	0.98803216	0.48739496	0.7199503
PID_FOXO_PATHWAY	47	0.9858352	0.47629312	0.7240869
REACTOME_ADHERENS_JUNCTIONS_INTERACTIONS	27	0.98372626	0.4729459	0.72782224
REACTOME_TRAF6_MEDIADED_IRF2_ACTIVATION	28	0.9835073	0.47244096	0.72669244
PID_TRKR_PATHWAY	61	0.9815089	0.4989775	0.7301676
REACTOME_REGULATION_OF_INSULIN_LIKE_GROWTH_FACTOR_IGF_ACTIVITY_BY_INSULIN_LIKE_GROWTH_FACTOR_BINDING_PROTEINS_IGFBPs	16	0.9807426	0.4785276	0.73050046
KEGG_COMPLEMENT_AND_COAGULATION CASCADES	69	0.98016787	0.4888438	0.73028886
REACTOME_POST_TRANSLATIONAL_MODIFICATION_SYNTHESIS_OF_GPI_ANCHORED_PROTEINS	25	0.9784213	0.48552337	0.7331017
PID_S1P_META_PATHWAY	20	0.97728026	0.49565217	0.73438674
REACTOME_TRNA_AMINOACYLATION	39	0.97507006	0.47233203	0.7383962
ST_DIFFERENTIATION_PATHWAY_IN_PC12_CELLS	44	0.9737855	0.5150905	0.74000406
REACTOME_RORA_ACTIVATES_CIRCADIAN_EXPRESSIONION	22	0.97334576	0.47544205	0.7394834
BIOCARTA_EIF4_PATHWAY	20	0.96975935	0.5091278	0.74701697
BIOCARTA_VEGF_PATHWAY	28	0.9695914	0.47764227	0.7457991
REACTOME_COLLAGENFORMATION	51	0.96637636	0.506986	0.7523834
ST_ERK1_ERK2_MAPK_PATHWAY	32	0.96310556	0.53974897	0.75907
KEGG_PENTOSE_PHOSPHATE_PATHWAY	25	0.9629634	0.51669943	0.75777364
PID_TNF_PATHWAY	44	0.9627708	0.5122449	0.7566101
REACTOME_CONVERSION_FROM_APc_C_CD20_TO_APc_C_CDH1_IN_LATE_ANAPHASE	16	0.960817	0.5212766	0.7598589
BIOCARTA_BCELLSURVIVAL_PATHWAY	15	0.96061987	0.51458335	0.758664
PID_RHOA_PATHWAY	41	0.9564449	0.53070176	0.7679599
KEGG_AUTOIMMUNE_THYROID_DISEASE	50	0.9556277	0.5080972	0.7683724
PID_HDAC_CLASSI_PATHWAY	64	0.953194	0.529661	0.77289903
PID_RAC1_REG_PATHWAY	37	0.9510934	0.51004016	0.77645016
REACTOME_DOWNSTREAM_SIGNAL_TRANSDUCTION	88	0.9507793	0.5708502	0.7785537
REACTOME_TRAFFICKING_OF_AMPA_RECEPTORS	26	0.95053345	0.5308642	0.7744876
REACTOME_CTNNB1_PHOSPHORYLATION CASCADE	15	0.94855654	0.5487805	0.77783495

REACTOME_SYNTHESIS_OF_PIPES_AT_THE_PLASMA_MEMBRANE	29	0.94768554	0.54393303	0.77841055
BIOCARTA_HDAC_PATHWAY	27	0.9475117	0.5546219	0.77715164
PID_S1P_S1P1_PATHWAY	20	0.9458978	0.5173913	0.77969074
REACTOME_DNA_REPLICATION	181	0.9454168	0.5897436	0.7793615
KEGG_COLON_CARCINOMA	60	0.94195765	0.5531915	0.7866234
BIOCARTA_LONGEVITY_PATHWAY	15	0.9404234	0.5326316	0.7887831
KEGG_NITROGEN_METABOLISM	22	0.9394777	0.5407098	0.78939533
KEGG_RIG_I_LIKE_RECEPTOR_SIGNALING_PATHWAY	67	0.9394243	0.56707317	0.7878405
BIOCARTA_MAPK_PATHWAY	83	0.93856436	0.55424064	0.78829104
PID_THROMBIN_PAR1_PATHWAY	42	0.9371623	0.5714286	0.7901412
KEGG_STEROID_BIOSYNTHESIS	16	0.93631625	0.5521739	0.79057276
KEGG_FC_GAMMA_R_MEDIATED_PHAGOCYTOSIS	91	0.9347213	0.5587629	0.79314935
KEGG ubiquitin_mediator_proteolysis	133	0.9312708	0.60965794	0.8001168
REACTOME_INHIBITION_OF_VOLTAGE_GATED_CA2_CHANNELS_VIA_GBETA_G_AMMA_SUBUNITS	25	0.9312163	0.5691383	0.7985174
PID_ERBB_NETWORK_PATHWAY	15	0.9296474	0.5513627	0.8008671
REACTOME_PLATELET_SENSITIZATION_BY_LDL	16	0.9295457	0.5532787	0.79943085
BIOCARTA_G1_PATHWAY	27	0.92873275	0.533195	0.79993737
REACTOME_NUCLEAR_RECECTOR_TRANSCRIPTION_PATHWAY	47	0.9242538	0.6080508	0.80959
REACTOME_TRANSCRIPTIONAL_REGULATION_OF_WHITE_ADIPOCYTE_DIFFERENTIATION	67	0.9239644	0.6064257	0.808733
REACTOME_PD1_SIGNALING	17	0.9237196	0.5382979	0.80766356
KEGG_NUCLEOTIDE_EXCISION_REPAIR	43	0.92290473	0.5856031	0.8080818
KEGG_AMINOACYL_TRNA BIOSYNTHESIS	38	0.9214303	0.5995763	0.8099778
BIOCARTA_MCALPAIN_PATHWAY	23	0.9213864	0.56512606	0.80841553
BIOCARTA_ARAP_PATHWAY	15	0.9176202	0.5414938	0.8163195
KEGG_OOCYTE_MEIOSIS	109	0.9171119	0.6350211	0.8159249
PID_MET_PATHWAY	77	0.9170191	0.61087865	0.81448615
KEGG_AMYOTROPHIC_LATERAL_SCLEROSIS_ALS	50	0.9166203	0.59417474	0.81375885
PID_HIF1A_PATHWAY	18	0.91490084	0.5728953	0.8164861
REACTOME_PROCESSING_OF_CAPPED_INTRON_CONTAINING_PRE_MRNA	123	0.914439	0.6494024	0.8159613
BIOCARTA_IGF1MTOR_PATHWAY	20	0.91271466	0.5687885	0.81842315
KEGG_ALPHA_LINOLENIC_ACID_METABOLISM	17	0.9111396	0.5705394	0.8207373
REACTOME_ZINC_TRANSPORTERS	15	0.90814656	0.57947683	0.8266995
PID_CXCR4_PATHWAY	99	0.90768623	0.6647174	0.8261195
KEGG_ADIPOCYTOKINE_SIGNALING_PATHWAY	64	0.90529555	0.6388309	0.8303025
KEGG_PRIMARY_IMMUNODEFICIENCY	34	0.9047902	0.59615386	0.8298624
BIOCARTA_EGF_PATHWAY	29	0.90476006	0.6124197	0.8282537
REACTOME_CELL_CELL_JUNCTION_ORGANIZATION	56	0.9002157	0.64025694	0.83731145
PID_EPHB_FWD_PATHWAY	40	0.8998171	0.62007874	0.8366475
KEGG_WNT_SIGNALING_PATHWAY	145	0.8994792	0.6983471	0.8358215
PID_IGF1_PATHWAY	29	0.8994531	0.61924684	0.8342314
REACTOME_GAP_JUNCTION_TRAFFICKING	26	0.8932848	0.5954825	0.84746975
REACTOME_ACYL_CHAIN_REMODELLING_OF_PE	21	0.89175284	0.6004184	0.84947795
REACTOME_PI3K_EVENTS_IN_ERBB2_SIGNALING	42	0.8902045	0.6268344	0.8515751
PID_ER_NONGENOMIC_PATHWAY	41	0.8894592	0.6772152	0.8517595
REACTOME_PROCESSING_OF_CAPPED_INTRONLESS_PRE_MRNA	22	0.88879645	0.63708085	0.85165256
PID_NCADHERIN_PATHWAY	32	0.88737357	0.60764587	0.85329187

Y				
PID_P38_MK2_PATHWAY	20	0.88533485	0.6109937	0.8564066
BIOCARTA_P38MAPK_PATHWAY	35	0.8846373	0.6310273	0.85636514
PID_KIT_PATHWAY	52	0.8801426	0.68346775	0.8649143
REACTOME_SR_PDEPENDENT_COTRANSLATIONAL_PROTEIN_TARGETING_TO_MEMBRANE	86	0.8795764	0.7006237	0.8644327
PID_PS1_PATHWAY	45	0.87906986	0.67330676	0.8639964
KEGG_CELL_CYCLE	122	0.8787839	0.75396824	0.86300147
REACTOME_INWARDLYRECTIFYING_K CHANNELS	31	0.8775433	0.6459227	0.864039
REACTOME_PIP3_ACTIVATES_AKT_SIGNALING	27	0.8739272	0.65368855	0.8707533
KEGG_EPITHELIAL_CELL_SIGNALING_IN_Helicobacter_pylori_infection	64	0.8734306	0.69894737	0.870218
KEGG_GNRH_SIGNALING_PATHWAY	97	0.870431	0.7145709	0.87557554
SIG_INSULIN_RECEPтор PATHWAY_IN_CARDIAC_MYOCTES	50	0.8688852	0.67975205	0.8773002
PID_IL3_PATHWAY	27	0.86387026	0.6422594	0.88707346
REACTOME_MUSCLE_CONTRACTION	44	0.8579755	0.6911447	0.8984137
REACTOME_INTERACTION_BETWEEN_L1_AND_ANKYRINS	20	0.8568577	0.6789588	0.89924407
REACTOME_SYNTHESIS_AND_INTERCONVERSION_OF_NUCLEOTIDE_DL_AND_TRIPHOSPHATES	15	0.85673505	0.6572008	0.89781004
BIOCARTA_KERATINOCTYE_PATHWAY	44	0.8563876	0.72317594	0.89689535
REACTOME_TIGHT_JUNCTION_INTERACTIONS	29	0.8556426	0.6773504	0.8967854
BIOCARTA_PAR1_PATHWAY	36	0.85548604	0.6963563	0.8954051
REACTOME_RNA_POL_III_TRANSCRIPTION	32	0.85493106	0.69033533	0.8950134
KEGG_RIBOSOME	66	0.854607	0.7292111	0.89403427
REACTOME_DOWNSTREAM_TCR_SIGNALING	33	0.85453206	0.68172485	0.8924853
BIOCARTA_PTDINS_PATHWAY	21	0.85161495	0.7022587	0.89724326
REACTOME_ACTIVATION_OF_CHAPERONE_GENES_BY_XBP1S	38	0.8514116	0.6966068	0.8959777
REACTOME_ACYL_CHAIN_REMOELLING_OF_PS	15	0.84953785	0.6809422	0.89824224
KEGG_TYROSINE_METABOLISM	40	0.8484863	0.7133621	0.89882404
BIOCARTA_TH1TH2_PATHWAY	19	0.84842706	0.66935486	0.89724183
BIOCARTA_NDKDYNAMIN_PATHWAY	16	0.84838426	0.6607843	0.89562535
REACTOME_POST_NMDA_RECECTOR_ACTIVATION_EVENTS	33	0.84801674	0.6979167	0.8947092
BIOCARTA_IL3_PATHWAY	15	0.8476119	0.6585366	0.8938772
REACTOME_TRANSMISSION_ACROSS_CHEMICAL_SYNAPSES	178	0.84683114	0.8231707	0.89384764
KEGG_VASOPRESSIN_REGULATED_WATER_REABSORPTION	43	0.84677845	0.71991247	0.89230126
REACTOME_PI3K_AKT_ACTIVATION	35	0.84676874	0.6913043	0.8906726
REACTOME_HIV_INFECTION	181	0.8459638	0.8634454	0.89078647
REACTOME_BILE_ACID_ANDBILE_SALT_METABOLISM	26	0.8448487	0.6889353	0.89154327
REACTOME_SIGNALING_BY_FGFR	106	0.84317696	0.796334	0.8933076
KEGG_SELENOAMINO_ACID_METABOLISM	25	0.84275216	0.7064579	0.8926225
PID_PI3K_PLC_TRK_PATHWAY	35	0.84093994	0.72669494	0.894628
PID_ERBB2_ERBB3_PATHWAY	43	0.8406051	0.75053304	0.89367855
ST_GA12_PATHWAY	23	0.83868986	0.7276507	0.89588
KEGG_GAP_JUNCTION	87	0.8383125	0.8203593	0.89502853
REACTOME_TRANSLATION	116	0.8367547	0.8183716	0.896519
REACTOME_PEPTIDE_CHAIN_ELONGATION	63	0.8367083	0.7808765	0.89498395
PID_P38_MKK3_6PATHWAY	25	0.8365783	0.6784141	0.89364403
KEGG_RENAL_CELL_CARCINOMA	65	0.8348432	0.7883495	0.89560527

KEGG_ETHER_LIPID_METABOLISM	29	0.8331327	0.73137254	0.89742726
PID_CERAMIDE_PATHWAY	47	0.83114576	0.7368421	0.8996968
REACTOME_CHYLOMICRON_MEDIATED_LIPID_TRANSPO RT	15	0.8303974	0.66324437	0.8995939
PID_HNF3B_PATHWAY	43	0.8292749	0.7388535	0.90000486
REACTOME_MRNA_PROCESSING	142	0.8288461	0.860835	0.8992302
BIOCARTA_CTCF_PATHWAY	22	0.8287531	0.72245765	0.8977909
REACTOME_DOWNSTREAM_SIGNALING_OF_ACTIVATED_FGFR	95	0.82823277	0.845679	0.89715844
BIOCARTA_EPO_PATHWAY	18	0.82756484	0.70258623	0.8968794
REACTOME_THE_ROLE_OF_NEF_IN_HIV1_REPLICATION_AND_DISEASE_PATHOGENESIS	26	0.8258349	0.7121535	0.89870507
REACTOME_ENERGY_DEPENDENT_REGULATION_OF_MTOR_BY_LKB1_AMPK	17	0.8233533	0.70564514	0.9019288
KEGG_FRUCTOSE_AND_MANNOSE_METABOLISM	33	0.82312006	0.7313131	0.90080273
REACTOME_GABA_SYNTHESIS_RELEASE_ReUPTAKE_AND_DEGRADATION	15	0.82245165	0.675	0.9004557
REACTOME_LIPID_DIGESTION_MOBILIZATION_AND_TRANSPORT	44	0.821653	0.7710843	0.90038484
KEGG_MATURITY_ONSET_DIABETES_OF_THE_YOUNG	24	0.81949043	0.72392637	0.90292686
BIOCARTA_MAL_PATHWAY	19	0.8181502	0.7245509	0.9038405
BIOCARTA_IGF1_PATHWAY	21	0.81737816	0.7219917	0.9036876
KEGG_LINOLEIC_ACID_METABOLISM	26	0.8117299	0.7645788	0.91235405
REACTOME_LIPOPROTEIN_METABOLISM	27	0.810476	0.72938687	0.9129367
REACTOME_ACTIVATED_AMPK_STIMULATES_FATTY_ACID_OXIDATION_IN_MUSCLE	18	0.8096152	0.71398747	0.9129946
BIOCARTA_MET_PATHWAY	36	0.8093269	0.7590361	0.91191614
REACTOME_SIGNALLING_T_ERKS	35	0.8069507	0.78028744	0.91453344
KEGG_FC_EPSILON_RISIGNALING_PATHWAY	74	0.80688566	0.82340425	0.9130451
BIOCARTA_STRESS_PATHWAY	24	0.8059007	0.7394958	0.91325223
REACTOME_TRAFFICKING_OF_GLUR2_CONTAINING_AMPA_RECEPtors	15	0.80345273	0.74327123	0.91591054
KEGG_ENDOMETRIAL_CANCER	51	0.7992038	0.82086617	0.9217984
REACTOME_FATTY_ACYL_COA BIOSYNTHESIS	16	0.7948234	0.73852295	0.92771226
REACTOME_NONSENSE_MEDiated_DECAY_ENHANCED_BY_THE_EXON_JUNCTION_COMPLEX	83	0.79475594	0.8901099	0.92622167
PID_FAS_PATHWAY	37	0.794055	0.7827004	0.9258585
KEGG_ENDOCYTOSIS	169	0.79044974	0.9361277	0.93021363
REACTOME_AMYLOIDS	68	0.79036504	0.86577183	0.9287395
REACTOME_PHOSPHOLIPASE_C_MEDIATED_CASCADE	51	0.78994626	0.84823287	0.92774075
REACTOME_MICRORNA_MIRNA_BIOGENESIS	17	0.7866602	0.7698574	0.93145883
BIOCARTA_PGC1A_PATHWAY	22	0.7851434	0.8080169	0.9322584
PID_TCR_CALCIUM_PATHWAY	27	0.78088266	0.77440345	0.9374031
REACTOME_FORMATION_OF_TUBULIN_FOLDING_INTERMEDIATES_BY_CCT_TRIC	19	0.77784115	0.7839506	0.94045234
PID_IL12_STAT4_PATHWAY	33	0.77720726	0.802	0.93991643
REACTOME_SIGNALLING_BY_THE_B_CELL_RECEPtor_BCR	118	0.77589446	0.9229209	0.94023013
PID_TELOMERASE_PATHWAY	66	0.7758787	0.87323946	0.9386561
BIOCARTA_TFF_PATHWAY	21	0.77003664	0.78630704	0.9456807
KEGG_STEROID_HORMONE_BIOSYNTHESIS	43	0.76543146	0.85544556	0.95066434
REACTOME_PREFOLDIN_MEDIATED_TRANSFER_OF_SUBSTRATE_TO_CCT_TRIC	24	0.76470506	0.793617	0.9500987
REACTOME_ABC_FAMILY	33	0.7639818	0.8377823	0.9495072

PROTEINS_MEDIATED_TRA_NSPORT				
KEGG_VIRAL_MYOCARDITIS	67	0.76375395	0.8949495	0.9482509
KEGG_BLADDER_CANCER	39	0.7626837	0.8510204	0.94812787
REACTOME_GLOBAL_GENOMIC_NER_NER	32	0.7621747	0.8391039	0.9471598
KEGG_PANCREATIC_CANCER	68	0.7615029	0.8798371	0.9464661
PID_ERA_GENOMIC_PATHWAY	61	0.7600164	0.8913934	0.9469572
REACTOME_SIGNALING_BY_ERBB4	87	0.75794214	0.9175476	0.9483724
REACTOME_ENDOGENOUS_STEROLS	15	0.75373507	0.78418803	0.9524702
REACTOME_TELOMERE_MAINTENANCE	68	0.75322366	0.91268194	0.9516016
REACTOME_TERMINATION_OF_OGLYCAN BIOSYNTESIS	20	0.74997836	0.827957	0.95431805
PID_CONE_PATHWAY	23	0.74378407	0.8460039	0.9606654
KEGG_THYROID_CANCER	29	0.7430283	0.84313726	0.9599241
REACTOME_SIGNALLING_TO_RAS	27	0.7423138	0.8476821	0.95922995
KEGG_BASAL_CELL_CARCIOMA	53	0.74220157	0.9171843	0.95778304
KEGG_HEDGEHOG_SIGNALLING_PATHWAY	55	0.741056	0.89830506	0.95766294
REACTOME_AMINE_COMPOUND_SLC_TRANSPORTERS	27	0.73975444	0.8729839	0.9576899
REACTOME_MITOTIC_MM_G1_PHASES	161	0.73665184	0.98455596	0.95982784
BIOCARTA_CERAMIDE_PATHWAY	21	0.7357312	0.82051283	0.9593055
PID_ILK_PATHWAY	43	0.7353843	0.9032967	0.95822537
PID_SYNDECAN_3_PATHWAY	16	0.7349529	0.8185745	0.95714194
REACTOME_PHOSPHORYLATION_OF_CD3_AND_TCR_ZETA_CHAINS	15	0.7343487	0.805492	0.9562833
BIOCARTA_SPPA_PATHWAY	21	0.73372746	0.86157024	0.95542353
KEGG_LONG_TERM_DEPRESSION	68	0.73070544	0.92727274	0.9574225
REACTOME_METABOLISM_OF_STEROID_HORMONES_AND_VITAMINS_A_AND_D	34	0.7302648	0.86070687	0.95638824
BIOCARTA_INTEGRIN_PATHWAY	35	0.7294541	0.8857143	0.9557243
REACTOME_ACTIVATION_OF_NMDA_RECECTOR_UPON GLUTAMATE_BINDING_AND_POSTSYNAPTIC_EVENTS	37	0.7279207	0.8661088	0.9558355
REACTOME_INFLUENZA_VIRAL_RNA_TRANSCRIPTION_AND_REPLICATION	79	0.72521037	0.9437751	0.9572174
REACTOME_SIGNALLING_TO_P38_VIA_RIT_AND_RIN	15	0.7218852	0.8312236	0.95947325
ST_INTERLEUKIN_4_PATHWAY	26	0.72126263	0.85655737	0.958554
REACTOME_TRANSCRIPTION_COUPLED_NER_TC_NEUR	41	0.717672	0.89285713	0.9607349
BIOCARTA_NOS1_PATHWAY	21	0.7135105	0.86382115	0.9636503
ST_INTEGRIN_SIGNALING_PATHWAY	76	0.71073645	0.9589322	0.9648604
REACTOME_REGULATION_OF_BETA_CELL DEVELOPMENT	29	0.70680076	0.8929293	0.9672362
BIOCARTA_AT1R_PATHWAY	31	0.6934525	0.91268194	0.97822565
KEGG_PENTOSE_AND_GLCURONATE_INTERCONVERSIONS	17	0.69332045	0.88438135	0.976764
KEGG_BASAL_TRANSCRIPTION_FACTORS	32	0.68737864	0.91803277	0.98026747
PID_FANCONI_PATHWAY	43	0.6736614	0.9580838	0.9894448
REACTOME_NUCLEOTIDE_EXCISION_REPAIR	46	0.67333484	0.9389474	0.9881173
BIOCARTA_CCR3_PATHWAY	23	0.6700779	0.90515465	0.9889568
PID_NEPHRIN_NEPH1_PATHWAY	28	0.6669936	0.9254902	0.98960584
REACTOME_REGULATORY_RNA_PATHWAYS	20	0.66089803	0.8978723	0.99212813
BIOCARTA_HCMV_PATHWAY	17	0.65401274	0.90128756	0.9950112

REACTOME_CYTOCHROME_P450_ARRANGED_BY_SUBSTRATE_TYPE	49	0.6531078	0.96370965	0.9940178
BIOCARTA_GCR_PATHWAY	19	0.6502828	0.9001957	0.9941775
REACTOME_ENDOSOMAL_SORTING_COMPLEX_REQUIRED_FOR_TRANSPORT_ELEMENTS_OF_SCRT	25	0.64776725	0.9585153	0.99416214
KEGG_RNA_DEGRADATION	55	0.6424494	0.9795082	0.9956522
REACTOME_NUCLEAR_SIGNALING_BY_ERBB4	38	0.6396886	0.960334	0.9956471
REACTOME_ABORTIVE_ELONGATION_OF_HIV1_TRANSLATIONAL_SCRIPT_IN_THE_ABSENCE_OF_TAT	18	0.63927543	0.91684437	0.9943255
PID_HEDGEHOG_2PATHWAY	21	0.6381688	0.9166667	0.99337465
BIOCARTA_CHREBP2_PATHWAY	42	0.63730603	0.9761431	0.9922984
KEGG_ERBB_SIGNALING_PATHWAY	83	0.6311795	0.9900398	0.9938757
BIOCARTA_VIP_PATHWAY	25	0.6281859	0.94650203	0.9938426
REACTOME_METABOLISM_OF_NON_CODING_RNA	45	0.62661487	0.976834	0.9930435
REACTOME_ACTIVATION_OF_THE_MRNA_UPON_BINDING_OF_THE_CAP_BINDING_COMPLEX_AND_EIFS_AND_SUBSEQUENT_BINDING_TO_43S	45	0.62577415	0.99185336	0.991913
PID_IL8_CXCR2_PATHWAY	33	0.624432	0.95578945	0.9910609
REACTOME_STEROID_HORMONES	29	0.6220332	0.9639066	0.9906562
BIOCARTA_ACH_PATHWAY	16	0.61122954	0.94600433	0.9940123
REACTOME_GLYCOLYSIS_SA_TRKA_RECECTOR	25	0.59298855	0.9726891	0.99921495
17	0.5839974	0.9419087	1	
PID_WNT_CANONICAL_PATHWAY	18	0.57809037	0.9628099	1
REACTOME_INFLUENZA_LIFE_CYCLE	110	0.56918806	1	1
BIOCARTA_PTEN_PATHWAY	18	0.55913323	0.96450937	1
REACTOME_ABCA_TRANSPORTERS_IN_LIPID_HOMEOSTASIS	17	0.55065644	0.97095436	1
REACTOME_3_UTR_MEDIA_TE_DISTRIBUTION_TRANSLATIONAL_REGULATION	80	0.54499364	1	1
ST_G_ALPHA_S_PATHWAY	16	0.5348369	0.989339	1
BIOCARTA_MTOR_PATHWAY	19	0.5301952	0.98221344	1
REACTOME_SHC1_EVENTS_IN_EGFR_SIGNALING	15	0.52890605	0.9717391	1
BIOCARTA_NO2IL12_PATHWAY	17	0.5147179	0.979716	1
REACTOME_CYTOSOLIC_T_RNA_AMINOACYLATION	22	0.5003817	0.9979716	1
PID_THROMBIN_PAR4_PATHWAY	15	0.4918635	0.98715204	1
PID_PDGFR_ALPHA_PATHWAY	21	0.49103978	0.9940711	0.9987714
REACTOME_PROLONGED_ERK_ACTIVATION_EVENTS	18	0.4747968	0.9897541	0.99846566
KEGG_PROTEIN_EXPORT	22	0.46754628	0.99375	0.99742883

Table S 2.7 Core enriched gene set from REACTOME_INTEGRIN_CELL_SURFACE_INTERACTION signature

Gene	RANK IN GENE LIST	RANK METRIC SCORE	RUNNING ES	CORE ENRICHMENT	Fold Change (Parental/ NUAK1-KO) > 2
FN1	0	4.957	0.1002	Yes	745
THBS1	17	3.305	0.1662	Yes	8.33
F11R	107	1.971	0.2015	Yes	3.52
ITGB5	110	1.951	0.2409	Yes	2.49
ITGB8	114	1.892	0.279	Yes	10.21
ITGA3	228	1.555	0.3046	Yes	
ICAM2	252	1.509	0.334	Yes	
COL4A1	276	1.481	0.3627	Yes	2.54
ITGB4	321	1.367	0.3881	Yes	
COL4A2	325	1.358	0.4154	Yes	
ITGA2B	476	1.162	0.4313	Yes	
APBB1IP	546	1.105	0.4501	Yes	
COL4A5	571	1.091	0.4709	Yes	
LAMB1	620	1.048	0.4897	Yes	
LAMC1	734	0.98	0.5037	Yes	
LAMA1	897	0.9	0.5137	Yes	
FBN1	1034	0.853	0.524	Yes	
ITGAE	1220	0.784	0.5304	Yes	
COL4A4	1992	0.596	0.5031	No	
VTN	2111	0.574	0.5086	No	
ITGAX	3489	0.402	0.4465	No	
CSK	3503	0.4	0.4539	No	
COL2A1	3660	0.385	0.4537	No	
AKT1	4176	0.331	0.4341	No	
BCAR1	4379	0.313	0.4302	No	
GRB2	4894	0.27	0.4094	No	
FGG	4906	0.27	0.4143	No	
SRC	5571	0.218	0.3848	No	
JAM2	5995	0.188	0.367	No	
CDH1	6196	0.174	0.3603	No	
BSG	6835	0.134	0.3304	No	
AMICA1	6964	0.125	0.3264	No	
RAP1A	7201	0.11	0.3166	No	
FGA	7351	0.1	0.311	No	
PDPK1	7372	0.098	0.312	No	
ITGAL	7418	0.096	0.3116	No	
JAM3	7461	0.094	0.3114	No	
ITGAV	7520	0.091	0.3103	No	
VWF	7564	0.088	0.3099	No	
ITGA10	7815	0.075	0.2986	No	
SYK	8302	0.046	0.2747	No	
TNC	8349	0.043	0.2733	No	
SOS1	8591	0.028	0.2615	No	
ITGA5	9026	0.004	0.2395	No	
RAPGEF4	9118	-0.001	0.2349	No	
FGB	9460	-0.019	0.2178	No	
CRK	10222	-0.061	0.1802	No	
COL1A1	10369	-0.071	0.1742	No	
VCAM1	10823	-0.095	0.153	No	
SHC1	10880	-0.099	0.1522	No	
RASGRP2	12010	-0.164	0.0978	No	
RAP1B	12083	-0.169	0.0976	No	
PTK2	12406	-0.188	0.0849	No	
COL4A3	13809	-0.278	0.019	No	
PTPN1	14152	-0.304	0.0077	No	
ITGB6	14681	-0.341	-0.0124	No	
ITGB1	14747	-0.346	-0.0087	No	
ICAM4	14757	-0.347	-0.0021	No	
RAPGEF3	15142	-0.376	-0.0141	No	
ITGB2	15330	-0.389	-0.0158	No	
ITGB7	15962	-0.444	-0.0391	No	
COL1A2	16155	-0.46	-0.0396	No	
LAMB2	16215	-0.466	-0.0332	No	
ITGA8	16915	-0.536	-0.058	No	
IBSP	16920	-0.536	-0.0474	No	
PECAM1	17004	-0.544	-0.0406	No	
ITGB3	17587	-0.621	-0.0578	No	
ITGA9	17678	-0.634	-0.0495	No	
ITGA11	18103	-0.707	-0.0569	No	
LAMA2	18399	-0.769	-0.0564	No	
ITGAM	18631	-0.834	-0.0513	No	
ICAM3	18725	-0.865	-0.0386	No	
ICAM1	18856	-0.912	-0.0268	No	
RASGRP1	19046	-0.991	-0.0164	No	
ITGA2	19214	-1.099	-0.0027	No	
SPP1	19372	-1.271	0.015	No	

Table S 2.8 Core enriched genes from HALLMARK_ TNFA_SIGNALING_VIA_NF- κ B

GENE	RANK IN GENE LIST	RANK METRIC SCORE	RUNNING ES	CORE ENRICHMENT	NF- κ B Target Gene (Gilmore lab's NF- κ B Target Genes list)
IL6	6	3.944	0.0273	No	Liebermann & Baltimore, 1990; Shimizu et al, 1990; Son et al, 2008
PMEPA1	14	3.484	0.0514	No	
LITAF	24	2.927	0.0714	No	
IL7R	43	2.569	0.0885	No	
HES1	65	2.233	0.1031	No	
IFIT2	66	2.201	0.1185	No	
SMAD3	70	2.143	0.1333	No	
KLF9	122	1.869	0.1438	No	
DUSP1	148	1.771	0.155	No	
DRAM1	168	1.729	0.1661	No	
PLK2	208	1.613	0.1754	No	
SAT1	281	1.473	0.182	No	
PPAP2B	288	1.452	0.1919	No	
IFIH1	297	1.428	0.2015	No	
ATF3	318	1.368	0.21	No	
TSC22D1	323	1.362	0.2194	No	
EFNA1	351	1.312	0.2272	No	
TNF	377	1.277	0.2348	No	
IER3	378	1.27	0.2437	No	
MARCKS	390	1.255	0.252	No	
RHOB	542	1.107	0.252	No	
IRF1	557	1.101	0.259	No	
JUNB	588	1.076	0.265	No	
DDX58	655	1.026	0.2688	No	
CXCL11	856	0.921	0.2649	No	
PDLIM5	857	0.92	0.2714	No	
EGR1	945	0.881	0.2731	No	
GADD45B	951	0.88	0.279	No	
CEBDPD	1061	0.842	0.2793	No	
JAG1	1074	0.835	0.2845	No	
DUSP4	1207	0.788	0.2833	No	
CCL20	1450	0.72	0.2759	No	
INHBA	1577	0.688	0.2743	No	
CSF1	1647	0.669	0.2754	No	
SPHK1	2181	0.562	0.252	No	
LIF	2185	0.561	0.2558	No	
CXCL10	2256	0.549	0.256	No	
TAP1	2360	0.533	0.2545	No	
JUN	2751	0.484	0.2378	No	
PDE4B	2762	0.482	0.2407	No	
TNFAIP2	2787	0.479	0.2428	No	
ZFP36	2834	0.472	0.2437	No	
MSC	2862	0.469	0.2456	No	
TUBB2A	2916	0.464	0.2462	No	
GPR183	2944	0.461	0.248	No	
SGK1	3036	0.451	0.2465	No	
SOD2	3275	0.426	0.2373	No	
PTPRE	3625	0.388	0.2221	No	
TGIF1	3731	0.377	0.2193	No	
NFE2L2	3758	0.374	0.2206	No	
CXCL1	3760	0.373	0.2232	No	
SPSB1	3813	0.368	0.2231	No	
CCRL2	3889	0.361	0.2217	No	
KLF4	3971	0.352	0.22	No	
EGR3	4200	0.329	0.2106	No	
PNRC1	4212	0.328	0.2124	No	
FOSL2	4244	0.325	0.2131	No	
OLR1	4402	0.312	0.2072	No	
CXCL3	4574	0.298	0.2005	No	
BHLHE40	4621	0.294	0.2002	No	
B4GALT1	4940	0.267	0.1857	No	
CEBPB	5018	0.26	0.1836	No	
NINJ1	5114	0.252	0.1805	No	
CYR61	5155	0.248	0.1802	No	
SOCS3	5327	0.236	0.173	No	
EHD1	6195	0.174	0.1297	No	
TLR2	6214	0.173	0.13	No	
TNFSF9	6585	0.15	0.1121	No	
REL	6611	0.149	0.1118	No	
KLF6	6805	0.136	0.1029	No	
ID2	6902	0.129	0.0989	No	
IER2	6945	0.126	0.0976	No	
NAMPT	6951	0.126	0.0982	No	
NR4A3	6983	0.123	0.0975	No	

EDN1	7197	0.11	0.0873	No	
HBEGF	7271	0.105	0.0843	No	
TNC	8349	0.043	0.0293	No	
SIK1	8456	0.037	0.0241	No	
NR4A1	8468	0.036	0.0238	No	
STAT5A	8507	0.033	0.0221	No	
B4GALT5	8708	0.022	0.012	No	
DENND5A	8806	0.016	0.0071	No	
DUSP2	8825	0.015	0.0063	No	
PTGS2	9281	-0.01	-0.017	No	
SNN	9284	-0.01	-0.017	No	
BIRC2	9287	-0.01	-0.0171	No	
ICOSLG	9353	-0.014	-0.0203	No	
IL18	9415	-0.017	-0.0233	No	
SLC16A6	10019	-0.049	-0.0539	No	
TIPARP	10634	-0.085	-0.0849	No	
IL12B	11470	-0.132	-0.1268	No	
FOS	11545	-0.137	-0.1297	No	
AREG	11548	-0.137	-0.1288	No	
IRS2	11708	-0.146	-0.1359	No	
MYC	11710	-0.146	-0.135	No	
TNFAIP6	11818	-0.153	-0.1394	No	
NFIL3	11906	-0.158	-0.1428	No	
SLC2A6	12080	-0.168	-0.1505	No	
VEGFA	12206	-0.177	-0.1556	No	
BTG2	12276	-0.182	-0.1579	No	
DNAJB4	12383	-0.187	-0.162	No	
RCAN1	12545	-0.197	-0.1689	No	
CD80	12588	-0.2	-0.1697	No	
NR4A2	12628	-0.202	-0.1703	No	
GCH1	12730	-0.208	-0.174	No	
PLAU	12769	-0.211	-0.1745	No	
CD69	12866	-0.217	-0.1779	No	
CCNL1	12879	-0.218	-0.177	No	
EIF1	13038	-0.229	-0.1835	No	
PANX1	13364	-0.25	-0.1984	No	
IL23A	13568	-0.263	-0.207	No	
MAP3K8	13873	-0.283	-0.2206	No	
SQSTM1	14337	-0.317	-0.2422	No	
CCL5	14444	-0.324	-0.2453	No	
TNIP2	14576	-0.334	-0.2497	No	
NFKBIA	14604	-0.335	-0.2488	No	
MAP2K3	14723	-0.344	-0.2524	No	
CLCF1	15043	-0.368	-0.2662	No	
TNFAIP3	15044	-0.368	-0.2636	No	
CD44	15179	-0.378	-0.2679	No	
FOSB	15351	-0.391	-0.2739	No	
BMP2	15456	-0.4	-0.2765	No	
EGR2	15462	-0.401	-0.2739	No	
CSF2	15656	-0.416	-0.2809	No	
PFKFB3	15866	-0.436	-0.2886	No	
IL15RA	16067	-0.453	-0.2957	No	
TNFAIP8	16080	-0.454	-0.2931	No	
BCL6	16320	-0.476	-0.302	No	
TANK	16344	-0.479	-0.2999	No	
IFNGR2	16535	-0.497	-0.3061	No	
YRDC	16547	-0.499	-0.3032	No	
SLC2A3	16783	-0.522	-0.3116	No	
PPP1R15A	16863	-0.53	-0.312	No	
RELA	16867	-0.531	-0.3084	No	
PLEK	17199	-0.569	-0.3214	Yes	
TRIP10	17234	-0.572	-0.3191	Yes	
KDM6B	17267	-0.577	-0.3167	Yes	
IER5	17401	-0.596	-0.3194	Yes	
SERPINB2	17488	-0.608	-0.3196	Yes	
CXCL6	17575	-0.62	-0.3196	Yes	
KYNU	17576	-0.62	-0.3153	Yes	
MAFF	17628	-0.627	-0.3135	Yes	
ETS2	17672	-0.632	-0.3113	Yes	
ZBTB10	17817	-0.659	-0.3141	Yes	
CXCL2	17853	-0.664	-0.3112	Yes	
GEM	17872	-0.668	-0.3075	Yes	
RELB	17910	-0.674	-0.3046	Yes	
PTGER4	17938	-0.678	-0.3013	Yes	
SERPINB8	17982	-0.686	-0.2987	Yes	
TNIP1	18110	-0.708	-0.3002	Yes	
CFLAR	18162	-0.717	-0.2978	Yes	
CCND1	18208	-0.727	-0.295	Yes	
NFKB1	18314	-0.749	-0.2952	Yes	
PTX3	18443	-0.782	-0.2963	Yes	
TRIB1	18492	-0.794	-0.2932	Yes	
FUT4	18536	-0.807	-0.2897	Yes	
SDC4	18553	-0.813	-0.2849	Yes	
CDKN1A	18633	-0.835	-0.2831	Yes	
KLF2	18652	-0.839	-0.2781	Yes	
CCL2	18653	-0.839	-0.2722	Yes	
F3	18695	-0.853	-0.2684	Yes	

TNFRSF9	18702	-0.856	-0.2627	Yes	
BTG3	18718	-0.862	-0.2574	Yes	
KLF10	18768	-0.879	-0.2538	Yes	
ICAM1	18856	-0.912	-0.2518	Yes	
RNF19B	18909	-0.932	-0.248	Yes	
GADD45A	18920	-0.937	-0.2419	Yes	
IL6ST	18988	-0.964	-0.2386	Yes	
TRAF1	19012	-0.974	-0.233	Yes	
NFAT5	19061	-1.004	-0.2284	Yes	
FOSL1	19084	-1.014	-0.2224	Yes	
MXD1	19087	-1.018	-0.2154	Yes	
FJX1	19120	-1.037	-0.2098	Yes	
ABCA1	19153	-1.064	-0.2039	Yes	
RIPK2	19197	-1.084	-0.1986	Yes	
ATP2B1	19209	-1.092	-0.1915	Yes	
MCL1	19233	-1.111	-0.1849	Yes	
G0S2	19278	-1.148	-0.1791	Yes	
SERPINE1	19281	-1.152	-0.1711	Yes	
F2RL1	19353	-1.237	-0.1661	Yes	
CD83	19410	-1.34	-0.1596	Yes	
NFKBIE	19455	-1.415	-0.1519	Yes	
PHLDA2	19460	-1.421	-0.1422	Yes	
DUSP5	19511	-1.562	-0.1338	Yes	
BIRC3	19563	-1.787	-0.1239	Yes	You et al, 1997; Stehlík et al, 1998a, 1998b; Simon et al. 2007
PHLDA1	19568	-1.819	-0.1114	Yes	
GFP72	19610	-2.244	-0.0977	Yes	
IL1A	19627	-2.446	-0.0814	Yes	Mori & Prager, 1996
BCL2A1	19632	-2.546	-0.0638	Yes	Lombardi et al, 1995
PLAUR	19633	-2.578	-0.0457	Yes	
NFKB2	19635	-2.589	-0.0276	Yes	Lombardi et al, 1995
IL1B	19664	-4.164	0.0001	Yes	Hiscott et al, 1993

Chapter 3

3 Discussion

3.1 Summary of Findings

Advanced-stage EOC is characterized by the accumulation of ascites fluid in the peritoneal cavity (Al Habyan et al., 2018; Sodek et al., 2009). Ascites contains spheroids which are a key mediator of peritoneal metastasis and can facilitate chemoresistance (Al Habyan et al., 2018; Desoize & Jardillier, 2000; Lengyel et al., 2014; Pease et al., 2012). Our group previously reported that the master kinase LKB1 is required for efficient ovarian cancer metastasis (Buensuceso et al., 2018; Peart et al., 2015). Therefore, the aim for this study was to elucidate the downstream target eliciting the pro-metastatic function of LKB1. We identified NUAK1 as a top candidate substrate and confirmed that its expression in spheroids and tumor samples is regulated by LKB1. NUAK1 is down-regulated in quiescent spheroids compared to proliferative monolayer cells and this differential expression is regulated by lysosome degradation and the UPS. To investigate the function of NUAK1 in ovarian cancer, we generated lines in which NUAK1 was knocked out by CRISPR/Cas9 or overexpressed by stable transfection. OVCAR8 *NUAK1*-KO cells had significantly lower cell adhesion while HEYA8 and OVCAR3 *NUAK1* overexpressing lines had significantly increased cell adhesion. Moreover, OVCAR8 *NUAK1*-KO spheroids had impaired spheroid integrity and OVCAR8 *NUAK1*-KO-GFP spheroids had an abundance of dead cells accumulate around the periphery. To identify a molecular basis for this adhesion phenotype, we completed transcriptome analysis using OVCAR8 parental spheroids and OVCAR8 *NUAK1*-KO spheroids. Using GSEA, we identified a cell attachment signature that was up-regulated in OVCAR8 parental spheroids compared to OVCAR8 *NUAK1*-KO spheroids. We validated multiple adhesion genes in this gene set by qPCR, including *FNI*, *LICAM*, *ITGB8*, *ITGB5*, *THBS1*, and *F11R*. We continued to confirm this signature on the protein level, focusing on *FNI* because it was the most differentially expressed gene with a 745-fold change. By western blot and immunofluorescence we showed that OVCAR8 *NUAK1*-KO spheroids had no detectable expression of *FNI* compared to OVCAR8 parental spheroids. In the reciprocal system, there was a dramatic increase in FN expression in HEYA8 *NUAK1*

overexpressing spheroids compared to their respective control. To demonstrate that NUAK1 is controlling spheroid integrity through fibronectin deposition, we added plasma fibronectin to OVCAR8 *NUAK1*-KO spheroids and completely restored the native phenotype. These findings suggest that through LKB1 regulation NUAK1 is promoting spheroid integrity through increasing fibronectin deposition.

In addition to examining the role of NUAK1 in cell adhesion, we tested whether it controls cell growth. *NUAK1*-KO spheroids had significantly increased viability and this was corroborated with our knockdown data. *NUAK1* overexpressing spheroids had significantly decreased viability. Surprisingly, we found no change in doubling time when NUAK1 was knocked out or chemically inhibited with the WZ4003 compound. Cells that were treated with the WZ4003 compound also showed no difference in thymidine incorporation. These results suggest that loss of NUAK1 increases spheroid viability however this effect is not due to increased cell proliferation. To understand the mechanism behind this increased viability, we completed GSEA and found that a NF- κ B pathway was enriched in OVCAR8 *NUAK1*-KO spheroids compared to OVCAR8 parental spheroids. To validate this gene set, we found increased nuclear translocation of p65 in OVCAR8 *NUAK1*-KO spheroids compared to the respective control. qPCR confirmed that NF- κ B target genes were also up-regulated, including *IL-1 β* , *IL-1 α* , *NF- κ B2*, *BCL2A1*, and *BIRC3*. Interestingly, previous work has implicated NF- κ B signaling as having pro-metastatic functions in ovarian cancer (House et al. 2017). Therefore, NUAK1 loss increases spheroid viability potentially through up-regulation of NF- κ B signaling.

3.2 LKB1-NUAK1 Signaling

LKB1 is known as a master kinase due to its ability to regulate AMPK as well as 12 AMPK-related kinases (Shackelford & Shaw, 2009). Through these substrates, LKB1 can have multiple functions related to cell polarity, metabolism and growth. While LKB1 is commonly known as a tumor suppressor, there is a growing body of literature implicating it as having pro-metastatic roles under certain contexts (S. W. Lee et al., 2015; Shackelford et al., 2013; Shackelford & Shaw, 2009). In fact, we previously demonstrated that LKB1 is required for EOC spheroid viability and metastasis in xenograft models (Buensuceso et al., 2018; Peart et al., 2015) Because LKB1 can have a

broad range of functions it is critical to elucidate its downstream targets to identify specific substrates that could serve as more suitable therapeutic targets. Most of the literature examining targets of LKB1 have focused on AMPK, which is a regulator of metabolic stress (Shackelford & Shaw, 2009). However, our prior work indicated that in EOC, LKB1 elicits its tumorigenic functions through AMPK-independent signaling (Buensuceso et al., 2018; Peart et al., 2015). Thus to determine the critical target for LKB1 in EOC, we completed multiplex inhibitor bead-mass spectrometry and identified the ARK NUAK1 as a top candidate substrate. To confirm these findings, we showed that LKB1 regulates the phosphorylation and expression of NUAK1 in EOC adherent cells, spheroids, and tumor samples. We found that early in spheroid formation NUAK1 is highly expressed and this correlates with the levels of phosphorylated-LKB1. However, later during spheroid formation NUAK1 levels decrease but are still expressed at detectable levels. Total LKB1 expression starts to increase later during spheroid formation and this is consistent with our data showing that this kinase has pro-metastatic functions in EOC. The down-regulation of NUAK1 was observed in several HGSOC established cell lines and patient-derived ascites cells cultured as spheroids. We showed that the UPS and lysosome degradation both contribute to the down-regulation of NUAK1 in spheroids. Indeed, previous studies have shown that the UPS plays a role in regulating NUAK1. NUAK1 can be phosphorylated by cyclin-dependent kinases and polo kinase which leads to the recruitment of SCF^{BTrcp} E3 ligase, NUAK1 ubiquitination and subsequent degradation (Banerjee et al., 2014). NUAK1 was also shown to be ubiquitinated by unique Lys29 and or Lys33 linkages which block phosphorylation and activation by LKB1 (Al-Hakim et al., 2008). USP9X can bind to NUAK1 and cleave the polyubiquitin modification, allowing for LKB1 phosphorylation and activation. In this report, we show that USP9X also regulates NUAK1 expression in EOC spheroids. Therefore, we found that NUAK1 is a target of LKB1 in EOC and is differentially expressed in proliferative adherent cells and quiescent spheroids.

3.3 Pro-metastatic function of NUAK1 in ovarian cancer

Multiple studies have provided evidence that NUAK1 can have tumor-promoting functions. In human hepatoma cells, NUAK1 blocked cell death by inhibiting caspase 8 (Atsushi Suzuki et al., 2003). Along with increasing cell survival through inhibiting

apoptosis, NUAK1 can induce the S-phase in the cell cycle and increase cell proliferation (Banerjee et al., 2014). Several reports have shown that NUAK1 can also enhance cancer survival through supporting metabolic homeostasis in tumors overexpressing myc (Liu et al., 2012). A tumor-promoting role for NUAK1 is strengthened by studies showing that elevated levels of NUAK1 correlate with poor prognosis (Phippen et al., 2016; Port et al., 2018). High NUAK1 transcript levels in serous ovarian cancer patients was correlated with lower progression free survival and overall survival (Phippen et al., 2016). The molecular basis underlying the poor prognosis in EOC had not previously been elucidated. Herein, we found that NUAK1 regulates EOC cell adhesion and the formation of spheroids, which are key mediators of metastasis in ovarian cancer.

In the context of EOC metastasis, cell adhesion is critical as cancer cells aggregate through cell-ECM interactions to form spheroids which then spread through the peritoneal cavity (Casey et al., 2001). Previous research has suggested NUAK1 controls cell adhesion due to its roles in promoting EMT and invasion. In ovarian cancer cells, NUAK1 increases EMT and migration of cells by inhibiting miR-1181 (Zhang et al., 2015). Furthermore, NUAK1 overexpression in a pancreatic cancer mouse model increased *in vivo* metastasis (Kusakai et al., 2004). Mechanistically, NUAK1 has been shown to promote cell detachment by controlling the myosin phosphatase complex in HEK293 and MEF cells (Zagórska et al., 2010). Moreover, in colorectal cancer, loss of NUAK1 reduced tumor-initiating capacity because spheroids appeared smaller in size and were less abundant. To identify the molecular basis for this phenotype, the authors proposed that NUAK1 protects tumors from oxidative stress through nuclear translocation of Nrf2 (Port et al., 2018). In our study, we show that loss of NUAK1 impairs single cell adhesion and spheroid formation as spheroids appeared less compact. By examining spheroid formation in real-time, we observed *NUAK1*-KO-GFP spheroids exhibiting decreased integrity with an accumulation of dead cells around the spheroid. We propose that the ability of NUAK1 to control adhesion molecules is likely the primary mechanism mediating EOC spheroid formation. Two of the top signatures up-regulated in OVCAR8 parental spheroids compared to OVCAR8 *NUAK1*-KO spheroids were related to cell attachment. Interestingly, in the Nrf2 study described above they also

observed several cell adhesion pathways using the Metacore GeneGO analysis (Port et al., 2018). These cell adhesion pathways had a higher ranking than the Nrf2 oxidative stress response pathway yet were not pursued in that study. We observed *FNI* as the most differentially expressed gene in OVCAR8 *NUAK1*-KO spheroids with a 745-fold decrease. Importantly, the addition of soluble fibronectin to *NUAK1*-KO spheroids also completely restored the native phenotype. Altogether, we have elucidated a novel mechanism of NUAK1 in promoting EOC cell adhesion and spheroid compaction through fibronectin matrix production.

Our GSEA indicated a cell attachment signature that was enriched in OVCAR8 spheroids compared to OVCAR8 *NUAK1*-KO spheroids. Multiple adhesion molecules were identified in the signature, including *FNI*, *LICAM*, *ITG β 8*, *ITG β 5*, *THBS1*, and *F11R*, (Table 2.7), suggesting that NUAK1 regulates a network of adhesion molecules. We focused our validation experiments on fibronectin because it demonstrated the greatest differential expression and prior studies have shown it plays a key role in spheroid formation. Previous work in OVCAR5 cells showed that fibronectin mediates the formation of spheroids (Casey et al., 2001). The authors showed that the fibronectin receptor $\alpha 5\beta 1$ integrin also contributes to spheroid integrity. Interestingly, the canonical fibronectin receptor subunits were not present in our transcriptome analysis with only the *ITG β 5* and *ITG β 8* subunits being differentially expressed (Table 2.4). A prior study showed that $\beta 8$ -integrin may interact with fibronectin, however this interaction has only been shown in chick sensory neurons and the alpha subunit has not yet been elucidated (Venstrom & Reichardt, 1995). In addition, *ITG β 8* had a smaller fold change of 10, while *FNI* had a fold change of 745, suggesting that regulation of matrix expression is the principal mechanism by which NUAK1 is controlling cell adhesion in spheroids. Another study similarly demonstrated the importance of fibronectin in spheroids generated from fallopian tube epithelial (FTE) cells, which represent the putative cell of origin in HGSC (Iwanicki et al., 2016; Labidi-Galy et al., 2017). FTE cells with *TP53* mutations have an increased propensity to aggregate into spheroids due to autocrine fibronectin deposition. Besides *FNI*, *LICAM* was differentially expressed in our analysis with a fold change of 10. Indeed, L1CAM was previously shown to promote OVCAR8 and FTE

spheroid formation (Doberstein et al., 2018). In FTE spheroids, L1CAM up-regulated expression of integrins and fibronectin to facilitate spheroid formation. In our study, we similarly showed an interesting relationship between L1CAM and fibronectin expression. In OVCAR8 *NUAK1*-KO spheroids there was no detectable levels of either L1CAM or fibronectin expression. Therefore, we may have identified a novel signaling pathway controlling fibronectin and its molecules that mediates the formation of EOC spheroids.

3.4 Loss of NUAK1 up-regulates NF-κB signaling

Besides controlling cell adhesion and spheroid integrity, we examined whether NUAK1 could be playing a role in cell growth. While loss of NUAK1 increased spheroid viability there was no change in cell proliferation. Interestingly, GSEA revealed that a NF-κB pathway was up-regulated in OVCAR8 *NUAK1*-KO spheroids compared to OVCAR8 parental spheroids. We validated this pathway by showing enhanced nuclear translocation of the p65 transcription factor and increased expression of its target genes. House et al. (2017) demonstrated that in the ovarian cancer cell lines, OV90 and ACI-23, NF-κB activation can support tumor heterogeneity. They showed that the canonical NF-κB pathway promotes cell proliferation, while the non-canonical NF-κB pathway supports spheroid formation, chemoresistance, and a stem cell population in spheroids. But the function of NF-κB in ovarian cancer may be more complex as it was shown to have a biphasic role by either inhibiting or promoting ovarian cancer growth (Gill et al., 2011). In chemosensitive ovarian cancer cells (SKOV3 and HEY), NF-κB has pro-apoptotic functions. In chemoresistant cell lines (SKOV3i.p1 and HEYA8), NF-κB could be reprogrammed to function as an oncogene. Furthermore, increased nuclear localization of the p65 transcription factor was correlated with enhanced chemosensitivity and longer overall survival in patients. Altogether, our data suggests that loss of NUAK1 leads to increased spheroid viability. This enhanced viability could be due to enhanced NF-κB signaling. Alternatively, it is also possible that because *NUAK1*-KO spheroids are less compact it might have been easier to dissociate the spheroids prior to measuring cell counts with trypan blue, leading to increased viability readings as compared with parental cell spheroids. Future studies will need to be completed to test whether up-regulated NF-κB signaling is contributing to enhanced spheroid viability.

3.5 Limitations of current study and future studies

To examine how levels of NUAK1 change in an *in vitro* model system of metastasis, I compared NUAK1 expression between proliferative adherent cells and quiescent spheroids. I found an interesting trend where NUAK1 was commonly down-regulated in HGSOC established cells lines and patient-derived cells cultured as spheroids compared to monolayer cells. Using a proteasome inhibitor, I determined that the UPS contributes to the differential expression of NUAK1 in spheroids. Therefore, I sought to determine whether NUAK1 may be more highly ubiquitinated in spheroids compared to monolayer cells. To test this, endogenous ubiquitinated proteins were first pulled down using TUBEs. Following this precipitation, the ubiquitinated protein of interest could be detected by immunoblotting with the NUAK1 antibody. While I detected ubiquitinated c-myc (positive control) in spheroids, I did not identify ubiquitinated-NUAK1 in adherent cells or spheroids. Multiple modifications were made in an attempt to troubleshoot this precipitation experiment. For example, to preserve the ubiquitin modification on proteins for the pull-down I treated cells with a proteasome inhibitor and a deubiquitinase inhibitor (PR-619). This deubiquitinase inhibitor was also included into the lysis buffer. I collected spheroids at both early times points and late time points in case ubiquitinated-NUAK1 was being rapidly cleared by the proteasome at 72 hours. The western blot protocol was also optimized for ubiquitin proteins by altering the transfer conditions and keeping the stacking gel to avoid discarding high molecular weight proteins (Emmerich & Cohen, 2015). My results suggest that NUAK1 may not be highly ubiquitinated in ovarian cancer cells or potentially TUBEs are not an effective method to detect certain ubiquitinated proteins. It is possible that levels of ubiquitinated NUAK1 are very low in the cell and other more highly ubiquitinated species are saturating the agarose-TUBEs. Alternatively, the epitope for the NUAK1 antibody may be blocked by the ubiquitin modification. A future experiment could be implemented to examine the levels of ubiquitinated-NUAK1 in spheroids by overexpressing ubiquitin in OVCAR8 cells with HA-ubiquitin using the PMT123 plasmid (provided by C. Schild-Poulter, Western University). Following immunoprecipitation of ubiquitinated proteins, ubiquitinated-NUAK1 could be detected by immunoblotting with the NUAK1 antibody. By over-expressing ubiquitinated proteins, this alternative experiment may be able to detect

ubiquitinated-NUAK1 in EOC cells. I predict that spheroids have higher levels of ubiquitinated-NUAK1 compared to adherent cells.

Another future experiment would investigate the molecular basis for the increased viability in *NUAK1*-KO spheroids. We suggested that this result could be because the spheroids are less compact or because loss of NUAK1 enhances NF-κB signaling. To test whether up-regulated NF-κB signaling contributes to this increased viability, we could treat our OVCAR8 *NUAK1*-KO spheroids with an inhibitor of the NF-κB pathway. The BAY 11-7082 compound hinders the phosphorylation and subsequent degradation of IκBa, leading to the sequestration of the NF-κB subunits in the cytoplasm (Lee, Rhee, Kim, & Cho, 2012). I predict that treating OVCAR8 *NUAK1*-KO spheroids with the BAY 11-7082 compound would decrease their viability. This experiment would clarify at least one mechanism behind the increased viability in *NUAK1*-KO spheroids.

3.6 Therapeutic implications

Our results suggest that NUAK1 may have pro-metastatic functions because it enhances ovarian cancer spheroid formation. Thus, the use of a NUAK1 inhibitor may be therapeutically beneficial in ovarian cancer metastasis. In fact, the ON123300 dual NUAK1/CDK4 inhibitor was developed to address the modest efficacy with single agent CDK inhibitors in multiple myeloma (Perumal et al., 2016). ON123300 led to cell cycle arrest and apoptosis in multiple myeloma cells. This inhibitor also reduced tumor growth in multiple myeloma mouse models. Similarly, in ovarian cancer the addition of a NUAK1 inhibitor to the standard combination therapy of carboplatin and paclitaxel may provide a therapeutic advantage by targeting spheroid formation. Spheroids are a key mediator of metastasis and have the potential to acquire chemoresistance (Al Habyan et al., 2018; Desoize & Jardillier, 2000; Lengyel et al., 2014; Pease et al., 2012). There is an urgent need to identify novel therapeutic targets because with the current standard of care majority of patients will go on to develop disease recurrence and chemoresistance (Bowtell et al., 2015a).

3.7 Overall Conclusion

In conclusion, we have identified NUAK1 as a key target of LKB1 in EOC. We show that NUAK1 has pro-metastatic functions because it increases EOC cell adhesion and promotes spheroid integrity. Mechanistically, NUAK1 controls the deposition of fibronectin in spheroids to facilitate spheroid formation. Altogether, we provide evidence that the LKB1 substrate NUAK1 could serve as a potential therapeutic target in ovarian cancer metastasis.

3.8 References

Ahmed, N., & Stenvers, K. L. (2013). Getting to Know Ovarian Cancer Ascites:

- Opportunities for Targeted Therapy-Based Translational Research. *Frontiers in Oncology*. <https://doi.org/10.3389/fonc.2013.00256>
- Al-Hakim, A. K., Zagorska, A., Chapman, L., Deak, M., Peggie, M., & Alessi, D. R. (2008). Control of AMPK-related kinases by USP9X and atypical Lys 29 /Lys 33 - linked polyubiquitin chains . *Biochemical Journal*. <https://doi.org/10.1042/bj20080067>
- Al Habyan, S., Kalos, C., Szymborski, J., & McCaffrey, L. (2018). Multicellular detachment generates metastatic spheroids during intra-abdominal dissemination in epithelial ovarian cancer. *Oncogene*. <https://doi.org/10.1038/s41388-018-0317-x>
- Altevogt, P., Doberstein, K., & Fogel, M. (2016). L1CAM in human cancer. *International Journal of Cancer*. <https://doi.org/10.1002/ijc.29658>
- American College of Obstetricians and Gynecologists. (2002). ACOG Committee Opinion Number 280: The Role of the Generalist Obstetrician-Gynecologist in the Early Detection of Ovarian Cancer. *Obstetrics & Gynecology*, 100(6), 1413–1416. [https://doi.org/10.1016/s0029-7844\(02\)02630-3](https://doi.org/10.1016/s0029-7844(02)02630-3)
- Banerjee, Sourav, Zagórska, A., Deak, M., Campbell, D. G., Prescott, A. R., & Alessi, D. R. (2014). Interplay between Polo kinase, LKB1-activated NUAK1 kinase, PP1 β MYPT1 phosphatase complex and the SCF β TrCP E3 ubiquitin ligase . *Biochemical Journal*. <https://doi.org/10.1042/bj20140408>
- Banerjee, Susana, Kaye, S. B., & Ashworth, A. (2010). Making the best of PARP inhibitors in ovarian cancer. *Nature Reviews Clinical Oncology*. <https://doi.org/10.1038/nrclinonc.2010.116>
- Bast, R. C., Hennessy, B., & Mills, G. B. (2009). The biology of ovarian cancer: New opportunities for translation. *Nature Reviews Cancer*. <https://doi.org/10.1038/nrc2644>
- Beer, S., Oleszewski, M., Gutwein, P., Geiger, C., & Altevogt, P. (1999). Metalloproteinase-mediated release of the ectodomain of L1 adhesion molecule. *Journal of Cell Science*.
- Beggs, A. D., Latchford, A. R., Vasen, H. F. A., Moslein, G., Alonso, A., Aretz, S., ... Hodgson, S. V. (2010). Peutz - Jeghers syndrome: A systematic review and recommendations for management. *Gut*. <https://doi.org/10.1136/gut.2009.198499>
- Bell, D., Berchuck, A., Birrer, M., Chien, J., Cramer, D. W., Dao, F., ... Thomson, E. (2011). Integrated genomic analyses of ovarian carcinoma. *Nature*. <https://doi.org/10.1038/nature10166>
- Bondong, S., Kiefel, H., Hielscher, T., Zeimet, A. G., Zeillinger, R., Pils, D., ... Altevogt, P. (2012). Prognostic significance of L1CAM in ovarian cancer and its role in constitutive NF- κ B activation. *Annals of Oncology*. <https://doi.org/10.1093/annonc/mdr568>
- Bonnans, C., Chou, J., & Werb, Z. (2014). Remodelling the extracellular matrix in development and disease. *Nature Reviews. Molecular Cell Biology*. <https://doi.org/10.1038/nrm3904>
- Bowtell, D. D., Böhm, S., Ahmed, A. A., Aspuria, P.-J., Bast, R. C., Beral, V., ... Balkwill, F. R. (2015a). Rethinking ovarian cancer II: reducing mortality from high-grade serous ovarian cancer. *Nature Reviews. Cancer*. <https://doi.org/10.1038/nrc4019>
- Bowtell, D. D., Böhm, S., Ahmed, A. A., Aspuria, P.-J., Bast, R. C., Beral, V., ...

- Balkwill, F. R. (2015b). Rethinking ovarian cancer II: reducing mortality from high-grade serous ovarian cancer. *Nature Reviews Cancer*, 15(11), 668–679.
<https://doi.org/10.1038/nrc4019>
- Bright, N. J., Thornton, C., & Carling, D. (2009). The regulation and function of mammalian AMPK-related kinases. *Acta Physiologica*.
<https://doi.org/10.1111/j.1748-1716.2009.01971.x>
- Buensuceso, A., Valdes, Y. R., Figueredo, R., DiMatta, G. E., & Shepherd, T. G. (2018). Abstract A12: The metabolic stress mediator LKB1 is required for ovarian cancer metastasis. <https://doi.org/10.1158/1557-3265.ovca17-a12>
- Casey, R. C., Burleson, K. M., Skubitz, K. M., Pambuccian, S. E., Oegema, T. R., Ruff, L. E., & Skubitz, A. P. N. (2001). β 1-integrins regulate the formation and adhesion of ovarian carcinoma multicellular spheroids. *American Journal of Pathology*.
[https://doi.org/10.1016/S0002-9440\(10\)63058-1](https://doi.org/10.1016/S0002-9440(10)63058-1)
- Cho, A., Howell, V. M., & Colvin, E. K. (2015). The Extracellular Matrix in Epithelial Ovarian Cancer – A Piece of a Puzzle. *Frontiers in Oncology*.
<https://doi.org/10.3389/fonc.2015.00245>
- Coleman, R. L., Monk, B. J., Sood, A. K., & Herzog, T. J. (2013). Latest research and treatment of advanced-stage epithelial ovarian cancer. *Nature Reviews Clinical Oncology*. <https://doi.org/10.1038/nrclinonc.2013.5>
- Correa, R. J. M., Valdes, Y. R., Peart, T. M., Fazio, E. N., Bertrand, M., McGee, J., ... Shepherd, T. G. (2014). Combination of AKT inhibition with autophagy blockade effectively reduces ascites-derived ovarian cancer cell viability. *Carcinogenesis*.
<https://doi.org/10.1093/carcin/bgu049>
- Correa, R. J. M., Valdes, Y. R., Shepherd, T. G., & DiMatta, G. E. (2015). Beclin-1 expression is retained in high-grade serous ovarian cancer yet is not essential for autophagy induction in vitro. *Journal of Ovarian Research*.
<https://doi.org/10.1186/s13048-015-0182-y>
- Desoize, B., & Jardillier, J. C. (2000). Multicellular resistance: A paradigm for clinical resistance? *Critical Reviews in Oncology/Hematology*.
[https://doi.org/10.1016/S1040-8428\(00\)00086-X](https://doi.org/10.1016/S1040-8428(00)00086-X)
- Doberstein, K., Spivak, R., Feng, Y., Stuckelberger, S., Mills, G. B., Devins, K. M., ... Affiliations. (2018). Fallopian tube precursor lesions of serous ovarian carcinoma require L1CAM for dissemination and metastasis. *BioRxiv Preprint First*.
<https://doi.org/10.1101/270785>
- Domcke, S., Sinha, R., Levine, D. A., Sander, C., & Schultz, N. (2013). Evaluating cell lines as tumour models by comparison of genomic profiles. *Nature Communications*. <https://doi.org/10.1038/ncomms3126>
- Duncan, J. S., Whittle, M. C., Nakamura, K., Abell, A. N., Midland, A. A., Zawistowski, J. S., ... Johnson, G. L. (2012). Dynamic reprogramming of the kinaseome in response to targeted MEK inhibition in triple-negative breast cancer. *Cell*.
<https://doi.org/10.1016/j.cell.2012.02.053>
- Emmerich, C. H., & Cohen, P. (2015). Optimising methods for the preservation, capture and identification of ubiquitin chains and ubiquitylated proteins by immunoblotting. *Biochemical and Biophysical Research Communications*.
<https://doi.org/10.1016/j.bbrc.2015.08.109>
- Emmings, E., Mullany, S., Chang, Z., Landen, C. N., Linder, S., & Bazzaro, M. (2019).

- Targeting Mitochondria for Treatment of Chemoresistant Ovarian Cancer. *International Journal of Molecular Sciences*, 20(1).
<https://doi.org/10.3390/ijms20010229>
- Espín-Palazón, R., & Traver, D. (2016). The NF-κB family: Key players during embryonic development and HSC emergence. *Experimental Hematology*.
<https://doi.org/10.1016/j.exphem.2016.03.010>
- F Ann Ran, Patrick D Hsu, Jason Wright, Vineeta Agarwala, D. A. S. & F. Z. (2013). Genome engineering using crispr-cas9 system. *Nature Protocols*, 8(11), 2281–2308.
https://doi.org/10.1007/978-1-4939-1862-1_10
- Franke, F. E., Von Georgi, R., Zygmunt, M., & Münstedt, K. (2003). Association between Fibronectin Expression and Prognosis in Ovarian Carcinoma. *Anticancer Research*.
- Gill, R. K., Yang, S. H., Meerzaman, D., Mechanic, L. E., Bowman, E. D., Jeon, H. S., ... Jen, J. (2011). Frequent homozygous deletion of the LKB1/STK11 gene in non-small cell lung cancer. *Oncogene*. <https://doi.org/10.1038/onc.2011.98>
- Goff, B. A. (2012). Advanced ovarian cancer: What should be the standard of care? *Journal of Gynecologic Oncology*. <https://doi.org/10.3802/jgo.2013.24.1.83>
- Gopal, S., Veracini, L., Grall, D., Butori, C., Schaub, S., Audebert, S., ... Van Obberghen-Schilling, E. (2017). Fibronectin-guided migration of carcinoma collectives. *Nature Communications*. <https://doi.org/10.1038/ncomms14105>
- Guldberg, P., Straten, P. T., Ahrenkiel, V., Seremet, T., Kirkin, A. F., & Zeuthen, J. (1999). Somatic mutation of the Peutz-Jeghers syndrome gene, LKB1/STK11, in malignant melanoma. *Oncogene*. <https://doi.org/10.1038/sj.onc.1202486>
- Hardie, D. G., & Alessi, D. R. (2013). LKB1 and AMPK and the cancer-metabolism link - ten years after. *BMC Biology*. <https://doi.org/10.1186/1741-7007-11-36>
- Hemminki, a, Avizienyte, E., Roth, S., Loukola, A., Aaltonen, L. a, Järvinen, H., & de la Chapelle, A. (1998). A serine/threonine kinase gene defective in Peutz-Jeghers syndrome. *Nature*, 391(January), 184–187. Retrieved from <http://www.ncbi.nlm.nih.gov/pubmed/11524750>
- Hernandez, L., Kim, M. K., Lyle, L. T., Bunch, K. P., House, C. D., Ning, F., ... Annunziata, C. M. (2016). Characterization of ovarian cancer cell lines as in vivo models for preclinical studies. *Gynecologic Oncology*.
<https://doi.org/10.1016/j.ygyno.2016.05.028>
- Hew, K. E., Miller, P. C., El-Ashry, D., Sun, J., Besser, A. H., Ince, T. A., ... Simpkins, F. (2016). MAPK activation predicts poor outcome and the MEK inhibitor, selumetinib, reverses antiestrogen resistance in ER-positive high-grade serous ovarian cancer. *Clinical Cancer Research*. <https://doi.org/10.1158/1078-0432.CCR-15-0534>
- Hou, X., Liu, J.-E., Liu, W., Liu, C.-Y., Liu, Z.-Y., & Sun, Z.-Y. (2011). A new role of NUAK1: directly phosphorylating p53 and regulating cell proliferation. *Oncogene*.
<https://doi.org/10.1038/onc.2011.19>
- House, C. D., Jordan, E., Hernandez, L., Ozaki, M., James, J. M., Kim, M., ... Annunziata, C. M. (2017). NFkB promotes ovarian tumorigenesis via classical pathways that support proliferative cancer cells and alternative pathways that support ALDH β cancer stem-like cells. *Cancer Research*.
<https://doi.org/10.1158/0008-5472.CAN-17-0366>

- Humbert, N., Navaratnam, N., Augert, A., Da Costa, M., Martien, S., Wang, J., ... Bernard, D. (2010). Regulation of ploidy and senescence by the AMPK-related kinase NUAK1. *EMBO Journal*. <https://doi.org/10.1038/emboj.2009.342>
- Iwanicki, M. P., Chen, H.-Y., Iavarone, C., Zervantonakis, I. K., Muranen, T., Novak, M., ... Brugge, J. S. (2016). Mutant p53 regulates ovarian cancer transformed phenotypes through autocrine matrix deposition. *JCI Insight*. <https://doi.org/10.1172/jci.insight.86829>
- Johansson, S., Svineng, G., Wennerberg, K., Armulik, A., & Lohikangas, L. (1997). Fibronectin-integrin interactions. *Frontiers in Bioscience : A Journal and Virtual Library*.
- Karst, A. M., & Drapkin, R. (2009). Ovarian Cancer Pathogenesis: A Model in Evolution. *Journal of Oncology*. <https://doi.org/10.1155/2010/932371>
- Kedves, A. T., Gleim, S., Liang, X., Bonal, D. M., Sigoillot, F., Harbinski, F., ... Forrester, W. C. (2017). Recurrent ubiquitin B silencing in gynecological cancers establishes dependence on ubiquitin C. *Journal of Clinical Investigation*. <https://doi.org/10.1172/JCI92914>
- Keller, A., Nesvizhskii, A. I., Kolker, E., & Aebersold, R. (2002). Empirical statistical model to estimate the accuracy of peptide identifications made by MS/MS and database search. *Analytical Chemistry*, 74(20), 5383–5392. <https://doi.org/10.1021/ac025747h>
- Kenny, H. A., Chiang, C. Y., White, E. A., Schryver, E. M., Habis, M., Romero, I. L., ... Lengyel, E. (2014). Mesothelial cells promote early Ovarian cancer metastasis through fibronectin secretion. *Journal of Clinical Investigation*. <https://doi.org/10.1172/JCI74778>
- Kusakai, G., Suzuki, A., Ogura, T., Kaminishi, M., & Esumi, H. (2004). Strong association of ARK5 with tumor invasion and metastasis. *Journal of Experimental & Clinical Cancer Research : CR*.
- Labidi-Galy, S. I., Papp, E., Hallberg, D., Niknafs, N., Adleff, V., Noe, M., ... Velculescu, V. E. (2017). High grade serous ovarian carcinomas originate in the fallopian tube. *Nature Communications*. <https://doi.org/10.1038/s41467-017-00962-1>
- Lee, J., Rhee, M. H., Kim, E., & Cho, J. Y. (2012). BAY 11-7082 is a broad-spectrum inhibitor with anti-inflammatory activity against multiple targets. *Mediators of Inflammation*. <https://doi.org/10.1155/2012/416036>
- Lee, S. W., Li, C. F., Jin, G., Cai, Z., Han, F., Chan, C. H., ... Lin, H. K. (2015). Skp2-Dependent Ubiquitination and Activation of LKB1 Is Essential for Cancer Cell Survival under Energy Stress. *Molecular Cell*. <https://doi.org/10.1016/j.molcel.2015.01.015>
- Lengyel, E., Burdette, J. E., Kenny, H. A., Matei, D., Pilrose, J., Haluska, P., ... Stack, M. S. (2014). Epithelial ovarian cancer experimental models. *Oncogene*. <https://doi.org/10.1038/onc.2013.321>
- Leung, B. M., Lesher-Perez, S. C., Matsuoka, T., Moraes, C., & Takayama, S. (2015). Media additives to promote spheroid circularity and compactness in hanging drop platform. *Biomaterials Science*. <https://doi.org/10.1039/c4bm00319e>
- Lheureux, S., Gourley, C., Vergote, I., & Oza, A. M. (2019). Epithelial ovarian cancer. *The Lancet*. [https://doi.org/10.1016/S0140-6736\(18\)32552-2](https://doi.org/10.1016/S0140-6736(18)32552-2)

- Lilienbaum, A. (2013). Relationship between the proteasomal system and autophagy. *International Journal of Biochemistry and Molecular Biology*.
- Lin, R. Z., Chou, L. F., Chien, C. C. M., & Chang, H. Y. (2006). Dynamic analysis of hepatoma spheroid formation: Roles of E-cadherin and β 1-integrin. *Cell and Tissue Research*. <https://doi.org/10.1007/s00441-005-0148-2>
- Linke, R., Babic, R., & Gossner, W. (1988). Fibrin-Fibronectin Compounds in Human Ovarian Tumor Ascites and Their Possible Relation to the Tumor Stroma. *Cancer Research*.
- Liu, F., Yang, X., Geng, M., & Huang, M. (2018). Targeting ERK, an Achilles' Heel of the MAPK pathway, in cancer therapy. *Acta Pharmaceutica Sinica B*. <https://doi.org/10.1016/j.apsb.2018.01.008>
- Liu, G., Zhang, J., Larsen, B., Stark, C., Breitkreutz, A., Lin, Z.-Y., ... Gingras, A.-C. (2010). ProHits: integrated software for mass spectrometry-based interaction proteomics. *Nature Biotechnology*. <https://doi.org/10.1038/nbt1010-1015>
- Liu, L., Ulbrich, J., Müller, J., Wüstefeld, T., Aeberhard, L., Kress, T. R., ... Murphy, D. J. (2012). Deregulated MYC expression induces dependence upon AMPK-related kinase 5. *Nature*. <https://doi.org/10.1038/nature10927>
- Livak, K. J., & Schmittgen, T. D. (2001). Analysis of relative gene expression data using real-time quantitative PCR and the $2^{-\Delta\Delta CT}$ method. *Methods*. <https://doi.org/10.1006/meth.2001.1262>
- Lizcano, J. M., Göransson, O., Toth, R., Deak, M., Morrice, N. A., Boudeau, J., ... Alessi, D. R. (2004). LKB1 is a master kinase that activates 13 kinases of the AMPK subfamily, including MARK/PAR-1. *EMBO Journal*. <https://doi.org/10.1038/sj.emboj.7600110>
- Lu, Z., Luo, R. Z., Lu, Y., Zhang, X., Yu, Q., Khare, S., ... Bast, R. C. (2008). The tumor suppressor gene ARHI regulates autophagy and tumor dormancy in human ovarian cancer cells. *Journal of Clinical Investigation*. <https://doi.org/10.1172/JCI35512>
- MacDonald, J., Ramos-Valdes, Y., Perampalam, P., Litovchick, L., DiMatta, G. E., & Dick, F. A. (2016). A Systematic Analysis of Negative Growth Control Implicates the DREAM Complex in Cancer Cell Dormancy. *Molecular Cancer Research*. <https://doi.org/10.1158/1541-7786.mcr-16-0323-t>
- Manning, G., Whyte, D. B., Martinez, R., Hunter, T., & Sudarsanam, S. (2002). The protein kinase complement of the human genome. *Science*. <https://doi.org/10.1126/science.1075762>
- Martin, L. P., Hamilton, T. C., & Schilder, R. J. (2008). Platinum resistance: The role of DNA repair pathways. *Clinical Cancer Research*. <https://doi.org/10.1158/1078-0432.CCR-07-2238>
- Matulonis, U. A. (2018). Management of newly diagnosed or recurrent ovarian cancer. *Clinical Advances in Hematology and Oncology*.
- Monteverde, T., Tait-Mulder, J., Hedley, A., Knight, J. R., Sansom, O. J., & Murphy, D. J. (2018). Calcium signalling links MYC to NUAK1. *Oncogene*. <https://doi.org/10.1038/onc.2017.394>
- Nagase, T., Kikuno, R., Hattori, A., Kondo, Y., Okumura, K., & Ohara, O. (2000). Prediction of the coding sequences of unidentified human genes. XIX. The complete sequences of 100 new cDNA clones from brain which code for large proteins in vitro. *DNA Research : An International Journal for Rapid Publication of Reports on*

- Genes and Genomes.* <https://doi.org/10.1093/dnares/7.6.347>
- Nakamura, K., Nakayama, K., Ishikawa, N., Ishikawa, M., Sultana, R., Kiyono, T., & Kyo, S. (2017). Reconstitution of high-grade serous ovarian carcinoma from primary fallopian tube secretory epithelial cells. *Oncotarget*, 9(16), 12609–12619. <https://doi.org/10.18632/oncotarget.23035>
- Nesvizhskii, A. I., Keller, A., Kolker, E., & Aebersold, R. (2003). A statistical model for identifying proteins by tandem mass spectrometry. *Analytical Chemistry*.
- Pankov, R., & Yamada, K. M. (2002). Fibronectin at a glance. *Journal of Cell Science*, 115(Pt 20), 3861–3863. <https://doi.org/10.1242/jcs.00059>
- Peart, T., Valdes, Y. R., Correa, R. J. M., Fazio, E., Bertrand, M., McGee, J., ... Shepherd, T. G. (2015). Intact LKB1 activity is required for survival of dormant ovarian cancer spheroids. *Oncotarget*. <https://doi.org/10.18632/oncotarget.4211>
- Pease, J. C., Brewer, M., & Tirnauer, J. S. (2012). Spontaneous spheroid budding from monolayers: a potential contribution to ovarian cancer dissemination. *Biology Open*. <https://doi.org/10.1242/bio.2012653>
- Perumal, D., Leshchenko, V. V., Kuo, P. Y., Jiang, Z., Divakar, S. K. A., Jay Cho, H., ... Parekh, S. (2016). Dual targeting of CDK4 and ARK5 using a novel kinase inhibitor ON123300 exerts potent anticancer activity against multiple myeloma. *Cancer Research*. <https://doi.org/10.1158/0008-5472.CAN-15-2934>
- Phippen, N. T., Bateman, N. W., Wang, G., Conrads, K. A., Ao, W., Teng, P., ... Conrads, T. P. (2016). NUAK1 (ARK5) Is Associated with Poor Prognosis in Ovarian Cancer. *Frontiers in Oncology*. <https://doi.org/10.3389/fonc.2016.00213>
- Port, J., Muthalagu, N., Raja, M., Ceteci, F., Monteverde, T., Kruspig, B., ... Murphy, D. J. (2018). Colorectal tumors require NUAK1 for protection from oxidative stress. *Cancer Discovery*. <https://doi.org/10.1158/2159-8290.CD-17-0533>
- Roett, M. A., & Evans, P. (2009). Ovarian cancer: An overview. *American Family Physician*.
- Sabio, G., & Davis, R. J. (2014). TNF and MAP kinase signalling pathways. *Seminars in Immunology*. <https://doi.org/10.1016/j.smim.2014.02.009>
- Sant, S., & Johnston, P. A. (2017). The production of 3D tumor spheroids for cancer drug discovery. *Drug Discovery Today: Technologies*. <https://doi.org/10.1016/j.ddtec.2017.03.002>
- Schauer, I. G., Zhang, J., Xing, Z., Guo, X., Mercado-Uribe, I., Sood, A. K., ... Liu, J. (2015). Interleukin-1 β Promotes Ovarian Tumorigenesis through a p53/NF- κ B-Mediated Inflammatory Response in Stromal Fibroblasts. *Neoplasia*, 15(4), 409-IN18. <https://doi.org/10.1593/neo.121228>
- Scherer, S. E., Muzny, D. M., Buhay, C. J., Chen, R., Cree, A., Ding, Y., ... Gibbs, R. A. (2006). The finished DNA sequence of human chromosome 12. *Nature*. <https://doi.org/10.1038/nature04569>
- Schiller, H. B., & Fässler, R. (2013). Mechanosensitivity and compositional dynamics of cell-matrix adhesions. *EMBO Reports*. <https://doi.org/10.1038/embor.2013.49>
- Shackelford, D. B., Abt, E., Gerken, L., Vasquez, D. S., Seki, A., Leblanc, M., ... Shaw, R. J. (2013). LKB1 Inactivation Dictates Therapeutic Response of Non-Small Cell Lung Cancer to the Metabolism Drug Phenformin. *Cancer Cell*. <https://doi.org/10.1016/j.ccr.2012.12.008>
- Shackelford, D. B., & Shaw, R. J. (2009). The LKB1-AMPK pathway: Metabolism and

- growth control in tumour suppression. *Nature Reviews Cancer.* <https://doi.org/10.1038/nrc2676>
- Shepherd, T. G., Thériault, B. L., Campbell, E. J., & Nachtigal, M. W. (2007). Primary culture of ovarian surface epithelial cells and ascites-derived ovarian cancer cells from patients. *Nature Protocols.* <https://doi.org/10.1038/nprot.2006.328>
- Shteynberg, D., Deutsch, E. W., Lam, H., Eng, J. K., Sun, Z., Tasman, N., ... Nesvizhskii, A. I. (2011). iProphet: Multi-level Integrative Analysis of Shotgun Proteomic Data Improves Peptide and Protein Identification Rates and Error Estimates. *Molecular & Cellular Proteomics.* <https://doi.org/10.1074/mcp.M111.007690>
- Siegel, R. L., Miller, K. D., & Jemal, A. (2019). Cancer statistics, 2019. *CA: A Cancer Journal for Clinicians.* <https://doi.org/10.3322/caac.21551>
- Sodek, K. L., Murphy, K. J., Brown, T. J., & Ringuette, M. J. (2012). Cell-cell and cell-matrix dynamics in intraperitoneal cancer metastasis. *Cancer and Metastasis Reviews.* <https://doi.org/10.1007/s10555-012-9351-2>
- Sodek, K. L., Ringuette, M. J., & Brown, T. J. (2009). Compact spheroid formation by ovarian cancer cells is associated with contractile behavior and an invasive phenotype. *International Journal of Cancer.* <https://doi.org/10.1002/ijc.24188>
- Stuhlmiller, T. J., Miller, S. M., Zawistowski, J. S., Nakamura, K., Beltran, A. S., Duncan, J. S., ... Johnson, G. L. (2015). Inhibition of lapatinib-induced kinase reprogramming in ERBB2-positive breast cancer by targeting BET family bromodomains. *Cell Reports.* <https://doi.org/10.1016/j.celrep.2015.03.037>
- Subramanian, A., Tamayo, P., Mootha, V. K., Mukherjee, S., Ebert, B. L., Gillette, M. A., ... Mesirov, J. P. (2005). Gene set enrichment analysis: a knowledge-based approach for interpreting genome-wide expression profiles. *Proceedings of the National Academy of Sciences of the United States of America.* <https://doi.org/10.1073/pnas.0506580102>
- Suzuki, A., Lu, J., Kusakai, G. -i., Kishimoto, A., Ogura, T., & Esumi, H. (2004). ARK5 Is a Tumor Invasion-Associated Factor Downstream of Akt Signaling. *Molecular and Cellular Biology.* <https://doi.org/10.1128/MCB.24.8.3526-3535.2004>
- Suzuki, Atsushi, Kusakai, G. I., Kishimoto, A., Lu, J., Ogura, T., Lavin, M. F., & Esumi, H. (2003). Identification of a novel protein kinase mediating Akt survival signaling to the ATM protein. *Journal of Biological Chemistry.* <https://doi.org/10.1074/jbc.M206025200>
- Teo, G., Kim, S., Tsou, C. C., Collins, B., Gingras, A. C., Nesvizhskii, A. I., & Choi, H. (2015). MapDIA: Preprocessing and statistical analysis of quantitative proteomics data from data independent acquisition mass spectrometry. *Journal of Proteomics,* 129, 108–120. <https://doi.org/10.1016/j.jprot.2015.09.013>
- Tomida, J., Kitao, H., Kinoshita, E., & Takata, M. (2008). Detection of phosphorylation on large proteins by western blotting using Phos-tag containing gel. *Protocol Exchange.* <https://doi.org/10.1038/nprot.2008.232>
- Tsou, C. C., Avtonomov, D., Larsen, B., Tucholska, M., Choi, H., Gingras, A. C., & Nesvizhskii, A. I. (2015). DIA-Umpire: Comprehensive computational framework for data-independent acquisition proteomics. *Nature Methods.* <https://doi.org/10.1038/nmeth.3255>
- Venstrom, K., & Reichardt, L. (1995). Beta 8 integrins mediate interactions of chick

- sensory neurons with laminin-1, collagen IV, and fibronectin. *Molecular Biology of the Cell*. <https://doi.org/10.1091/mbc.6.4.419>
- Viatour, P., Merville, M. P., Bouras, V., & Chariot, A. (2005). Phosphorylation of NF- κ B and IkkB proteins: Implications in cancer and inflammation. *Trends in Biochemical Sciences*. <https://doi.org/10.1016/j.tibs.2004.11.009>
- Wang, Q., Bu, S., Xin, D., Li, B., Wang, L., & Lai, D. (2018). Autophagy Is Indispensable for the Self-Renewal and Quiescence of Ovarian Cancer Spheroid Cells with Stem Cell-Like Properties. *Oxidative Medicine and Cellular Longevity*. <https://doi.org/10.1155/2018/7010472>
- Ware, M. J., Colbert, K., Keshishian, V., Ho, J., Corr, S. J., Curley, S. A., & Godin, B. (2016). Generation of Homogenous Three-Dimensional Pancreatic Cancer Cell Spheroids Using an Improved Hanging Drop Technique. *Tissue Engineering Part C: Methods*. <https://doi.org/10.1089/ten.tec.2015.0280>
- Weaver, B. A. (2014). How Taxol/paclitaxel kills cancer cells. *Molecular Biology of the Cell*, 25(18), 2677–2681. <https://doi.org/10.1091/mbc.e14-04-0916>
- Weiswald, L. B., Bellet, D., & Dangles-Marie, V. (2015). Spherical Cancer Models in Tumor Biology. *Neoplasia (United States)*. <https://doi.org/10.1016/j.neo.2014.12.004>
- White, E. S., & Muro, A. F. (2011). Fibronectin splice variants: Understanding their multiple roles in health and disease using engineered mouse models. *IUBMB Life*. <https://doi.org/10.1002/iub.493>
- Ye, Z., Chen, X., & Chen, X. (2018). ARK5 promotes invasion and migration in hepatocellular carcinoma cells by regulating epithelial-mesenchymal transition. *Oncology Letters*, 15(2), 1511–1516. <https://doi.org/10.3892/ol.2017.7453>
- Zagórska, A., Deak, M., Campbell, D. G., Banerjee, S., Hirano, M., Aizawa, S., ... Alessi, D. R. (2010). New roles for the LKB1-NUAK pathway in controlling myosin phosphatase complexes and cell adhesion. *Science Signaling*. <https://doi.org/10.1126/scisignal.2000616>
- Zhang, H. Y., Li, J. H., Li, G., & Wang, S. R. (2015). Activation of ARK5/miR-1181/HOXA10 axis promotes epithelial-mesenchymal transition in ovarian cancer. *Oncology Reports*. <https://doi.org/10.3892/or.2015.4113>

Curriculum Vitae

Name:	Jamie Lee Fritz
Post-secondary Education and Degrees:	Western University London, Ontario, Canada 2013-2017 Bachelor of Medical Sciences
	Western University London, Ontario, Canada 2017- present Master's in Anatomy and Cell Biology
Honours and Awards:	Obstetrics and Gynaecology Graduate Scholarship 2017-2018
	Oncology Research and Education Day: Oral Presentation Award 2019
	Paul Harding Research Day: Poster Award 2018
	Canadian Conference on Ovarian Cancer Research: Travel Award 2018
	Western Graduate Scholarship 2017-2018; 2018- 2019
Related Work Experience	Teaching Assistant (Histology 3309) Western University 2017-2018; 2018- 2019